**US Army Corps
of Engineers**
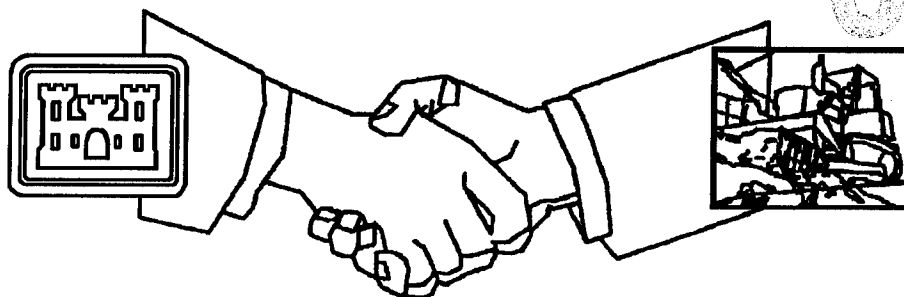Waterways Experiment
Station

CONSTRUCTION PRODUCTIVITY ADVANCEMENT RESEARCH (CPAR) PROGRAM

Masonry Research for Limit-States Design

by

Michael I. Hammons, Richard H. Atkinson,
Michael P. Schuller, Paul J. Tikalsky

Approved For Public Release; Distribution Is Unlimited

**A Corps/Industry Partnership to Advance
Construction Productivity and Reduce Costs**

**Construction Productivity Advancement
Research (CPAR) Program**

Masonry Research for Limit-States Design

by Michael I. Hammons
U.S. Army Corps of Engineers
Waterways Experiment Station
3909 Halls Ferry Road
Vicksburg, MS   39180-6199

Richard H. Atkinson, Michael P. Schuller
Atkinson - Noland & Associates
2619 Spruce Street
Boulder, CO   80302

Paul J. Tikalsky
Santa Clara University
Santa Clara, CA   75053

Final report

19941205 007

Prepared for   U.S. Army Corps of Engineers
Washington, DC   20314-1000

**US Army Corps
of Engineers**
Waterways Experiment
Station

N

INFORMATION
TECHNOLOGY
LABORATORY

GEOTECHNICAL
LABORATORY

HEADQUARTERS
BUILDING

MAIN
ENTRANCE

HYDRAULICS
LABORATORY

COASTAL ENGINEERING
RESEARCH CENTER

ENVIRONMENTAL
LABORATORY

STRUCTURES
LABORATORY

FOR INFORMATION CONTACT :
PUBLIC AFFAIRS OFFICE
U. S. ARMY ENGINEER
WATERWAYS EXPERIMENT STATION
3909 HALLS FERRY ROAD
VICKSBURG, MISSISSIPPI 39180-6199
PHONE : (601)634-2502

SCALE
500   0   500 m

AREA OF RESERVATION = 2.7 sq km

Contents

SF 298

Preface

The investigation described in this report was conducted for the Head-quarters, U.S. Army Corps of Engineers (HQUSACE), by the U.S. Army Engineer Waterways Experiment Station (WES) in cooperation with Atkinson-Noland and Associates (ANA), Boulder, CO. This cooperative research and development agreement was a part of the Fiscal Year 1990 Construction Productivity Advancement Research (CPAR) Program. The CPAR Technical Monitor was Mr. C. Gutberlet (CEMP-ET).

The testing was performed at WES by members of the staff of the Structures Laboratory (SL) and by Dr. Paul J. Tikalsky, Santa Clara University, California, under the general supervision of Messrs. Bryant Mather, Director, SL; J. T. Ballard, Assistant Director, SL; and K. L. Saucier, Chief, Concrete Technology Division (CTD), SL. Mr. William F. McCleese, CTD, was the CPAR Program Manager at WES. Direct supervision was provided by Mr. Steven A. Ragan, Chief, Engineering Mechanics Branch (EMB), CTD. Mr. Michael I. Hammons, EMB, was the Principal Investigator for this research. Test concept and data analysis were provided by Dr. Richard H. Atkinson and Mr. Michael P. Schuller, ANA. This report was prepared by Mr. Hammons, Dr. Atkinson, Mr. Schuller, and Dr. Tikalsky. The authors wish to acknowledge Dr. James L. Noland, ANA, and Messrs. Dan Wilson, Cliff Gill, Billy D. Neeley, Willie McDonald, and Donald M. Smith, and Mrs. Linda Mayfield, EMB, for their assistance during this investigation.

At the time of preparation of this report, Director of WES was Dr. Robert W. Whalin. Commander was COL Bruce K. Howard, EN.

Conversion Factors, Non-SI to SI Units of Measurement

Non-SI units of measurement used in this report can be converted to SI units as follows:

Multiply	By	To Obtain
degrees (angle)	0.01745329	radians
feet	0.3048	metres
inches	25.4	millimetres
kips (force)	4.448222	kilonewtons
pounds (mass) per cubic foot	16.01846	kilograms per cubic metre
pounds (force) per square inch	0.006894757	megapascals
*To obtain Celsius (C) temperature readings from Fahrenheit (F) readings, use the following formula: C = (5/9) (F-32). To obtain Kelvin (K) readings, use: K = (5/9) (F-32) + 273.15.		

1 Introduction

Background

Reinforced masonry provides an attractive, low-cost alternative to conventional steel or reinforced-concrete construction. Experience in California has shown that when reinforced masonry is properly designed and constructed, adequate ductility can be provided for seismic resistance. Reinforcing in masonry also provides resistance to wind and gravity loads and will be required in all future Corps of Engineers masonry structures.

Existing masonry design codes and design methods (Uniform Building Code 1992, American Concrete Institute (ACI) 1988a) are a mixture of empirical rules and linear-elastic working-stress methods. These methods are unsatisfactory for designing masonry buildings to provide an assured level of ductility to meet seismic and other loadings. In addition, because multiple and sometimes unknown factors of safety are involved, existing design methods for masonry are considered to be uneconomical when compared to limit-states methods adopted for use in reinforced concrete and structural steel design.

The Masonry Standards Joint Committee (MSJC), formed in 1989 by the ACI, the American Society of Civil Engineers (ASCE), and The Masonry Society (TMS), develops consensus-based, material design standards for masonry. A subcommittee of the MSJC is presently developing a limit-states-based design standard for masonry. This new design standard, which is to be based on rational engineering principles rather than on empirical rules, will require an in-depth understanding of the behavior reinforced masonry.

The investigation reported in this report was conducted under the U. S. Army Corps of Engineers Construction Productivity Advancement Research (CPAR) Research Program under a Cooperative Research and Development Agreement (CRDA) between the U.S. Army Engineer Waterways Experiment Station (WES), Vicksburg, MS, and Atkinson-Noland and Associates, Boulder, CO. This research was conducted in conjunction with the U.S. Coordinated Program for Masonry Building Research (Noland 1990), which is a comprehensive program of research in the

structural aspects of reinforced masonry supported by the masonry industry of the United States and the National Science Foundation. Technical direction of this program is provided by the Technical Coordinating Committee for Masonry Research (TCCMAR). The research conducted in this CPAR program complements the work of TCCMAR by filling in certain critical areas in the TCCMAR Program.

Objective

The objective of the research conducted under this CPAR program was to determine the critical material and design parameters of reinforced masonry necessary for formulation of the new limit-states design standard for masonry. The study identified several of these parameters, conducted the necessary research, and presented the results and recommendations in a form usable by the subcommittee drafting the limit-states design standard. Actual drafting of design standards, however, is a function of the voluntary committees operating under auspices of professional organizations.

Scope

Three specific areas of deficient knowledge of reinforced masonry behavior are addressed in this study:

a. Lap-splice requirements for reinforced masonry.

b. Tension-stiffening behavior of reinforced masonry and its effect on minimum and maximum reinforcing steel requirements.

c. Behavior of masonry when loaded under in-plane biaxial compression and tension loadings.

Results from studies on these topics will provide knowledge of masonry behavior which will have immediate impact on the limit-states design code being drafted. The results will also provide the means for better methods of analysis, especially in the area of finite element analysis of masonry structures.

In this report, Chapters 2, 3, and 4 present the results of the lap-splice, tension-stiffening, and biaxial behavior of reinforced masonry, respectively. Each chapter is complete in itself covering all aspects of the work including problem statement, literature review, test procedures, results, analysis, and conclusions. Chapter 5 presents a summary of the program as well as recapitulates the major conclusions from this study. Material properties common to all three components of this research study are contained in Appendix A. A compendium of all research data generated from

this study is contained in an unpublished appendix. These data are stored in both print and magnetic media and can be obtained from WES on request for future study and evaluation.

2 Lap-Splice Tests

Introduction

Tests were conducted to investigate lap splices in reinforced masonry. These tests focused on investigating parameters which affect the strength and ductility of lap splices for grouted concrete and clay masonry construction. Data from the investigation were used to conduct a comprehensive examination of the effects of masonry unit width, masonry unit type, reinforcing bar diameter, and lap length on both the strength and monotonic behavior of lap splices in masonry. The range of unit and reinforcement sizes tested provides information for development of recommendations regarding reinforcement size limitations and required lap lengths.

Current design codes governing the use of lap splices in reinforced masonry use working stress methods and are based largely upon results from research with reinforced concrete. Research on lap splices in masonry suggests that the behavior of splices in masonry may, in fact, be somewhat similar to that in concrete construction. However, masonry research to date has been limited to only a few bar and unit sizes, and the research has not convincingly verified this assumption. One of the main goals of the study was to expand upon current knowledge of lap splices in reinforced masonry so that an educated assessment of current design provisions can be established.

The model for designing lap length adopted for use in the proposed Masonry Limit-States Design Standard (MLSDS) (Masonry Standards Joint Committee 1992) is evaluated by comparing the model with CPAR experimental results. The MLSDS method considers reinforcing-bar diameter and yield strength, grout tensile strength, and masonry unit thickness when determining splice length. Experimental results are in good agreement with values provided by this analysis and have been used to further verify the applicability of the model. Recommendations for required lap lengths and maximum reinforcement ratios are provided, based upon experimental results obtained in this study.

Background

Overview of past research

A comprehensive review of literature pertaining to reinforcement bond and anchorage has been compiled by Scrivener (1986) as background material for the TCCMAR program. This effort indicated that research on lap splices in reinforced masonry has been limited; the majority of past investigations concentrated on reinforcement behavior in concrete. Reinforced masonry is sufficiently similar to reinforced concrete to allow some comparisons to be made, but the tensile behavior of masonry is quite different. Reinforced masonry is a composite material, consisting of an assemblage of clay or concrete units, mortar, grout, and reinforcement, and behavior is complicated by the interaction of these materials during loading. In addition, masonry possesses regular planes of weakness at the mortar joints which tend to promote the development of tension cracks at predetermined intervals. Several of the more significant efforts investigating reinforcement anchorage and lap splice behavior in reinforced masonry are described in the following text.

Scrivener (1986) compiled a comprehensive literature review of nearly 70 publications relating to bond, slip, and anchorage of reinforcement in hollow-unit masonry. The majority of this compilation is concerned with reinforced concrete simply due to the lack of available data relating to reinforced masonry. However, there have been several recent investigations in this field that have concentrated specifically on reinforced masonry. The findings of these recent inquiries are presented here, along with results of several of the more significant studies described by Scrivener.

Several noteworthy projects have investigated lap splices in reinforced concrete and provide useful background information on the general behavior of lap splices. A state-of-the-art report published by ACI in 1966 identifies research in the field of anchorage as early as 1938 (Ferguson et al. 1966). This report describes the nature of bond and splitting failure in addition to factors influencing the different failure modes. Forces on reinforcing bars are resisted by bond stress. This is described as the combined action of chemical adhesion at the surface of the steel, friction along the surface of the bar, and mechanical interaction between the bar deformations and the surrounding concrete. Lutz and Gergely (1967) found that chemical adhesion provides little resistance and is destroyed soon after slip begins, after which the bar is restrained primarily by bearing of the ribs against the concrete as shown in Figure 1. Bearing causes compressive and shear stresses to develop along the length of the bar, and tensile stresses perpendicular to the bar surface resulting from the radial component of the bearing stresses. Failure of the anchorage can occur by crushing of the concrete in front of the ribs, shear of the concrete along the ribs, or by longitudinal tensile splitting of the cross section.
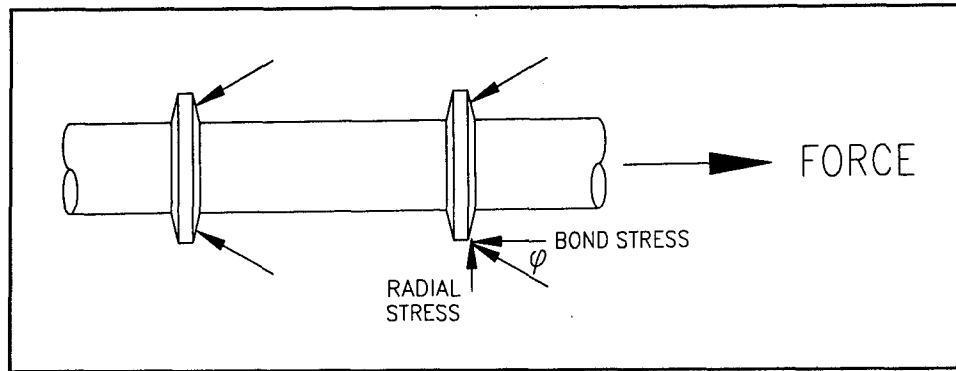
Figure 1.   Bond and radial stresses developed by bearing of
             reinforcement deformations against grout

Most design codes are based upon a limiting value for bond stress and consider the bond to be distributed evenly along the length of the bar. Several projects have investigated bond stress distributions during both monotonic and cyclic loadings (Soric and Tulin 1987, Perry and Jundi 1969, Wantanabe 1985). Local bond stresses are greatest at the location of primary cracks and over the first one-third of the anchorage length (Lutz and Gergely 1967). When the magnitude of bond stress exceeds the capacity of the concrete, bond slip occurs and stress is distributed over a greater length (Figure 2). At the ultimate load, bond stress distribution becomes more evenly distributed.
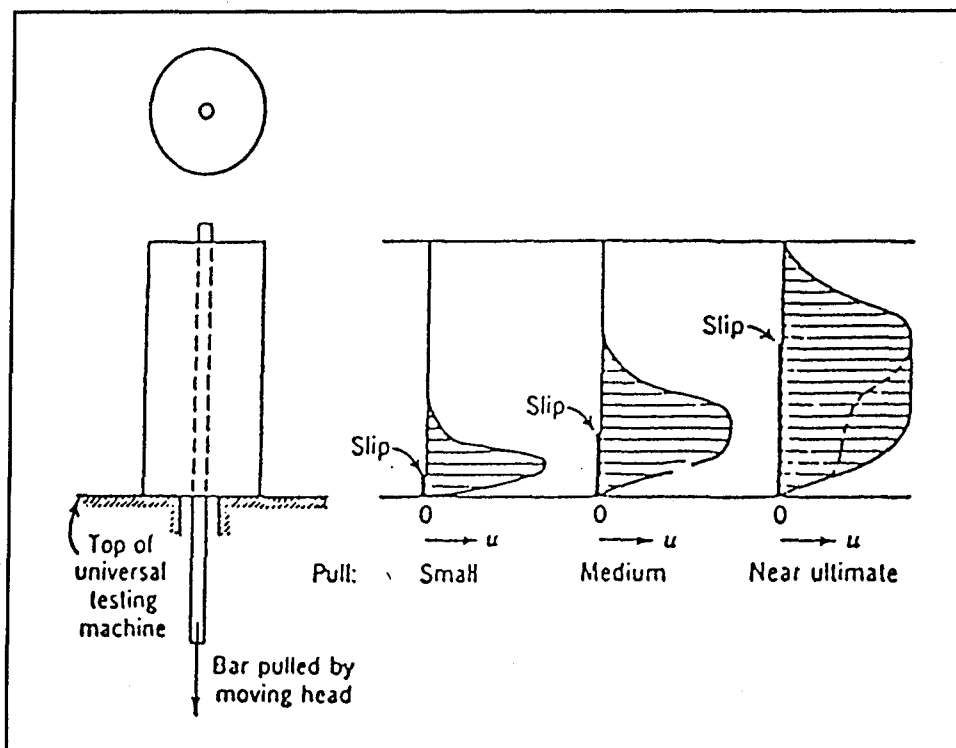
Figure 2.   Bond stresses become redistributed as cracking occurs (from
             Ferguson (1979); permission to print granted by Wiley and
             Sons, New York, NY)

6

Cheema and Klingner (1985) conducted a series of monotonic pull-out tests on individual bars grouted in single-wythe concrete masonry wall specimens. The test setup was chosen to minimize interference with the stress state around the test bar. These tests showed that while anchorage failure mechanisms in masonry are similar to what has been observed in concrete, there is an additional failure mode of separation and uplift at the mortar joints. It is expected that this is unique for single bar anchorages, since there has been no mention of this type of failure during the testing of lap splices. Cheema offers suggestions for minimum bar spacing to prevent uplift failure and developed an analytical model to predict the pullout strength of the bar. This model is based upon failure by tensile splitting of the masonry or pullout of the reinforcement.

Full-scale beam specimens were tested by Suter and Fenton (1985) in an investigation of the performance of lap splices in concrete masonry. Reinforcing bars were spliced at midheight of a vertical wall section, and out-of-plane loads were applied at the third points to create a region of constant moment and zero shear at the splice. The effect of grout type, misplaced bars, and multiple splices in a single core were considered. The splice strength was more accurately predicted by grout compressive strength rather than masonry prism compressive strength. All of Suter's tests showed considerably higher bond strengths than could be predicted by current working stress and limit-states design theories, with all splices failing by yield of the reinforcement. No pull-out or splitting failures were observed, even though the splice lengths tested were 25 percent to 50 percent less than what is required by design codes. This suggests that current code provisions for lap splice length may be over-conservative.

A comprehensive study of bond and slip in reinforced masonry has been conducted by Soric and Tulin (1987) under the auspices of TCCMAR as part of the U.S.-Japan Coordinated Program for Masonry Building Research. Tests included specimens with single bar anchorages and lap splices. Three analytical models were developed to describe bond stress distributions, considering linearly elastic and cracking phases. A model based upon analysis by Cheema and Klingner (1985) was also developed to determine the appropriate lap length for spliced reinforcement in masonry structures (Soric and Tulin 1988). This model provides the basis for the draft Masonry Limit-States Design Standard described later.

Kubota and Kamogawa (1985) and Watanabe (1985) investigated anchorage and splice strength with a series of monotonic tests on grouted masonry. Kubota's investigation considered only a single bar size and a relatively long lap length but was successful in verifying the effectiveness of lap splices in masonry. In all cases, the bars exceeded their yield capacity under the applied tensile loads. Watanabe tested single bar anchorages and demonstrated that, for 19-mm (No. 6) bars in 190-mm (7.44-in.) concrete and clay unit specimens, a lap length of only 14 bar diameters is capable of developing the full yield stress of the bar.

A direct comparison between anchorage behavior in reinforced concrete and reinforced masonry was conducted by Matsumura (1990), during an experimental program which was concerned specifically with the tensile behavior of lap splices in masonry. To determine the effect of masonry versus concrete on the reinforcing bar behavior, several monolithic concrete specimens with identical dimensions and similar properties as the masonry specimens were tested. The tests showed there to be little difference in either strength or ductility for lap splices in the different materials. The main difference was in the cracking pattern: cracks occurred in nearly every mortar joint in the masonry specimens, whereas cracks in the concrete specimens were more limited. Bond stress was not investigated in this study, but it is expected that the stress distribution in the masonry specimens would be affected by the increased number of cracks perpendicular to the bar.

Failure modes of lap splices

Past research (Cheema 1981) has identified four possible failure modes for reinforcing bars in tension anchorages or lap splices in reinforced masonry:

a. Yielding of reinforcement.

b. Pullout of reinforcing bars.

c. Splitting of grout and masonry unit.

d. Uplift of a masonry course due to creation of a new primary crack.

Yielding of the reinforcement provides the optimal combination of strength and ductility and would be the preferred limit state for design purposes.

Under the application of tensile loads, small cracks occur around the reinforcing bar (Figure 3) due to a difference in modulus between the grout and the steel. As tensile stress is transferred from the bars to the surrounding masonry, primary cracks form perpendicular to the bars when stress in the grout exceeds its tensile capacity. Weak planes at the mortar joints are the preferred locations for the occurrence of primary cracks. In the vicinity of these cracks, the steel must carry the entire tensile load and, if there is sufficient anchorage capacity available in the uncracked regions, the reinforcing bar will yield. For the case of a single-bar anchorage, the masonry above the location of a primary crack does not contribute to the anchorage strength and, thus, is ineffective in carrying any of the tensile load (Figure 4a). Cracks occurring at a lap-splice location (Figure 4b) do not affect the transfer of stress as drastically. The masonry is still effective at transferring load from one bar to the other outside of the cracked region.
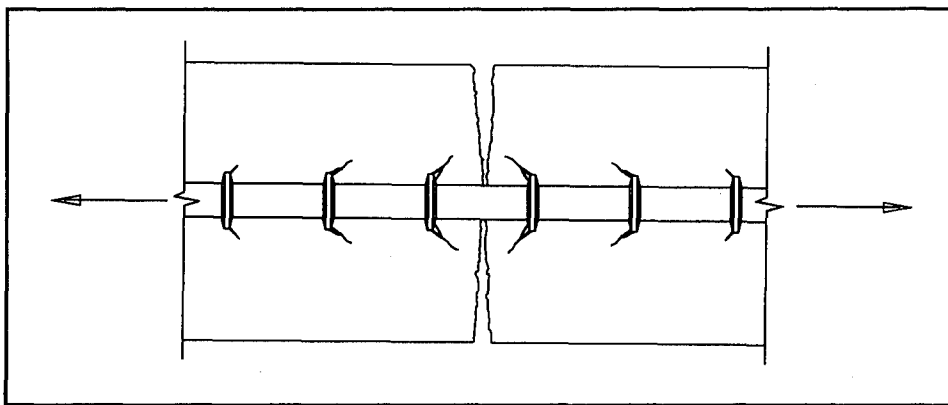
Figure 3.   Primary tensile cracks occur where masonry tensile strength is exceeded. Secondary cracks occur where bond stress is large
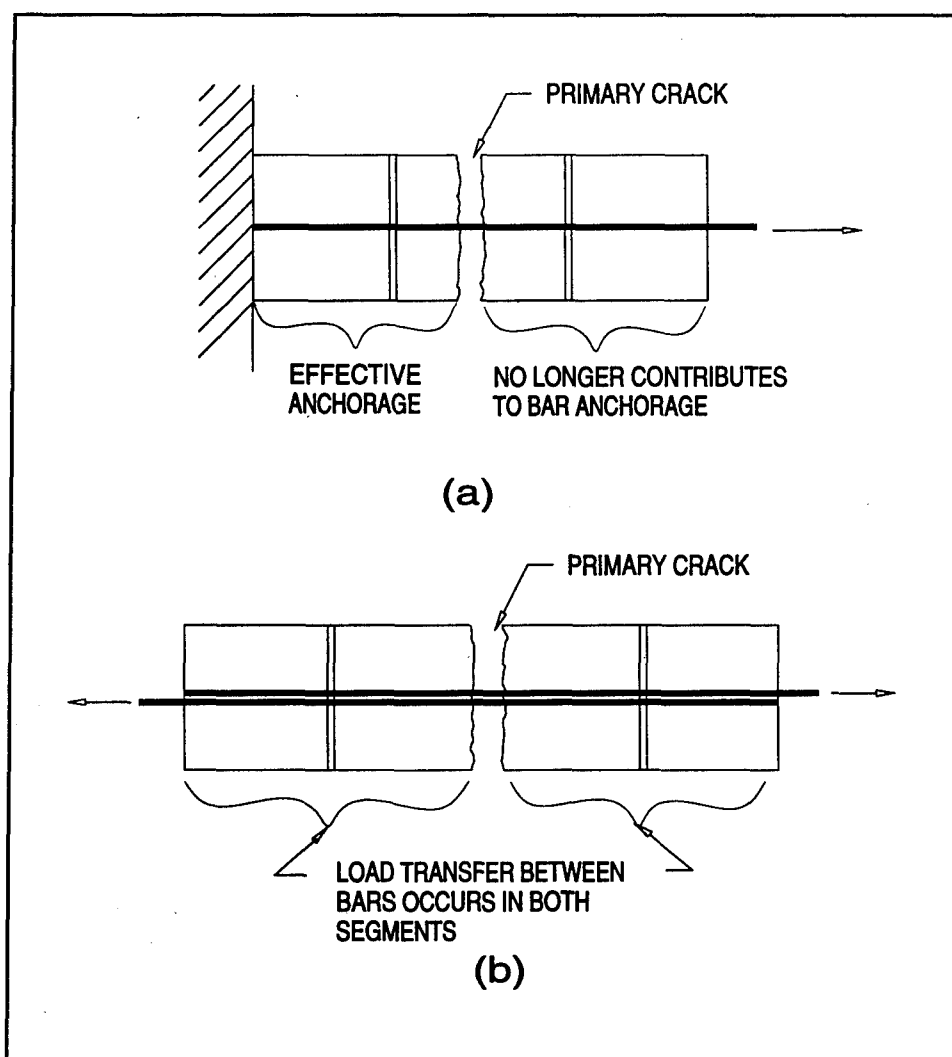
Figure 4.   Effect of primary crack on stress transfer in (a) single-bar anchorage; (b) lap splice

Pull-out failure is most often observed for single-bar anchorages. Pull-out of the reinforcement is resisted by bond stress, which consists mainly of mechanical interactions between ribs on the reinforcing bars and the grout. Grout failures (Figure 5) are initiated by crushing in front of the ribs or shear along a cylindrical surface between adjacent ribs, depending upon the dimensions and spacing of the deformations and the properties of the grout.
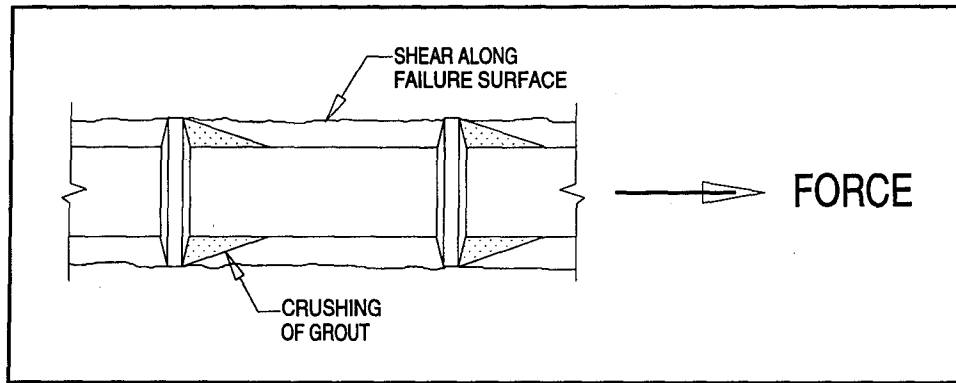
Figure 5.   Grout failure by compressive crushing or shear

Reinforcing bar pullout has not been identified as an ultimate failure mode by any of the researchers investigating lap splices and rarely occurs in these situations due to bar-to-bar deformation compatibility constraints along the length of the splice. Small slip displacements will, however, increase tensile splitting forces already present, precipitating failure by longitudinal splitting of the masonry along the splice. As shown previously in Figure 1, mechanical interaction between reinforcement deformations and grout results in a compressive grout stress inclined at an angle ϕ from the longitudinal axis of the bar. The radial component of this force causes circumferential tensile stresses in the masonry, and because the radial forces act equally in all directions, the masonry ring resisting splitting forces can be approximated (Figure 6a) for a single-bar anchorage. Additional tensile stresses may also be caused by eccentricity of tensile forces on the bars and the grout and by relative movement between two spliced reinforcing bars. Relative movement resulting from slip displacements increase the splitting forces on the surrounding masonry when one bar rides up on the other (Figure 7).

The resisting ring of tensile forces is distorted slightly for the case of lapped bars; and if additional stress due to transverse movement of the two closely spaced bars is included, the resisting ring can take on the elliptical shape (Figure 6b). Splitting cracks occur when the circumferential tensile stresses exceed the tensile strength of the grout. Splitting cracks are often initiated at stress concentrations, such as the tip of the bar being spliced, and will propagate along the critical plane (Figure 6b).

10
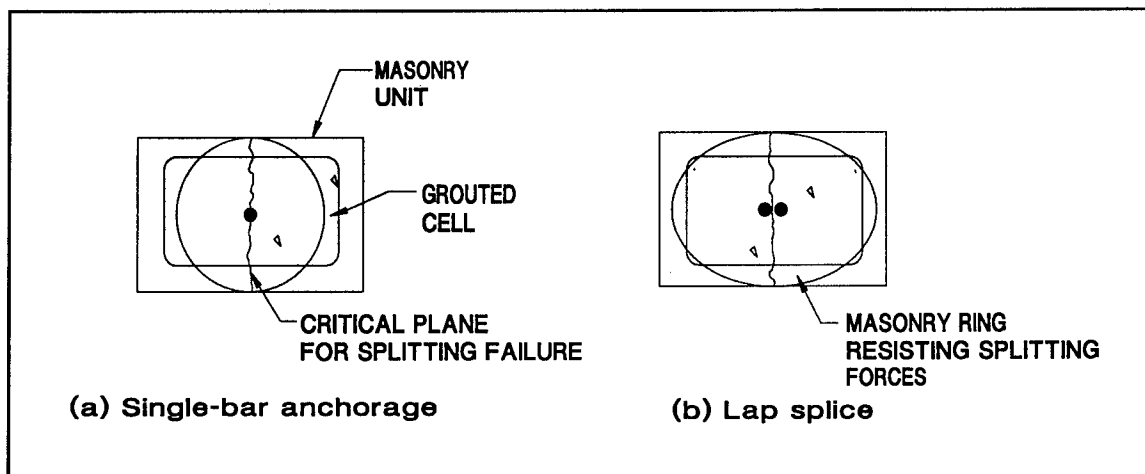
Figure 6. Masonry ring resisting splitting forces
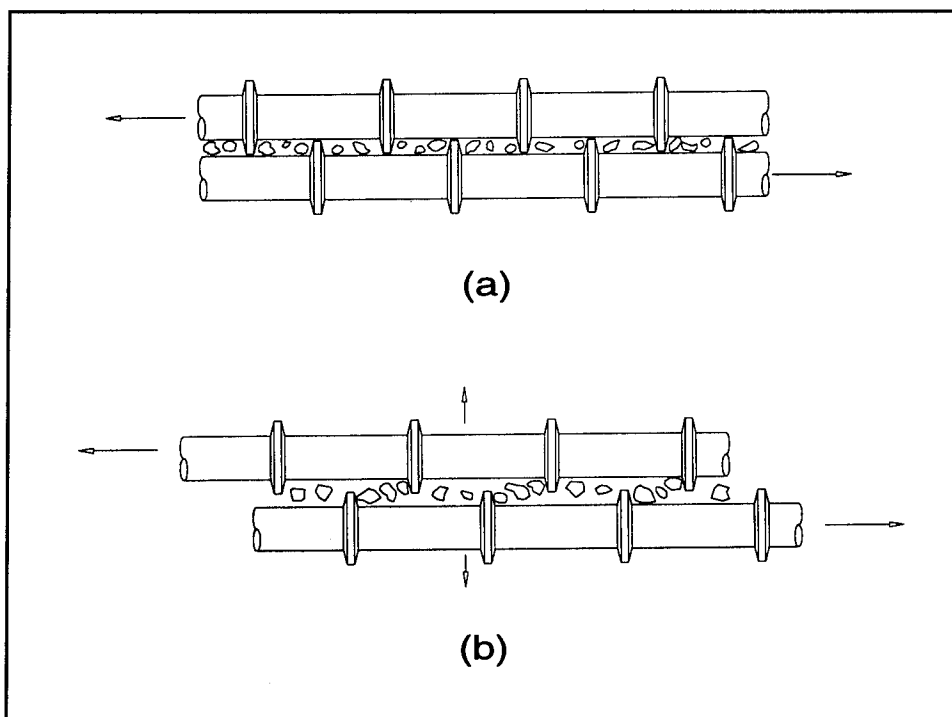
Figure 7. Movement of one bar, relative to the next (a) results in the development of additional lateral splitting forces as bars ride up on one another (b)

Splitting failure is most often observed for larger bars in masonry units with limited thickness (Soric and Tulin 1987) or in splices with inadequate lap length (Thompson et al. 1979), whereas rebar yield was the main failure mode for specimens tested by Suter and Fenton (1985). Cheema and Klingner (1985) divide anchorage length into three different classifications, based upon the failure mode:

a. Short, where the bars cannot yield, in which pullout initiates the formation of longitudinal splitting cracks.

b. Intermediate, where bars yield, but ultimately fail by longitudinal splitting of the masonry.

c. Long, with failure by yield of the reinforcement, where few splitting cracks form.

Observed failure of lap splices during CPAR testing agrees well with this classification.

Current design code requirements

The rationale behind existing design code requirements for lap splices in reinforced masonry is not explicitly stated, but it appears that most requirements are derived from early working stress criteria for reinforced concrete. Currently, the design of reinforced masonry in the United States is governed by two working stress design codes: the Uniform Building Code (UBC) (International Conference of Building Officials 1988), and ACI 530-92/ASCE 5-92/TMS 402/92 *Building Code Requirements for Masonry Structures* (American Concrete Institute 1988a). Criteria contained in these standards for anchorage of reinforcement determine development lengths necessary to develop working stress levels in the reinforcing bars based upon a limiting value for bond stress and consider the bond to be distributed evenly along the length of the bar. Lap splices must be designed for a lower bond stress than single-bar anchorages, because large stress concentrations at the cutoff end of the bar and the close proximity of the bars both act to promote splitting failure. Most of the design codes recognize these effects by requiring lap lengths which are greater than single-bar anchorage values. Lap splices are also required to develop a minimum tensile strength equivalent to 125 percent of the yield strength of the reinforcing bars being spliced to provide adequate splice ductility.

Section 2409 of the UBC lists criteria for lap splices in reinforced masonry. A commentary to the UBC (The Masonry Society Codes and Standards Committee 1990) states that the development-length formula is based upon a maximum nominal bond stress of 125 psi (0.86 MPa) and a grout compressive strength of 2,000 psi (13.8 MPa), which is the minimum allowed for reinforced masonry. Lap-splice length for reinforcing bars in tension is calculated as the maximum of

$$l_d = 40 d_b \tag{1}$$

or

$$l_d = 0.002 d_b f_s \tag{2}$$

where

l_d = splice development length (in.)

d_b = diameter of the reinforcing bar (in.)

f_s = steel stress (psi) calculated at the splice

For the case of Grade 60 (413 MPa) rebar, fully stressed to its allowable limit of 24,000 psi (165 MPa), the lap splice length specified by Equation 2 becomes

$$l_d = 48 \, d_b \tag{3}$$

However, recognizing that failure of lap splices is often brittle, the UBC imposes a stiff penalty upon splices which are located in critical areas. A 50-percent increase in the lap length is required for splices of bars which are stressed to more than 80 percent of the specified allowable stress, increasing the lap length to 72 bar diameters. Results from research into lap splices in masonry indicate that this criteria may be overly conservative (Soric and Tulin 1987, Suter and Fenton 1985, Matsumura 1990); however, current test data are not convincing enough to relax these requirements.

Requirements listed by the ACI/ASCE/TMS masonry code are similar to the UBC provisions. Lap length is determined by Equation 2 with the additional stipulation that the lap length be greater than 12 in. Thus, for Grade 60 (413 MPa), reinforcement stressed to its allowable limit of 24,000 psi (165 MPa), the required lap length is again determined using Equation 3.

It is useful to discuss requirements for lap splices in reinforced concrete because these criteria appear to offer an improvement over the simple linear relationships described previously. ACI 318-89 (ACI Committee 1989) contains a formula for lap splice length determination that considers the effect of concrete tensile strength, represented as the square root of the compressive strength f'c, in addition to the area of the reinforcing bar A_b

$$l_d = 0.04 \, \frac{A_b f_y}{\phi \sqrt{f'_c}} \tag{4}$$

If the reinforcement nominal yield stress is equal to 60,000 psi (413 MPa) and the concrete compressive strength is equal to 2,000 psi (13.8 MPa) (for comparison with UBC and the ACI/ASCE/TMS masonry code), this formula reduces to

$$l_d = 42.1 \, d_b^2 \tag{5}$$

Note that for this case the splice length is proportional to the square of the bar diameter, resulting in much greater splice lengths for large diameter bars. This may account for the tendency of larger diameter bars to fail at lower nominal bond stresses by splitting rather than pullout or yield. An additional stipulation is that the splice length be greater than $0.0004d_b f_y$ or for Grade 60 reinforcement, greater than $24\ d_b$.

Immediately obvious from Figure 8 is that the ACI 318/89 (ACI Committee 1989) requirements are less conservative for smaller bar diameters, supporting research findings which have determined smaller bars can tolerate greater bond stresses before failure (Soric and Tulin 1987, Cheema 1981).

The MLSDS for the design of reinforced masonry structures is currently being compiled by a committee consisting of members of The Masonry Society, ACI, and ASCE (Masonry Standards Joint Committee 1992) and is based upon expected values, rather than minimum or specified values. This standard appears to provide a more rational determination of lap-splice length where lap length is based upon a formula that, in
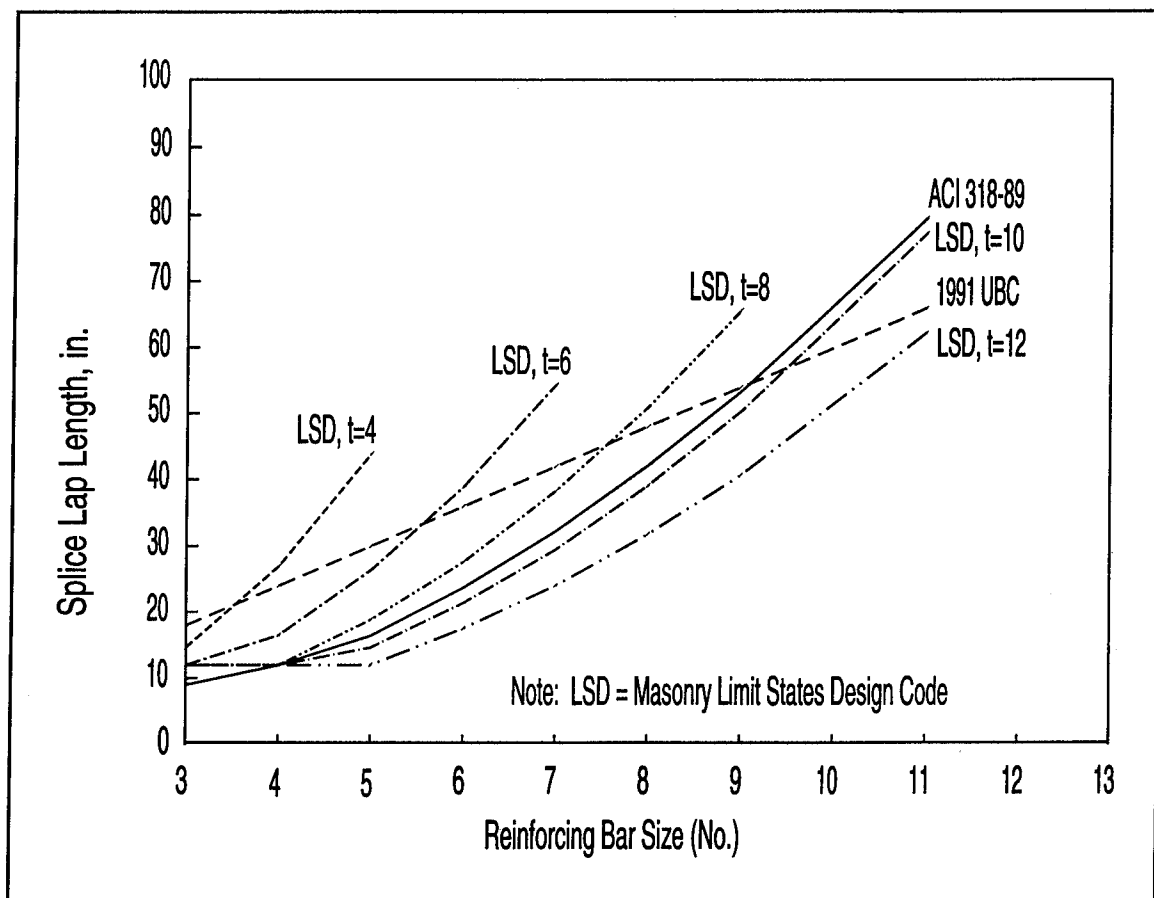
Figure 8. Comparison of lap-splice lengths`required by different design codes as a function of bar size. Shown are curves for Grade 60 reinforcement and grout compressive strength of 2,000 psi

its original form, considers reinforcing bar diameter, the expected yield strength of the reinforcement, expected grout tensile strength, and masonry thickness at the splice location. The expected values used in the MLSDS are mean values of material properties determined by physical testing.

The relationship for splice length used by the MLSDS was originally developed by Soric and Tulin (1987) for the case of lap splices in grouted hollow-unit concrete masonry and uses a model that regards the radial stress due to bond action on the grout as an outward acting hydraulic pressure. The surrounding masonry resists this pressure by acting as a thick-walled pressure vessel, and failure occurs when the circumferential tensile stress exceeds the tensile strength of the masonry. In its original form, the required lap length is as follows:

$$l_d = \frac{C\, d_b^2 f_y}{(t - d_b)\, f_{gt}}$$

(6)

where:

t = masonry thickness

f_{gt} = grout tensile strength

d_b = reinforcing bar diameter

f_y = steel yield strength

C = empirical constant

The coefficient C is used to account for nonuniformity of bond stresses along the length of the bar. Note that this formula is nondimensional and may be used with SI or U. S. customary units. Soric conducted experimental tests with No. 4 and No. 7 bars in 6-in. hollow concrete units and calculated a mean value of 1.75 for the coefficient C (Soric and Tulin 1987). This determination is based upon the criteria that the lap splice develops a strength which is greater than 125 percent of the reinforcement yield strength. The MLSDS adopted this value for C and assumed a grout tensile strength of 400 psi (2.75 MPa)

$$\phi\, l_d = \frac{0.0045\, d_b^2 f_{ye}}{(t - d_b)}$$

(7)

where:

ϕ = 0.8 (capacity reduction factor)

f_{ye} = expected yield strength of the steel

The splice length must also be 12 in. or greater. Splice length curves for different masonry unit thicknesses using this formula are plotted in Figure 8 along with lap lengths required by other design standards. The MLSDS requirements are significantly different than the UBC and the ACI/ASCE/TMS masonry code requirements and generally require shorter lap lengths for small bars in large units. In addition, the long lap lengths required for large bars in small units may act to prevent brittle splitting failure which is prevalent in this type of splice. Both the UBC and ACI/ASCE masonry codes are somewhat less conservative for lap splices than the MLSDS requirements in this case.

The formula adopted in the draft MLSDS (Equation 7) provides a rational approach to the determination of lap-splice length and considers the important parameters of grout tensile strength, reinforcement yield strength, and the thickness of the grouted masonry. This approach provides for economical splices of small bars and poses a severe penalty for large bars in small units, which exhibit a tendency toward splitting failure. However, this model relies on an accurate determination for the coefficient C, which must be verified for additional combinations of bar diameter, unit size, and grout strength. Results from the CPAR study are used in the Results section of this chapter to investigate the value of this coefficient and the overall validity of the model.

It is interesting to note that with the exception of the limit-states code, all requirements are based upon a limiting value for bond stress, suggesting that pull-out failure will govern splice strength. However, as previously discussed, this is not consistent with the findings of other researchers who have found that splitting failure is normally the controlling mode for the case of lap splices in masonry. Only the limit-states standard explicitly considers the tendency of splices of large bars in thin walls to undergo a splitting failure mode. All of the design codes do limit the maximum reinforcement percentage in a single grouted cell to 4 percent (draft limit-states standard) or 6 percent (UBC) of the cell area, which may be aimed at limiting the use of large bars in thin units.

Test Program

Test specimens

Variables investigated during the CPAR program included the effects of reinforcing bar diameter, masonry unit width, masonry unit type, and splice length on lap splice behavior. A total of 124 specimens were tested for 62 different combinations of these parameters, with two replications of each type of specimen. Figure 9 shows the range of lap lengths and specimen sizes tested for both concrete and clay masonry specimens. A listing of all specimens tested is provided in Table 1. Note that splice development lengths were based upon modular 4-in. increments.

16

All test specimens were fabricated in the laboratory at WES using materials selected to be similar, to the greatest extent possible, with the materials used by other TCCMAR researchers. A complete compilation of test results from index and material properties tests conducted on all materials used for this research program is contained in Appendix A. A general quality assurance plan for the test specimens is summarized in Table 2.

Specimens were constructed in stack bond using half units to provide a single vertical cell. To reduce the variability introduced by inconsistent workmanship, all specimens were constructed with the aid of a prism building jig designed by Atkinson-Noland (Figure 10). The jig consists of four vertical, slotted angles bolted to an aluminum base plate, with two moveable, horizontal bars attached to the uprights. The vertical members can be adjusted laterally and longitudinally to accommodate units of
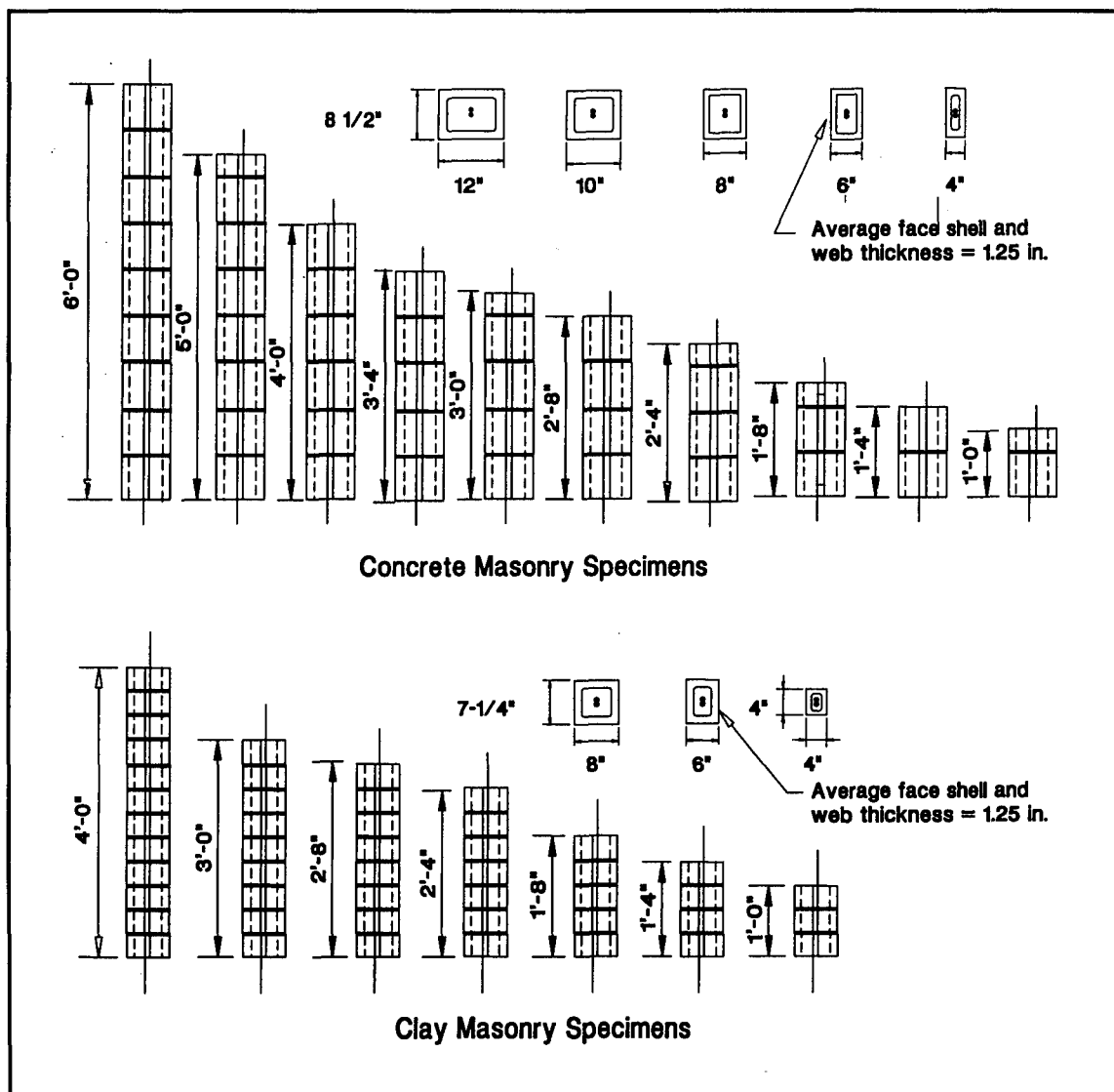
Figure 9. Schematic of lap splice test specimens

various sizes. The horizontal bars are raised in predetermined increments to allow the uniform placement of mortar and units during prism construction.

After the hollow prisms were constructed, they were placed on a bench fabricated from a double thickness of 2- by 12-in. lumber and concrete masonry blocks. These benches provided a stable platform for placement of the grout and elevated the bottom the prisms sufficiently that the lapped bars could be placed in the hollow prisms prior to grouting. Holes were drilled in the lumber near the center of each prism so that the protruding reinforcing bars could be positioned in the prism.

Typically, within a few days after the units were laid, the lapped steel reinforcing bars were placed in the hollow prisms. The bars were cut to a length approximately 17 in. longer than the required lap length to provide adequate length of bar for attaching instrumentation and for adequate protrusion of the bars beyond the grouted prism for gripping during the test.

All test specimens were fully grouted (Figure 11) after the reinforcing bars were placed in the prisms. The grout was batched in the laboratory. Grout was placed by hand into the hollow masonry and immediately vibrated using a small hand-held concrete vibrator. After approximately 5 min, the grout was reconsolidated using the same vibrator.

Table 1
Concrete and Clay Masonry Test Specimens

Reinf. Size (No.)	4-in. Unit	6-in. Unit	8-in. Unit	10-in. Unit	12-in. Unit
4	24 = 12 in. 32 = 16 in. 40 = 20 in. CL - 24 = 12 in. CL - 32 = 16 in. CL - 40 = 20 in.	24 = 12 in. 32 = 16 in. 40 = 20 in. CL - 24 = 12 in. CL - 32 = 16 in. CL - 40 = 20 in.	24 = 12 in. 32 = 16 in. 40 = 20 in. CL - 24 = 12 in. CL - 32 = 16 in. CL - 40 = 20 in.		
6	37 = 28 in. 48 = 36 in. CL - 37 = 28 CL - 48 = 36	27 = 20 in. 37 = 28 in. 48 = 36 in. CL - 27 = 20 CL - 37 = 28 CL - 48 = 36	27 = 20 in. 37 = 28 in. 48 = 36 in. CL - 27 = 20 CL - 37 = 28 CL - 48 = 36	27 = 20 in. 37 = 28 in. 48 = 36 in.	27 = 20 in. 37 = 28 in. 48 = 36 in.
8		CL - 32 = 32 in. CL - 48 = 48 in.	32 = 32 in. 40 = 40 in. 48 = 48 in. 60 = 60 in. CL - 32 = 32 in. CL - 40 = 40 in. CL - 48 = 48 in.	32 = 32 in. 40 = 40 in. 48 = 48 in.	32 = 32 in. 40 = 40 in. 48 = 48 in.
11			52 = 72 in.	35 = 48 in. 44 = 60 in. 52 = 72 in.	35 = 48 in. 44 = 60 in. 52 = 72 in.

Note: Lap lengths tested are shown as l/d_b = in., where d_b is the reinforcing bar diameter. Clay masonry specimens designated as "CL." The full-size bar tests are representative of actual bar behavior and are used in all subsequent calculations relating to bar yield strength.

Materials

Tables 3 and 4 contain a matrix of test specimens, dates of fabrication and testing, grout and mortar batches, and strength of constituent materials for the concrete and clay masonry specimens, respectively. Additional information on the properties of the various materials can be found in Appendix A. A general description of the materials used in this study follows.

Units. Test specimens were fabricated using hollow concrete units or hollow clay brick units with 3/8-in.-thick fully bedded mortar joints and type S mortar. Hollow concrete masonry units with nominal widths of 4,

Table 2
Laboratory Quality Control Plan

Component/ Process	ASTM Standard[1]	Other Standards	Comments/Sample Size
Mortar			
Proportions	C 270	UBC 24-20[2] UBC 24-21[2]	Type S, 1:½:4½ (cement:lime:sand, by volume) Volumetric proportions converted to weight proportions based on unit weights of local materials.
Mixing Sampling	C 305 C 780	Atkinson-Noland (1988)	Use ASTM C 305 for small batch mixing for cubes. Use ASTM C 780-90 (1990s) for sampling mortar during specimen construction.
Cube Test	C 109 C 780	Atkinson-Noland (1988)	Test three 2- × 2- × 2-in. cubes per sample.
Cylinder Test	C 780	UBC 24-22[2]	Test three 2- × 4-in. cylinders per sample
Grout			
Proportions	C 476 C 404	UBC 24-23[2]	1:3:2 (cement:sand:gravel) Included Sika Grout Aid per manufacturer's instructions.
Mixing			Batched in laboratory. Ensure that batching is done by weight. Add final water and Grout Aid immediately prior to pouring. Slump should be at least 8 in.
Standard Test	C 1019	UBC 24-28[2]	Test three 3- × 3- × 6-in. specimens per sample.
Core Test			Remove and test three 2- × 4-in. cylinders from grout placed in normal unit hollow cells (without bond-break). Consolidate as for walls. Cure these in laboratory air. Cut ends to 4-in. length and cap with gypsum or grind smooth, flat, and parallel.
Masonry Units			
Compressive Strength	C 140		Test 5 each type
Initial Rate of Absorption	C 67		Test 5 each type
Reinforcing			
Steel	ASTM A 370-88a (1990a)		Coupons and bars are to be labelled such that coupon properties can be related to the bars in the test structure.

[1] ASTM Standards are listed in references following main text.
[2] International Conference of Building Officials. (1992). *Uniform building code.* Whittier, CA.

Figure 10. Constructing masonry prisms in jig

Figure 11. Grouting prisms

Table 3
Test Matrix, Concrete Masonry Lap Splice Tests

Specimen Name	Nominal Specimen Height, in.	Program Phase	Date Constructed	Mortar Batch*	Date Grouted	Grout Batch*	Date Tested	Unit	Mortar Cube	Mortar Cylinder	Grout	Tensile Mortar	Tensile Grout	Reinforcing Bar
4-in. Concrete Masonry Units														
4CON-4-24-1	12	II	9/15/92	M259-1	9/24/92	G268-1	11/17/92	1,900	4,390	3,770	4,400			72,300
4CON-4-24-2	12	II	9/15/92	M259-1	9/24/92	G268-1	11/17/92	1,900	4,390	3,770	4,400			72,300
4CON-4-32-1	16	II	9/15/92	M259-1	9/24/92	G268-1	11/16/92	1,900	4,390	3,770	4,400			72,300
4CON-4-32-2	16	II	9/15/92	M259-1	9/24/92	G268-1	11/16/92	1,900	4,390	3,770	4,400			72,300
4CON-4-40-1	20	II	9/15/92	M259-1	9/24/92	G268-1	11/17/92	1,900	4,390	3,770	4,400			72,300
4CON-4-40-2	20	II	9/15/92	M259-1	9/24/92	G268-1	11/17/92	1,900	4,390	3,770	4,400			72,300
4CON-6-37-1	28	I	4/29/91	M119-1	6/13/91	G164-1	8/13/91	1,900	2,420	2,240	3,340			66,400
4CON-6-37-2	28	I	4/29/91	M119-1	6/13/91	G164-1	8/15/91	1,900	2,420	2,240	3,340			66,400
4CON-6-48-1	36	I	5/2/91	M122-2	6/13/91	G164-1	8/29/91	1,900	1,900		3,340			66,400
4CON-6-48-2	36	I	5/2/91	M122-2	6/13/91	G164-1	8/29/91	1,900	1,900		3,340			66,400
6-in. Concrete Masonry Unit														
6CON-4-24-1	12	II	9/15/92	M259-1	9/24/92	G268-1	11/18/92	3,090	1,900	4,390	3,770			72,300
6CON-4-24-2	12	II	9/15/92	M259-1	9/24/92	G268-1	11/18/92	3,090	1,900	4,390	3,770			72,300
6CON-4-32-1	16	II	9/15/92	M259-1	9/24/92	G268-1	11/18/92	3,090	1,900	4,390	3,770			72,300
6CON-4-32-2	16	II	9/15/92	M259-1	9/24/92	G268-1	11/18/92	3,090	1,900	4,390	3,770			72,300
6CON-4-40-1	20	II	9/15/92	M259-1	9/24/92	G268-1	11/19/92	3,090	1,900	4,390	3,770			72,300
6CON-4-40-2	20	II	9/15/92	M259-1	9/24/92	G268-1	11/20/92	3,090	1,900	4,390	3,770			72,300

*Additional information on material properties can be found in Appendix A.

(Sheet 1 of 5)

Table 3 (Continued)

Specimen Name	Nominal Specimen Height, in.	Program Phase	Date Constructed	Mortar Batch*	Date Grouted	Grout Batch*	Date Tested	Compressive Strength, psi*				Tensile Strength, psi*		
								Unit	Mortar		Grout	Mortar	Grout	Reinforcing Bar
									Cube	Cylinder				
6CON-6-27-1	20	I	4/25/91	M115-1	5/9/91	G129-2	7/25/91	3,090	2,060	1,980	2,130		430	66,400
6CON-6-27-2	20	I	4/25/91	M115-1	5/9/91	G129-2	7/25/91	3,090	2,060	1,980	2,130		430	66,400
6CON-6-37-1	28	I	4/25/91	M115-1	5/9/91	G129-2	8/23/91	3,090	2,060	1,980	2,130		430	66,400
6CON-6-37-2	28	I	4/25/91	M115-1	5/9/91	G129-2	8/23/91	3,090	2,060	1,980	2,130		430	66,400
6CON-6-48-1	36	I	5/2/91	M122-1	7/26/91	G207-1	9/11/91	3,090	3,240	2,705	2,700			66,400
6CON-6-48-2	36	I	5/2/91	M122-1	7/26/91	G207-1	9/11/91	3,090	3,240	2,705	2,700			66,400
8-In. Concrete Masonry Unit														
8CON-4-24-1	12	I	4/24/91	M114-2	5/9/91	G129-2	7/11/91	3,690	2,490	2,150	2,130		430	72,300
8CON-4-24-2	12	I	4/24/91	M114-2	5/9/91	G129-2	7/10/91	3,800	2,490	2,150	2,130		430	72,300
8CON-4-24-3	12	I	8/1/91	M213-1	8/5/91	G217-1	1/28/92	3,800	2,430	1,860	3,460	250		72,300
8CON-4-32-1	16	I	4/24/91	M114-2	5/9/91	G129-2	7/15/91	3,800	2,490	2,150	2,130		430	72,300
8CON-4-32-2	16	I	4/24/91	M114-2	5/9/91	G129-2	7/16/91	3,800	2,490	2,150	2,130		430	72,300
8CON-4-40-1	20	I	4/24/91	M114-2	5/9/91	G129-2	7/18/91	3,800	2,490	2,150	2,130		430	72,300
8CON-4-40-2	20	I	4/24/91	M114-2	5/9/91	G129-2	7/18/91	3,800	2,490	2,150	2,130		430	72,300
8CON-6-27-1	20	I	4/24/91	M114-2	5/9/91	G129-2	7/22/91	3,800	2,490	2,150	2,130		430	66,400
8CON-6-27-2	20	I	4/24/91	M114-2	5/9/91	G129-2	7/23/91	3,800	2,490	2,150	2,130		430	66,400
8CON-6-37-1	28	I	4/25/91	M115-1	6/13/91	G164-1	8/12/91	3,800	2,060	1,980	3,340			66,400
8CON-6-37-2	28	I	4/25/91	M115-1	6/13/91	G164-1	8/12/91	3,800	2,060	1,980	3,340			66,400
8CON-6-48-1	36	I	5/2/91	M122-1	6/13/91	G164-1	8/29/91	3,800	3,240	2,850	3,340			66,400
8CON-6-48-2	36	I	5/2/91	M122-1	6/13/91	G164-1	8/29/91	3,800	3,240	2,850	3,340			66,400

(Sheet 2 of 5)

Table 3 (Continued)

Specimen Name	Nominal Specimen Height, in.	Program Phase	Date Constructed	Mortar Batch*	Date Grouted	Grout Batch*	Date Tested	Compressive Strength, psi* — Unit	Compressive Strength — Mortar Cube	Compressive Strength — Mortar Cylinder	Compressive Strength — Grout	Tensile Strength, psi* — Mortar	Tensile Strength — Grout	Tensile Strength — Reinforcing Bar
8CON-8-32-1	32	I	5/2/91	M122-1	6/13/91	G164-1	8/29/91	3,800	3,240	2,850	3,340			68,700
8CON-8-32-2	32	I	5/2/91	M122-1	6/13/91	G164-1	8/26/91	3,800	3,240	2,850	3,340			68,700
8CON-8-40-1	40	I	5/3/91	M123-1	7/26/91	G207-1	10/24/91	3,800	1,910	1,655	3,000			68,700
8CON-8-40-2	40	I	5/3/91	M123-1	7/26/91	G207-1	10/24/91	3,800	1,910	1,655	3,000			68,700
8CON-8-40-3	40	I	8/1/91	M213-1	8/5/91	G217-1	10/25/91	3,800	2,430	1,860	3,460	250		68,700
8CON-8-48-1	48	I	7/31/91	M212-1	8/5/91	G217-1	1/16/92	3,800	2,750	1,950	3,460			68,700
8CON-8-48-2	48	I	7/31/91	M212-1	8/5/91	G217-1	1/16/92	3,800	2,750	1,950	3,460			68,700
8CON-8-60-1	60	I-A	8/2/91	M214-1	10/22/91	G295-1	1/23/92	3,800						68,700
8CON-8-60-2	60	I-A	8/2/91	M214-1	10/22/91	G295-1	1/22/92	3,800						68,700
8CON-11-35-1	48	I	8/2/91	M214-1	10/22/91	G295-1		3,800						68,000
8CON-11-35-2	48	I	8/2/91	M214-1	10/22/91	G295-1		3,800						68,000
8CON-11-52-1	72	I	8/2/91	M214-1	8/5/91	G217-1	1/27/92	3,800			3,460			68,000
8CON-11-52-2	72	I	8/2/91	M214-1	8/5/91	G217-1	1/24/92	3,800			3,460			68,000
10-in. Concrete Masonry Unit														
10CON-6-27-1	20	I	4/24/91	M114-2	5/9/91	G129-2	7/22/91	3,850	2,490	2,150	2,130		430	66,400
10CON-6-27-2	20	I	4/24/91	M114-2	5/9/91	G129-2	7/19/91	3,850	2,490	2,150	2,130		430	66,400
10CON-6-37-1	28	I	4/25/91	M115-1	6/13/91	G164-1	8/13/91	3,850	2,060	1,980	3,340			66,400
10CON-6-37-2	28	I	4/25/91	M115-1	6/13/91	G164-1	8/13/91	3,850	2,060	1,980	3,340			66,400
10CON-6-48-1	36	I	5/2/91	M122-1	6/13/91	G164-1	8/28/91	3,850	3,240	2,705	3,340			66,400
10CON-6-48-2	36	I	5/2/91	M122-1	6/13/91	G164-1	8/28/91	3,850	3,240	2,705	3,340			66,400

(Sheet 3 of 5)

Table 3 (Continued)

Specimen Name	Nominal Specimen Height, in.	Program Phase	Date Constructed	Mortar Batch*	Date Grouted	Grout Batch*	Date Tested	Unit	Cube	Cylinder	Grout	Mortar (Tensile)	Grout (Tensile)	Reinforcing Bar
10CON-8-32-1	32	II	9/16/92	M260-2	10/20/92	G294-1	11/23/92	3,850	3,580	2,370	3,220			68,700
10CON-8-32-2	32	II	9/16/92	M260-2	10/20/92	G294-1	11/23/92	3,850	3,580	2,370	3,220			68,700
10CON-8-40-1	40	II	9/16/92	M260-1	10/20/92	G294-2	11/30/92	3,850	4,580	3,030	1,900			68,700
10CON-8-40-2	40	II	9/16/92	M260-1	10/20/92	G294-2	12/1/92	3,850	4,580	3,030	1,900			68,700
10CON-8-48-1	48	II	9/16/92	M260-1	10/20/92	G294-2	12/7/92	3,850	4,580	3,030	1,900			68,700
10CON-8-48-2	48	II	9/16/92	M260-1	10/20/92	G294-2	12/7/92	3,850	4,580	3,030	1,900			68,700
10CON-11-35-1	48	II	9/16/92	M260-1	9/24/92	G268-1	12/9/92	3,850	4,580	3,030	4,400			68,000
10CON-11-35-2	48	II	9/16/92	M260-1	9/24/92	G268-1	12/10/92	3,850	4,580	3,030	4,400			68,000
10CON-11-44-1	60	II	10/15/92	M289-1	10/20/92	G294-1	1/5/93	3,850	4,530	3,960	3,220			68,000
10CON-11-44-2	60	II	10/15/92	M289-1	10/20/92	G294-1	1/5/93	3,850	4,530	3,960	3,220			68,000
10CON-11-52-1	72	II	10/16/92	M290-1	10/20/92	G294-2	1/21/93	3,850	5,800	4,390	1,900			68,000
10CON-11-52-2	72	II	10/16/92	M290-1	10/20/92	G294-1	1/20/93	3,850	5,800	4,390	3,220			68,000
12-in. Concrete Masonry Unit														
12CON-6-27-1	20	I	4/24/91	M114-2	5/9/91	G129-2	7/23/91	6,280	2,490	2,150	2,130		430	66,400
12CON-6-27-2	20	I	4/24/91	M114-2	5/9/91	G129-2	7/23/91	6,280	2,490	2,150	2,130		430	66,400
12CON-6-37-1	28	I	4/29/91	M119-1	6/13/91	G164-1	8/24/91	6,280	2,420	2,240	3,340			66,400
12CON-6-37-2	28	I	4/29/91	M119-1	6/13/91	G164-1	8/24/91	6,280	2,420	2,240	3,340			66,400
12CON-6-48-1	36	I	5/2/91	M122-2	7/26/91	G207-1	9/9/91	6,280	1,900		3,000			66,400
12CON-6-48-2	36	I	5/2/91	M122-2	6/13/91	G164-1	9/4/91	6,280	1,900		3,340			66,400
12CON-8-32-1	32	II	10/16/92	M290-1	10/20/92	G294-1	12/1/92	6,280	5,800	4,390	3,220			68,700

(Sheet 4 of 5)

Table 3 (Concluded)

| Specimen Name | Nominal Specimen Height, in. | Program Phase | Date Constructed | Mortar Batch* | Date Grouted | Grout Batch* | Date Tested | Compressive Strength, psi* | | | | Tensile Strength, psi* | | |
| | | | | | | | | Unit | Mortar | | Grout | Mortar | Grout | Reinforcing Bar |
									Cube	Cylinder				
12CON-8-32-2	32	II	10/16/92	M290-1	10/20/92	G294-1	12/2/92	6,280	5,800	4,390	3,220			68,700
12CON-8-40-1	40	II	10/16/92	M290-2	10/20/92	G294-2	12/2/92	6,280	5,010	4,650	1,900			68,700
12CON-8-40-2	40	II	10/16/92	M290-2	10/20/92	G294-2	12/2/92	6,280	5,010	4,650	1,900			68,700
12CON-8-48-1	48	II	10/16/92	M290-2	10/20/92	G294-2	12/8/92	6,280	5,010	4,650	1,900			68,700
12CON-8-48-2	48	II	10/19/92	M293-1	10/20/92	G294-2	12/8/92	6,280	4,370	4,030	1,900			68,700
12CON-11-35-1	48	II	10/19/92	M293-1	10/20/92	G294-1	12/10/92	6,280	4,370	4,030	3,220			68,000
12CON-11-35-2	48	II	10/19/92	M293-1	10/20/92	G294-1	12/14/92	6,280	4,370	4,030	3,220			68,000
12CON-11-44-1	60	II	10/19/92	M293-1	10/20/92	G294-1	1/21/93	6,280	4,370	4,030	3,220			68,000
12CON-11-44-2	60	II	10/19/92	M293-2	10/20/92	G294-2	1/20/93	6,280	2,430	2,250	1,900			68,000
12CON-11-52-1	72	II	10/19/92	M293-2	10/20/92	G294-2	2/3/93	6,280	2,430	2,250	1,900			68,000
12CON-11-52-2	72	II	10/19/92	M293-2	10/20/92	G294-1	2/3/93	6,280	2,430	2,250	3,220			68,000

(Sheet 5 of 5)

Table 4
Test Matrix, Clay Masonry Lap Splice Tests

| Specimen Name | Nominal Specimen Height, in. | Program Phase | Date Constructed | Mortar Batch* | Date Grouted | Grout Batch* | Date Tested | Compressive Strength, psi* | | | | Tensile Strength, psi* | | |
								Unit	Mortar Cube	Mortar Cylinder	Grout	Mortar	Grout	Reinforcing Bar
4-In. Clay Masonry Unit														
4CLAY-4-24-1	12	II	9/15/92	M259-1	9/24/92	G268-1	11/13/92	15,640	4,390	3,770	4,770			72,300
4CLAY-4-24-2	12	II	9/15/92	M259-1	9/24/92	G268-1	11/13/92	15,640	4,390	3,770	4,770			72,300
4CLAY-4-32-1	16	II	9/15/92	M259-1	9/24/92	G268-1	11/16/92	15,640	4,390	3,770	4,770			72,300
4CLAY-4-32-2	16	II	9/15/92	M259-1	9/24/92	G268-1	11/13/92	15,640	4,390	3,770	4,770			72,300
4CLAY-4-40-1	20	II	9/15/92	M259-1	9/24/92	G268-1	11/20/92	15,640	4,390	3,770	4,770			72,300
4CLAY-4-40-2	20	II	9/15/92	M259-1	9/24/92	G268-1	11/20/92	15,640	4,390	3,770	4,770			72,300
4CLAY-6-37-1	28	I	5/1/91	M121-1	6/13/91	G164-1	8/15/91	15,640	2,070	2,030	3,450			66,400
4CLAY-6-37-2	28	I	5/1/91	M121-1	6/13/91	G164-1	8/16/91	15,640	2,070	2,030	3,450			66,400
4CLAY-6-48-1	36	I	8/1/91	M213-1	8/5/91	G217-1	9/13/91	15,640	2,430	1,860	3,440	250		66,400
4CLAY-6-48-2	36	I	8/1/91	M213-1	8/5/91	G217-1	9/13/91	15,640	2,430	1,860	3,440	250		66,400
6-In. Clay Masonry Unit														
6CLAY-4-24-1	12	I	4/24/91	M114-2	5/9/91	G129-2	7/12/91	14,200	2,490	2,150	3,700		500	72,300
6CLAY-4-24-2	12	I	8/1/91	M213-1	8/5/91	G217-1	1/28/92	14,200	2,430	1,860	3,440	250		72,300
6CLAY-4-24-3	12	I	8/1/91	M213-1	8/5/91	G217-1	1/28/92	14,200	2,430	1,860	3,440	250		72,300
6CLAY-4-32-1	16	I	4/24/91	M114-2	5/9/91	G129-2	7/15/91	14,200	2,490	2,150	3,700		500	72,300
6CLAY-4-32-2	16	I	4/24/91	M114-2	5/9/91	G129-2	7/15/91	14,200	2,490	2,150	3,700		500	72,300
6CLAY-4-32-3	16	I	8/1/91	M213-1	8/5/91	G217-1	1/28/92	14,200	2,430	1,860	3,440	250		72,300

*Additional information on material properties can be found in Appendix A.

(Sheet 1 of 3)

Table 4 (Continued)

Specimen Name	Nominal Specimen Height, in.	Program Phase	Date Constructed	Mortar Batch*	Date Grouted	Grout Batch*	Date Tested	Compressive Strength, psi* Unit	Mortar Cube	Mortar Cylinder	Grout	Tensile Strength, psi* Mortar	Grout	Reinforcing Bar
6CLAY-4-40-1	20	I	4/25/91	M115-1	5/9/91	G129-2	8/6/91	14,200	2,060	1,980	3,700		500	72,300
6CLAY-4-40-2	20	I	4/25/91	M115-1	5/9/91	G129-2	8/6/91	14,200	2,060	1,980	3,700		500	72,300
6CLAY-6-27-1	20	I	4/25/91	M115-1	5/9/91	G129-2	7/25/91	14,200	2,060	1,980	3,700		500	66,400
6CLAY-6-27-2	20	I	4/29/91	M119-1	5/9/91	G129-2	7/25/91	14,200	2,420	2,240	3,700		500	66,400
6CLAY-6-37-1	28	I	5/1/91	M121-1	6/13/91	G164-1	8/19/91	14,200	2,070	2,030	3,450			66,400
6CLAY-6-37-2	28	I	5/1/91	M121-1	6/13/91	G164-1	8/19/91	14,200	2,070	2,030	3,450			66,400
6CLAY-6-48-1	36	I	5/2/91	M122-2	7/26/91	G207-1	9/10/91	14,200	1,900		2,700			66,400
6CLAY-6-48-2	36	I	5/2/91	M122-2	7/26/91	G207-1	9/10/91	14,200	1,900		2,700			66,400
6CLAY-8-32-1	32	I	5/1/91	M121-1	6/13/91	G164-1	8/26/91	14,200	2,070	2,030	3,450			68,700
6CLAY-8-32-2	32	I	5/1/91	M121-1	6/13/91	G164-1	8/26/91	14,200	2,070	2,030	3,450			68,700
6CLAY-8-48-1	48	I	9/12/91	M255-1	10/22/91	G295-1	1/22/92	14,200	1,830	1,860		250		68,700
6CLAY-8-48-2	48	I	9/12/91	M255-1	10/22/91	G295-1	1/22/92	14,200	1,830	1,860		250		68,700
8-In. Clay Masonry Unit														
8CLAY-6-27-1	20	I	4/29/91	M119-1	6/13/91	G164-1	8/7/91	10,890	2,420	2,240	3,450			66,400
8CLAY-6-27-2	20	I	4/29/91	M119-1	6/13/91	G164-1	8/7/91	10,890	2,420	2,240	3,450			66,400
8CLAY-6-37-1	28	I	5/1/91	M121-1	6/13/91	G164-1	8/19/91	10,890	2,070	2,030	3,450			66,400
8CLAY-6-37-2	28	I	5/1/91	M121-1	6/13/91	G164-1	8/23/91	10,890	2,070	2,030	3,450			66,400
8CLAY-6-48-1	36	I	5/2/91	M122-2	7/26/91	G207-1	9/13/91	10,890	1,900		2,700			66,400
8CLAY-6-48-2	36	I	5/2/91	M122-2	7/26/91	G207-1	9/11/91	10,890	1,900		2,700			66,400
8CLAY-8-32-1	32	II	9/16/92	M260-1	9/24/92	G268-1	11/24/92	10,890	4,580	3,030	4,770			68,700

(Sheet 2 of 3)

Table 4 (Concluded)

Specimen Name	Nominal Specimen Height, in.	Program Phase	Date Constructed	Mortar Batch*	Date Grouted	Grout Batch*	Date Tested	Compressive Strength, psi*					Tensile Strength, psi*	
								Unit	Mortar			Grout	Mortar	Grout	Reinforcing Bar
									Cube	Cylinder	Grout			
8CLAY-8-32-2	32	II	9/16/92	M260-1	9/24/92	G268-1	11/30/92	10,890	4,580	3,030	4,770			68,700
8CLAY-8-40-1	40	II	9/16/92	M260-1	9/24/92	G268-1	12/4/92	10,890	4,580	3,030	4,770			68,700
8CLAY-8-40-2	40	II	9/16/92	M260-1	9/24/92	G268-1	12/4/92	10,890	4,580	3,030	4,770			68,700
8CLAY-8-48-1	48	II	9/16/92	M260-2	9/24/92	G268-1	12/4/92	10,890	3,580	2,370	4,770			68,700
8CLAY-8-48-2	48	II	9/16/92	M260-2	9/24/92	G268-1	12/4/92	10,890	3,580	2,370	4,770			68,700

(Sheet 3 of 3)

6, 8, 10, and 12 in. and hollow clay units with nominal widths of 4, 6, and 8 in. were used. Specimens were constructed in stack bond with a prism-building jig (Atkinson-Noland & Associates 1985) using half-units to provide a single vertical cell. Half-units were obtained by cutting one full cell (i.e., two face shells and two webs) from full-size units. Nominal specimen dimensions are provided in Figure 9. Lap splices were centered within the cell in the orientation shown in Figure 9.

Hollow concrete units were tested in compression in accordance with ASTM C 140-75, Method for Sampling and Testing Concrete Masonry Units (American Society of Testing and Materials (ASTM) 1990h). Test values are fairly consistent with the exception of the 10-in. units, which had an average compressive strength of 2,570 psi, whereas all remaining CMU sizes had compressive strengths of 3,380 to 3,690 psi. There is no immediate explanation for the discrepancy, since all units were obtained from the same manufacturer and the same materials and base concrete mix were supposedly used for all units. Tests were also conducted to determine 24-hour absorption for each unit type. Results of absorption tests are listed in Appendix A.

Clay masonry units, tested in compression according to ASTM C 67-89a, Method of Sampling and Testing Brick and Structural Clay Tile (ASTM 1990c), were somewhat stronger than the concrete masonry units. Compressive strengths of clay masonry ranged from 15,640 psi for 4-in. units to 10,890 psi for 8-in. units. Test results for determination of 24-hr and initial rates of absorption are listed in Appendix A.

Four compression prisms were tested per ASTM E 447-84, Test Methods for Compressive Strength of Masonry Prisms (ASTM 1990u), to determine compression stress-strain behavior of the finished assemblage. Two concrete and two clay-unit prisms were tested. The prisms were not reinforced but were fully grouted. Concrete masonry prisms had an average compressive strength of 3,120 psi; prisms constructed with clay units had an average compressive strength of 4,160 psi.

Mortar. Type S mortar with volumetric proportions of cement:lime: sand equal to 1:1/2:4-1/2 was used for all specimens. Mortar was proportioned by weight and mixed in small batches. Mortar cubes (2-in.) were prepared for each batch of mortar and tested in accordance with ASTM C 109-90, Test Method for Compressive Strength of Hydraulic Cement Mortars (ASTM 1990d). An average mortar compressive strength of 3,120 psi was measured for the 20 batches used during specimen construction.

A small number of mortar cylinders were tested to determine mortar tensile strength. ASTM C 496-90, Test Method for Splitting Tensile Strength of Cylindrical Concrete Specimens (ASTM 1990r), was used for determination of tensile splitting strength. Cylinders for testing were prepared in accordance with UBC 24-22 (International Conference of Building Officials (1992)), Field Test for Mortar, using 2-in.-diam by 4-in.-long cylinders.

Grout. All specimens were fully grouted using a coarse grout with volumetric proportions of 1:3:2 (cement:sand:gravel) and maximum aggregate size of 3/8 in. A water-cement ratio of approximately 0.7 was used to provide a slump of 9-1/2 to 10 in. Sika Grout-Aid expansive admixture was used in the grout in the amount of 1 percent Grout-Aid by weight of cement to offset shrinkage due to migration of mix water from the grout to the surrounding masonry. The same grout mix design was used for both concrete and clay masonry specimens. A total of eight separate grout batches were used.

Specimens for grout compression testing were prepared using the method described in ASTM C 1019-89a, Method of Sampling and Testing Grout (ASTM 1990t). Three 3-in. by 3-in. by 6-in. grout prisms were prepared for each grout batch.

Several grout cylinders were tested in accordance with ASTM C 496-90, Test Method for Splitting Tensile Strength of Cylindrical Concrete Specimens (ASTM 1990r), to determine tensile splitting strength of the grout. Cylinders for splitting tension testing obtained by coring 2-in.-diam by 4-in. cores from grouted hollow masonry units. It was expected that different types of units would have an effect on grout strength due to variations in absorptive properties of the different unit types and sizes.

Reinforcing Steel. Reinforcing steel used in this study included No. 4, 6, 8, and 11 Grade 60 bars, conforming to the requirements of ASTM A 615, Specification for Deformed and Plain Billet-Steel Bars for Concrete Reinforcement (ASTM 1990b). Deformations are in a diagonal pattern, at an angle of 70 deg to the longitudinal axis of the bar, with three longitudinal ribs. Three sample bars of each size were tested in tension to determine steel yield strength. The reinforcing steel tensile yield strengths listed in Appendix A were determined by testing full-size reinforcing bars approximately 4 ft in length.

Testing and Instrumentation

The test setup for the lap-splice study simulated actual conditions present at lap splices in reinforced masonry by subjecting the reinforcing bars to pure tension, while the masonry is unrestrained against lateral splitting failure. Tensile loads were applied directly to the ends of the bars protruding from the masonry using hydraulically activated tension grips. Loads were applied monotonically in displacement control at a rate which allowed adequate acquisition of data and observation of crack formation. Load application was continued until some type of failure occurred which caused a significant drop in load resistance.

The direct tension forces to the lapped bars were provided by a 300-kip servo-controlled, closed-loop hydraulic loading system. The 300-kip capacity ram was attached to a 20-ft-tall tripodal load frame that was fixed

to the structurally strong floor. The upper cross beam in the load frame could be adjusted up or down to adjust to different length specimens.

The ends of the reinforcing bars were gripped by hydraulically acti-vated tension grips. The upper tension grip was attached to a load cell in line with the 300-kip hydraulic ram. The lower tension grip was attached to a solid steel beam that was connected to the structurally strong floor. The position of the lower tension grip could be adjusted to account for the eccentricity caused by the lap in the reinforcing bars. Also, the lower beam could be raised or lowered hydraulically to allow the test specimens to be loaded conveniently. A schematic of the overall test setup is shown in Figure 12. Figure 13 shows the actual test setup with splitting failure.

One of the main goals of this study was to determine load-displacement behavior of reinforced masonry containing lap splices, and the specimen was instrumented to obtain the necessary information to describe this be-havior. The instrumentation was selected to allow recording of overall load-deformation behavior, overall bond slip, and relative slip between the spliced bars.
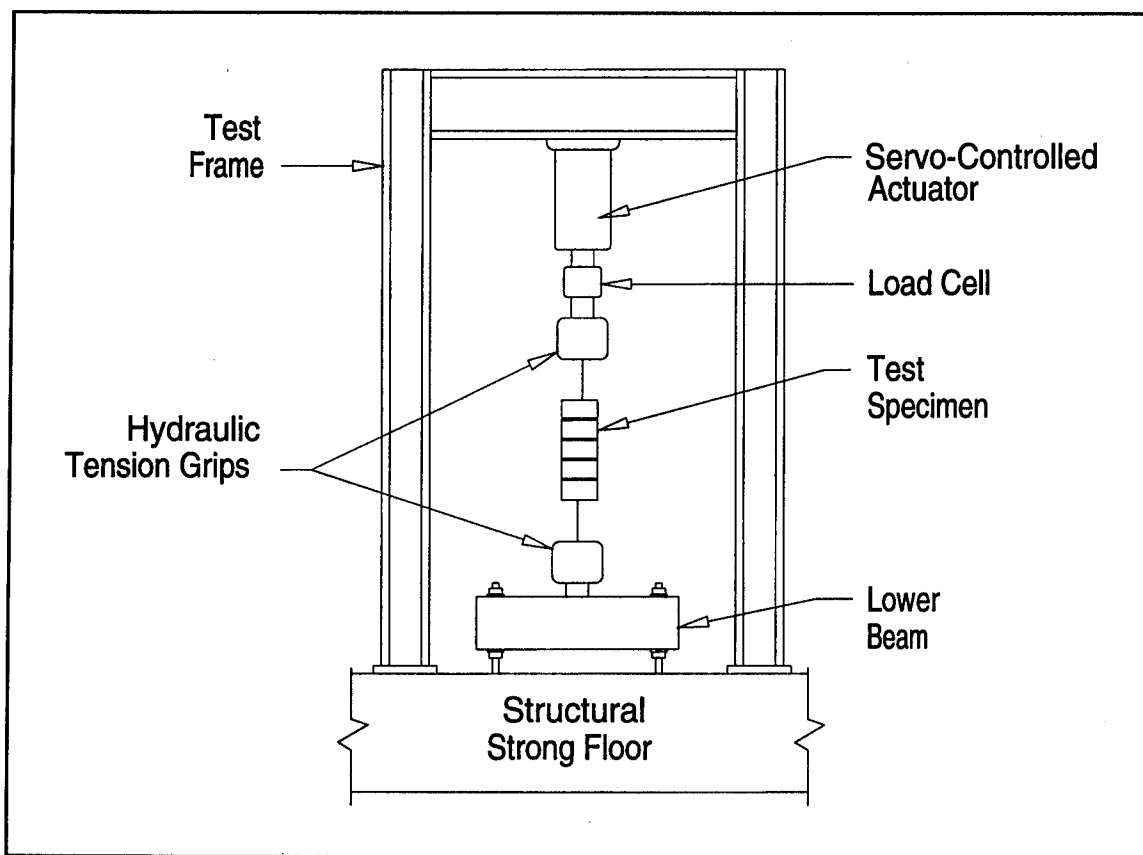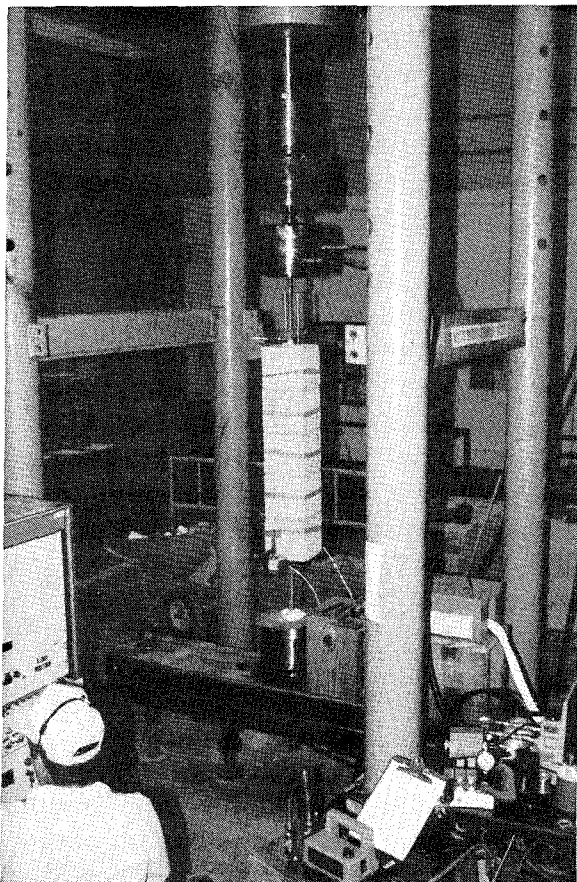

Figure 12.   Schematic of lap-splice experimental setup

a. Overall view of test setup

Bond slip relationships between the reinforcement and the grout were determined by measuring overall bond slip. Relative movement between two spliced bars was measured to identify how relative displacements influence splitting failures.

Sufficient postpeak data were obtained to allow ductility and energy absorption to be determined. At large strain levels, there was considerable specimen damage due to spalling, cracking, and splitting. This damage would have an adverse effect on deformation measurements obtained using surface-mounted devices. For this reason, no surface mount linear variable differential transducers (LVDT) were used.

An conceptual view of the test instrumentation is shown in Figure 14. All instrumentation was attached to a yoke, which was clamped to the reinforcing bar protruding from the test specimen. Instrumentation for the lap splice tests consisted of the following items:

b. Typical splitting failure mode

Figure 13. Actual test setup and typical failure mode

a. Axial load, as measured by a 400-kip capacity load cell in series with the test specimen and the 300-kip ram.

b. Head-to-head displacement, as measured by a reel-type position transducer mounted between the hydraulic tension grips.

c. Bar-to-bar displacement, as measured by reel-type position transducers (in the Phase I tests) or by alternating current (AC) LVDT's. These gauges were mounted to vee-notched 3/4-in.-thick acrylic yokes clamped to the reinforcing bars protruding above and below the prism.

d. Bar-to-grout displacement, as measured by AC LVDT's mounted to the yoke clamped to one of the protruding reinforcing bars. The probe of the LVDT rested on the grout adjacent to the splice.

e. Bar-to-bar displacement, as measured by AC LVDT's mounted to the yoke clamped to one of the protruding reinforcing bars. The probe of the LVDT rested on top of the other reinforcing bar comprising the splice.
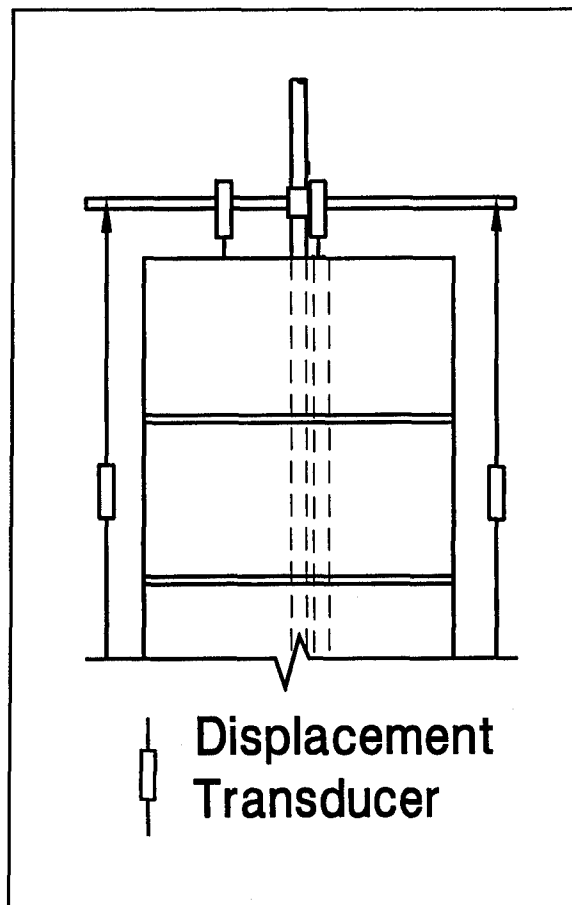

Figure 14. Schematic of lap splice instrumentation

All data were acquired by a microcomputer-controlled digital data acquisition system programmed to acquired data at equal time intervals of approximately 5 sec.

Results

Table 5 contains a tabulation of the as-built dimensions of all lap splice test specimens and measured cover. Tables 6 and 7 contain information on the reinforcement ratio maximum load and ratio of maximum load to yield load. Determination of material properties is described in Appendix A. Note that the reinforcement ratios listed in the database are based upon the area of a *single* lapped bar in the grouted cell area or the gross area of the specimen. A photograph of a typical splitting failure mode is shown in Figure 13b.

Table 5
As-Built Dimensions of Lap-Splice Test Specimens

Specimen Name	Actual Specimen Height, in.	Measured Cover, in.			
		W1	W2	L1	L2
4-in. Concrete Masonry Units					
4CON-4-24-1	11.5	1.8	1.5	3.8	4.4
4CON-4-24-2	11.5	1.8	1.8	4	3.5
4CON-4-32-1	15.5	1.8	1.8	4	4
4CON-4-32-2	15.5	1.5	1.5	3.75	4
4CON-4-40-1	19.5	1.8	1.5	4	4
4CON-4-40-2	19.5	1.8	1.8	4	4
4CON-6-37-1	27.5	1.75	1.75	3.75	3.75
4CON-6-37-2	27.5	2	1.75	4	3.75
4CON-6-48-1	35.5	1.5	1.5	4.75	3.75
4CON-6-48-2	35.5	2	1.625	3.75	4.25
6-in. Concrete Masonry Units					
6CON-4-24-1	11.5	2.8	2.8	4	3.5
6CON-4-24-2	11.5	2.8	2.8	4	3.8
6CON-4-32-1	15.5	2.8	2.8	3.8	4
6CON-4-32-2	15.5	2.8	2.8	4	4
6CON-4-40-1	19.5	2.8	2.8	4	4
6CON-4-40-2	19.5	2.8	2.8	4	4
6CON-6-27-1	19.5	2.75	2.5	3.75	4.75
6CON-6-27-2	19.5	2.75	2.75	4	4
6CON-6-37-1	27.5	2.75	2.75	4	3.5
6CON-6-37-2	27.5	2.75	3	4.25	3.75
6CON-6-48-1	35.5	2.5	3	4.25	3.5
6CON-6-48-2	35.5	3	2.25	4.5	3.5
8-in. Concrete Masonry Units					
8CON-4-24-1	11.5	NA*	NA	4	4
8CON-4-24-2	11.5	NA	NA	NA	NA
8CON-4-24-3	11.5	3.7	3.5	4	4
8CON-4-32-1	15.5	3.5	3.75	4	4
8CON-4-32-2	15.5	3.75	3.75	4	4
8CON-4-40-1	19.5	3.75	3.5	4.5	4
8CON-4-40-2	19.5	4	3.5	4.25	4.25
8CON-6-27-1	19.5	3.75	3.75	4	3.75

(Sheet 1 of 4)

*Information not available.

Table 5 (Continued)

Specimen Name	Actual Specimen Height, in.	Measured Cover, in.			
		W1	W2	L1	L2
8CON-6-27-2	19.5	4	3.5	4	3.75
8CON-6-37-1	27.5	3.75	4	4	4.25
8CON-6-37-2	27.5	3.75	3.75	4	4
8CON-6-48-1	35.5	NA	NA	NA	NA
8CON-6-48-2	35.5	3.5	4	4.25	3.75
8CON-8-32-1	31.5	3.75	3.75	4.5	3.75
8CON-8-32-2	31.5	3.75	3.5	4.5	3.5
8CON-8-40-1	39.5	3.5	3.75	4.25	4.25
8CON-8-40-2	39.5	3.75	3.75	4.25	4
8CON-8-40-3	39.5	4	3.5	4	4.25
8CON-8-48-1	47.5	3.5	3.8	4.3	4.3
8CON-8-48-2	47.5	3.8	3.8	4	4
8CON-8-60-1	59.5	3.5	3.5	4	4
8CON-8-60-2	59.5	3.8	3.5	4	4
8CON-11-35-1	47.5	NA	NA	NA	NA
8CON-11-35-2	47.5	NA	NA	NA	NA
8CON-11-52-1	71.5	4.3	4	4	4
8CON-11-52-2	71.5	3.5	3.5	4	4
10-in. Concrete Masonry Units					
10CON-6-27-1	19.5	4	4.25	5	4.75
10CON-6-27-2	19.5	4.75	4	4.75	4.25
10CON-6-37-1	27.5	4	4.75	4.5	4.5
10CON-6-37-2	27.5	4.75	4.75	4	4.25
10CON-6-48-1	35.5	4	4.5	4	4
10CON-6-48-2	35.5	4.25	4	3.75	4
10CON-8-32-1	31.5	4.8	4.8	4	4.3
10CON-8-32-2	31.5	4.8	4.8	4	4.1
10CON-8-40-1	39.5	4.5	4.5	NA	NA
10CON-8-40-2	39.5	4.8	4.8	NA	NA
10CON-8-48-1	47.5	4.8	4.8	4	4
10CON-8-48-2	47.5	4.5	4.8	4.5	4.8
10CON-11-35-1	47.5	4.3	4.5	3.8	4.3
10CON-11-35-2	47.5	4.3	4.2	4.3	4.2
10CON-11-44-1	59.5	4	4.8	4	4
10CON-11-44-2	59.5	4.5	4.8	3.5	4
10CON-11-52-1	71.5	5	5	4	4

(Sheet 2 of 4)

Table 5 (Continued)

Specimen Name	Actual Specimen Height, in.	Measured Cover, in.			
		W1	W2	L1	L2
10CON-11-52-2	71.5	4.75	4.75	4	4
12-in. Concrete Masonry Unit					
12CON-6-27-1	19.5	5.5	5.75	4.25	3.75
12CON-6-27-2	19.5	6	5.5	3.75	3.75
12CON-6-37-1	27.5	6	5.5	4.5	3.375
12CON-6-37-2	27.5	5.75	5.25	4	4
12CON-6-48-1	35.5	4.25	4.25	6	5.25
12CON-6-48-2	35.5	6	5.5	4	4
12CON-8-32-1	31.5	5.5	5.5	3.8	4
12CON-8-32-2	31.5	5.5	5.8	3.8	4.3
12CON-8-40-1	39.5	5.8	5.8	4.3	4.3
12CON-8-40-2	39.5	5.8	5.8	4	4
12CON-8-48-1	47.5	5.8	5.8	4	4
12CON-8-48-2	47.5	5.8	5.8	4.3	
12CON-11-35-1	47.5	5.5	5.5	3.5	4.3
12CON-11-35-2	47.5	5.3	5.8	3.8	3.8
12CON-11-44-1	59.5	NA	NA	NA	NA
12CON-11-44-2	59.5	5.75	NA	4	NA
12CON-11-52-1	71.5	5.75	5.75	4	4
12CON-11-52-2	71.5	5.75	5.75	4	4
4-in. Clay Masonry Unit					
4CLAY-4-24-1	11.5	1.8	1.8	2	2.5
4CLAY-4-24-2	11.5	1.8	1.8	2.1	2.1
4CLAY-4-32-1	15.5	1.7	1.5	2.1	2
4CLAY-4-32-2	15.5	1.8	1.8	2.5	2.3
4CLAY-4-40-1	19.5	1.8	1.8	2	2
4CLAY-4-40-2	19.5	1.8	1.8	2.3	2.5
4CLAY-6-37-1	27.5	1.25	1.75	2.75	2.25
4CLAY-6-37-2	27.5	1.5	1.5	2.5	2.5
4CLAY-6-48-1	35.5	1.25	2	2.5	2.25
4CLAY-6-48-2	35.5	1.75	1.75	2.5	2.25
6-in. Clay Masonry Unit					
6CLAY-4-24-1	11.5	NA	NA	3.5	3.5
6CLAY-4-24-2	11.5	2.8	2.8	3.5	3.6
6CLAY-4-24-3	11.5	2.8	2.3	3.3	3.3

(Sheet 3 of 4)

Table 5 (Continued)

Specimen Name	Actual Specimen Height, in.	Measured Cover, in.			
		W1	W2	L1	L2
6CLAY-4-32-1	15.5	3	3	3.5	3.5
6CLAY-4-32-2	15.5	2.75	2.75	3.5	3.75
6CLAY-4-32-3	15.5	NA	NA	NA	NA
6CLAY-4-40-1	19.5	3.25	2.5	3.5	3.75
6CLAY-4-40-2	19.5	2.75	2.75	3.25	3.25
6CLAY-6-27-1	19.5	2.5	2.75	3.5	3.25
6CLAY-6-27-2	19.5	2.5	3	3.75	3.5
6CLAY-6-37-1	27.5	2.5	2.5	3.5	3
6CLAY-6-37-2	27.5	2.75	2.75	4	2.5
6CLAY-6-48-1	35.5	3	2	3.25	3.25
6CLAY-6-48-2	35.5	3	2.5	2.5	3
6CLAY-8-32-1	31.5	2.5	2.625	3.5	3
6CLAY-8-32-2	31.5	2.5	2.5	3	3
6CLAY-8-48-1	47.5	NA	NA	3.4	3
6CLAY-8-48-2	47.5	3	2.6	3.6	3
8-in. Clay Masonry Unit					
8CLAY-6-27-1	19.5	3.875	3.5	3.25	3.75
8CLAY-6-27-2	19.5	3.875	3.75	3.5	3.625
8CLAY-6-37-1	27.5	4	3.5	2.75	3.75
8CLAY-6-37-2	27.5	3.5	3.5	4	3
8CLAY-6-48-1	35.5	3.5	3.5	3.5	3.25
8CLAY-6-48-2	35.5	3.5	3.75	4	3.25
8CLAY-8-32-1	31.5	3.8	3.5	3.5	3.5
8CLAY-8-32-2	31.5	3.8	3.8	3.5	3.3
8CLAY-8-40-1	39.5	3.8	3.8	3.5	3.5
8CLAY-8-40-2	39.5	3.8	3.8	3.5	3.5
8CLAY-8-48-1	47.5	4	4	3.5	3.5
8CLAY-8-48-2	47.5	3.8	3.8	3.6	3.6

(Sheet 4 of 4)

Table 6
Strength Test Results, Concrete Masonry Lap-Splice Tests

| Specimen Name | Reinforcement Ratio, percent | | A_s sq in. | P_{max} kips | P_{max}/P_y |
	Gross Area	Cell Area			
4-in. Concrete Masonry Unit					
4CON-4-24-1	0.71	2.63	0.2	9.8	0.678
4CON-4-24-2				10.7	0.740
4CON-4-32-1				13.2	0.913
4CON-4-32-2				12.9	0.892
4CON-4-40-1				12.3	0.851
4CON-4-40-2				13.1	0.906
4CON-6-37-1	1.56	5.80	0.44	21.9	0.750
4CON-6-37-2				22.4	0.765
4CON-6-48-1				26.2	0.897
4CON-6-48-2				25.4	0.869
6-in. Concrete Masonry Unit					
6CON-4-24-1	0.46	0.96	0.2	14.2	0.982
6CON-4-24-2				14.6	1.010
6CON-4-32-1				18.0	1.245
6CON-4-32-2				17.5	1.210
6CON-4-40-1				20.9	1.445
6CON-4-40-2				20.8	1.438
6CON-6-27-1	1.01	2.11	0.44	21.8	0.744
6CON-6-27-2				21.2	0.727
6CON-6-37-1				28.0	0.957
6CON-6-37-2				28.0	0.959
6CON-6-48-1				29.0	0.993
6CON-6-48-2				29.2	0.999
8-in. Concrete Masonry Unit					
8CON-4-24-2	0.34	0.72	0.20	19.9	1.377
8CON-4-24-3				19.7	1.363
8CON-4-32-1				19.5	1.351
8CON-4-32-2				15.7	1.086
8CON-4-40-2				12.8	0.884
8CON-6-27-1	0.74	1.58	0.44	28.2	0.964
8CON-6-27-2				28.0	0.958
8CON-6-37-1				31.7	1.085
8CON-6-37-2				30.8	1.054

(Sheet 1 of 3)

Table 6 (Continued)

Specimen Name	Reinforcement Ratio, percent		A_s sq in.	P_{max} kips	P_{max}/P_y
	Gross Area	Cell Area			
8CON-6-48-1				31.6	1.083
8CON-6-48-2				33.8	1.156
8CON-8-32-1	1.33	2.84	0.79	44.0	0.810
8CON-8-32-2				42.8	0.787
8CON-8-40-1				48.6	0.894
8CON-8-40-2				50.8	0.935
8CON-8-40-3				48.1	0.886
8CON-8-48-1				50.8	0.936
8CON-8-48-2				51.3	0.944
8CON-8-60-1				54.1	0.996
8CON-8-60-2				54.1	0.997
8CON-11-35-1	2.63	5.60	1.56		0
8CON-11-35-2					0
8CON-11-52-1				80.2	0.756
8CON-11-52-2				77.8	0.733
10-in. Concrete Masonry Unit					
10CON-6-27-1	0.59	1.21	0.44	29.0	0.992
10CON-6-27-2				28.8	0.987
10CON-6-37-1				32.7	1.118
10CON-6-37-2				33.0	1.095
10CON-6-48-1				34.2	1.171
10CON-6-48-2				34.9	1.196
10CON-8-32-1	1.05	2.17	0.79	48.2	0.888
10CON-8-32-2				48.8	0.899
10CON-8-40-1				50.8	0.936
10CON-8-48-1				56.8	1.047
10CON-8-48-2				53.6	0.988
10CON-11-35-1	2.08	4.29	1.56	71.2	0.671
10CON-11-35-2				67.5	0.636
10CON-11-44-1				76.9	0.725
10CON-11-44-2				82.4	0.777
10CON-11-52-1				91.9	0.866
10CON-11-52-2				91.0	0.858

(Sheet 2 of 3)

Table 6 (Concluded)

Specimen Name	Reinforcement Ratio, percent		A_s sq in.	P_{max} kips	P_{max}/P_y
	Gross Area	Cell Area			
12-in. Concrete Masonry Unit					
12CON-6-27-1	0.49	0.98	0.44	28.8	0.984
12CON-6-27-2				28.4	0.973
12CON-6-37-1				33.9	1.162
12CON-6-37-2				33.3	1.139
12CON-6-48-1				42.5	1.453
12CON-6-48-2				36.7	1.254
12CON-8-32-1	0.87	1.76	0.79	47.0	0.866
12CON-8-32-2				46.6	0.859
12CON-8-40-1				53.2	0.980
12CON-8-40-2				52.2	0.962
12CON-8-48-1				56.1	1.034
12CON-8-48-2				53.1	0.978
12CON-11-35-1	1.72	3.48	1.56	65.9	0.621
12CON-11-35-2				70.0	0.660
12CON-11-44-1				78.5	0.740
12CON-11-44-2				83.3	0.785
12CON-11-52-1				74.3	0.700
12CON-11-52-2				90.7	0.855

(Sheet 3 of 3)

Table 7
Strength Test Results, Clay Masonry Lap-Splice Tests

Specimen Name	Reinforcement Ratio, percent		A_s sq in.	P_{max} kips	P_{max}/P_y
	Gross Area	Cell Area			
4-in. Clay Masonry Unit					
4CLAY-4-24-1	0.75	0.56	0.2	11.4	0.788
4CLAY-4-24-2	0.75	0.56	0.2	10.4	0.719
4CLAY-4-32-1	0.75	0.56	0.2	14.5	1.003
4CLAY-4-32-2	0.75	0.56	0.2	14.6	1.010
4CLAY-4-40-1	0.75	0.56	0.2	14.5	1.003
4CLAY-4-40-2	0.75	0.56	0.2	14.3	0.988
4CLAY-6-37-1	1.66	1.24	0.44	25.4	0.868
4CLAY-6-37-2	1.66	1.24	0.44	19.2	0.656

(Continued)

Table 7 (Concluded)

Specimen Name	Reinforcement Ratio, percent		A_s sq in.	P_{max} kips	P_{max}/P_y
	Gross Area	Cell Area			
4CLAY-6-48-1	1.66	1.24	0.44	26.7	0.912
4CLAY-6-48-2	1.66	1.24	0.44	27.1	0.929
6-in. Clay Masonry Unit					
6CLAY-4-24-2	0.47	0.33	0.2	15.1	1.041
6CLAY-4-24-3	0.47	0.33	0.2	14.0	0.967
6CLAY-4-32-1	0.47	0.33	0.2	13.6	0.941
6CLAY-4-32-2	0.47	0.33	0.2	14.4	0.998
6CLAY-4-32-3	0.47	0.33	0.2	18.1	1.248
6CLAY-4-40-1	0.47	0.33	0.2	18.1	1.252
6CLAY-4-40-2	0.47	0.33	0.2	13.5	0.936
6CLAY-6-27-1	1.03	0.74	0.44	22.6	0.776
6CLAY-6-27-2	1.03	0.74	0.44	24.6	0.842
6CLAY-6-37-1	1.03	0.74	0.44	27.9	0.957
6CLAY-6-37-2	1.03	0.74	0.44	29.1	0.996
6CLAY-6-48-1	1.03	0.74	0.44	28.9	0.990
6CLAY-6-48-2	1.03	0.74	0.44	29.3	1.004
6CLAY-8-32-1	1.85	1.32	0.79	36.8	0.677
6CLAY-8-32-2	1.85	1.32	0.79	37.1	0.683
6CLAY-8-48-1	1.85	1.32	0.79	29.2	0.538
8-in. Clay Masonry Unit					
8CLAY-6-27-1	0.74	0.41	0.44	26.1	0.894
8CLAY-6-27-2	0.74	0.41	0.44	29.2	0.999
8CLAY-6-37-1	0.74	0.41	0.44	33.7	1.152
8CLAY-6-37-2	0.74	0.41	0.44	37.6	1.286
8CLAY-6-48-1	0.74	0.41	0.44	32.0	1.094
8CLAY-6-48-2	0.74	0.41	0.44	35.2	1.205
8CLAY-8-32-1	1.34	0.73	0.79	45.6	0.840
8CLAY-8-32-2	1.34	0.73	0.79	43.6	0.803
8CLAY-8-40-1	1.34	0.73	0.79	50.2	0.925
8CLAY-8-40-2	1.34	0.73	0.79	50.6	0.932
8CLAY-8-48-1	1.34	0.73	0.79	52.2	0.962
8CLAY-8-48-2	1.34	0.73	0.79	58.5	1.078

Experimental precision

Two replications each of 62 different lap-splice specimens were tested. In general, the tests showed good repeatability between identical specimens. The distribution of experimental precision is plotted in Figure 15 for all 62 specimen pairs. Here the precision is calculated as the percentage variation of the recorded splice strength from the mean value for each pair. Concrete masonry specimen pairs displayed excellent repeatability, with lap-splice strengths for each pair generally in agreement to within 4 percent, with a mean variation of 2.61 percent. Clay masonry specimens displayed a somewhat greater variation, averaging 4.35 percent for each pair, presumably due to the predominance of relatively brittle failures for these specimens. Tested lap-splice strengths for all specimen pairs varied by an average of 3.18 percent. Nearly all of the specimen pairs had variabilities of less than 5 percent.
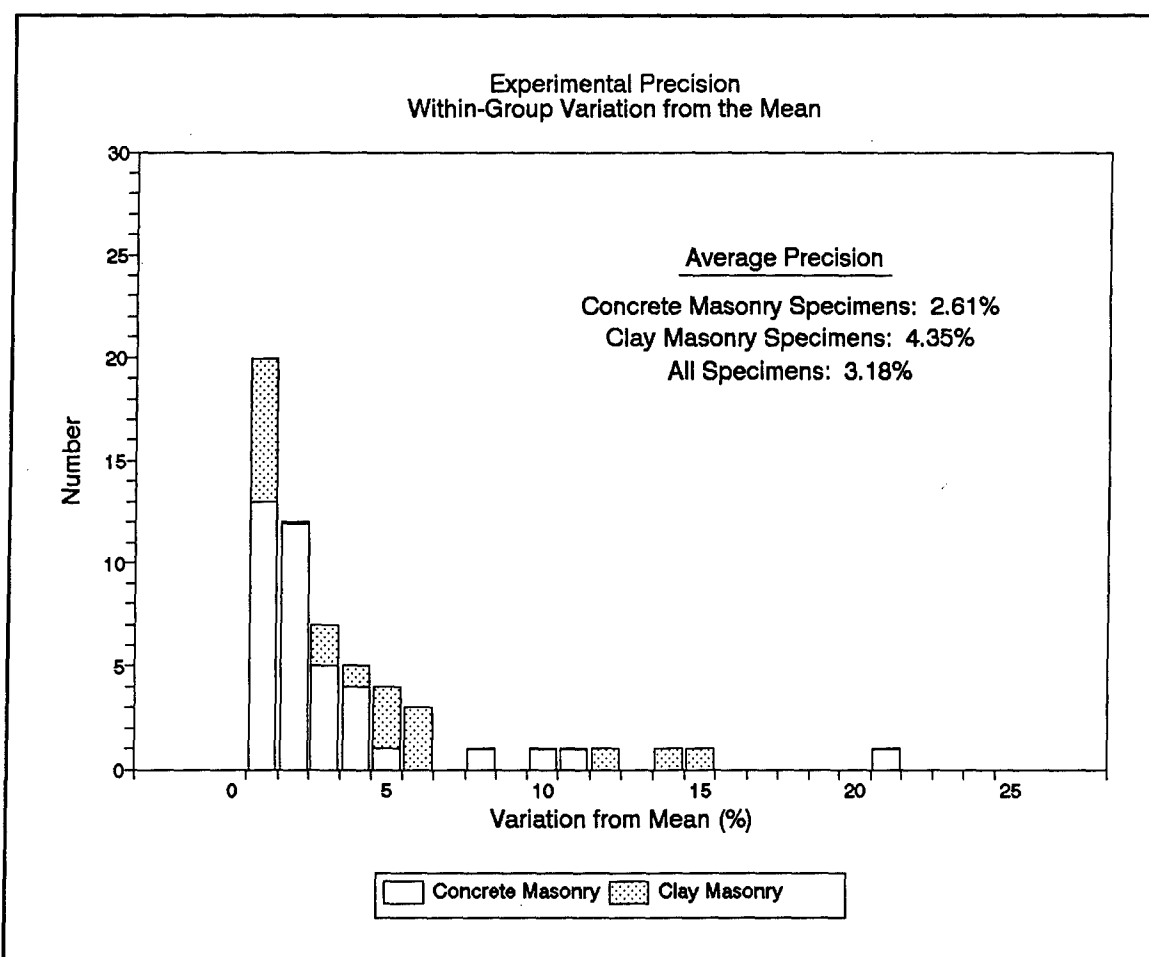
Figure 15. Experimental precision

Performance criteria

As discussed previously, current design codes require that lap splices develop a minimum tensile strength equivalent to 125 percent of the yield strength of the reinforcing bars being spliced. This criterion is intended to provide adequate splice ductility and will also be used here as a measure of splice performance. Hence, a splice which develops 1.25 times the yield force of the bar Py is considered to be adequate based upon strength alone. Most of the data in the plots which follow have been normalized by the bar yield strength to allow comparison between splices of different bar diameters.

Strength alone may not be sufficient for determining the acceptability of lap splices, however. The splice must also be ductile, and brittle splitting-type failures should be avoided. Splice performance in terms of ductility and failure mode is discussed later in the Results section of this chapter.

Effect of unit width

The effect of varying masonry unit width on lap-splice strength is shown in Figures 16 through 22, which show the ratio of the force resisted by the splice (Pmax) to the yield force of the bar (Py) versus lap splice length for No. 4, 6, 8, and 11 bars in different size concrete and clay
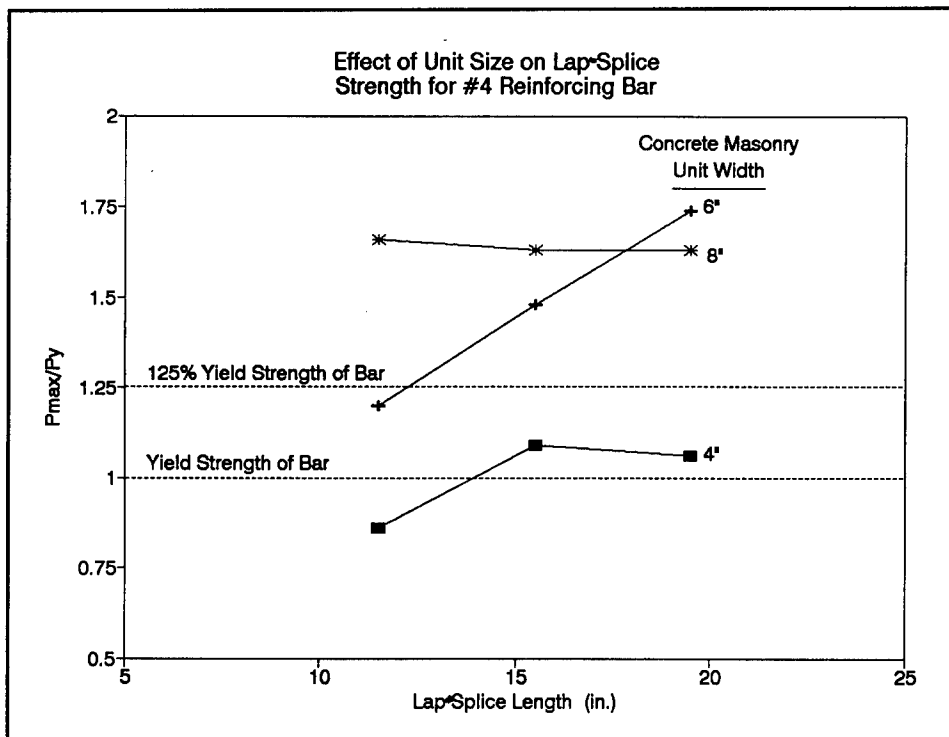
Figure 16. Effect of unit size on lap-splice strength, No. 4 reinforcing bar, CMU
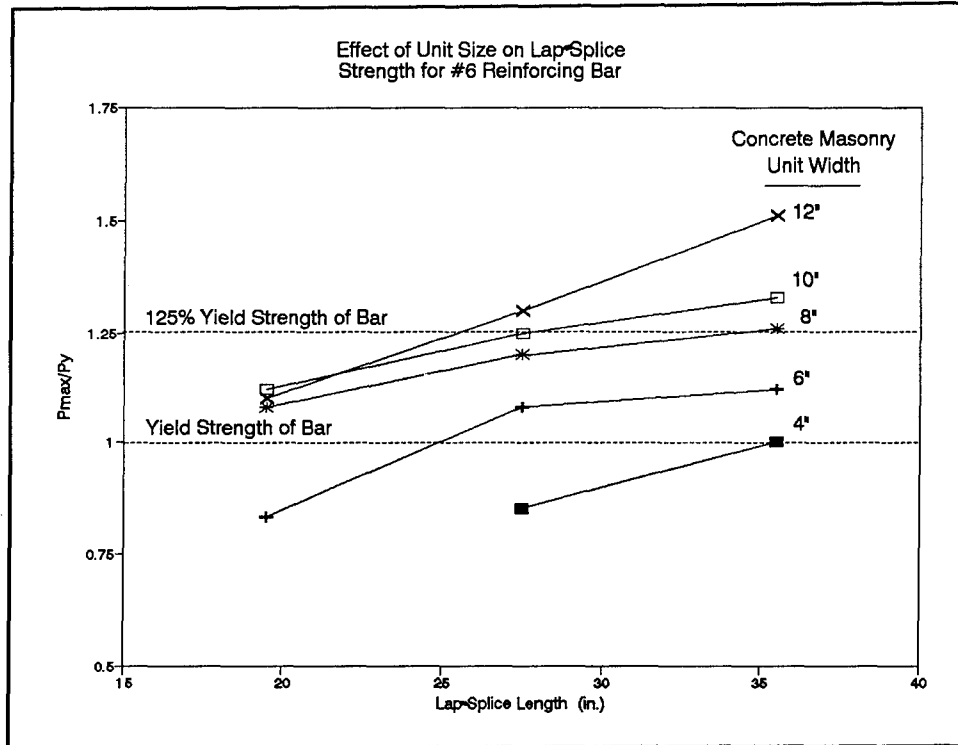
Figure 17. Effect of unit size on lap-splice strength, No. 6 reinforcing bar, CMU
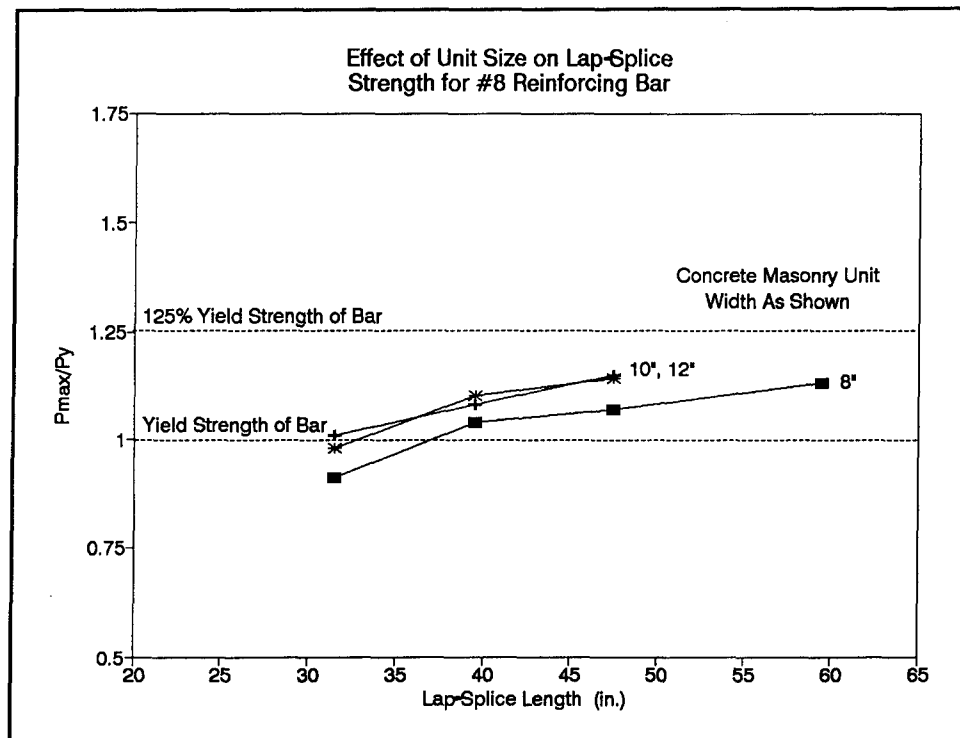
Figure 18. Effect of unit size on lap-splice strength for No. 8 reinforcing bar
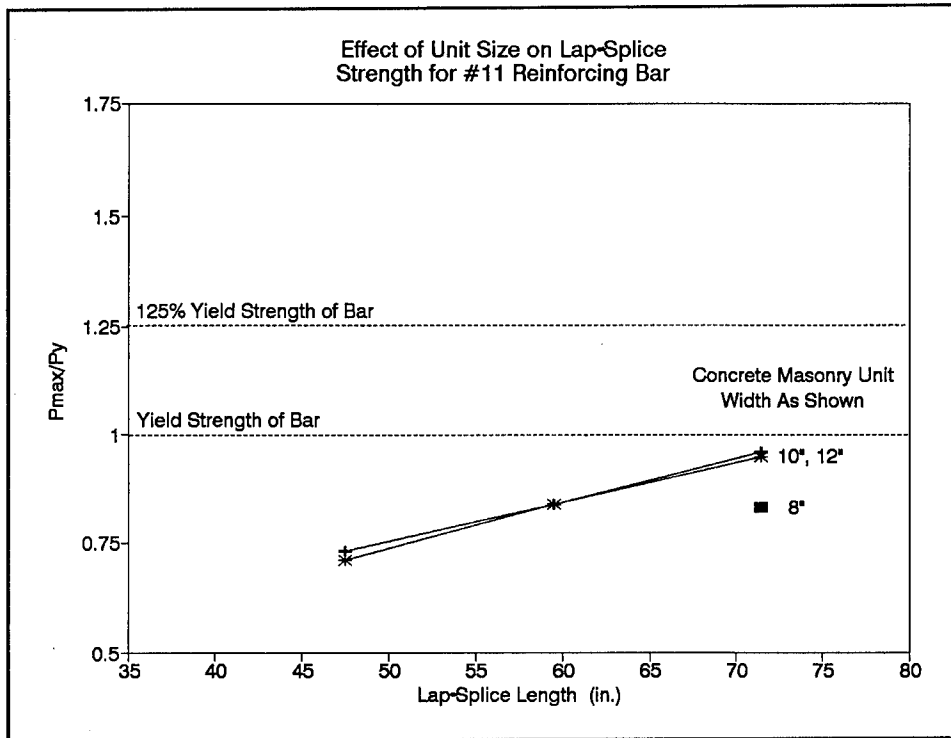
Figure 19.   Effect of unit size on lap-splice strength for No. 11 reinforcing bar
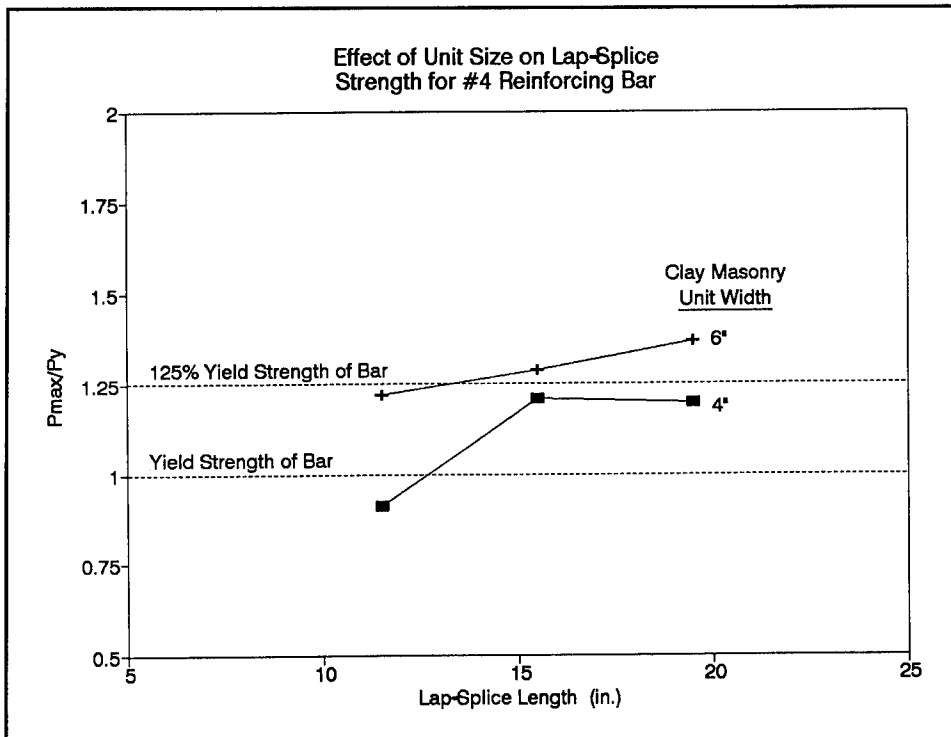
Figure 20.   Effect of unit size on lap-splice strength for No. 4 reinforcing bar, clay masonry unit
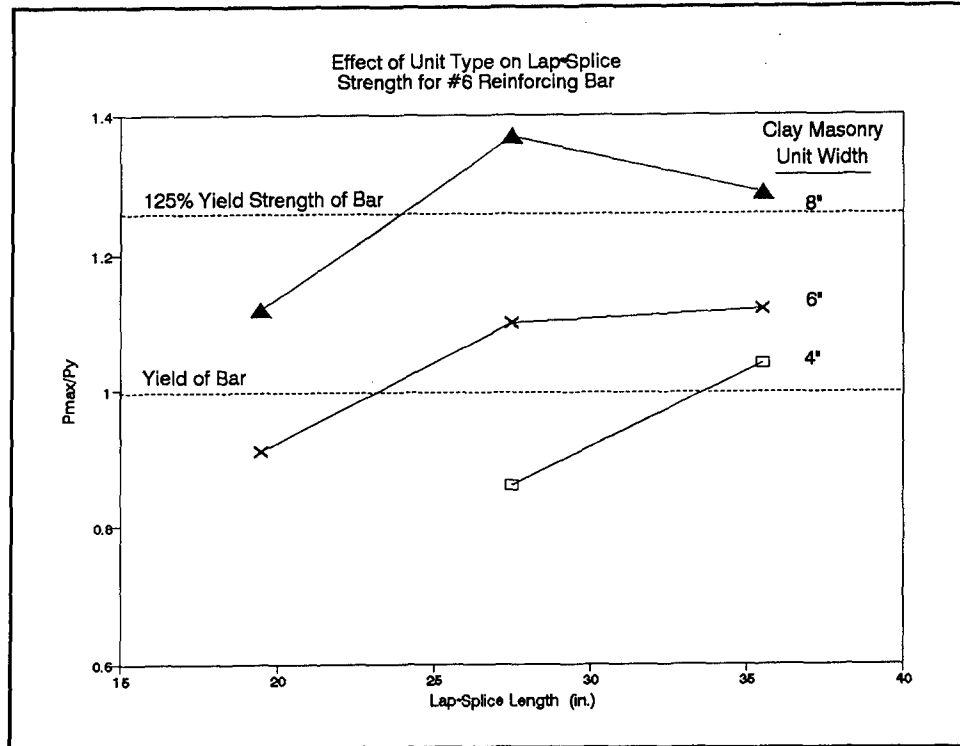
Figure 21.   Effect of unit type on lap-splice strength for No. 6 reinforcing
bar, clay masonry unit
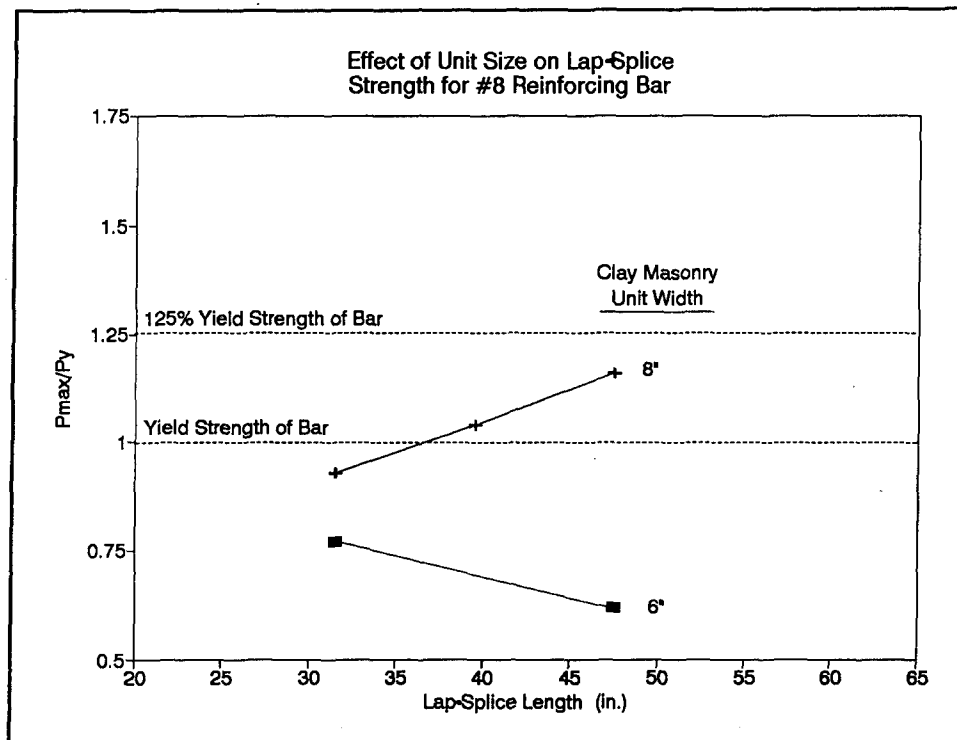
Figure 22.   Effect of unit size on lap-splice strength for No. 8 reinforcing
bar, clay masonry unit

masonry units. These plots show splice strength data for all specimens tested in Phases I and II. Several basic trends regarding failure type and the effect of splice cover are discussed below.

Splice strength is directly affected by unit width, and, more specifically, cover distance. Lap splices were contained within a single grouted cell constructed using half-units. Unit widths ranged from 3.625 to 11.625 in., however the unit length for all cases were all around 8.375 in. (this is equivalent to one grouted cell plus two end webs). Hence for 10- and 12-in.unit widths, the unit length governed minimum cover distances (see dimensions as shown in Figure 9). Reinforcing bar sizes No. 8 and 11 show an increase in splice strength when the unit width is increased from 8 to 10 in. (Figures 18 and 19), but show no significant effect when unit width is increased further to 12 in. Hence, the minimum cover distance and not unit width governs splice strength. For partially grouted walls, it would be necessary to consider the minimum of the unit width or thickness when determining lap length.

Three different types of failure were noted: bar pullout, pullout followed by splitting, and longitudinal splitting along the splice. In general, the strength of specimens dominated by tensile splitting were not affected by increasing splice length. For a given unit width, increasing lap length increased splice strength when bar pullout governed splice strength.

Specimens constructed with relatively large bars in a small unit width (large reinforcement ratio) did not provide sufficient cover to the lap splices to resist tensile splitting forces. For these specimens, where tensile splitting governed splice capacity, increasing the lap length had little or no effect on splice strength. This effect can be seen with No. 4 bars in 4-in. units, No. 6 bars in 6-in. units, and No. 8 bars in 8-in. units.

Increasing the lap-splice cover by using wider units increased resistance to tensile splitting, resulting in a stronger overall splice. The curves of Figure 17 display this trend. Where a No. 4 bar was spliced in 4-in. units, increasing lap length from 16 to 20 in. had no effect on splice capacity, presumably due to a splitting mode governing failure. Increasing the unit width by using 6- and 8-in. units results in a stronger splice where failure is governed by pull-out-induced splitting (splice in 6-in. specimen) and pure pullout (splice in 8-in. specimen).

It should be noted that only the specimens with No. 4 bars in 8-in. units displayed a classical pull-out type of failure. All other specimens failed by some type of tensile splitting. Where the cover was small (i.e., large reinforcement ratio) failure was predominated by brittle longitudinal splitting. Increasing the unit width slightly provides an intermediate reinforcement ratio and a more ductile splice; however, failure was ultimately tensile splitting initiated by large relative bar displacements. Specimens with No. 4 bars in 8-in. units had the lowest reinforcement ratio, with $\rho = 0.31$ percent; these specimens failed by pure pullout, fully developing the ultimate strength of the steel with no splitting observed.

Another observation can be made regarding the effect of increasing lap length on splice strength. All of the specimens displayed a linear relationship between lap length and splice strength up to yield. Hence, it was quite easy to develop the bar yield strength but disproportionately more difficult to develop 125 percent of the yield strength. As discussed previously, relative movement between two adjacent spliced bars will increase radial forces on the grout and increase tensile stresses. It appears that large displacements and bar slip associated with bar yielding accelerates splice failure in this regime.

Effect of bar size

A similar series of curves is shown in Figures 23 through 30, where splice strength of different size reinforcing bars is plotted for each unit size. These plots can be useful for help in determination of maximum bar sizes for each unit width. Data displayed in Figures 23 through 30 show that, for a given unit size, increasing the reinforcement ratio by increasing bar size has a distinct effect on splice strength.

A subjective evaluation of maximum bar size can be obtained by interpreting data shown in these plots. In some cases, a relatively short splice length was needed to develop 1.25 times the yield strength of the bar. For these specimens, it can be concluded that this combination of bar and unit
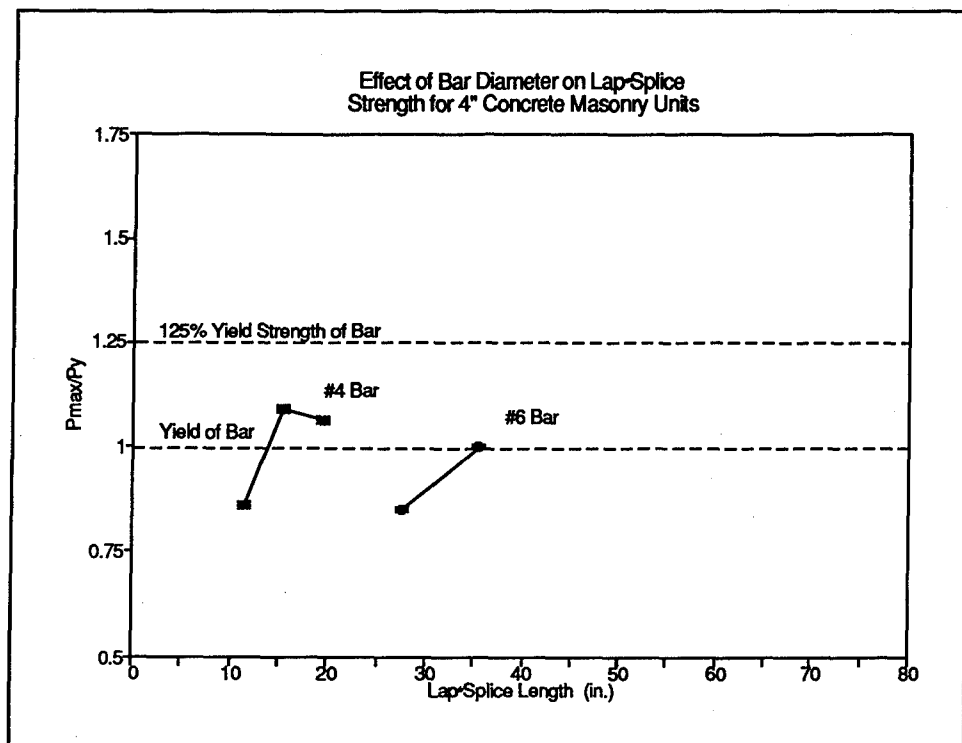
Figure 23. Effect of bar diameter on lap-splice strength for 4-in. concrete masonry units
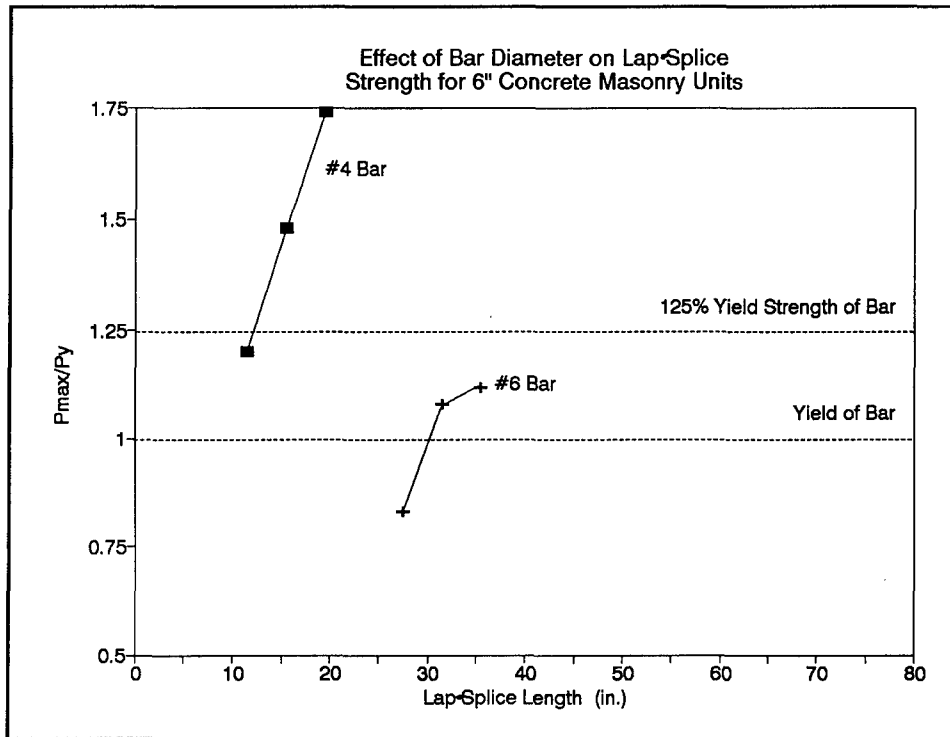
Figure 24.   Effect of bar diameter on lap-splice strength for 6-in. concrete
masonry units
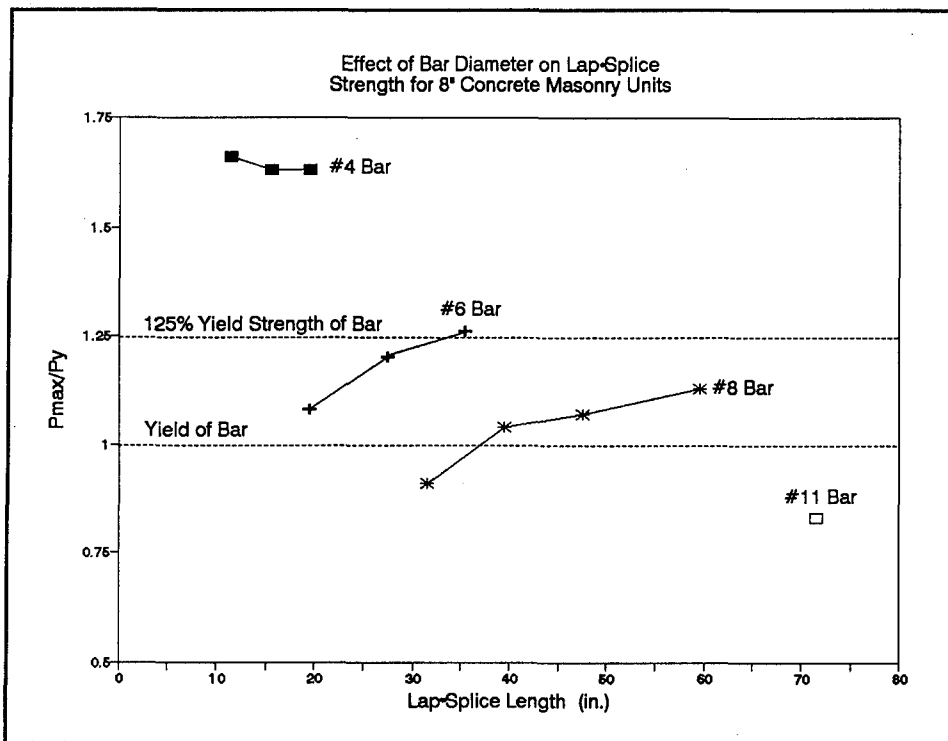
Figure 25.   Effect of bar diameter on lap-splice strength for 8-in. concrete
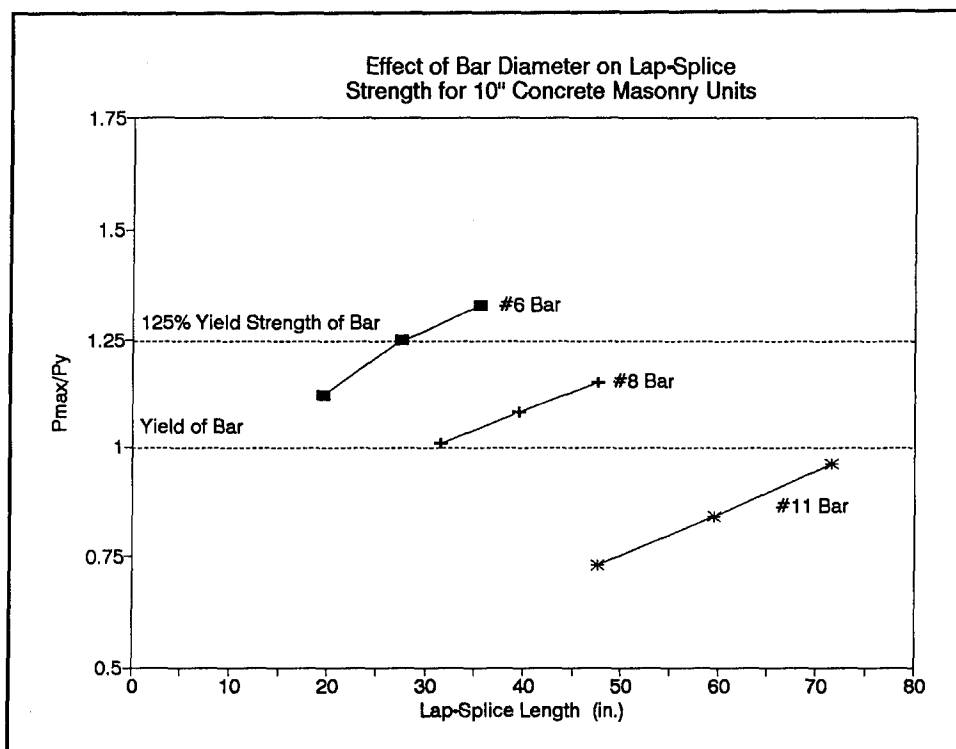masonry units

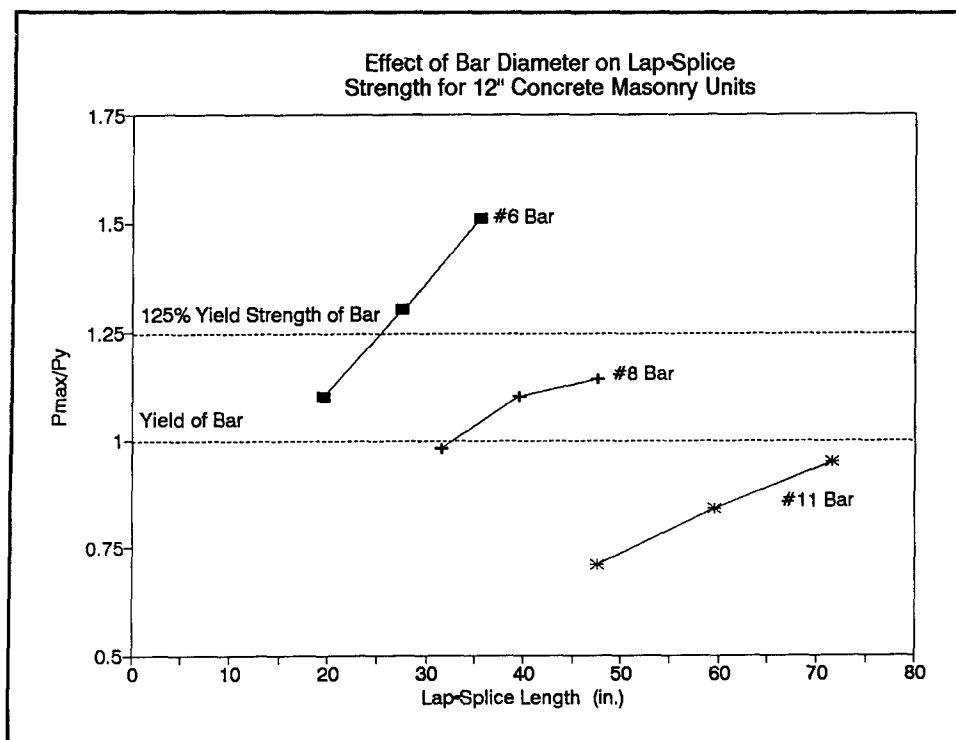Figure 26. Effect of bar diameter on lap-splice strength for 10-in. concrete masonry units

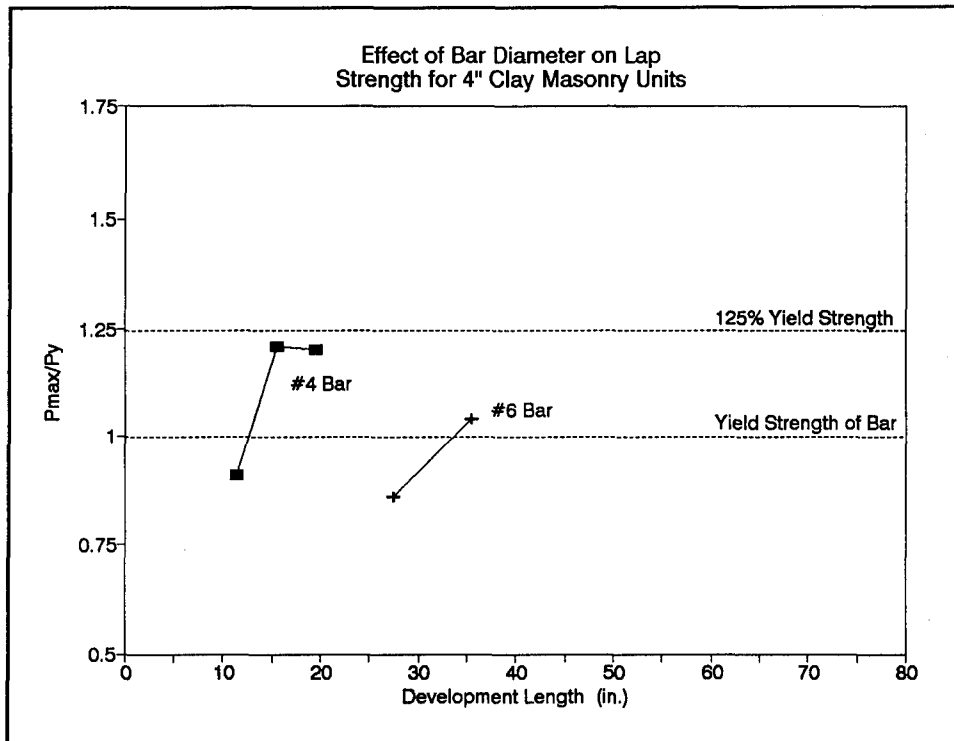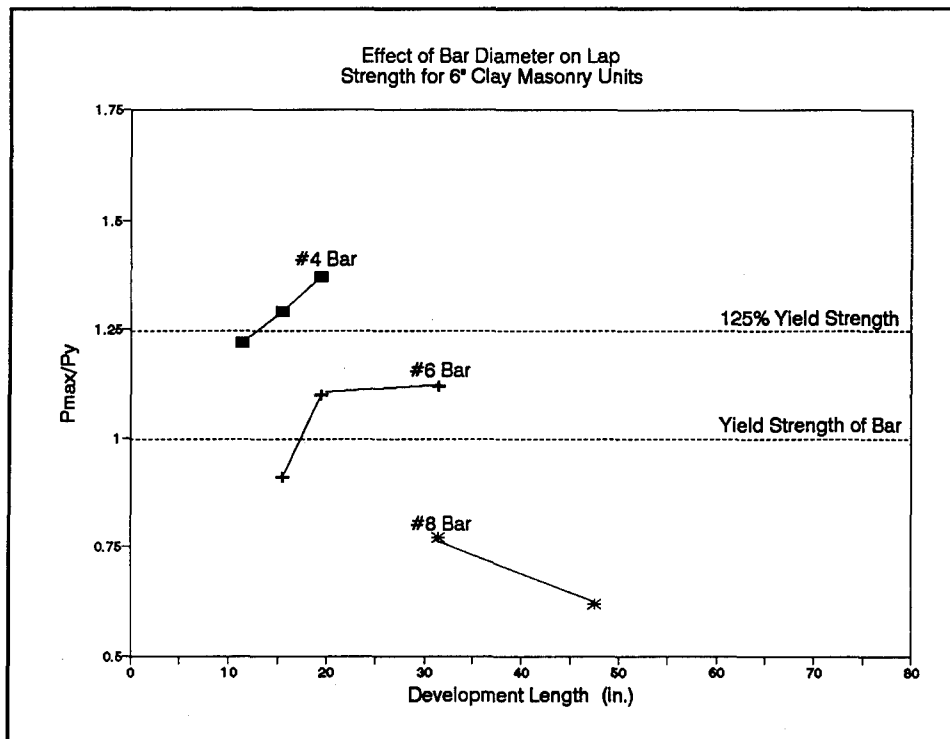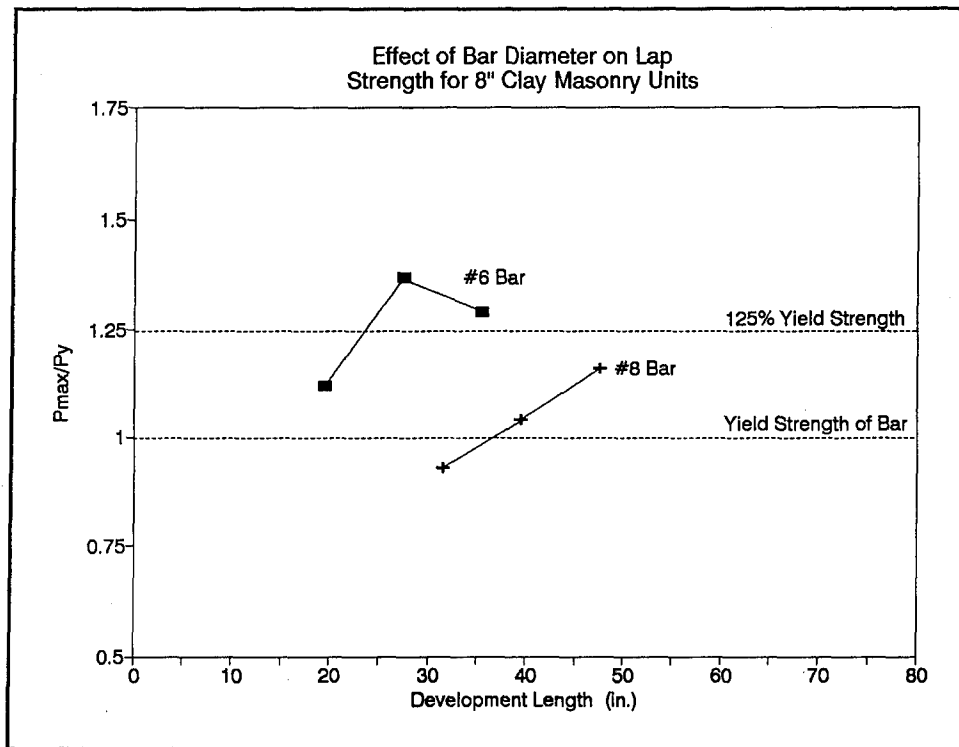Figure 27. Effect of bar diameter on lap-splice strength for 12-in. concrete masonry units

Figure 28.   Effect of bar diameter on lap strength for 4-in. clay masonry units

Figure 29.   Effect of bar diameter on lap strength for 6-in. clay masonry units

Figure 30. Effect of bar diameter on lap strength for 8-in. clay masonry
units

size provided sufficient ductility pullout and hence, would be acceptable.
Combinations which required large increases in lap length for a small in-
crease in strength indicate failure governed by longitudinal splitting.
These combinations of bar sizes and unit sizes may be deemed
unacceptable.

Effect of unit type

Specimens were constructed using both concrete and clay masonry
units to investigate the effect of unit type on lap splice capacity and behav-
ior. Average material properties listed in Appendix A for concrete and
clay units used in the CPAR study show significant variations in absorp-
tion, compressive strength, and tensile strength between the two unit
types. Concrete masonry units were significantly weaker in compression
and also had greater total absorption than the clay masonry units.

The measured compressive strength of the clay units was also three to
five times greater than the strength of the concrete units. Compressive
strength by itself is not expected to have a significant effect on lap-splice
strength, however, clay masonry units also have a greater compressive
modulus and tensile strength than the concrete units. Both the modulus
and tensile strength may have a direct effect on the masonry's resistance
to longitudinal splitting along lap splices.

52

Plots of lap strength versus lap length for different bar and unit types are shown in Figures 31 through 33. For these plots, P/P_y is normalized by the actual specimen width to account for the fact that the unit width of clay masonry specimens was 2 to 4 percent less than the unit width of concrete masonry specimens, due to slight differences in modular sizes. It should also be noted that the gross area of clay units varied from 50 to 12 percent less than the gross area of corresponding concrete masonry specimens due to differences in the configuration of grouted cells. This is because single-cell units were cut from full-size units for specimen construction, and the clay masonry units had three vertical cells: two large cells for rebar placement and one small intermediate cell. Concrete units, on the other hand, had two internal cells, each slightly larger than the clay unit cells. Unit widths, gross areas and cell areas for each unit type used are listed in Table 8.

As shown in Figures 31 through 33, the greater modulus and tensile strength associated with clay units appears to have a confining effect on the splice and increases resistance to tensile splitting failure. Splices in clay masonry are from 2 to 13 percent stronger than splices in corresponding concrete masonry specimens. The increase in strength is most noticeable for specimens with a large reinforcement ratio where failure was dominated by tensile splitting. This effect is less pronounced when bar pullout (small reinforcement ratio) governs splice strength.

There is one exception to the general trend. Splices of No. 4 bars in 6-in. clay masonry units were weaker than corresponding splices in 6-in. concrete masonry units. A possible explanation is that these splices were resisting loads in the range of 1.2 to 1.7 times the yield load. Splice behavior in this regime is dominated by large steel deformations, bar
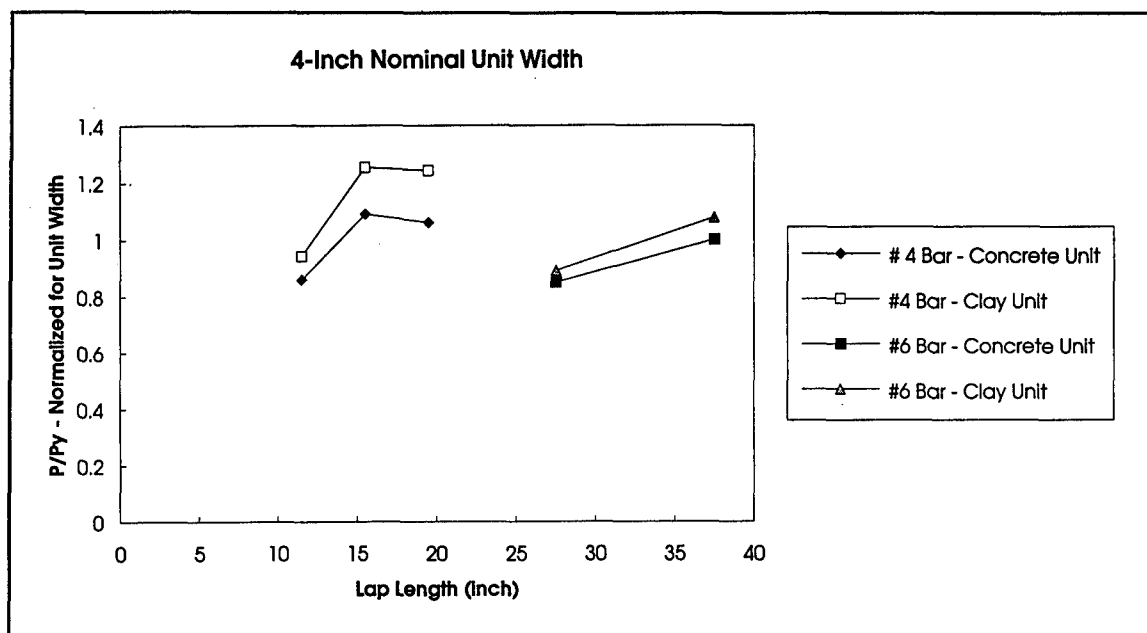

Figure 31.   Effect of masonry unit type on lap-splice strength, 4-in. units

slippage, and grout crushing in front of bar lugs. This behavior would be very sensitive to minor local variations in grout consolidation and material properties, rather than overall unit properties.

CPAR data on unit type effects does not agree with similar TCCMAR research conducted in Japan by Watanabe (1985). Watanabe found that for single-bar anchorages, clay brick masonry is not as effective at anchoring bars as concrete block masonry. However, this may be related to
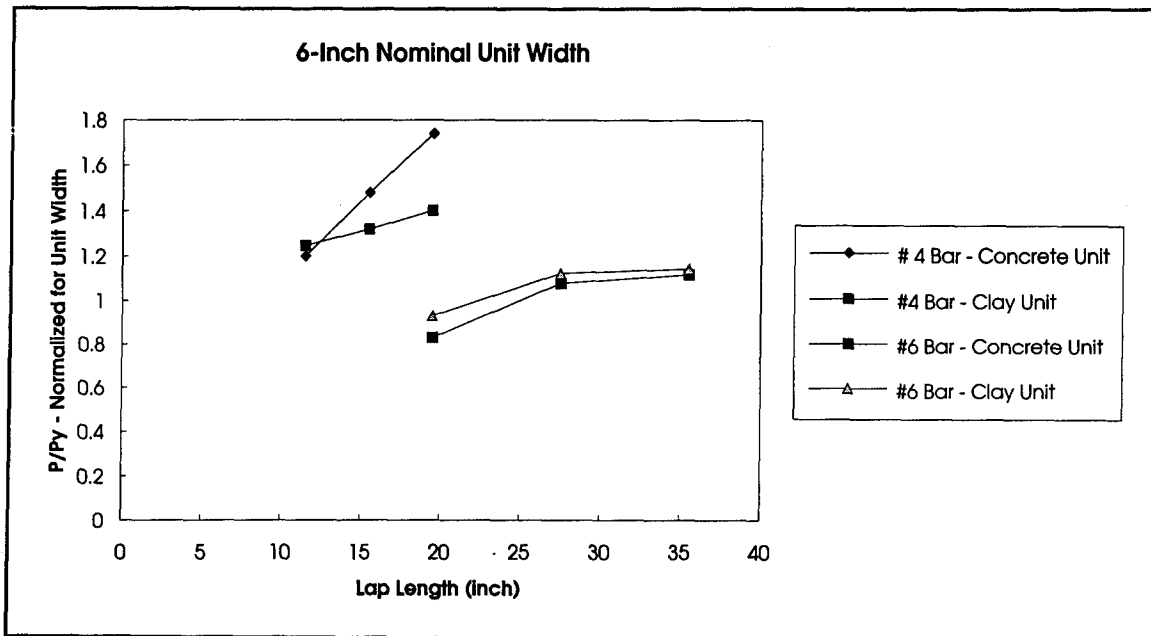
6-Inch Nominal Unit Width

Figure 32. Effect of masonry unit type on lap-splice strength, 6-in. units

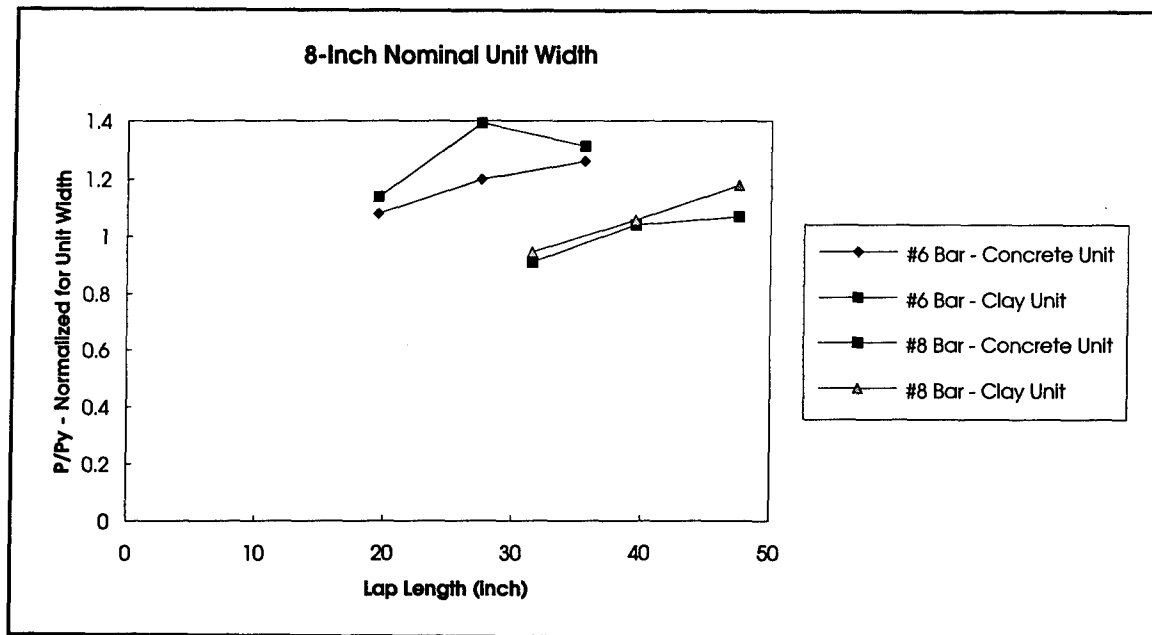**8-Inch Nominal Unit Width**

Figure 33. Effect of masonry unit type on lap-splice strength, 8-in. unit

Table 8
Unit Dimensions - Concrete and Clay Masonry Units

Unit Type	Gross Dim. in.	Cell Dim. in.	Gross Area, in.^{2}	Unit Net Area, in.^{2}	Cell Area, in.^{2}
4-in. CMU	8-3/8 × 3-5/8	5-7/8 × 1-1/2	30.36	21.55	8.81
6-in. CMU	8-1/8 × 5-5/8	6-1/8 × 3-1/2	45.70	24.27	21.44
8-in. CMU	8-1/8 × 5-5/8	6-1/8 × 3-1/2	61.95	32.21	29.74
10-in. CMU	8-1/4 × 9-5/8	5-3/4 × 6-3/4	79.41	40.59	38.81
12-in. CMU	8-1/2 × 11-5/8	5-5/8 × 8-1/2	98.81	51.00	47.81
4-in. CB	4-1/4 × 3-1/2	2-7/8 × 1-3/4	14.88	9.84	5.03
6-in. CB	7-1/8 × 5-1/2	4-3/4 × 2-3/4	39.19	26.13	13.06
8-in. CB	7-1/4 × 7-5/8	4-5/8 × 5	55.28	32.15	23.13

problems during specimen construction. Watanabe noted that the more absorptive clay units hampered grout placement, resulting in poor grout consolidation for these specimens. No problems were noted during grout placement in CPAR specimens, and examination of failed specimens revealed no significant voids present in the grout in clay or concrete masonry specimens.

Discussion of Results

Comparison with design code recommendations

A comparison between lap splice lengths required by different building codes was discussed in the background for this chapter. The 1992 Uniform Building Code (UBC) (International Conference of Building Officials 1992), ACI 530-88/ASCE 5-92/TMS 402/92 *Building Code Requirements for Masonry Structures* (ACI 1988a), ACI 318-89 *Building Code Requirements for Reinforced Concrete* (ACI 1989), and the proposed *Masonry Limit-States Design Standard* (Masonry Standards Joint Committee in preparation) were all compared. In the following section, the validity of the MLSDS formula is examined by comparing design lap lengths with lap lengths determined during experimental testing.

Lap length requirements based on CPAR data

Current masonry design standards require mechanical splice connections to develop a tensile strength greater than 125 percent of the reinforcement yield strength. This criteria have been adopted here, as well, as performance criteria for lap splices. Experimental results can be used to determine lap lengths required to develop 125 percent of the yield

strength by either interpolation or extrapolation of the experimental data curves in Figures 16 through 30. The points where the curves cross the line representing 125 percent of the reinforcement yield strength are then used to determine the appropriate lap. Data plots showing lap lengths required to develop 125 percent of bar yield strength for different size concrete masonry units are shown in Figures 34 through 37.

The experimental data obtained during the CPAR program fit the general shape of the design formula developed by Soric and Tulin (1987), yet appear to be shifted slightly upward for bar sizes 6, 8, and 11. This effect can be explained by the manner in which Soric determined the coefficient C in Equation 6. The empirical constant C can be determined as a function of material properties and geometry:

$$C = \frac{l_d (t - d_b) f_{gt}}{d_b^2 f_y}$$

(8)

Soric used results from lap splice tests using No. 4 and 7 bars in 6-in. units and determined an average value of $C = 1.75$. CPAR results are similar to Soric's but are not identical. The main discrepancy between Soric's original formulation and CPAR results arises in the values used for grout tensile strength: Soric measured a direct grout tensile strength of 439 psi (3.0 MPa) (tested using the briquette specimen of ASTM C 190, Test Method for Tensile Strength of Hydraulic Cement Mortars (1990k)) and grout cylindrical tensile splitting strength of 732 psi (5.0 MPa) (measured in accordance with ASTM C 496, Test Method for Splitting Tensile Strength of Cylindrical Concrete Specimens (1990r)) corresponding to a grout compressive strength of 3,760 psi (25.9 MPa). An average grout tensile splitting strength of 430 psi (2.9 MPa) for concrete masonry specimens and grout compressive strength of 2,910 psi (20.0 MPa) were measured during the CPAR program. Soric determined a mean value of $C = 1.75$ based upon the grout tensile strength using the briquette specimens, however only the grout tensile splitting strength was measured during the CPAR program. The relationship between grout compressive strength and tensile splitting strength is approximately equivalent for both sets of data; hence, it is possible to recalculate Soric's values for the coefficient C to (a) account for the fact that the CPAR grout strengths were lower; and (b) base the model upon tensile splitting strength rather than direct tensile strength. This approach may, in fact, be more useful for design purposes because the direct tensile test is rarely conducted in practice.

Curves representing lap lengths required by application of Soric's formula, with $C = 1.75$, are shown in Figures 34 through 37 along with CPAR data. For most cases, Soric's formula underestimates the required splice length. The general shape of Soric's formula matches CPAR data quite well and, if the coefficient C is recalculated for each bar size, the calculated lap length matches quite well with splice length determined experimentally. The coefficient C was determined for each bar size and does not
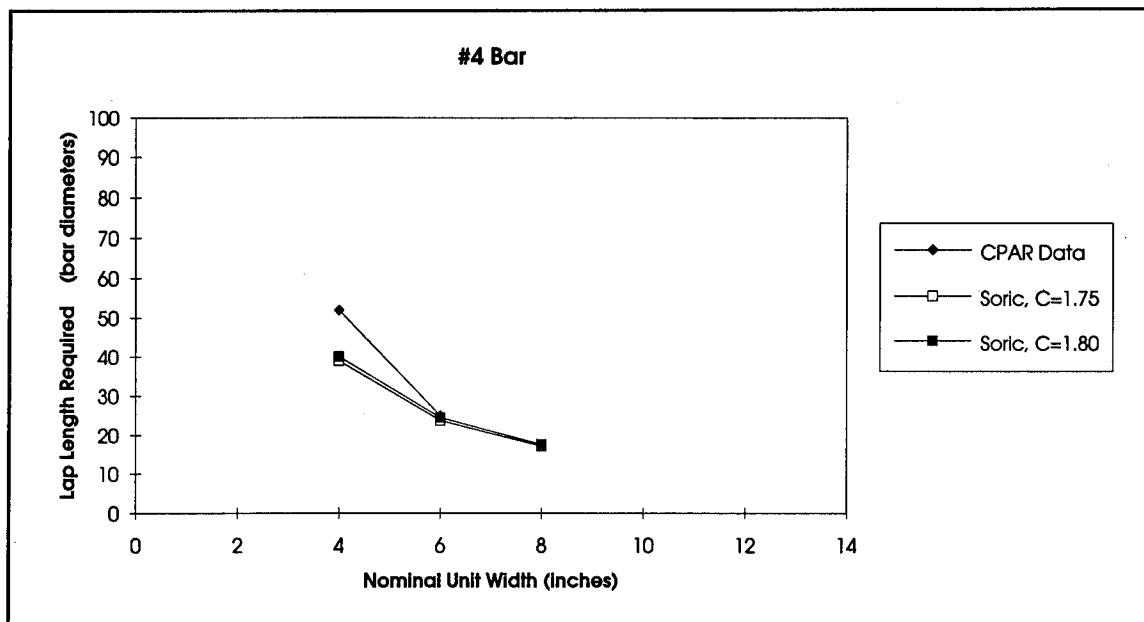
Figure 34.   Required lap length, No. 4 reinforcing bar
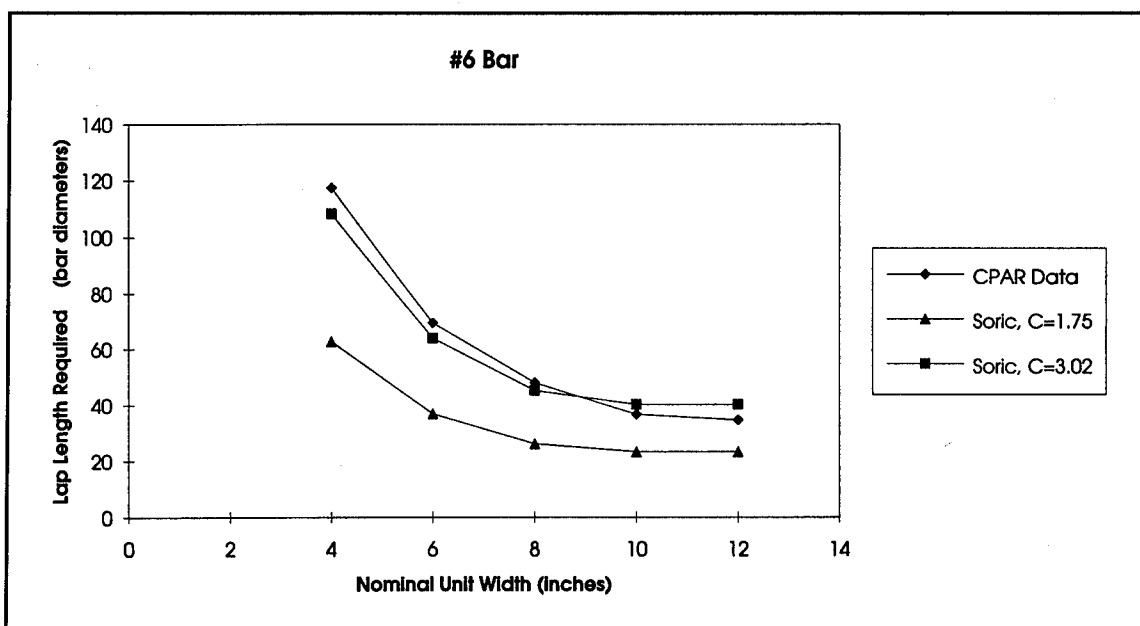

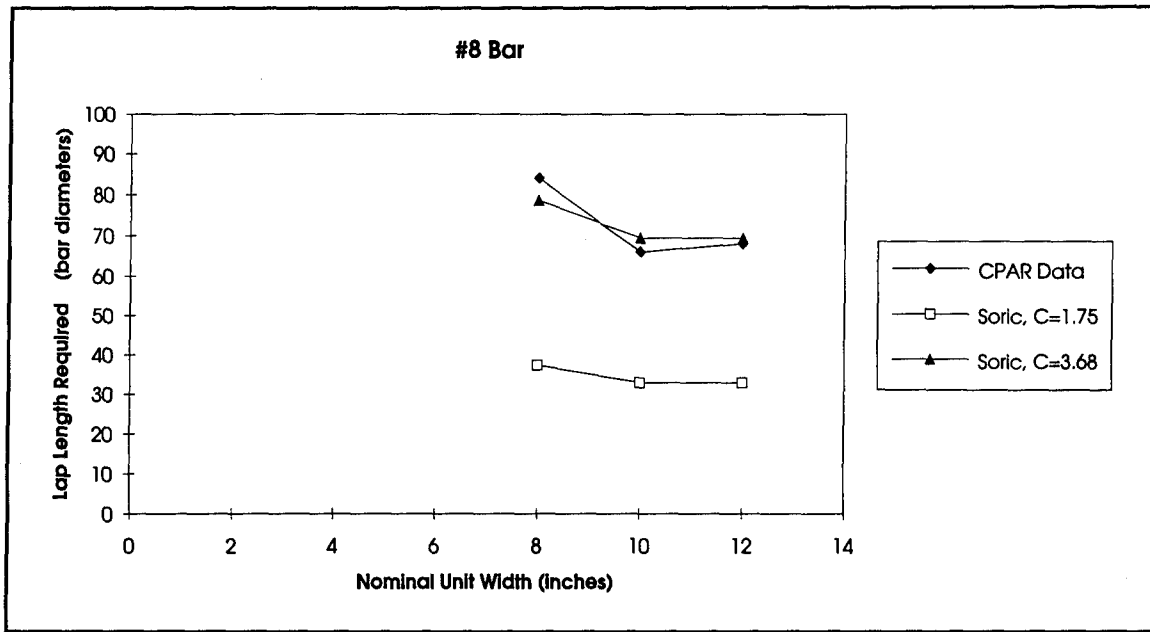Figure 35.   Required lap length, No. 6 reinforcing bar

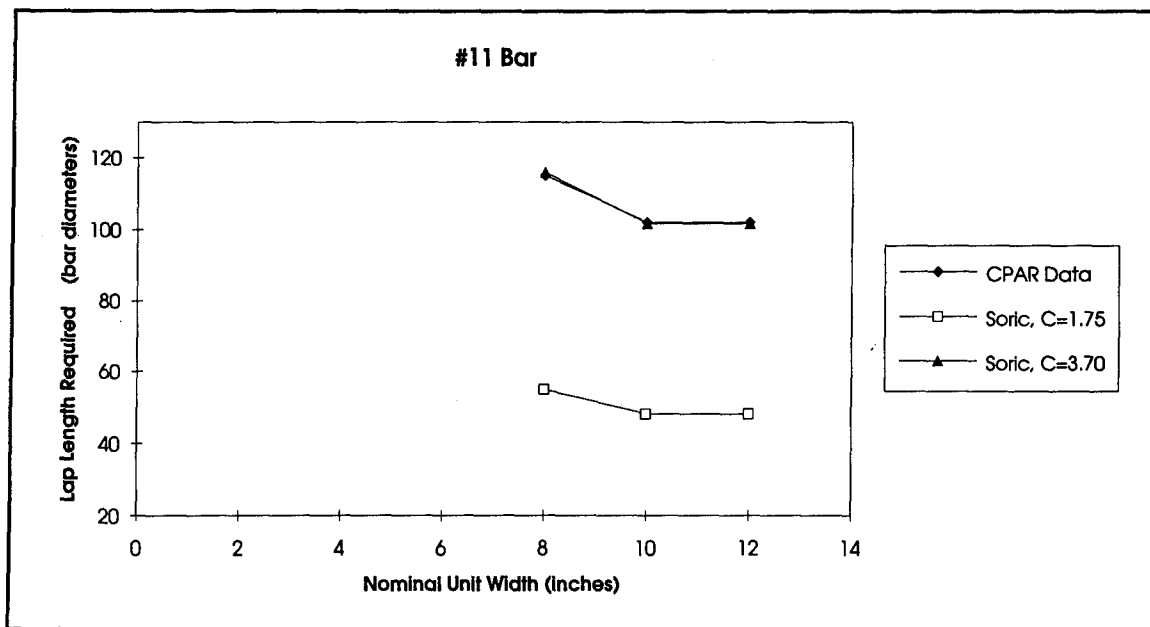Figure 36.   Required lap length, No. 8 reinforcing bar

Figure 37.   Required lap length, No. 11 reinforcing bar

appear to be a constant value, ranging from 1.8 for No. 4 bars to 3.02, 3.68, and 3.7 for No. 6, 8, and 11 bars, respectively.

Note that the data curves for No. 11 bars are suspect because no splices of No. 11 bars reached yield, let alone 125 percent yield. Hence, all information for No. 11 splice lengths are based upon extrapolation of CPAR data and may not be reliable.

CPAR lap-splice data suggest that the coefficient C, used in Equations 6, and 7 indirectly, for determination of lap-splice length, is not a constant value but varies dependent upon bar diameter. The analytical model derived by Soric is based upon the premise that bond stresses cause tensile stresses in the grout, precipitating splitting failure along the splice. Bond stress values are difficult to determine and most previous investigations and design codes have relied upon nominal or average bond stress values for anchorage and splice length determinations. However, bond stresses are not distributed evenly along the length of a spliced bar but instead range from a peak near the beginning of the splice to approximately zero at the end of the splice. It is the peak bond stress and distribution of peak stresses, not the nominal bond stress, that precipitates failure.

Soric investigated the distribution of bond stresses along spliced bars and proposed several analytical models for describing bond stresses. The coefficient C used in the formulation is based not upon the bond stress models but is described as an empirical parameter, "accounting for the nonuniformity of bond stresses along the rebar length." It would be interesting to investigate further the effect of peak bond stresses and the distribution of bond stresses on lap-splice failure; it may be possible to develop an analytical model for predicting which failure mode will predominate for different material and geometric parameters.

The coefficient C varies for different bar sizes, implying that the distribution of bond stresses also varies and is related to the bar diameter. This is not totally unexpected: bond stresses are distributed around the perimeter of the bar, where the perimeter varies directly with bar diameter. The total force that must be resisted by bond stresses (125 percent P_y), however, is related to the bar area, which varies with the square of the bar diameter. Therefore, for splices of larger diameter bars, it can be expected that peak bond stresses will be distributed along a greater initial bar length (assuming that the peak bond stress is governed by grout strength and is constant from one size to the next).

The preceding discussion may describe why the coefficient C varies for different bars sizes, however additional investigation into the exact cause for this variation is necessary. It would be interesting to determine if variations in peak bond stresses and the nature of bond stress distributions are related to tensile splitting failure of lap splices. Soric's model for bond stress distribution does have bond stresses varying as a function of the bar diameter, expressed as the reinforcement ratio (Soric and Tulin 1987); this model could be investigated further for insight into the situation.

Regardless of the outcome, Soric's model for determination of lap-splice length is a reasonable approximation of lap-splice behavior. The model accurately describes the tendency of splices in areas with a large reinforcement ratio (i.e., large-diameter bars in narrow units) to fail by tensile splitting and requires lap lengths of 100-bar diameters and greater for these cases. The model also requires a shorter lap length in splices where the reinforcement ratio is small. It appears as if the coefficient C varies from 1.8 for No. 4 bars, to 3.0 for No. 6 bars, to 3.7 for No. 8 bars.

Maximum reinforcement ratio and maximum bar size

In addition to satisfying strength requirements, lap splices must be sufficiently ductile to prevent sudden failure in the case of unanticipated loads. The preferred failure mode would be ductile yielding and/or pull-out of the spliced bars. Brittle failure by formation of longitudinal splitting cracks should be avoided. Hence, to prevent brittle splitting failure, the peak circumferential tensile stresses radiating from the spliced bars at $1.25 \, f_y$ must not exceed the tensile strength of grout/unit assemblage.

It should be possible to relate bond stresses at a bar stress of 1.25 fy to masonry tensile resistance and calculate the maximum reinforcement ratio. Work by Cheema (1981) and Soric and Tulin (1987) have addressed this with the use of iterative computerized simulations. This subject deserves additional attention.

The UBC limits the reinforcement ratio to 6 percent of the cell area for hollow unit construction, or 12 percent at lap splice locations. The MLSDS allows a maximum reinforcement ratio of 4 percent of the cell area; however, it does not explicitly address the reinforcement ratio at lap splice locations. For consistency, reinforcement ratio at lap splices is calculated here as the ratio of the area of *one* of the lapped bars to the net area of the grouted cell.

Observations during testing may also be used to qualitatively determine the maximum reinforcement ratio. Results from CPAR testing show a direct correlation between reinforcement ratio and splice behavior. Bar and unit size combinations with a small reinforcement ratio develop the requisite 125 percent of bar yield with a smaller splice length than specimens with a large reinforcement ratio. Specimens with a small reinforcement ratio were also more inclined toward a ductile failure, usually precipitated by pullout or pullout-induced splitting. Specimens with a large reinforcement ratio failed predominately by brittle longitudinal splitting before pullout was observed and in many cases before the bar yield strength was fully developed.

A problem remains, however: How is the difference between small and large reinforcement ratios to be quantified, and how is a limiting reinforcement ratio to be defined? The preferred behavior would be to have a "ductile" splice, and it would be best to prohibit splitting failure altogether.

60

Nearly all of the CPAR specimens ultimately failed by some type of splitting, however. Often this splitting was induced by large relative displacements between spliced bars occurring during yielding of the bars. The previously mentioned criteria requiring lap splices to develop 125 percent of the reinforcement yield strength may also be too prohibitive. At a force level of 125 percent of f_y, the steel is well into the strain-hardening portion of the curve and has undergone large deformations.

The previously adopted strength criteria, which stipulate that the splice develop 1.25 times the steel yield strength, actually imply a ductile splice. Hence, it may not be necessary to fully prohibit all types of splitting behavior. As the bar is loaded to 125 percent of the yield strength, large deformations associated with steel yielding provide adequate ductility. Displacement ductilities for lap splices of bar sizes No. 4, 6, and 8 are provided in Table 9.

Table 9	
Deformation Ductility of Steel Reinforcing Bars and Lap Splice Specimens	
Specimen	Ductility
Single No. 4 Bar	8.4
8CON4-32	3.3
Single No. 6 Bar	9.1
8CON6-36	6.7
Single No. 8 Bar	9.7
8CON8-48	8.3
Single No. 11 Bar	8.5
Note: Ductility calculated as deformation at 125 percent of yield strength divided by deformation measured at yield.	

Displacement ductility of single bars tested in tension are also shown for comparison. Displacement ductility is calculated in these cases as the measured specimen deformation at 125 percent of yield divided by the deformation at yield:

$$\mu = \frac{\Delta_{1.25 p_y}}{\Delta_{p_y}} \tag{9}$$

Specimen deformations were obtained by subtracting bar slip from measured overall specimen deformations. The values listed in Table 9 show that for reinforcing bars stressed to 125 percent of the yield stress deformation ductilities of 8.4 to 9.7 can be expected. It is interesting to note that for lap splices in masonry, the deformation ductility is reduced for every case, suggesting that most deformations are occurring in the vicinity of only a few discrete cracks. This effect is most noticeable for No. 4

bars in 6-in. units with a small reinforcement ratio and is less pronounced for No. 6 and 8 bars with larger reinforcement ratios.

Subjective evaluation of test data can also provide information on reinforcement ratio limitations. The plots of Figures 16 through 30 show splice strength as a function of lap splice length for different bar and unit sizes (i.e., different reinforcement ratios). When bar pullout or yielding governs splice strength, increasing the lap length correspondingly increases the splice strength. When the splitting mode of failure governs, increasing lap length has little or no effect on splice strength. Similarly, for a given bar size, increasing unit width will increase lap strength when splitting failure governs but will have little effect when pullout and bar slip govern.

Based upon empirical evaluation of test results as described, lap splices of different size bars in different unit widths can be split into two categories: those dominated by splitting failure, and those failing by pullout or bar slip. Results of a subjective overview of specimen behavior are listed in Table 10, where reinforcement ratios limiting splitting behavior are tabulated for different bar sizes in both concrete and clay unit masonry. It is interesting to note that in all cases the limiting reinforcement ratio in clay unit masonry is consistently greater than the limiting reinforcement ratio in concrete unit masonry. This agrees with the previous observation suggesting that the stronger clay units have a confining effect on lap splices, increasing resistance to tensile splitting. Another observation is that the limiting reinforcement ratio does not appear to be constant for all bar sizes, but appears to increase with increasing bar diameter.

Table 10
Reinforcement Ratios for Limiting Brittle Splitting Behavior of Lap Splices in Both Concrete and Clay Unit Masonry

Bar Size (No.), Unit Type*	Gross Area Reinforcement Ratio (Cell area reinforcement ratio listed in parentheses)		
	Splitting	No Splitting	Questionable
4,CMU	0.66 (2.10)	0.42 (0.90)	
4,CBU	1.31 (3.98)	0.50 (1.68)	
6,CMU	0.92 (1.98)	0.68 (1.46)	
6,CBU	1.10 (3.71)	0.80 (1.90)	
8,CMU			0.80-1.22 (1.63-2.62)
8,CBU	1.98 (6.65)		1.43 (3.42)
11,CBU			1.58-1.88 (3.22-4.02)

Note: The questionable category is used where splices behaved in a ductile manner but did not satisfy the strength criteria of 1.25 P_y
*CMU = Concrete masonry unit; CBU = Clay brick unit

Using this subjective criteria leads to the following recommendations for acceptable lap splices: no splices of any size reinforcement in 4-in. units; splices of No. 4 bars in 6-in. units; No. 4 through 6 bars in 8-in. units; and No. 4 through 8 bars in 8-, 10-, and 12-in. units. These recommendations suggest the gross area reinforcement ratio be limited to less than 1 percent (cell area reinforcement ratio less than 2 percent). Currently the MLSDS allows a maximum reinforcement ratio of 4 percent, based on the cell area, at splice locations. Based upon experimental data from the CPAR program, it appears that reinforcement ratio limitations at lap splice locations need to be reduced.

Conclusions

Based upon experimental data from the CPAR test program, there are several conclusions regarding lap-splice capacity and behavior in reinforced masonry.

Increasing unit width increases splice capacity and reduces the likelihood of failure by tensile splitting. Minimum cover distance (either unit width or length of a grouted cell) will control splice strength. For partially grouted walls, minimum cover distance, and not unit width alone, should be used in Equation 7 for calculation of required lap lengths.

Lap splices in clay masonry specimens were stronger than comparable lap splices in concrete unit masonry. Clay units have a greater tensile strength and modulus than concrete units, providing a slight confining effect to the splice and reducing the tendency toward formation of tensile splitting cracks.

Large bars in thin walls providing a large reinforcement ratio have a tendency to fail by brittle tensile splitting. This failure usually occurs at a load level that is much less than the specified strength criteria that the splice develop 125 percent of the reinforcement yield strength. The reinforcement ratio limiting splitting failure varies with bar size, from 1 percent for No. 4 bars to approximately 2 percent for No. 8 bars. Acceptable reinforcement ratios for lap splices in grouted clay masonry are from 10 to 20 percent greater due to a confining effect that the stronger clay units have on the splice.

The formula adopted for use by the Masonry Limit-States Design Standard describes general trends observed in CPAR data, but usually underpredicts required lap lengths. The coefficient C varies with bar diameter from 1.8 for No. 4 bars, to 3.0 for No. 6 bars, to 3.7 for No. 8 bars. The formula provides very accurate predictions of required lap lengths when modified values for C are used.

3   Tension-Stiffening Tests

Problem Statement

Analytical modeling of reinforced masonry to predict strength and deformation under load requires proper representation of material behavior. While considerable attention has been given to understanding masonry behavior under compressive stresses, little research has been conducted on the tensile behavior of reinforced masonry. Understanding the tensile behavior, especially in the postcracked state, is necessary for the analysis of flexural elements such as walls under in-plane horizontal loadings and walls under out-of-plane bending loads.

Before formation of tensile cracks, the behavior of reinforced masonry subject to direct tension is approximately linearly elastic with the steel bar and the other materials (grout, unit, and mortar) experiencing the same strain levels and stress levels proportionate to their individual elastic moduli. At some strain level, tensile cracking will occur resulting in a redistribution of stress, since that portion of load previously carried by the masonry materials is now carried by the steel across the crack (Figure 38). Beginning at the crack interface, a zone of stress transfer occurs where tensile load is transferred from the steel to the concrete. The transfer results primarily from mechanical interlock between the bar ribs and grout and to a much lesser extent from steel-grout adhesive bond. Additional tensile strain will cause additional tensile cracks to occur. Between tensile cracks there are zones in which the masonry materials carry a portion of the total tensile load and add stiffness to the cracked composite.

The cracking behavior and tensile stress redistribution is a complex phenomenon and has been extensively studied for reinforced concrete and, to a very limited extent, for masonry. Analytical expressions have been developed to account for this behavior (Soric and Tulin 1987, Gupta and Maestrini 1990, Hegemier, Murakami, and Hageman 1985), but they are not suitable for use in analysis of large structural elements, since this would require modeling of every reinforcing bar and crack in the structure.
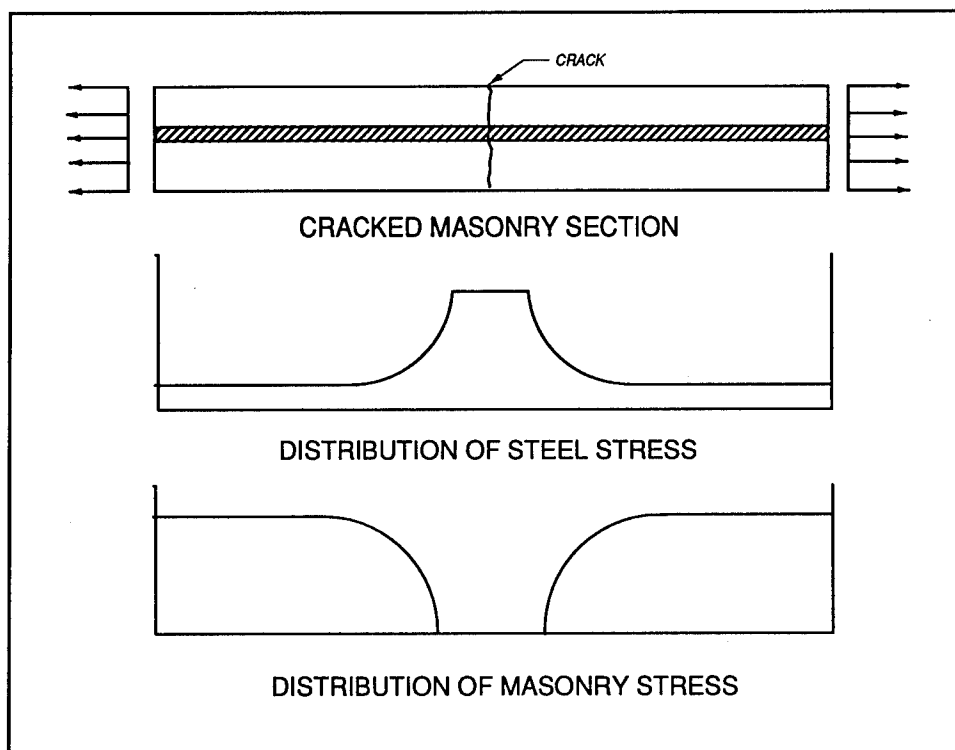
Figure 38. Schematic of reinforced masonry element subjected to tensile forces

To overcome this problem, averaged properties of reinforcing bar geometry and reinforcing bar-grout behavior are employed to model the tensile behavior of the masonry (Ewing, El-Mustaphe, and Kariotis 1987; Seible, LaRovere, and Kingsley 1989). As a result, the average stiffness of the cracked member is increased over that of the reinforcing bar alone. This effect is termed "tension stiffening." This represents, on an averaged basis, the cumulative effects of the very complex interaction that occurs between the reinforcing bar and the concrete as the tensile strain is progressively increased.

The increased stiffness which results from the interaction of the concrete and steel in tension can have a significant effect on overall structural response. If only the properties of the reinforcing steel are used, calculated deflections can be overestimated. The tension stiffening effect is most pronounced for response in the serviceability range and for lightly reinforced members (Massicotte, Elwi, and MacGregor 1990; Prakhya and Morley 1990; Goto 1971).

In the case of reinforced masonry, which is typically lightly reinforced to improve its ductile response, the tension stiffening effect must be accounted for to correctly calculate flexural response deflections. When limit-states design procedures are adopted in the United States (Masonry Standards Joint Committee 1993), accurate determination of deflections

will be essential because certain limit states will be based on structural deflections, e.g., maximum drift angles for shear walls.

This chapter discusses the available data relating to the tensile behavior of reinforced masonry including bond-slip data. Also reviewed is information relating to bond-slip, tension stiffening, and analytical modeling in reinforced concrete. Subsequently, the experimental program to investigate tension-stiffening behavior in masonry is presented and discussed.

Background

Review of bond/development length studies in masonry

Research into the interaction of reinforcing steel and masonry is limited. Many design practices and design standard requirements are based on information from reinforced concrete research in the absence of data for masonry. This practice may not be warranted because reinforced concrete is a two-component material (concrete, steel), while reinforced masonry is a four-component material (masonry unit, mortar, grout, and steel). The varying tensile strengths and moduli and bond strengths between these materials create a significantly more complex material for analysis and characterization than reinforced concrete.

Studies of reinforcing bar bond and development length in masonry have been conducted by several investigators. Soric and Tulin (1987) conducted a significant study of bond and slip in both concrete masonry and hollow unit clay masonry testing single bar anchorage and lap splice behavior using a number of testing configurations. A model for single-bar anchorage behavior was developed based on specimen geometry and the grout tensile strength.

Baynit (1990) studied the effects of bar diameter, multiple bars, embedment length, bar spacing, and grout strength and slump on ultimate bond strength in reinforced concrete masonry. A comparison of results from beam tests to those from pull-out tests showed that the pull-out tests overestimated ultimate bond stress.

Cheema (1981) investigated the pull-out resistance of single-bar anchorages grouted in the cells of concrete block masonry. These tests simulate behavior of foundation dowels or roof anchors grouted into masonry.

Japanese investigators (Matsumura 1990, Kubota and Kamogawa 1985, Watanabe 1985) have studied reinforcing bar development length in connection with lap splice design for masonry. These experimental studies were primarily directed toward establishing design criteria for anchorage and splice lengths.

Notably absent from all these studies have been either a discussion or measurement of possible tension stiffening behavior. Also lacking is information on expected cracking patterns in masonry as a function of reinforcement parameters.

Tension Stiffening of Reinforced Masonry

Only one study consisting of three specimens has been found which addresses the tension-stiffening effect in reinforced masonry loaded by in-plane loads (Nunn 1980, Hegemier, Nunn, and Arya 1978). Test panels, 64 in. by 64 in., were cut from a larger section to provide varying angles between the specimen edge and the masonry bedjoint. Test specimens were constructed from standard 8- by 8- by 16-in. fully grouted concrete blocks. A stiff biaxial load frame enclosed 16 servo-controlled 120-kip actuators which were used to load the specimen (four to a side).

Proportional loadings were applied to all biaxial specimens to produce zero stress on the head joints. The ratio of compressive stress, σ_c, to tensile stress, σ_t, is given by:

$$\frac{\sigma_c}{\sigma_t} = \cot^2 \theta$$

(10)

where θ is the angle between the bedjoint and applied compressive load direction.

Three reinforced masonry specimens were tested in this program. Two No. 5 bars were installed in each direction at a spacing of 32 in. on center, giving a steel ratio of 0.0013. The three specimens had layup angles of 0, 45, and 70 deg. The 45-deg specimen gave a stress ratio of 1:1, while the 70-deg specimen had a stress ratio of 7.5.

The 0-deg specimen was loaded by uniaxial tension-compression cycles with the tension loads producing progressively greater cracking strain levels. The compression side of the cycle produced low stress levels of approximately 40 psi.

The three specimens had on average a cracking stress in the range of 65 to 95 psi, followed by a drop in tensile stress to 55 psi. Subsequent load cycles produced increased masonry tensile stress to a level of about 75 psi at a hardening rate of 1.5×10^5 psi. The limited data suggest that the ultimate postcracking tensile strength is independent of the orthogonal compressive stress.
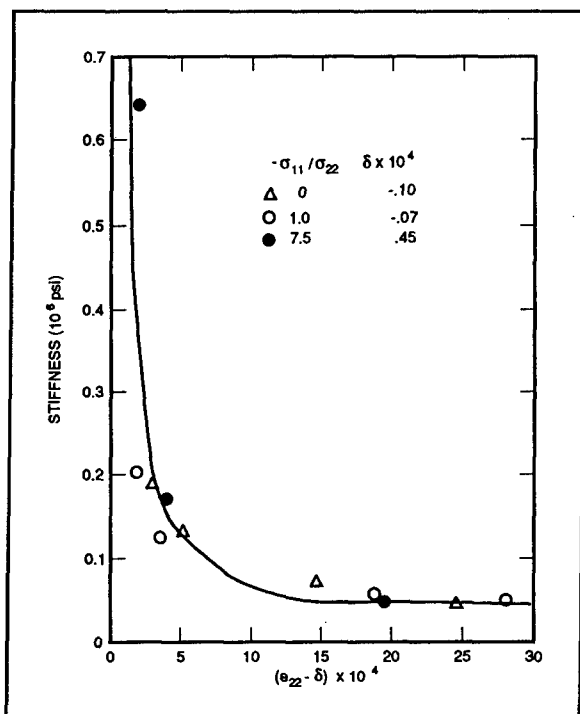
Figure 39. Tensile stiffness as a function of tensile strain (after Nunn 1980)

The postcracking tensile load-unload cycles permitted an evaluation of the tensile stiffness degradation as a function of tensile strain. The data from the three tests were plotted on the same curve once a strain offset was accounted for (Figure 39). The strain offset term has different values for the three layup angles tested. The curve has the form of $1/\varepsilon$ and becomes asymptotic to the steel stiffness at strains of about 20×10^4.

Houston and Tadros (1990) discuss deflection analysis methods for single-wythe reinforced masonry flexural members subject to out-of-plane loads. Six methods for computing deflections are presented and compared to experimental data from concrete masonry tests. Tension-stiffening effects had a significant influence in these analysis methods and can be incorporated by (a) developing a suitable masonry tensile stress-strain curve, (b) developing an empirical average moment of inertia for the entire length of beam, or (c) by developing empirical interpolation relations between cracked and uncracked section behavior. Predicted versus measured deflections were calculated using all six analytical methods for the experimental data available. Variations in predicted flexural deflections were over 100 percent dependent on the tension stiffening assumption used in the analysis.

Two recently developed finite element method programs for the in-plane analysis of reinforced masonry (Ewing, El-Mustapha, and Kariotis 1987; Seible, LaRovere, and Kingsley 1989) have used assumptions for tension stiffening behavior based on experimental data from reinforced concrete. These have included a tension-stiffening model developed by Vecchio and Collins (1982) as well as linear, bilinear, and exponential decay models. These models were chosen in the absence of any experimental data for reinforced masonry. Parametric studies have shown that calculated shear wall strengths and deflections will vary depending on the tension-stiffening model chosen.

68

Tension stiffening in reinforced concrete

Micromechanics approach. Considerable study has been directed toward determining the cracking behavior of reinforced concrete in tension. Experimental studies (Gerstle and Ingraffea 1991, Goto 1971) have shown that the adhesive bond between the bar and the concrete is destroyed at low stress levels with the stress transfer arising from the interaction of the concrete and the ribs of the bar accounting for the major part of the so-called bond stress. In reinforced concrete, cracking starts at the rib locations and grows outward forming a series of primary and secondary cracks. The width of the crack measured at the surface is greater than the width at the bar depth due to contraction of the partially stress-relieved concrete and to concrete-rib interaction (Lutz and Gergely 1967).

Many factors influence the distribution of tension cracks in a concrete member including bar spacing, bar diameter, steel ratio, cover distance, and angle between the crack and reinforcing steel. Formulae for calculating crack widths and spacings are discussed by Williams (1986) and evaluated using results of direct tension tests on large reinforced concrete panels.

Tensile cracking in concrete is not a perfectly brittle phenomenon as is often assumed but, under strain-controlled conditions, concrete will exhibit a finite postpeak decreasing or softening stress-strain curve (Figure 40) (Gopalaratnam and Shah 1985). For heavily reinforced members, the concrete tension softening curve is important in determining first cracking load and subsequent tension stiffening behavior (Bortolotti 1991).

Macromechanics approach. Measurement of local bond stress and slip along an embedded reinforcing bar subject to tension is difficult and sensitive to experimental error. Moreover, the relationship between bond stress and local slip varies along the length of the bar and with the magnitude of loading. For these reasons, the majority of finite element formulations have used averaged quantities to represent the concrete and steel behavior over a given domain rather than attempting to model discrete cracks.

In the need to employ averaged properties to account for discrete cracking (smeared crack models) and resulting reinforcing bar-concrete behavior in finite element analysis of reinforced concrete, modelers have given (a) the steel an artificial increase in stiffness to account for the stiffening effect of the concrete surrounding the bar; or (b) the concrete a pseudo strength increase in its tensile postpeak regime (ACI Committee 224 1986, Barzegar-Jamshidi and Schnobrich 1986, Stevens et al. 1991, Gupta and Maestrini 1990). The most common approach has been to assign to the concrete tensile strength at strain levels beyond the strain level at which the uniaxial postpeak strength equals zero (Figure 40). The shape of the residual concrete tensile strength curve (straight line, bilinear, exponential) and the strain where it reaches a zero magnitude are important variables (Barzegar-Jamshidi and Schnobrich 1986, Stevens et al. 1991).
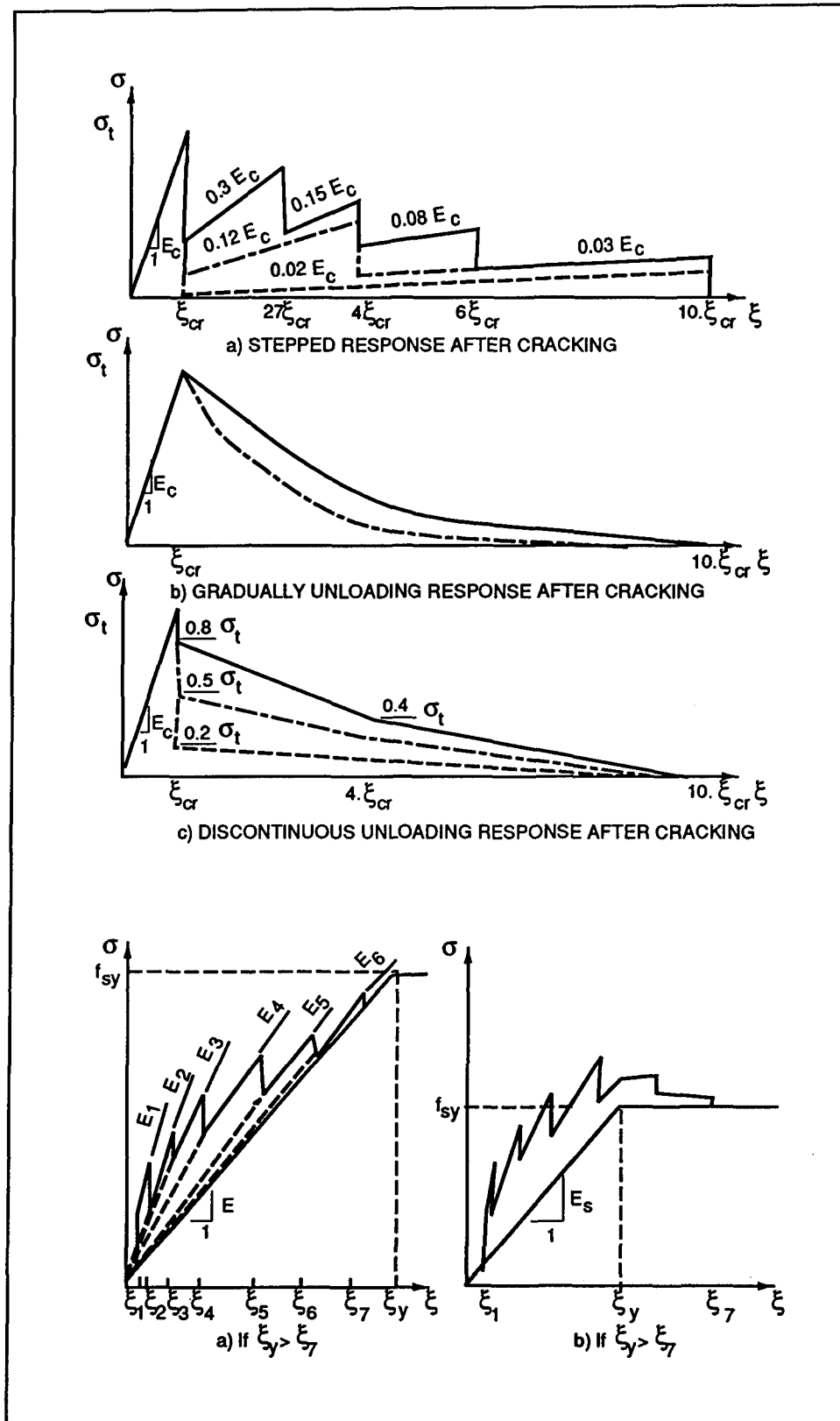
Figure 40. Tensile cracking in concrete

The strain at zero stress is typically given as a factor, α, times the cracking strain of the concrete. Gilbert and Warner (1978) utilized various models for tension stiffening in a smeared crack analysis of concrete slabs. In addition to the concrete referenced models mentioned previously, they employed a steel referenced model in which the stiffness of the reinforcing steel was increased to account for the surrounding concrete. Six levels of stiffness, ε_i, defined by seven strain levels, ε_i, which are based on cracking strain levels are defined as:

ε_1	ε_2	ε_3	ε_4	ε_5	ε_6	ε_7
ε_{cr}	$1.5\varepsilon_{cr}$	$3.0\varepsilon_{cr}$	5.0ε	$8.0\varepsilon_{cr}$	$11.0\varepsilon_{cr}$	$14.0\varepsilon_{cr}$

and

E_1	E_2	E_3	E_4	E_5	E_6
$4.0E_s$	$2.7E_s$	$2.0E_s$	$1.6E_s$	$1.15E_s$	$1.05E_s$

where the stiffness E_1, equal to 4.0 times the modulus of steel, E_s, occurs in the strain range from cracking to 1.5 times the cracking strain.

Experimental studies of tension stiffening in concrete have either been on members or panels subject to uniaxial tensile loads (Williams 1986) or the tension-stiffening behavior has been determined from large panels tested under a general state of in-plane stress (Vecchio and Collins 1982).

Williams (1986) subjected large reinforced concrete slabs (2,500 mm by 1,500 mm by 250 mm) to direct tension. Crack widths, crack spacing, and tension stiffening effects were measured. Parameters varied in the test program included:

Group 1: Fixed steel percentage (1 percent), varying bar size and spacing
Group 2: Fixed bar spacing, varying bars size and percentage (0.24 percent to 2.4 percent) (Note: this corresponds to masonry where bar spacing is fixed by unit cell spacing.)
Group 3: Fixed bar size (20 mm), varying spacing and percentage (0.84 percent, 1.0 percent, and 1.5 percent)
Group 4: Fixed bar size and spacing, varying cover distance
Group 5: Fixed bar size, spacing, and cover, with and without transverse steel

For a fixed steel percentage (1 percent), the smaller bar sizes and closer bar spacings resulted in closer crack spacings. For the Group 2 tests, yield was developed in the small rebars (8 and 10 mm) before full crack development occurred.

Tension-stiffening results show that the total perimeter of the bars in the specimen was a significant factor. The higher the surface area of the bar, the greater the tensile stress carried by the concrete. Small bars with a greater perimeter to area ratio are more efficient in transferring tensile

stress to the masonry. For Group 2 (masonry case) with equal bar spacing, the specimens with small bars had a higher concrete stress than specimens with larger bars (i.e., the tension stiffening effect is greater for a small reinforcement ratio). At a global tensile strain level of 200 microstrain, the concrete still carried up to 20 percent of its cracking stress for low steel percentages. The presence of transverse bars decreased the concrete tensile stress at high strain levels compared to the case with longitudinal bars only.

A series of panel tests at the University of Toronto (Vecchio and Collins 1982) have resulted in the development of the modified compression field theory, one component of which is the assumption of an effective tension stiffening effect applied to the tensile strength curve for the concrete. The original concrete postcracking tensile stress-strain curve is given by

$$f(\varepsilon) = \frac{f_{cr}}{(1 + \sqrt{200\varepsilon})} \qquad (11)$$

where

f_{cr} = tensile cracking strength

ε = tensile strain

Equation 11 was modified (Stevens et al. 1991) so that the concrete tensile stress reduces exponentially from cracking to a limiting tensile stress at large strains determined as a function of the steel ratio and bar diameter. In this approach, the steel stress is taken as a value less than yield to reflect the average steel stress which would be determined by averaging stress over the cracked and uncracked sections of the bar. These changes were reportedly made primarily for computational convenience.

Researchers have attempted to develop tension stiffening behavior using basic constitutive properties of the material including bond-slip relations. Gupta and Maestrini (1990) assumed a bilinear bond-slip curve and used basic equilibrium relations and linear material properties to develop an expression for concrete tensile stress as cracking occurs. The modular ratio and steel percentage were important parameters affecting response. They were forced to introduce a "damage parameter" to force their theory to match experiments; especially at high strains where their theory predicts a limiting concrete tensile stress equal to 50 percent of cracking stress.

Hegemier, Murakami, and Hageman (1985) and Hegemier, Murakami, and Kendall (1990) have developed a "mixture model" for the analysis of the behavior of reinforced concrete, reinforced masonry, or other composites under generalized loadings. A variational principle accounts for the constitutive relations of the component materials, the interface reactions, and the geometry. For the case of axial rebar-concrete interaction, a slip

initiation criterion and an incremental nonlinear slip rule are proposed based on experimental data from pull-out tests on specimens with short embedment lengths. Using this approach, good agreement was obtained with both pull-out test and direct tension test results. By adopting bond-slip relations for reversed loading, the use of the model was extended to cyclic loadings.

In an application specific to masonry, Hegemier, Murakami, and Kendall (1990) develop relations for a panel with orthogonal reinforcement loaded at an arbitrary angle to the reinforcement direction. For the case of alignment of load and reinforcement directions, the following equation is proposed for the secant modulus, C_{11}, of cracked concrete masonry as a function of tensile strain, ε_{11}.

$$\frac{C_{11}}{E^1} = \frac{C_{11}}{E^1} + \left(1 - \frac{C_{11}}{E^1}\right) \exp\left(\frac{-\gamma(\varepsilon_{11} - \sigma_t)}{E^1}\right) \tag{12}$$

where

$E^1 = $ tensile Young's modulus of the uncracked masonry

$\sigma_t = $ tensile cracking strength

$\gamma = $ an empirical numerical factor

For the case of a concrete masonry with a tensile strength of 400 psi and 1 percent steel with a yield stress level of 50 ksi, the use of the mixture model gave a ratio $C_{11}/E^1 = 0.10$ and $\gamma = 6,290$.

Most experimental studies of tension-stiffening behavior have assumed that zero stress exists in the materials before tensile loading begins. Cementitious materials have well known shrinkage behavior which, when occurring in a reinforced member, acts to produce tensile stresses in the concrete or grout and compressive stress in the steel bar. If deformation and loads are measured assuming that they are initially equal to zero, then the true tension-stiffening behavior may be masked by the initial but unknown stress conditions.

Test Plan

The masonry tension experiments were conducted in two phases with all specimens for each phase constructed at the same time. The first phase had as its main purpose to study the effect of the steel ratio on the tension stiffening behavior of masonry. This variation was achieved in two ways: first reinforcing bars ranging from a No. 3 to a No. 11 bar were grouted into 8-in. half-wide units. Next, a No. 4 bar was grouted into units of varying width ranging from 4-in. wide units to 12-in. wide units. This

produced steel ratios varying from 0.0015 to 0.0237. All units used in the first phase were nominal 8-in. high concrete masonry units. Two replications were made for each specimen.

In the Phase II tests, additional specimens were tested: (a) to provide additional variation in the ratio of steel to gross masonry area; (b) to determine the effect that unit material had on response by testing clay unit specimens; (c) to repeat certain Phase I tests to obtain better data at low strain levels; and (d) to investigate the behavior at single cracks. Because of the excellent reproducibility observed in the Phase I tests, no replications of specimens were tested in Phase II.

Specimen fabrication

All test specimens were fabricated in the laboratory at WES using materials selected to be similar, to the greatest extent possible, with the materials used by other TCCMAR researchers. A complete compilation of test results from index and material properties tests conducted on all materials used for this research program is contained in Appendix A. The general quality assurance plan for the tension stiffening test specimens was identical to that for the lap splice test specimens (Table 2).

All specimens consisted of concrete masonry units with 3/8-in. fully bedded mortar joints. Hollow concrete masonry units with nominal widths of 4, 6, 8, 10, and 12 in. and clay masonry units with nominal widths of 4, 6, and 8 in. were used to construct the test specimens. Results of index property tests on units are presented in Appendix A.

Specimens were constructed in stacked bond using half units to provide a single vertical cell. To reduce the variability introduced by inconsistent workmanship, all specimens were constructed with the aid of a prism building jig design by Atkinson-Noland. The jig consists of four vertical, slotted angles bolted to an aluminum base plate, with two moveable, horizontal bars attached the uprights. The vertical members can be adjusted laterally and longitudinally to accommodate units of various sizes. The horizontal bars are raised in predetermined increments to allow the uniform placement of mortar and units during prism construction.

The mortar proportions, selected to conform to ASTM C 270 (ASTM 1990n), were, by volume, 1:½:4½ (cement:lime:sand). The volumetric proportions were converted to weights of the locally available materials for batching in the laboratory. Results of compressive strength tests on mortar are given in Appendix A.

After the hollow prisms were constructed, they were placed on a bench fabricated from a double thickness of 2- by 12-in. lumber and concrete masonry blocks. These benches provided a stable platform for placement of the grout, and elevated the bottom of the prisms sufficiently that the bars could be placed in the hollow prisms prior to grouting. Holes were drilled

in the lumber near the center of each prism so that the protruding reinforcing bars could be positioned in the prism.

Typically, within a few days after the mortar was laid, the steel reinforcing bars were placed in the hollow prisms. The reinforcing steel used in this study included No. 3, 4, 6, 8, and 11 bars of Grade 60 steel conforming to the requirements of ASTM A 615, Specification for Deformed and Plain Billet-Steel Bars for Concrete Reinforcement (ASTM 1990b). Deformations were in a diagonal pattern at an angle of 70 deg to the longitudinal axis of the bar. The bars were cut to a length approximately 34 in. longer than the length of the masonry prism to provide 17 in. of bar on each end of the prism for attaching instrumentation and for adequate protrusion of the bars beyond the grouted prism for gripping during the test.

All test specimens were fully grouted after the reinforcing bars were placed in the prisms. The grout was batched in the laboratory. The volumetric proportions of the grout were 1:3:2 (sand:cement:gravel) with a water-cement ratio of approximately 0.7 to provide a slump in the range of approximately 9-1/2 to 10 in. Sika Grout-Aid, an expansive admixture, was added to the grout to offset shrinkage due to migration of the mix water from the grout to the surrounding masonry. Results of fresh and hardened tests on the grout are given in Appendix A. Grout was placed by hand into the hollow masonry and immediately vibrated using a small hand-held concrete vibrator. After approximately 5 min, the grout was reconsolidated using the same vibrator.

Table 11 contains a matrix of test specimens, dates of fabrication and testing, grout and mortar batches, and strength of constituent materials for the tension-stiffening specimens. Additional information on the properties of the various materials can be found in Appendix A.

Specimen loading

The test setup for the tension-stiffening study was very similar to that of the lap-splice study. Tensile loads were applied directly to the ends of the bar protruding from the masonry using hydraulically activated tension grips. Loads were applied monotonically in displacement control at a rate which allowed adequate acquisition of data and observation of crack formation. Load application was continued to very large vertical displacements, usually 4 or more inches.

The direct tension forces to the test specimens were provided by a 300-kip servo-controlled, closed-loop hydraulic loading system. The 300-kip capacity ram was attached to a 20-ft tall tripodal load frame that was fixed to the structural strong floor.

The ends of the reinforcing bars were gripped by hydraulically activated tension grips. The upper tension grip was attached to a load cell in line with the 300-kip hydraulic ram. The lower tension grip was attached

Table 11
Tension-Stiffening Test Matrix

Specimen Name	Program Phase	Date Const.	Mortar Batch	Date Grouted	Grout Batch	Date Tested	Compressive Strength, psi				Date Tested Yield Strength, psi
							Unit	Mortar Cube	Mortar Cylinder	Grout	
4-in. Concrete Masonry Unit											
TS4CON-4-1	I	08/01/91	M213-1	08/05/91	G217-1	12/17/91	1,900	2,430	1,860	3,460	72,300
TS4CON-4-2	I	08/01/91	M213-1	08/05/91	G217-1	12/18/91	1,900	2,430	1,860	3,460	72,300
TS4CON-4-3	II	05/12/93	M132-1	05/13/93	G133-1	06/24/93	1,900	5,050	4,760	4,850	72,300
6-in. Concrete Masonry Unit											
TS6CON-4-1	I	08/01/91	M213-1	08/05/91	G217-1	12/17/91	3,090	2,430	1,860	3,460	72,300
TS6CON-4-2	I	08/01/91	M213-1	08/05/91	G217-1	12/18/91	3,090	2,430	1,860	3,460	72,300
TS6CON-4-3	II	05/12/93	M132-1	05/13/93	G133-1	06/25/93	3,090	5,050	4,760	4,850	72,300
TS6CON-8-1	II	05/12/93	M132-1	05/13/93	G133-1	06/29/93	3,090	5,050	4,760	4,850	
8-in. Concrete Masonry Unit											
TS8CON-3-1	I	05/03/91	M123-1	07/26/91	G207-1	01/19/92	3,800	1,910	1,660	3,000	69,200
TS8CON-3-2	I	05/03/91	M123-1	07/26/91	G207-1	01/10/92	3,800	1,910	1,660	3,000	69,200
TS8CON-3-3	II	05/12/93	M132-1	05/13/93	G133-1	06/24/93	3,800	1,910	4,760	4,850	69,200
TS8CON-4-1	I	05/03/91	M123-1	07/26/91	G207-1	12/18/91	3,800	1,910	1,660	3,000	72,300
TS8CON-4-2	I	05/03/91	M123-1	07/26/91	G207-1	12/19/91	3,800	1,910	1,660	3,000	72,300
TS8CON-4-3	II	05/12/93	M132-1	05/13/93	G133-1	06/25/93	3,800	1,910	4,760	4,850	72,300
TS8CON-6-1	I	05/03/91	M123-1	07/26/91	G207-1	12/11/91	3,800	1,910	1,660	3,000	66,400
TS8CON-6-2	I	05/03/91	M123-1	07/26/91	G207-1	12/13/91	3,800	1,910	1,660	3,000	66,400
TS8CON-6-3	II	05/12/93	M132-2	05/13/93	G133-1	06/28/93	3,800	4,780	4,260	4,850	66,400
TS8CON-8-1	II	05/12/93	M132-2	05/13/93	G133-1	06/29/93	3,800	4,780	4,260	4,850	

(Continued)

Table 11 (Concluded)

Specimen Name	Program Phase	Date Const.	Mortar Batch	Date Grouted	Grout Batch	Date Tested	Compressive Strength, psi				Date Tested Yield Strength, psi
							Unit	Mortar Cube	Mortar Cylinder	Grout	
10-in. Concrete Masonry Unit											
TS8CON-11-1	I	05/03/91	M123-1	07/26/91	G207-1	12/20/91	3,800	1,910	1,660	3,000	68,000
TS8CON-11-2	I	05/03/91	M123-1	07/26/91	G207-1	01/07/92	3,800	1,910	1,660	3,000	68,000
TS10CON-4-1	I	07/31/91	M212-1	08/05/91	G217-1	12/19/91	3,850	2,750	1,950	3,460	72,300
TS10CON-4-2	I	07/31/91	M212-1	08/05/91	G217-1	12/17/91	3,850	2,750	1,950	3,460	72,300
TS10CON-4-3	II	05/12/93	M132-2	05/13/93	G133-1	06/24/93	3,850	4,780	4,260	4,850	72,300
12-in. Concrete Masonry Unit											
TS12CON-4-1	I	07/31/91	M212-1	08/05/91	G217-1	01/09/92	6,280	2,750	1,950	3,460	72,300
TS12CON-4-2	I	07/31/91	M212-1	08/05/91	G217-1	01/09/92	6,280	2,750	1,950	3,460	72,300
TS12CON-4-3	II	05/12/93	M132-2	05/13/93	G133-1	06/25/93	6,280	4,780	4,260	4,850	72,300
4-in. Clay Masonry Unit											
TS4CL-3-1	II	05/10/93	M130-1	05/13/93	G133-1	06/22/93	15,640	5,050	4,760		69,200
TS4CL-4-1	II	05/10/93	M130-1	05/13/93	G133-1	06/22/93	15,640	5,050	4,760		72,300
6-in. Clay Masonry Unit											
TS6CL-3-1	II	05/10/93	M130-1	05/13/93	G133-1	06/23/93	14,200	5,050	4,760		69,200
TS6CL-4-1	II	05/10/93	M130-1	05/13/93	G133-1	06/23/93	14,200	5,050	4,760		72,300
TS6CL-6-1	II	05/10/93	M130-1	05/13/93	G133-1	06/28/93	14,200	5,050	4,760		66,400
TS6CL-8-1	II	05/10/93	M130-1	05/13/93	G133-1	06/29/93	14,200	5,050	4,760		
8-in. Clay Masonry Unit											
TS8CL-3-1	II	05/10/93	M130-1	05/13/93	G133-1	06/23/93	10,890	5,050	4,760		69,200
TS8CL-4-1	II	05/10/93	M130-1	05/13/93	G133-1	06/24/93	10,890	5,050	4,760		72,300
TS8CL-6-1	II	05/10/93	M130-1	05/13/93	G133-1	06/28/93	10,890	5,050	4,760		66,400
TS8CL-8-1	II	05/10/93	M130-1	05/13/93	G133-1	06/29/93	10,890	5,050	4,760		

to a solid steel beam that was connected to the structural strong floor. Also, the lower beam could be raised or lowered hydraulically to allow the test specimens to be loaded conveniently. A schematic of the overall test setup is shown in Figure 41.
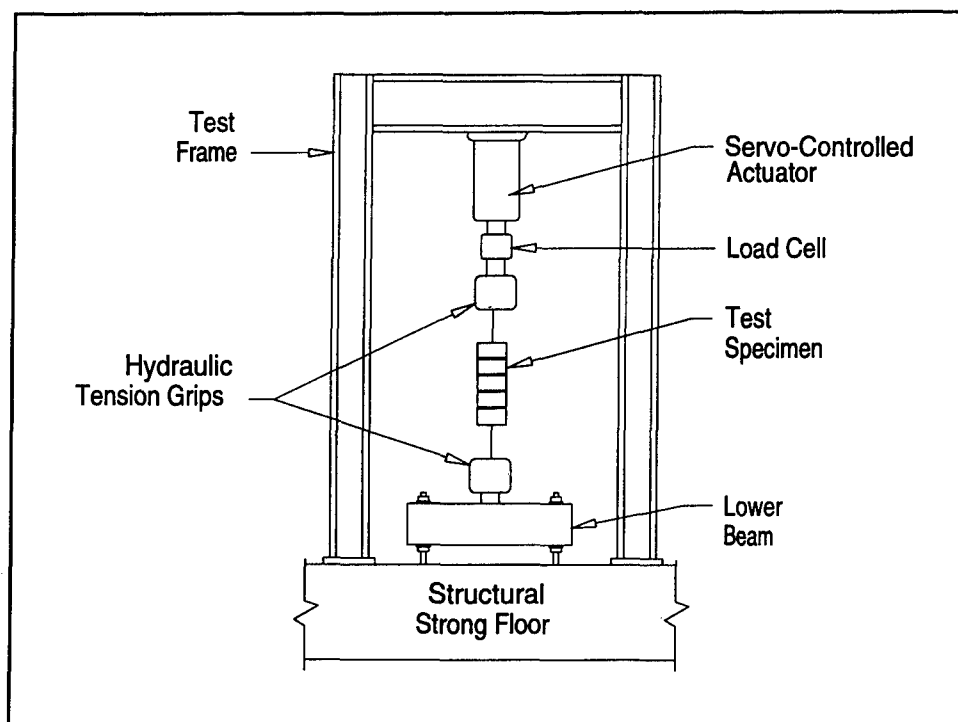

Figure 41. Schematic of test setup

Instrumentation

The instrumentation for the tension-stiffening tests was selected to allow recording of overall load-deformation behavior, tensile deformation of the masonry specimen, and bond slip between the ends of the specimen and reinforcing bar.

A conceptual view of the test instrumentation is shown in Figure 42. Instrumentation for the tension-stiffening tests consisted of the following items:

a. Axial load, as measured by a 400-kip capacity load cell in series with the test specimen and the 300-kip ram.

b. Head-to-head displacement, as measured by a reel-type position transducer mounted between the hydraulic tension grips.

c. Masonry displacement, as measured by LVDT's mounted to the surface of the masonry prisms.

d. Displacement across a mortar joint (Phase II only), as measured by LVDT's mounted to the surface of the masonry prisms.

e. Relative movement of the reinforcing bar and masonry at the ends, as measured by LVDT's mounted to the reinforcing bar by clamps.

All data were acquired by a microcomputer-controlled digital data acquisition system programmed to acquired data at equal time intervals of approximately 5 sec.

Analysis of Results

General

A total of 35 specimens were tested in the tension stiffening part of the CPAR program; 16 in Phase I and 19 in Phase II. For all tests, the loading was continued until large strain levels were obtained. Maximum strain levels measured on the specimen typically were in the range of 2 to 5 percent. In no case was a test terminated by failure of the reinforcing bar whether encased by masonry, outside the masonry, or in the tension grips. Tests were terminated by reaching the deformation limit of the test system. For each test, data from eight transducers were recorded for the entire deformation history of the test. This results in a considerable amount of data to be evaluated.

In the Phase I tests, a rotary potentiometer displacement gauge was used to measure deformation over large gauge lengths associated with the on-masonry deformation (span) and the deformation measured between the ends of the specimen (end-to-end). At low levels of displacement, these gauges often did not respond, and as a result no Phase I deformation data were measured until the load reached approximately one-third of the load to produce yield in the reinforcing bar. For the Phase II tests, the rotary potentiometers were replaced with conventional LVDT's with rigid links spanning between the two gauge points. The LVDT's provided much more sensitive measurement capacity at low deformation levels.

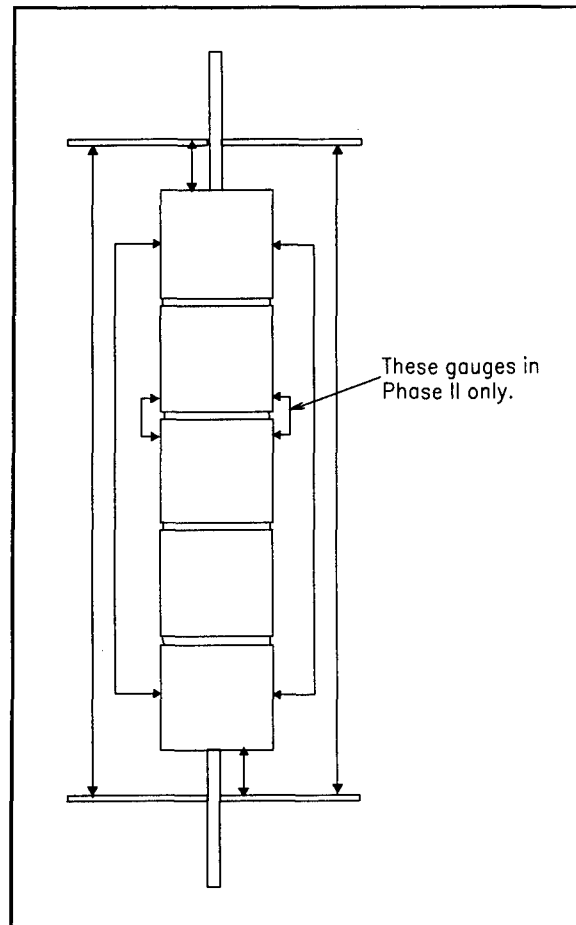

These gauges in Phase II only.

Figure 42. Conceptual view of instrumentation for tension-stiffening test

In the Phase II tests, data channels which had been used to measure the end-to-end deformations were used to measure crack opening at a single bed joint on the specimen. Many of the specimens only experienced one or two horizontal bedjoint cracks which did not always occur at the instrumented bedjoint, hence a complete record of crack opening data from the Phase II tests is not available.

In this section, the results of a typical test will be presented and described in detail to illustrate the nature of the data obtained. Next the results of several specialized studies on cracking behavior, the shape of the tensile stress-strain curve, initial stiffness and stiffness degradation will be presented to obtain measures of the tension-stiffening behavior.

Typical results

The response curves from Specimen 8CON-6-3 are presented to illustrate the general nature of the tensile behavior observed. The specimen consists of a single #6 reinforcing bar (0.75-in.-diam) grouted in one cell of an 8-in. concrete half-width unit. The specimen had a gross dimension of 8 by 7.5 in., giving an area of 60 sq. in. and a reinforcement ratio of 0.0073. Figure 43 shows the full tensile stress-strain curve to the maximum test strain of 6.0 percent, while Figure 44 shows the stress-strain
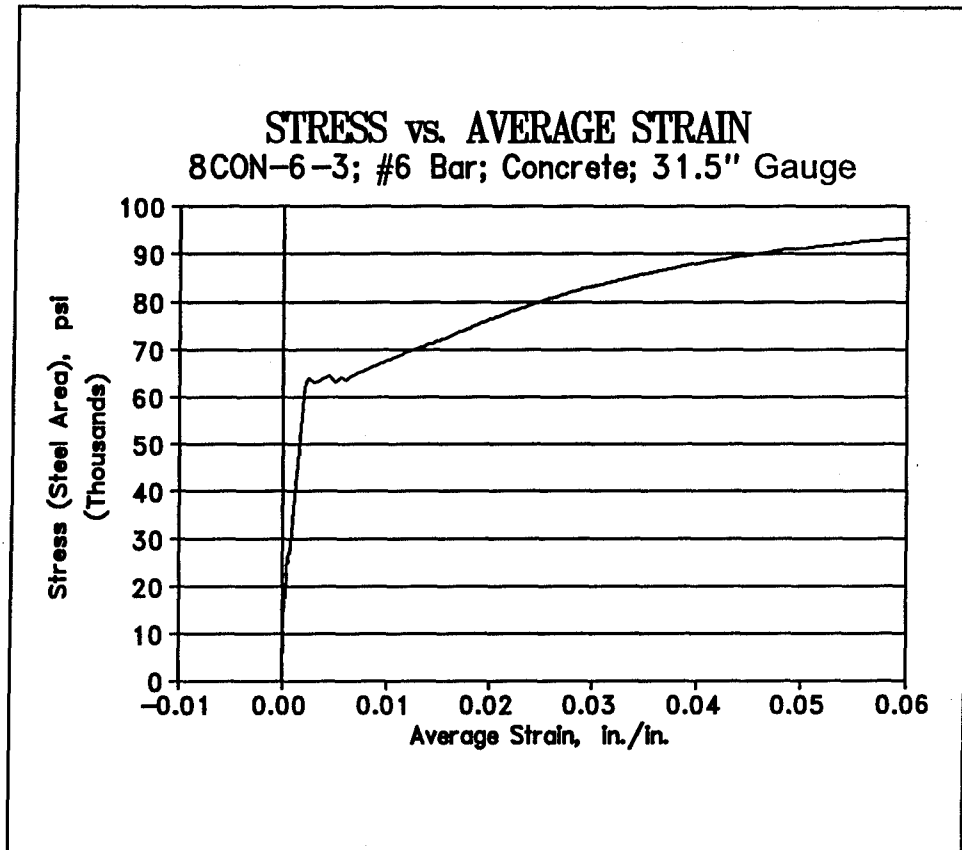

Figure 43. Full tensile stress-strain curve, test 8CON-6-3

curve up to the occurrence of steel yield. Both curves are plotted using the steel area to compute tensile stress and the deformations measured from the long span LVDT's mounted on the specimen to compute strain. In Figure 45 the stress-strain curve up to yield is plotted using the gross specimen area as the reference. This plot shows the occurrence of four clearly defined tensile cracks in the specimen. The plot of response up to yield shows the progressive softening of the specimen after each crack occurrence.

A complete presentation of the tensile stress-strain curves from the 35 specimens is given in Appendix B. In the Phase I experiments three unload-reload cycles were performed as part of the tensile loading sequence. The unloading typically amounted to one-half the load on the specimen at the time and was performed in an attempt to measure progressive softening of the specimen. Unfortunately, because of the insensitivity of the rotary potentiometers used in the Phase I tests, little useful data could be determined from these cycles.
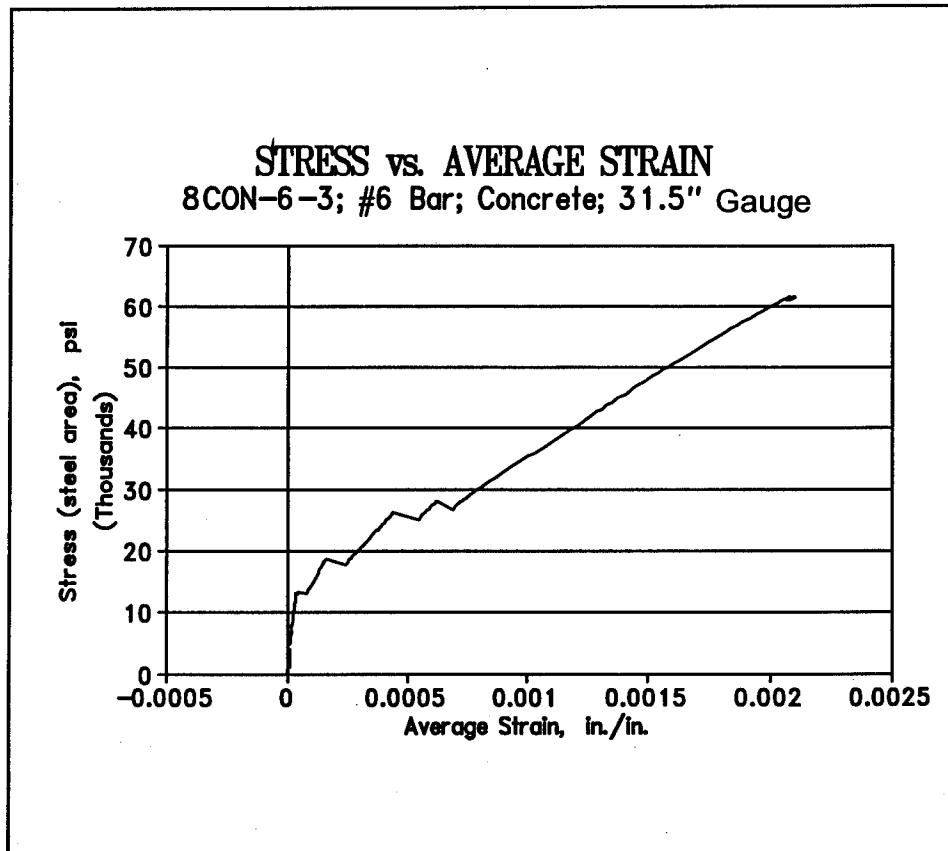

Figure 44. Tensile stress-strain curve to yield, test 8CON-6-3 (stress based on steel area)
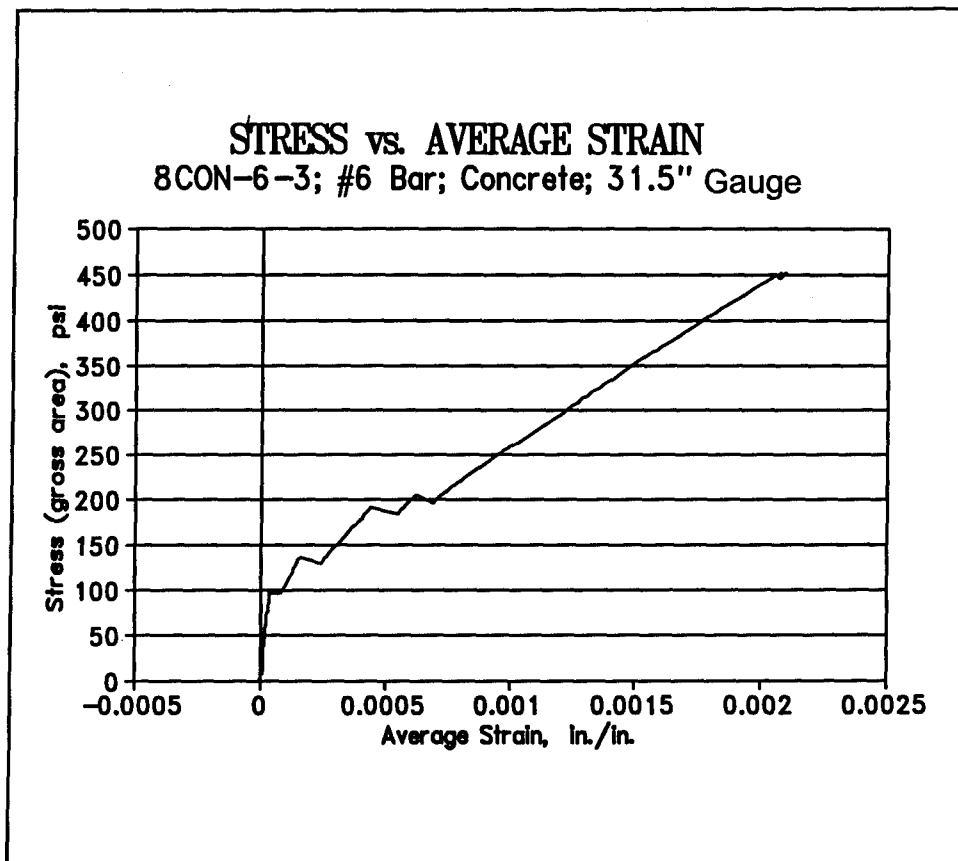
STRESS vs. AVERAGE STRAIN
8CON-6-3; #6 Bar; Concrete; 31.5" Gauge

Figure 45. Tensile stress-strain to yield, test 8CON-6-3 (stress based on gross area)

Cracking

These tests provide an excellent means to measure the tensile cracking strength of grouted reinforced masonry. As illustrated in Figure 45, cracking was characterized by a sudden increase in deformation and a slight decrease in load. Although the load was applied by a servo ram operated in stroke control, the residual softness of the overall system resulted in a deformation jump upon cracking.

The cracking tensile strengths determined from the stress-strain curve were corrected to account for the proportion of tensile force carried by the steel reinforcing bar in the specimen. The correction was made assuming that at the location of the crack both the masonry and the steel have the same linear elastic tensile strain prior to cracking. The steel was assumed to have an elastic modulus of 29,000 ksi (200 MPa) and the masonry a tensile modulus of 2,000 ksi (13.79 MPa). The proportion of load carried by the steel and the masonry was then determined based on their respective areas.

The results of the tensile strength survey for the case of all tensile cracks are plotted as a histogram in Figure 46. The data for the occurrence of the first tensile crack only are plotted in Figure 47. The distribution of tensile data in Figure 46 for all cracks is best represented by a log-normal or a Weibol distribution. When data from the first crack are plotted, a more normal distribution of data are observed having a mean tensile strength of 165.3 psi (1.14 MPa) with a standard deviation of 98.5 psi (0.68 MPa).

The specimen cracking patterns were recorded for every test. For the Phase I tests, the cracking pattern observed at the conclusion of each test was recorded. For the Phase II tests, crack patterns were recorded at the onset of yielding, at the onset of strain hardening, and at the conclusion of the test.

The number of complete horizontal cracks at each stage of loading are listed in Table 12, together with the steel ratio and the number of bed joints contained in the specimen. In Figure 48, the number of cracks at the final loading stage are plotted versus the steel ratio. A general trend for the number of cracks in the specimen to increase with an increase in the steel ratio is observed. Concrete masonry specimens with high steel ratios typically had horizontal cracks at the bedjoints and cracks through
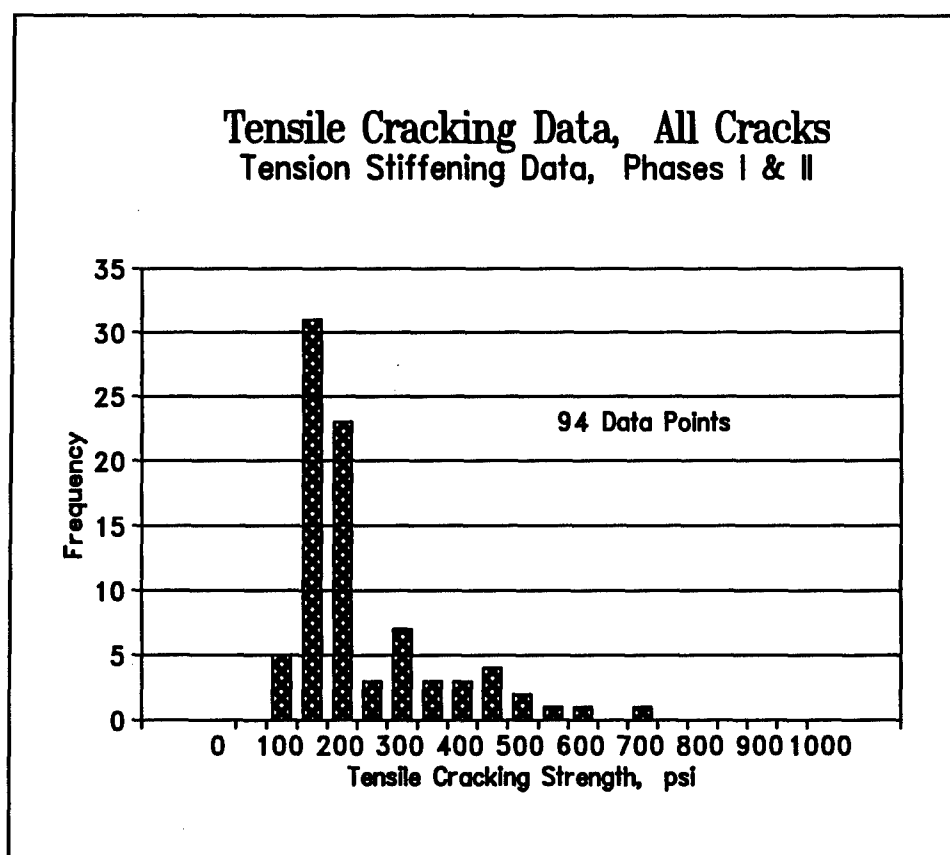

Figure 46. Histogram of tensile cracking strength

First Tensile Crack Data
Tension Stiffening Data, Phases I & II
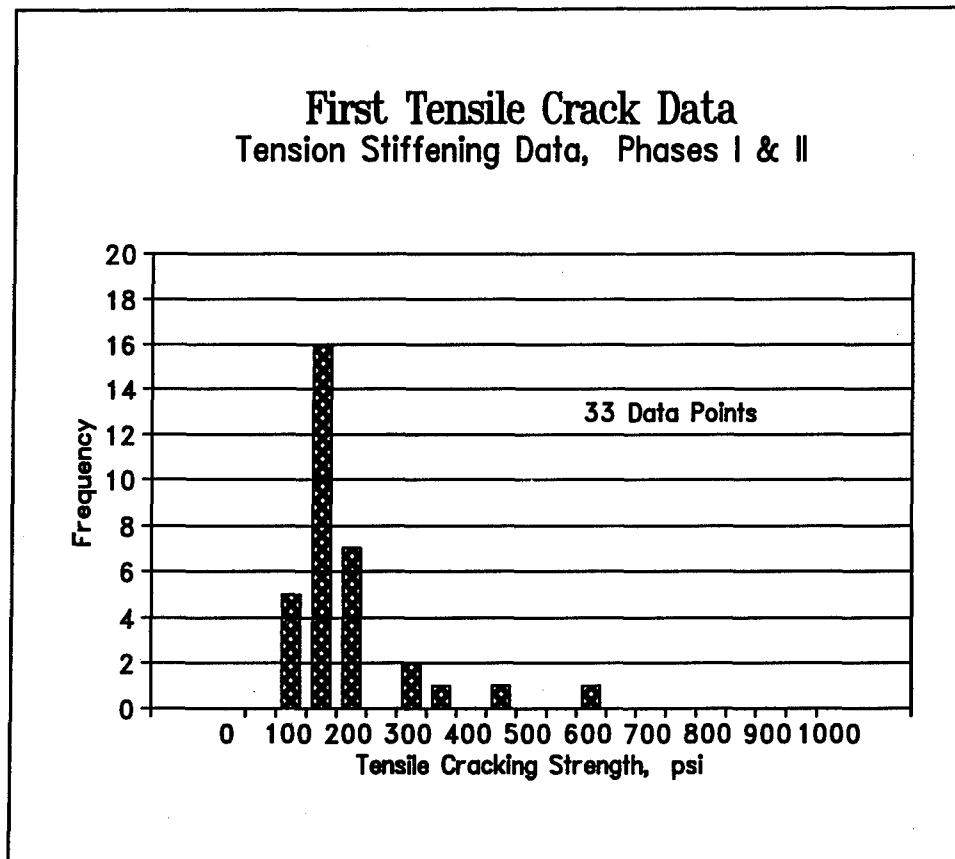
33 Data Points

Figure 47. Histogram of first tensile cracking strength

the middle of the units. The clay unit specimens only experienced horizontal cracks through the bedjoints.

The development of a large number of cracks with small openings is considered preferable to development of one or two cracks with large openings. In the later case the tensile strain demand from the structure is concentrated at one or two locations with the result that the reinforcing bar at the crack is subject to large plastic strain levels while the steel in the remainder of the section is at a much lower strain. Under loading conditions in which the applied load can not decrease as the deformations become large (as for example a simple beam under gravity loading), the concentration of strain at a single crack may lead to premature failure due to steel rupture. If the case of a single or small number of cracks occurs in a masonry wall subject to in-plane loading from a cyclic loading source, then on the reverse compression cycle the open cracks cannot be closed since the reinforcing bars have been plastically deformed in tension. As a result, all of the compressive force is carried by the bars and a situation leading to potential buckling in the lateral direction is created. This situation is discussed in detail by Paulay and Priestley (1993) who developed expressions for displacement ductility demands and geometric requirements to avoid lateral buckling.

Table 12
Examination of Horizontal Cracking Pattern and Number of Cracks

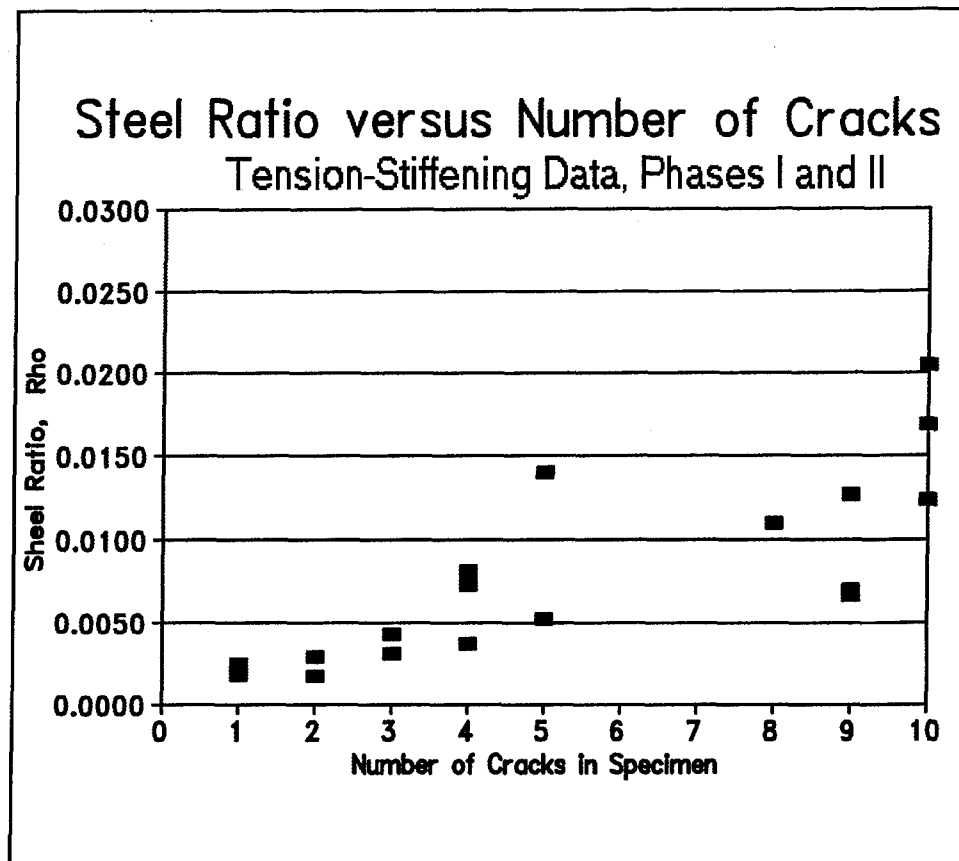| Specimen	Steel Ratio	Number of Joints	Number of Horizontal Cracks			Comments
			At Yield	At Onset of Strain Hardening	At Final	
4CO-4-1	0.0066	4	NA	NA	5	
4CO-4-2	0.0063	4	NA	NA	11	
6CO-4-1	0.0044	4	NA	NA	5	
6CO-4-2	0.0042	4	NA	NA	6	
8CO-3-1	0.0015	4	NA	NA	8	
8CO-3-2	0.0017	4	NA	NA	4	
8CO-4-1	0.0031	4	NA	NA	3	
8CO-4-2	0.0031	4	NA	NA	3	
8CO-6-1	0.0069	4	NA	NA	4	
8CO-6-2	0.0069	4	NA	NA	5	
10CO-4-1	0.0024	4	NA	NA	2	
10CO-4-2	0.0025	4	NA	NA	4	
12CO-4-1	0.0020	4	NA	NA	4	
12CO-4-2	0.0020	4	NA	NA	4	Phase I Tests Above
4CL-3-1	0.0070	9	3	9	9	Phase II Tests Below
4CL-4-1	0.0127	9	6	9	9	End fracture at end of test
6CL-3-1	0.0029	9	2	2	2	
6CL-4-1	0.0052	9	0	5	5	
6CL-6-1	0.0110	9	0	7	8	
6CL-8-1	0.0205	9	1	9	10	
8CL-3-1	0.0018	9	1	1	1	1-1/2" wide @ final
8CL-4-1	0.0037	9	4	4	4	Two very wide cracks
8CL-6-1	0.0081	9	2	3	4	End unit fractured
8CL-8-1	0.0140	9	2	5	5	
4CON-4-3	0.0067	4	3	5	9	Cracks in middle of all units
6CON-4-3	0.0043	4	3	3	3	
6CON-8-1	0.0169	4	4	9	10	
8CON-3-3	0.0017	4	0	0	2	
8CON-4-3	0.0031	4	2	2	3	
8CON-6-3	0.0073	4	3	4	4	
8CON-8-1	0.0124	4	0	9	10	
10CON-4-3	0.0025	4	1	1	1	
12CON-4-3	0.0022	4	0	0	1	

Figure 48. Steel ratio versus number of cracks

The sum of the length of longitudinal cracks measured on all four sides for each specimen were recorded and entered into Table 13 in addition to the steel ratio, the maximum tensile strain, and the cover distance measured from the edge of the bar to the nearest free surface of the specimen. Specimen 4CO-4-2 experienced cracking on opposite sides of the specimen for the full height of the specimen. All other specimens had no longitudinal cracking or limited longitudinal cracking. Where longitudinal cracking occurred, it was typically in the end units of the specimen. Of the 10 clay unit specimens tested in Phase II, only 1 specimen experienced longitudinal cracking. The LVDT data from Specimen No. 8CO-3-1 showed considerable bending that may account for the larger value of cracking measured on this specimen.

The occurrence of longitudinal cracking is far more serious than cracking normal to the axis of the reinforcing bars, since this type of cracking provides a mechanism for the loss of masonry material from around the bar which could lead to lateral bucking of the bars when loaded in compression. No correlation is noted between the steel ratio and the occurrence or extent of longitudinal cracking. A correlation, although weak, exists between the cover distance and longitudinal cracking. Of the 13 specimens with a cover distance less than 2.5 in. (63 mm), 6 were cracked and 7 were uncracked. Of the 22 specimens having a cover distance equal or greater than 2.5 in. (63 mm), 7 were cracked and 15 were uncracked. If

86

Table 13
Longitudinal Crack Length

Specimen	Steel Ratio	Maximum Strain	Length Longitudinal Cracks, in.	Cover Distance*	
				in.	Bar Diameters
4CO-4-1	0.0066	0.033	24	1.25	2.5
4CO-4-2	0.0063	0.032	80	1.25	2.5
6CO-4-1	0.0044	0.030	0	2.00	4.0
6CO-4-2	0.0042	0.028	8	2.00	4.0
8CO-4-1	0.0031	0.030	0	2.50	5.0
8CO-4-2	0.0031	0.034	0	3.00	6.0
10CO-4-1	0.0024	0.026	8	3.75	7.5
10CO-4-2	0.0025	0.012	12	3.75	7.5
12CO-4-1	0.0020	0.031	0	3.50	7.0
12CO-4-2	0.0020	0.021	0	3.25	6.5
8CO-3-1**	0.0015	0.020	20	3.25	8.7
8CO-3-2	0.0017	0.032	0	3.00	8.0
8CO-6-1	0.0069	0.029	8	3.00	4.0
8CO-6-2	0.0069	0.031	12	3.00	4.0
8CO-11-1†	0.0237	0.013	0	2.00	1.5
8CO-11-2†	0.0213	0.015	8	2.12	1.5
4CL-3-1	0.0070	0.014	0	1.56	4.2
4CL-4-1	0.0127	NA	0	1.50	3.0
6CL-3-1	0.0029	0.048	0	2.56	6.8
6CL-4-1	0.0052	0.057	0	2.25	4.5
6CL-6-1	0.0110	0.065	0	2.37	3.2
6CL-8-1	0.0205	0.060	0	2.25	2.3
8CL-3-1	0.0018	0.053	0	3.56	9.5
8CL-4-1	0.0037	0.055	0	3.25	6.5
8CL-6-1	0.0081	0.042	16	3.37	4.5
8CL-8-1	0.0140	0.065	0	3.25	3.3
4CO-4-3	0.0067	0.055	24	1.50	3.0
6CO-4-3	0.0043	0.046	0	2.50	5.0
6CO-8-1	0.0169	0.057	20	2.25	2.3
8CO-3-3	0.0017	0.035	0	3.56	9.5
8CO-4-3	0.0031	0.050	0	3.50	7.0
8CO-6-3	0.0073	0.060	8	3.37	4.5
8CO-8-1	0.0124	0.062	0	3.25	3.3
10CO-4-3	0.0025	0.019	0	4.00	8.0
12CO-4-3	0.0022	0.045	0	4.00	8.0

*   Cover distance is measured to the edge of the bar.
** Specimen exhibited significant bending strain.
†   Test stopped slightly above yield plateau due to tension grip capacity.

the cover distance is expressed in terms of bar diameters, then of the six specimens with a cover of less than three bar diameters, four were cracked and two were uncracked. Of the 29 specimens with cover equal to or greater than three bar diameters, 9 were cracked and 20 were uncracked.

It should be noted that maximum tensile strains generated were quite large ranging from 2 to 3 percent for the Phase I specimens and up to 6.5 percent for the Phase II specimens. Also, the lack of horizontal cracks and only one occurrence of longitudinal cracking in specimens fabricated using clay units can be attributed to the greater tensile strength inherent in the clay unit compared to the CMU.

Stress-strain response prior to yield

Because of the initial insensitivity of the deformation gauges placed on the specimen, the initial deformation data obtained from the Phase I tests are not considered reliable for determining early tension stiffening response. The Phase II data were used to calculate a steel referenced modulus for the deformation response up to yield as shown in Figure 49 for specimen 8CON-6-3. The modulus was calculated as a chord modulus in the data spreadsheet using a span of five data readings for the stress and strain intervals. This results, on occasion, in very high or very low modulus readings when, for example, the deformation or load readings are influenced by sudden changes such as caused by tensile cracking. Figure 50 shows high initial modulus in the range of approximately 300 to 400 $\times$ 10^6 psi. After occurrence of the first crack, the modulus drops to the range of
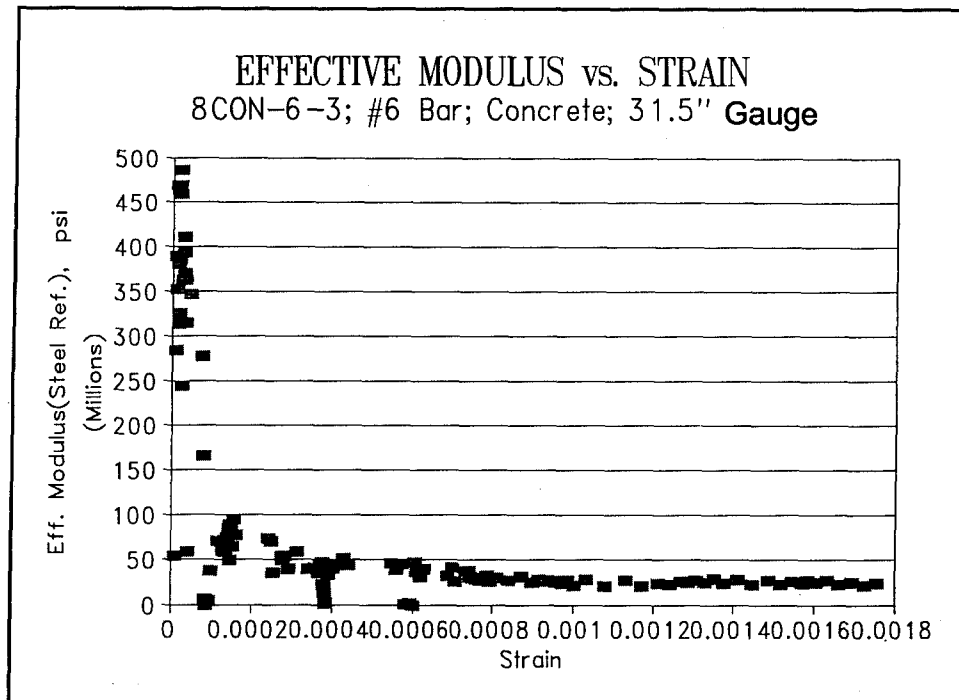

Figure 49. Effective modulus versus strain, test 8CON-6-3

50 to 100×10^6 psi followed by further decreases up to a tensile strain of about 0.0008 at which point it reaches a value approximately equal to the steel modulus.

For the elastic precracked case, the steel referenced tensile modulus should be given by the masonry modulus divided by the steel ratio. For specimen 8CON6-3, the steel ratio is 0.0073. If the masonry modulus is assumed to be 2.5×10^6 psi, an initial modulus of 342×10^6 psi is calculated which is in the range determined from the data.

Results from similar plots from the Phase II tests were used to establish an average modulus curve for the masonry expressed as a function of the tensile strain. The initial portion of the modulus versus strain curve was expanded. From this curve, strain levels associated with steel referenced modulus values of 30, 60, 150, and 300×10^6 psi were determined. Where the strain response experienced large jumps associated with occurrence of cracking, as for example with specimen 6CL-3-1, the strains associated with the cracking were subtracted from the overall strain response. These large strain jumps are considered to be an artifact of the test setup rather than the masonry response.

Results of the tension stiffening study are listed in Table 14 for the 14 test results which provided useful data. These data show a very rapid loss of stiffness as the tensile strain increases. There is a drop from 300×10^6 psi at a low strain level of 15 microstrain to a value of 30×10^6 psi at a strain level of 256 microstrain. These results are also plotted in Figure 50.

Table 14
Averaged Tension-Stiffening Results

Steel Referenced Stiffness million psi	Average Strain, millionths	Ration (Strain/Cracking Strain)
30	256	3.7
60	131	1.9
150	55	0.8
300	15	0.22

If the average stress occurring at the first crack of 165 psi is divided by an assumed gross elastic tensile modulus of 2.5×10^6 psi for the masonry, an average strain at first crack of 66 microstrain is obtained. If the average strain determined at each of the four stiffness values is divided by this value of cracking strain, the list of values given in the third column of Table 14 is obtained. This expresses stiffness in terms of cracking strain, a form often used to express tension stiffening in reinforced concrete (Gilbert and Warner 1978).

Thus, the effective stiffness of a masonry section in tension is given by the composite elastic properties up to the point of initial elastic cracking. After the initial tensile crack occurs, the stiffness drops to approximately
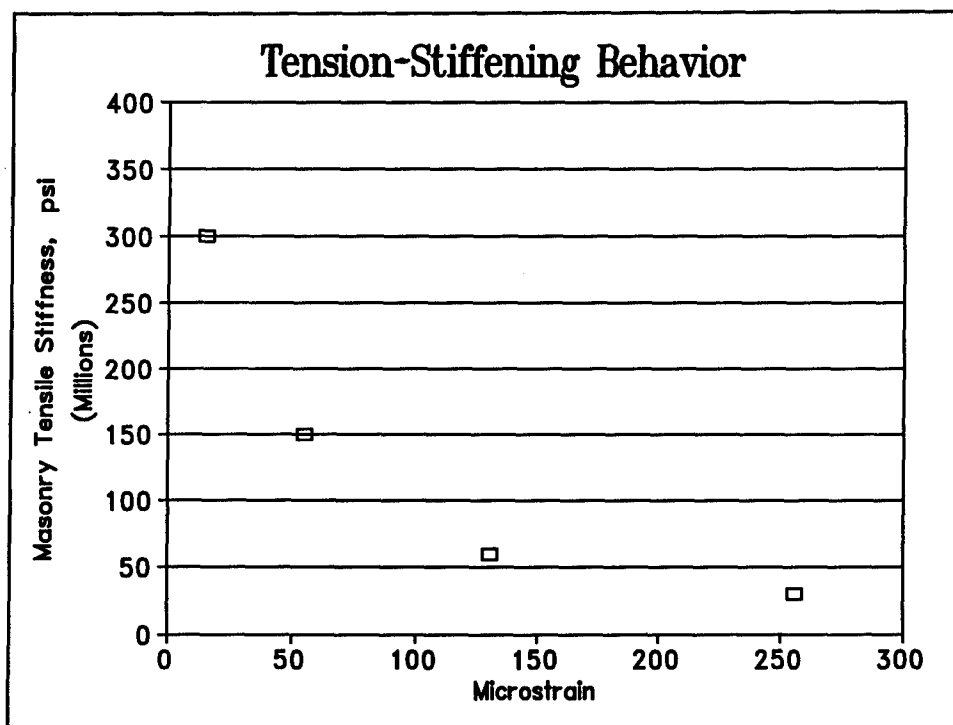
Figure 50. Stiffness versus strain

150×10^6 psi or five times the steel modulus. At a strain level equal to approximately twice the cracking strain, the stiffness drops to 60×10^6 psi or twice the steel stiffness. At a strain level equal to four times the cracking strain, the masonry tensile stiffness drops to a value equal to the steel stiffness. This rate of stiffness decrease is considerably greater than reported for reinforced concrete (Gilbert and Warner 1978).

Stress-strain response after yield

In addition to affecting the stress-strain response prior to yield as usually considered by tension-stiffening equations for reinforced concrete, the observed response from this series of masonry tension tests showed considerable influence on the shape of the stress-strain curve after yield. As the ratio of the steel area to masonry area decreases, the length of the yield plateau decreases and the stiffness of stress-strain curve in the strain hardening region increases. This is illustrated in Figures 51 and 52 for results obtained from the Phase I test series. In Figure 51 are shown the stress-strain response curves for specimens having a No. 3, 4, and 6 reinforcing bar in an 8-in. concrete masonry unit. Also shown for comparison is the stress-strain curve for a bare steel bar. In Figure 52 are shown the stress-strain response curves for a No. 4 reinforcing bar in a 6-, 8-, and 10-in. CMU. Also shown is the stress-strain curve from a No. 4 reinforcing bar without masonry.
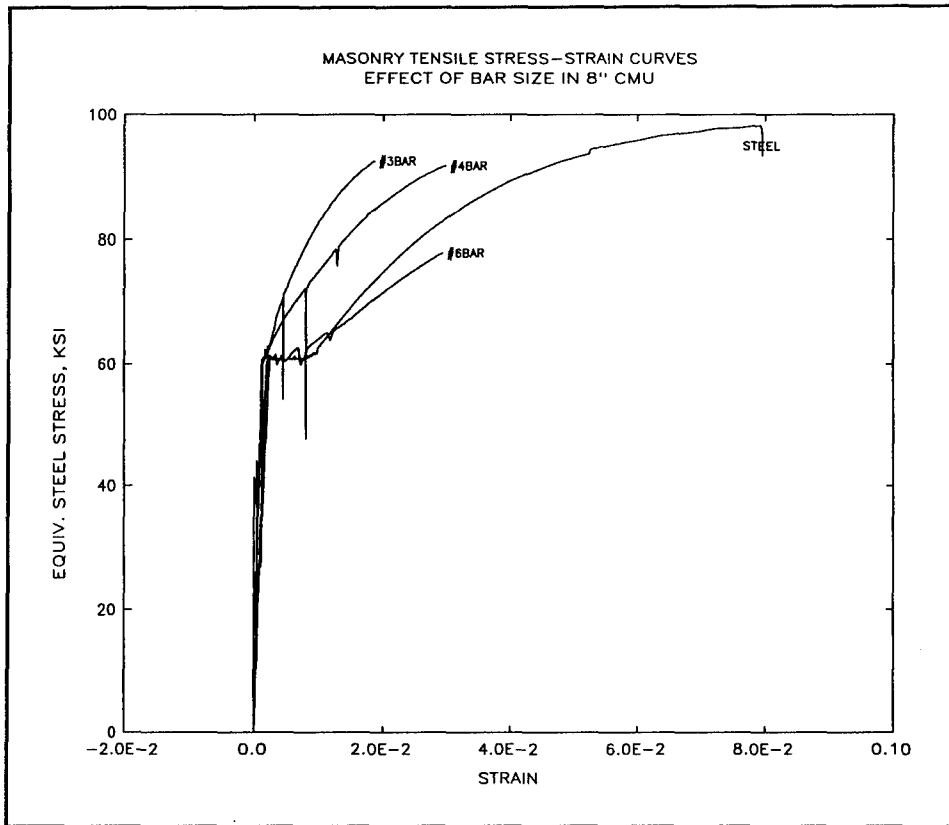
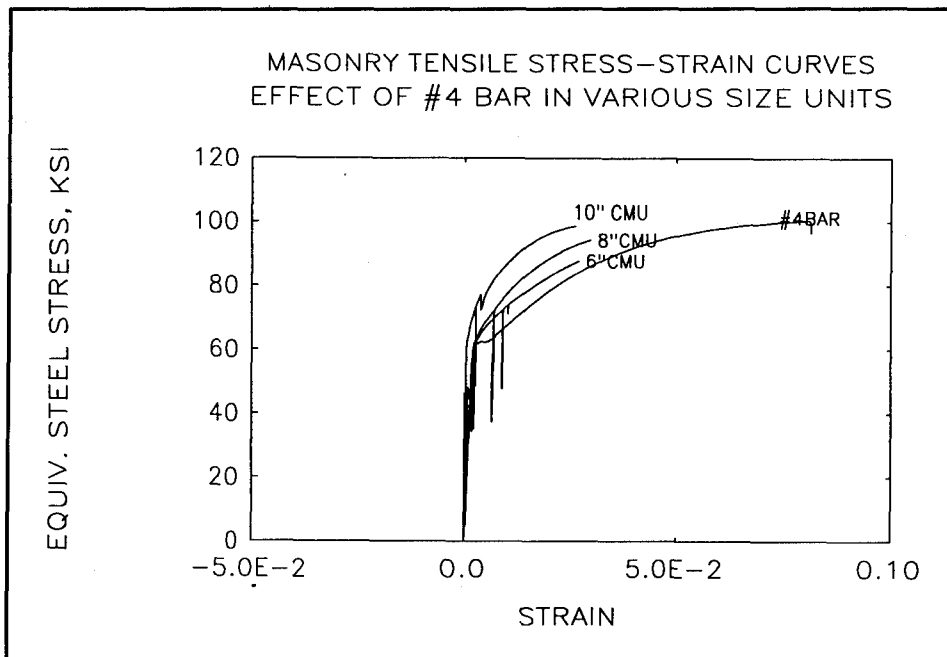Figure 51.   Masonry tensile stress-strain curves, 8-in. CMU

Figure 52.   Masonry tensile stress strain curves, No. 4 bar

As the steel ratio becomes large, the effect of the surrounding masonry becomes minimal as illustrated in Figure 51 by a comparison of the response of the specimen with a No. 6 reinforcing bar in an 8-in. unit to the stress-strain response of the steel alone. As the steel ratio becomes small, the tensile response becomes much less ductile as illustrated by the response of the No. 4 bar in an 8-in. unit in Figure 52. For this case, no yield plateau is present.

Effect of steel ratio on ductility

An examination was made of the effect of the ratio of the steel area to the gross area on the overall ductility of the masonry specimens loaded in direct tension. The stress-strain curves obtained from the surface mounted LVDT's having a nominal 32-in. gauge length were examined to determine the stress and strain level associated with the onset of reinforcing bar yielding. Next, the strain level associated with a stress level equal to 125 percent of the yield stress level was determined. The values for individual specimens are contained in Table 15. Figure 53 illustrates how these values were determined.

Table 15				
Comparison of Strain Values at Yield and at 125 Percent of Yield				
Specimen Number	**Steel Ratio**	**Strain @ Yield**	**Strain @ 125% Yield**	**Strain Ratio 125% Yield/100% Yield**
4CO-4-1	0.0066	0.002010	0.019500	9.70
4CO-4-2	0.0063	0.001230	0.017500	14.23
6CO-4-1	0.0044	0.002530	0.014300	5.65
6CO-4-2	0.0042	0.002250	0.014700	6.53
8CO-4-1	0.0031	0.002130	0.009560	4.49
8CO-4-2	0.0031	0.001899	0.011310	5.96
10CO-4-1	0.0024	0.000528	0.005400	10.23
10CO-4-2	0.0025	Low deformation readings unreliable		
12CO-4-1	0.0020	0.001660	0.010700	6.45
12CO-4-2	0.0020	0.001900	0.007500	3.95
8CO-3-1	0.0015	0.001380	0.006670	4.83
8CO-3-2	0.0017	0.001990	0.010900	5.48
8CO-6-1	0.0069	0.002460	0.026500	10.77
8CO-6-2	0.0069	0.001850	0.022000	11.89
8CO-11-1	0.0237	Machine load limit exceeded just beyond onset of strain hardening.		
8CO-11-2	0.0213			
4CO-4-3	0.0067	0.005233	0.068790	13.15
6CO-4-3	0.0043	0.005440	0.025850	4.75
				(Continued)

Table 15 (Concluded)

| Specimen Number	Steel Ratio	Strain @ Yield	Strain @ 125% Yield	Strain Ratio 125% Yield/100% Yield
6CO-8-1	0.0169	0.005330	0.032410	6.08
8CO-3-3	0.0017	0.000057	0.000075	1.32 (Cracking Strain > Yield)
8CO-4-3	0.0031	0.003930	0.029740	7.57
8CO-6-3	0.0073	0.004370	0.046820	10.71
8CO-8-1	0.0124	0.005017	0.033080	6.59
10CO-4-3	0.0025	0.001574	0.007912	5.03
12CO-4-3	0.0022	0.000081	0.019610	Cracking Strain > Yield
4CY-3-1	0.0070	0.003528	0.058875	16.69
4CY-4-1	0.0127	0.003517	LVDT out of range	
6CY-3-1	0.0029	0.002250	0.025680	11.41
6CY-4-1	0.0052	0.004280	0.033000	7.71
6CY-6-1	0.0110	0.004870	0.054900	11.27
6CY-8-1	0.0205	0.005900	0.035900	6.08
8CY-3-1	0.0018	0.001880	0.043100	22.93
8CY-4-1	0.0037	0.003482	0.025630	7.36
8CY-6-1	0.0081	0.004005	0.043190	10.78
8CY-8-1	0.0140	0.005432	0.037220	6.85
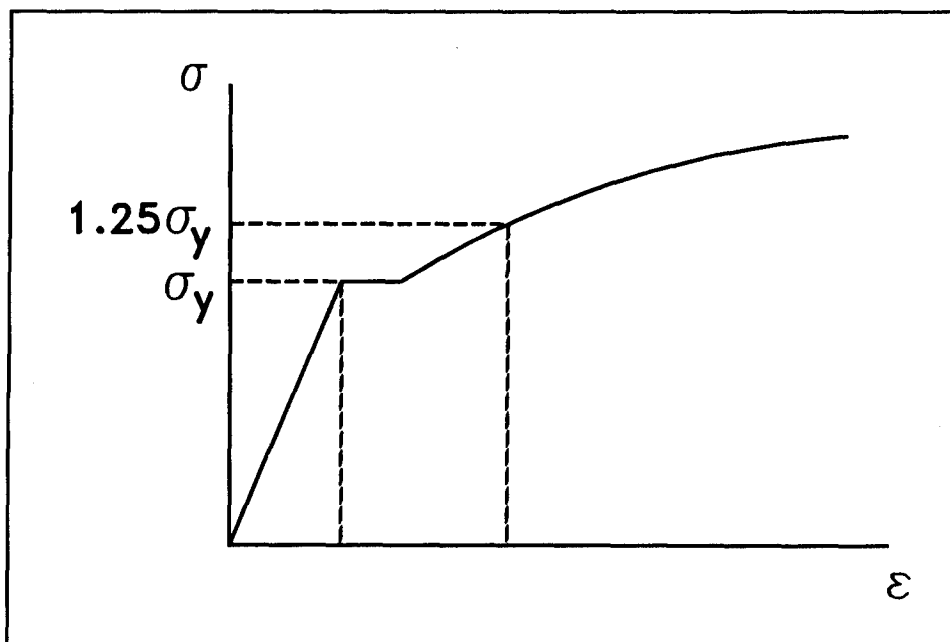
Figure 53. Idealized tensile stress-strain curve

A similar procedure was applied to the stress-strain curves obtained for the direct tension tests conducted on the full-size bars. These tests were conducted in the same loading apparatus used for the tension-stiffening tests and the deformation readings were also obtained over a 32-in. gauge length. The results are presented in Table 16. A considerable scatter in the ductility defined as the ratio of strain at 125 percent of yield to the strain at yield is observed between the various size bars.

Table 16
Influence of Steel Ratio on Ductility

Specimen	Steel Ratio	Ductility
8CO-3-1	0.0015	4.83
8CO-4-3	0.0031	7.57
8CO-6-2	0.0069	11.89

A plot was made of the ductility of the tension-stiffening specimens, defined as the ratio of strain at 125 percent of yield stress to the strain at yield stress versus the steel ratio, Figure 54. The four plotted data points associated with the highest steel ratios were all from Phase II of the test program and all had No. 8 size reinforcing bars from the same lot. An examination of Table 17 for the ductility of the reinforcing bars reveals that the ductility of this particular lot was 5.52 compared to an average ductility of 12.60 for all bars excluding this No. 8 bar. If the four data points associated with the No. 8 bar, Phase II specimens are excluded, then a general trend of increasing ductility with increasing steel ratio occurs.
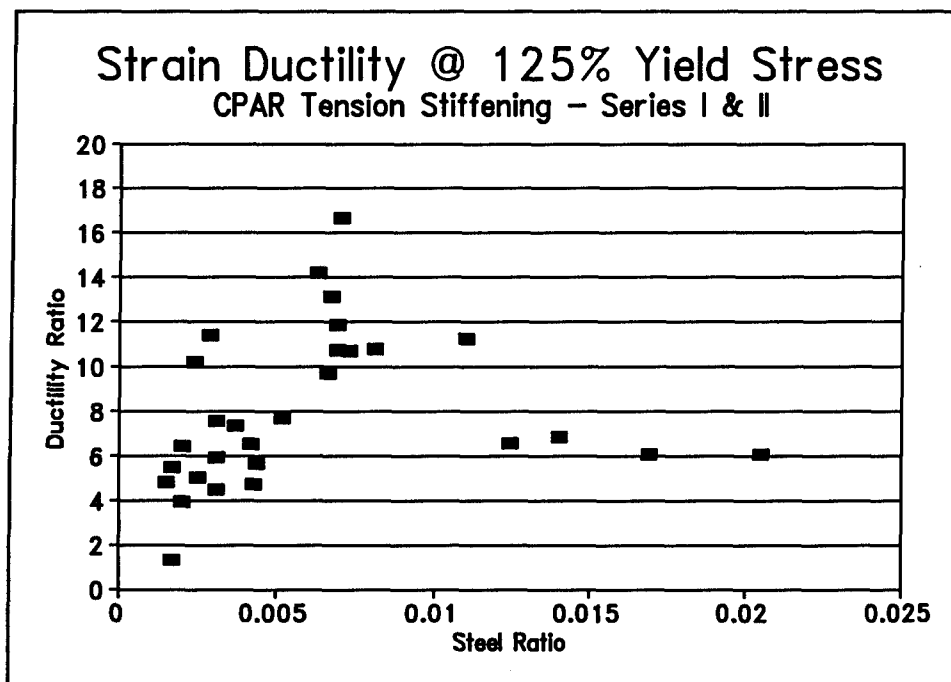

Figure 54. Strain ductility at 125 percent of yield stress

This behavior is illustrated in Figure 51 and Table 16 where the influence of steel ratio on ductility is presented.

Table 17
Results of Tests on Steel Reinforcing Bars

Bar Specimen	Bar Size No.	Strain at Yield	Strain at 125% Yield	Strain Ratio (125% Yield/100% Yield)
PBAR3	3	0.002152	0.024690	11.47
PBAR3-1	3	0.002386	0.028370	11.89
#3-PHII	3	0.001886	0.037160	19.70
4BAR1	4	0.002643	0.021830	8.26
PBAR4	4	0.002319	0.019870	8.57
#4-PHII	4	0.002886	0.033693	11.67
6BAR3	6	0.001855	0.027620	14.89
#6-PHII	6	0.001958	0.035789	18.28
8BAR1	8	0.002258	0.019510	8.64
#8-PHII	8	0.00322	0.017772	5.52
11BAR1	11	0.002309	*	
	Average	0.002352		12.60**

* Testing machine lacked capacity to reach 125% of yield
** Specimen #8-PHII not included in average

Length of debonding

The data from the end LVDT's of the Phase I specimens and from the crack gauges of the Phase II specimens were used to estimate the amount of debonding between the reinforcing bar and the grout at a crack. "Debonding" includes all mechanisms which serve to separate the steel bar from the masonry grout including wedge formation, relative slip, and pull-out. The debonding is taken as the length of steel at a crack sufficiently free to undergo yielding.

The first series of tension stiffening tests had an LVDT attached to the bar 1/2 in. from each end of the specimen to measure the relative bar-masonry displacement. The output of the LVDT includes the 1/2-in. exposed rebar plus the pullout of the bar relative to masonry. This pullout includes steel deformation down to point of steel-masonry strain compatibility. The pullout at the end of the specimen also can be considered as representing bar behavior in one-half of an interior crack. For the selected test data, the length of the flat yield plateau was measured. From this length was subtracted the length of the yield plateau that would occur from 1/2 in. of exposed bar.

From 16 tension tests on full-size bars, the average length of the strain plateau was 0.0067 with a standard deviation of 0.0021. For the 1/2 in. of rebar exposed, this translates to a yield plateau deformation of 0.00335 in.

The assumption is made that once the rebar reaches yield, the yielding process will continue at constant stress (or load) until the strain hardening regime is reached. During this time any progressive "debonding" stops, since total load is constant. The length of "debonded" steel inside the masonry is determined by subtracting the steel plateau deformation of the 1/2-in. exposed bar from the total plateau deformation measured by the LVDT. The plateau deformation inside the masonry divided by the steel yield plateau strain of 0.0067 gives the length of "debonded" steel inside the masonry that is yielding.

Phase II specimens had one bedjoint instrumented with LVDT crack gauges. A similar procedure was used for reducing this data except that no adjustment for exposed reinforcing steel was necessary, and it was recognized that the gauges measured debonding from both sides of the crack.

Data were rejected for inclusion in this study for several reasons. Phase I data were rejected when the end pullout failure cone intercepted the bearing point of the LVDT. Specimens where the cracking load was near the yield load often displayed erratic response on first cracking and were therefore rejected. Other specimens, which displayed erratic response for no known reason, were also rejected.

Data are presented in Table 18 and plotted in Figure 55. In Figure 55, a general trend of increasing debond length is observed as the perimeter of the steel bar increases. The reason for the large scatter in the data from No. 4 bars is not known except that the two data points with the largest debond lengths came from Phase II tests. These data are in agreement with general bar development theories in which larger bars require greater lengths for development.

While the method used for determination of the length of debonding is only approximate, the results indicate that a sufficient length of debonding exists to prevent severe strain concentration at cracks in reinforced masonry, even for very lightly reinforced sections.

Conclusions

Results from a total of 35 direct tension tests on reinforced masonry were available. The 16 specimens tested in Phase I employed instrumentation which failed to give reliable deformation measurements for the initial loading behavior prior to yield of the reinforcing bars. Improved instrumentation in the Phase II tests corrected this problem and provided reliable data over the entire deformation range.

Table 18
Reinforcing Bar Debonding Data

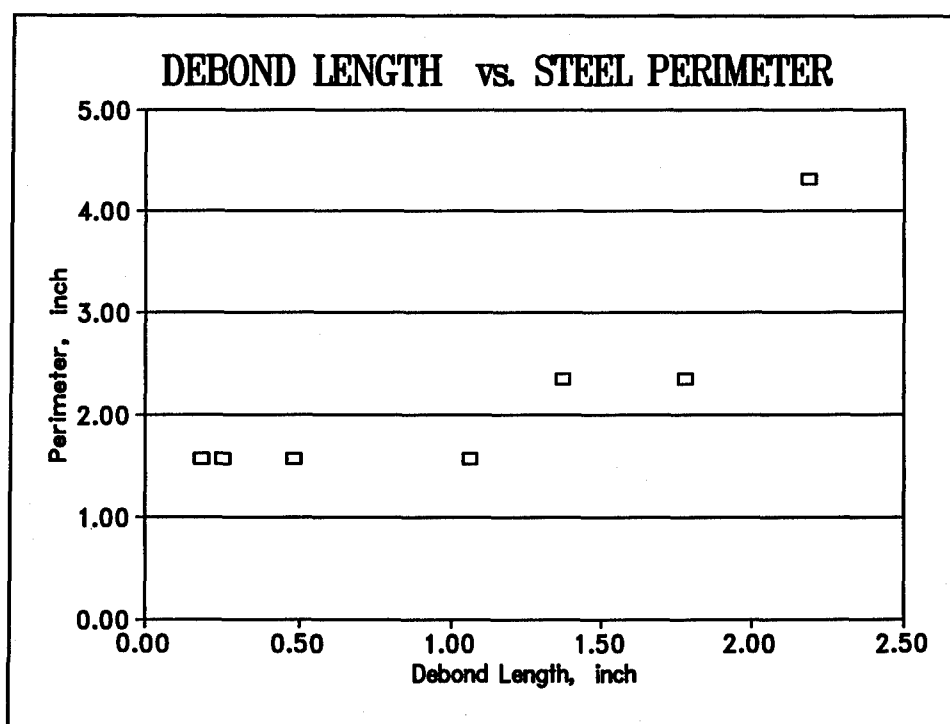| Specimen Number	Debond Length, in.	Steel Area, in.^{2}	Steel Perimeter, in.
8CO-11-2t	2.19	1.56	4.32
8CO-6-2t	1.78	0.44	2.35
8CO-6-2b	1.37	0.44	2.35
6CO-4-1	0.25	0.2	1.57
4CO-4-2t	1.06	0.2	1.57
4CO-4-2b	0.18	0.2	1.57
6CO-4-2	0.48	0.2	1.57
4CL-4-1	1.46	0.2	1.57
4CO-4-3	2.78	0.2	1.57
4CL-3-1	1.55	0.11	1.18
6CL-6-1	1.46	0.44	2.35
8CO-6-3	1.49	0.44	2.35

Figure 55.   Debond length

The average first cracking strength from all tests was 165 psi. When subsequent second, third, and fourth cracks could be identified, the resulting distribution of strength was distinctly nonnormal having a log-normal or Weibol distribution tailing to the higher cracking strengths. Observed cracking normal to the tensile stress direction showed increasing numbers of cracks and a more uniform distribution of cracks as the steel ratio increased. For low values of the steel ratio, ≤0.0020, however, no occurrence of strain localization sufficient to produce bar failure was observed. The occurrence of cracks parallel to the reinforcing bar was observed to be primarily a function of the least cover distance of the bar.

The tensile stress-strain response prior to yielding was governed primarily by the progressive cracking of the masonry. Initial behavior was governed elastic properties. After cracking, a rapid decrease in effective stiffness was observed with the stiffness reduced to that of the reinforcing steel at a strain approximately equal to five times the cracking strain.

After yield, the influence of the surrounding masonry served to decrease the range of the yield plateau as well as to increase the stiffness of the strain hardening range compared to the response of the steel bar alone. Measures of this decreased ductility are given. Finally, an estimate was made of the length of debonding that occurs between the bar and the surrounding grout at a crack. Although this measure is only approximate, results confirm that extreme strain localization does not occur at cracks, at least not for the steel percentages studied.

4 Biaxial Tests of Reinforced Masonry

General

A reinforced masonry element subjected to biaxial in-plane loads is an important component of most masonry structures. Such an element, often in the form of a shear wall, provides resistance to horizontal loadings produced by seismic and wind forces, in addition to resisting vertical loads from dead and live loads. Under typical loading conditions, this element resists compressive stresses by compression of the masonry and tension in the reinforcement. Cyclic loading can produce alternating stress states in a reinforced masonry element with each stress state having its own orientation of principal stresses and strains.

Vecchio and Collins (1982), in their pioneering study of the in-plane response of reinforced concrete panels, observed that a degradation of concrete compressive strength resulted from transverse tensile strains in the postcracking range. They formulated an expression for this effect which has been used by a number of analysts in the development of finite element codes. The proper representation of this degradation effect has been essential for adequate modeling of reinforced concrete behavior (Cervenka 1985).

Presently no experimental data are available to permit an evaluation of the degradation of masonry compressive strength due to transverse tensile strain. Lacking such information, those developing finite element codes for masonry (Ewing, El-Mustapha, and Kariotis 1987; Seible, La Rovere, and Kingsley 1990) have used the Vecchio and Collins expressions for reinforced concrete. This approach has been questioned, however, given the significant differences in materials and structure between reinforced concrete and reinforced masonry.

The future adoption of limit-state design for reinforced masonry will require the determination of masonry behavior at several limit states, including those which produce biaxial yielding stresses, strains, and plastic behavior of biaxially loaded elements. A behavioral understanding and

description of load resistance and deformation is required to define design parameters and the limit states. In particular, material properties of composite elements (smeared crack properties) must be defined for analytic modeling and the design of reinforcing steel.

The biaxial state of stress in masonry wall elements relates directly to the prediction of failure stresses in masonry shear walls and diaphragms. High levels of strain in one direction may damage the masonry and reduce its carrying capacity in another direction. As such, the behavior of masonry with biaxial stress and strain states is of importance when defining the strength limit state of the structural system. In addition, the effect of preexisting cracks on the ultimate compressive strength can be used to determine the strength of a damaged structure to evaluate retrofit methods and options.

A literature review summarizes available information relating to biaxial behavior of masonry in both the cracked and uncracked states. Information relating to the compressive behavior of cracked reinforced concrete is also reviewed including details of experiments used to determine this behavior. The test plan is presented along with a description of the experimental equipment and test procedures used to investigate the compressive behavior of cracked reinforced masonry including variables to be considered and details of the experimental test setup. A description of the materials used in the study is presented. The results of the tests conducted on panels of reinforced masonry loaded in biaxial compression-tension are presented. The behavior of the test panels is analyzed to produce an equation describing the behavior in a form suitable for inclusion in finite element programs.

Problem Statement

The strength of reinforced masonry walls under complex loading conditions is currently not clearly understood. In particular, the biaxial strength of these walls has not been clearly defined. It is understood that the compressive strength of masonry walls deteriorates with lateral tension. However, the extent of deterioration and the relationship between lateral strain and compressive strength is not yet quantified for structural modeling and design.

Research Objectives

The primary objective of this research project is to determine the relationship between lateral strain and the ultimate compressive strength of reinforced concrete masonry walls under biaxial loading conditions. An expression is to be developed for the compressive stress-strain behavior as a function of transverse tensile strain in a form suitable for use in

finite element analysis of reinforced masonry. A secondary objective of the research program is to determine the postcracking strength of reinforced concrete masonry walls under both biaxial and uniaxial loading conditions.

Literature Review

The literature in the area of biaxial compressive strength and behavior is limited in the area of reinforced masonry construction. Reinforced masonry has largely been assumed to behave in a similar manner as reinforced concrete construction. However, recent tests have shown clear flaws in this assumption, and the biaxial behavior of reinforced masonry has received some focused attention to describe the biaxial stress-strain relationship for computer modeling and strength prediction.

Reinforced concrete biaxial behavior

The majority of related research performed in the area of biaxial tension-compression behavior has been performed on reinforced concrete specimens, not reinforced concrete masonry. These research studies have brought about a series of equations that approximately describe the behavior of reinforced concrete. Vecchio and Collins (1986) and Vecchio (1989) have conducted some of the most definitive work on this problem. They found that transverse tensile strains have a degrading effect on the compressive stress-strain behavior of concrete. The prepeak compressive stress degraded parabolically according to the equation

$$F_c = F_c' \left[2 \left(\frac{\varepsilon_c}{\varepsilon_o} \right) - \beta \left(\frac{\varepsilon_c}{\varepsilon_o} \right)^2 \right] \tag{13}$$

where

ε_c = vertical compressive strain

ε_o = uniaxial compressive strain at maximum strength

f_c = biaxial compressive stress

F_c' = uniaxial compressive strength

β = damage factor (ratio of biaxial compressive-tensile strength to uniaxial compressive strength)

The magnitude of the biaxial compressive-tensile strength was related to the ratio of $\varepsilon_t/\varepsilon_o$ as follows:

$$F_c = \frac{F_c'}{\beta} = \frac{F_c'}{0.80 + 0.34 \left(\dfrac{\varepsilon_t}{\varepsilon_o} \right)}$$

(14)

where

ε_t = lateral tensile strain

F_c = biaxial compressive strength

F_c' = uniaxial compressive strength

The postpeak behavior was described by the equation below.

$$f_c = F_c \left[1 - \frac{(\varepsilon_c - \varepsilon_p)^2}{(2\varepsilon_o - \varepsilon_p)^2} \right]$$

(15)

where

ε_p = the biaxial compressive strain at maximum strength.

The postpeak parabolic envelop developed by Vecchio and Collins (1986) was later modified to include a stress plateau at $f_c = 0.3F_c$ for large strains (Stevens et al. 1991).

Cervenka (1985) has formulated a different approach to account for the transverse strain in which the damage factor, β, is a linear function of the tensile strain,

$$\beta = \frac{\varepsilon_t}{0.005}$$

(16)

The concrete stress is given by a parabolic expression

$$f_c = E_{co} \left[2 - \frac{\varepsilon_c}{\Gamma\varepsilon_o} \right] \varepsilon_c$$

(17)

where

E_{co} = the secant modulus to the peak stress of the uniaxial stress-strain curve,

$E_{co} = F_c'/\varepsilon_o$, and the term Γ is given by

$$\Gamma = 1 - k_1 \beta$$

(18)

102

where

k_1 = a constant determined by experiments.

Cervenka (1985) used the above representation for concrete behavior to win a competition staged by Vecchio and Collins (1986) to predict the behavior of four additional panels tested in their load frame.

The decrease in compressive strength with increasing transverse tensile strains may arise from two sources. First, the presence of transverse tensile stress in the concrete sections between tensile cracks will reduce the compressive failure strength as has been shown by many studies defining the failure envelope for concrete in the compression-tension stress quadrant. Secondly, the "bond-slip" behavior associated with concrete and reinforcing bars in tension results in a complex three-dimensional system of radial and longitudinal cracks as illustrated by Gerstle and Ingraffea (1991). The progressive growth of these cracks interacting with the compressive stress field likely acts to reduce compressive strength as a function of average tensile strain.

While the reinforced concrete research has provided valuable information, it is not adequate to predict the behavior of reinforced masonry construction. Research conducted at the University of California at San Diego investigated the behavior of reinforced concrete masonry (Nunn 1980). Although concrete masonry block is anisotropic, the tension-compression tests were conducted to simulate isotropic conditions which were then partially corrected for anisotropic conditions. The results showed a linear decrease in tensile capacity as the orthogonal compressive stress increased.

Masonry biaxial behavior

A number of studies have been conducted into the biaxial behavior of unreinforced masonry panels loaded by in-plane biaxial stresses. These studies determined the biaxial failure envelope as a function of the applied stresses, the angle between the bedjoint and major principal stress direction (layup angle) and material properties of the masonry. In addition to allowing development of failure theories, these studies have also measured biaxial stress-strain behavior up to the failure state.

A limited amount of biaxial testing on masonry elements has been directed toward determining the failure envelope of unreinforced masonry under proportional loading. Hegemier, Nunn, and Arya (1978), Khattab and Drysdale (1992) and Naraine and Sinha (1992) are three notable studies in this area. Two of these studies found that isotropic failure theories do not apply to grouted concrete masonry. Although these studies found that grout provides continuity and decreases the anisotropic characteristics, grouted unreinforced concrete masonry still does not exhibit isotropic characteristics throughout the broadest range of loads and deflections.

Hegemier, Nunn, and Arya (1978) loaded grouted concrete block panels under in-plane, biaxial, tension-compression proportional loading states. While the majority of the panels were unreinforced, three reinforced panels with bedjoint angles of 0, 45, and 70 deg were also tested. The tensile behavior of the reinforced panels was approximately isotropic, although the authors commented that poor-quality head joints or grouting techniques could induce appreciable anisotropy. None of the tests in this program would allow determination of the reduction in compressive strength due to a preexisting normal tensile strain field.

Nunn (1980) proposed a constitutive model for biaxially stressed grouted masonry. The difficulty with this model is the inability to predict mortar or grout discontinuities. However, for the special case which has zero tensile stress normal to the head joint with varying bed joint angles of inclination, a linear relationship between tensile and compressive strength was proposed using a constant slope correction for biaxial conditions other than an angle of 0 deg. A slope of approximately 1/12 (tensile strength/compression strength) was found in this study. In the case of tension perpendicular to the head joints, the head joints were ineffective in carrying tensile loads, and the grouted block in opposite courses could be used to determine the cracking tensile strength of the masonry block assemblies. The primary tensile strength of a reinforced concrete masonry block wall is due to the reinforcement and was not included in Nunn's constitutive model.

A series of tests on 1.2-m-square panels of unreinforced concrete and clay brick masonry by Thürlimann and Ganz (1985) and Thürlimann, Lurati, and Graf (1990) under monotonic, proportional loading has produced a failure criteria for masonry based on four material parameters: uniaxial strengths in the vertical and horizontal directions and the joint friction angle and cohesion.

Khattab and Drysdale (1992) determined that the tensile strength of concrete masonry initially increases with increased perpendicular compression. Their study used grouted, unreinforced, concrete masonry unit panels under a system of biaxial compression-tension loads. A variable in their test program was the inclination of the bedjoint to the loading direction. The bedjoint direction had a marked effect only with primarily compressive loads. The biaxial failure envelop for a 45-deg bedjoint angle showed an approximately 30-percent increase in tensile stress at failure (σ_1) as the normal compressive stress (σ_2) increased from 0 to a value equal to 3.86 times the tensile stress. As the stress ratio (σ_1/σ_2) increased beyond this point, the tensile stress at failure decreased linearly to zero.

Khattab and Drysdale (1993) also tested six masonry panels reinforced with varying amounts of horizontal and vertical reinforcing steel. The panels were loaded under a state of pure shear obtained by loading the panel, at a 45-deg angle to the bedjoint, under equal magnitudes of tension and compression stress. They observed that, under a pure shear loading, proper detailing of the relative amounts of horizontal and vertical steel

and ensuring that the steel used had an adequate yield zone were necessary to obtain ductile panel behavior. Since their compression and tension loads were equal, their results can not be used to determine compressive strength degradation under varying amounts of tensile strain.

Naraine and Sinha (1992) have developed the concept of a "common point" and a "stability point" to describe stress-strain behavior of brick masonry in biaxial compression. The common point is a point on the reloading curve that intersects the previous unloading curve and represents an upper bound solution for elastic recovery. The stability point is a lower-bound solution for elastic recovery. It is defined as the maximum stress-strain where unloading results in a full elastic recovery. A locus of stability points and common points could be used as a stress-strain range for design purposes.

The above referenced biaxial studies on masonry have been primarily concerned with determining the material failure criteria as a function of biaxial load ratio, layup angle, and masonry properties. Only the paper by Khattab and Drysdale (1993) has considered the postcracking strength behavior of the masonry.

Loading mechanisms

The method of loading material specimens is important in any experiment but is especially important when multiaxial loads are to be applied. Under ideal conditions, one would like to apply a known and controllable set of tractions to a specimen to investigate its response. When loads are applied through rigid steel platens, the mismatch in moduli between the platen and the specimen leads to creation of surface shear tractions which act as confining stresses on the specimen.

Several investigators have successfully used brush platens to load small specimens in compression and tension (Dhanasekar, Page, and Kleeman 1985 and Dialer 1990). The brush platen significantly reduces lateral surface shear tractions but restricts any rotational deformations at the surface which Dialer has shown with unreinforced brick masonry. Hegemier, Nunn, and Arya (1978) used a polysulfide material having a very low shear modulus between the specimen and a rigid loading member to reduce shear tractions from compressive loads. For tensile loadings, he used a rigid epoxy to bond the specimen to the platen. Thürlimann and Ganz (1985) employed five pads composing a sandwich of neoprene, steel plate, and teflon sheet between the specimen and a load transfer beam.

The test setup used by Khattab and Drysdale (1992, 1993) bonds four steel channel sections to each tension side of the specimen using a structural epoxy. When the panel contains reinforcing bars, they are welded to the steel channels. Each channel section is free to rotate in the plane of the panel. Compression loads are transmitted to the specimen through four steel platens per side using a Hydrostone capping material between the

specimen and platen. Spherical heads are used with each compression platen to permit free rotation. While surface shear tractions are created with this design, the depth of their influence is limited to approximately the width of the channel or platen leaving the interior of the panel specimen free from boundary effects. The specimen design used for reinforced concrete panel tests by Vecchio and Collins (1986) and Vecchio (1989) welds the ends of the reinforcing bars to steel plates which are cast in the specimen. Individual external load rams connect to the embedded plates.

Full-scale biaxial panel tests require massive, rigid loading frames to resist the applied specimen forces. Hydraulic rams are the usual loading mechanism used to generate the loads. One problem to be overcome in the design of the loading mechanism is to allow the specimen to freely deform in a direction orthogonal to an applied load. The loading device of Thürlimann isolates the horizontal compression loading mechanism from the vertical mechanism by suspending the horizontal loader by cables. The biaxial load frame of Drysdale applies the compression loads through four independent ram-reaction mechanisms which are suspended from an overhead frame. This allows lateral specimen movements to be accommodated. His tensile load device is a whiffletree arrangement reacting against a rigid frame. The in-plane load frame of Vecchio and Collins fixes the specimen at two locations to provide stability. Each loading point is connected to two hydraulic rams at 90 deg to allow normal and shear tractions to be applied to the specimen edge.

Research Plan

The research plan for the biaxial testing of reinforced masonry wall panels was to conduct eight full-scale tests to compressive failure. The compressive strength of each grouted concrete masonry panel, 48 in. wide by 32 in. high, was determined under a prescribed lateral strain condition. The prescribed tensile strain was applied to each specimen, then the specimen was loaded to its ultimate compressive strength under displacement control. After ultimate compressive strength was reached, the compressive load was removed and the lateral tension force reduced. When possible, additional tests under different lateral strains were then conducted for postfailure strength analysis. Prisms, mortar cubes, and grout prisms were also tested to determine the relationship between the wall segments and standardized tests.

Test specimens

The test specimens were full-scale grouted concrete masonry unit wall panels. They consisted of four courses of hollow concrete masonry bond beam units (15.6-in. × 5.6-in. × 7.6 in.). Each wall specimen was 47.625 in. wide and 31.25 in. high. In each course, one horizontal No. 4 reinforcing bar was placed along the center line of the course. This gives a

reinforcement ratio of 0.0045. To accommodate the reinforcing bars at the center line, it was necessary to remove some material from the web of the bond beam units. The reinforcing bars were welded to an end plate. The end plates rested inside the hollow core of the outermost masonry block to be fully bonded after the grouting process. Two 1/2-in.-diam all-thread rods extended through the end plates and outside of the specimens in a manner that permitted use of these rods to tension the specimen (Figure 56). A test jig was constructed to accurately position the transverse reinforcing bars and bearing plates. A tension test was conducted on this assembly to assure that the reinforcing bar could be loaded into the strain hardening region prior to tensile failure of the assembly.

Instrumentation

Four different types of instruments were used in this testing program. The machine head displacement was controlled and monitored by two direct current (DC) displacement transducers. The lateral forces applied to the masonry panel were measured using four strain-gauged tensile links (two on each side of the panel) acting as load cells. Each link was calibrated against a verified universal testing machine prior to the tests. Twelve channels of alternating current (AC) linear variable differential transducers (LVDT), six on each side of the specimens, were used to determine horizontal and vertical displacements over prescribed gauge lengths
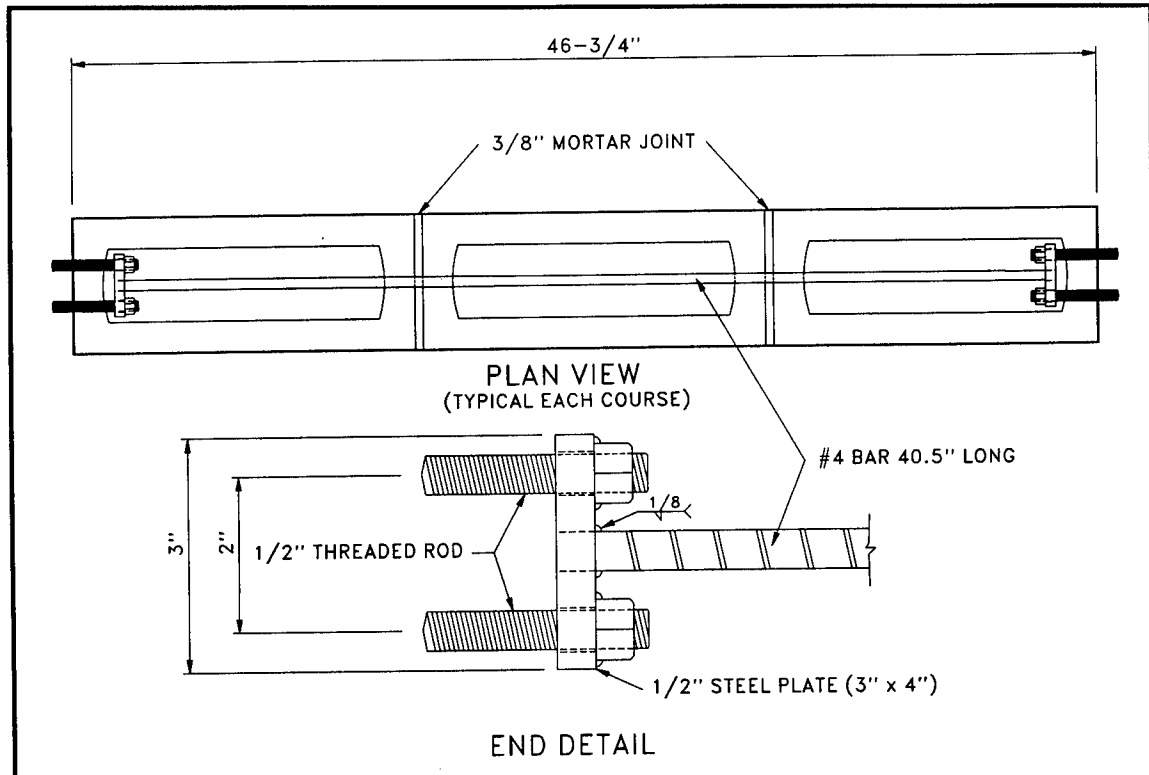

Figure 56.   Reinforcing bar details

on both sides of the masonry walls. The locations of the instruments are shown in Figure 57. Two pressure transducers were used to monitor the hydraulic pressure in the vertical and horizontal rams.

Each device used in the test program was calibrated by a traceable reference. The LVDT's were calibrated with micrometers, the load cells with a universal testing machine, and the pressure transducers with a dead weight tester. A Hewlett-Packard electronic data acquisition system was used to collect the conditioned signals for AC LVDT's, DC displacement transducers, pressure transducers, and load cells. The data were uploaded to a personal computer for reduction and analysis.

Loading system

The tests were performed at the Concrete Technology Division, Structures Laboratory, WES. The biaxial loading frame was designed by Atkinson-Noland and Associates, Boulder, CO. Figure 58 shows a schematic diagram of the loading system. The vertical loading system was a 2.4-million-pound (force) capacity Baldwin universal testing machine. The machine is controlled by a closed-loop servo-hydraulic system and is capable of both load and displacement control. The transverse loading system was comprised of a steel lateral frame with a wiffletree tension loading arrangement to distribute the loading to eight equal application points on the specimen.

The transverse tensile loading system had an active side and a passive side. On the active side, a 120-kip hydraulic ram provided the force for the tension loading system. The system was operated manually through a
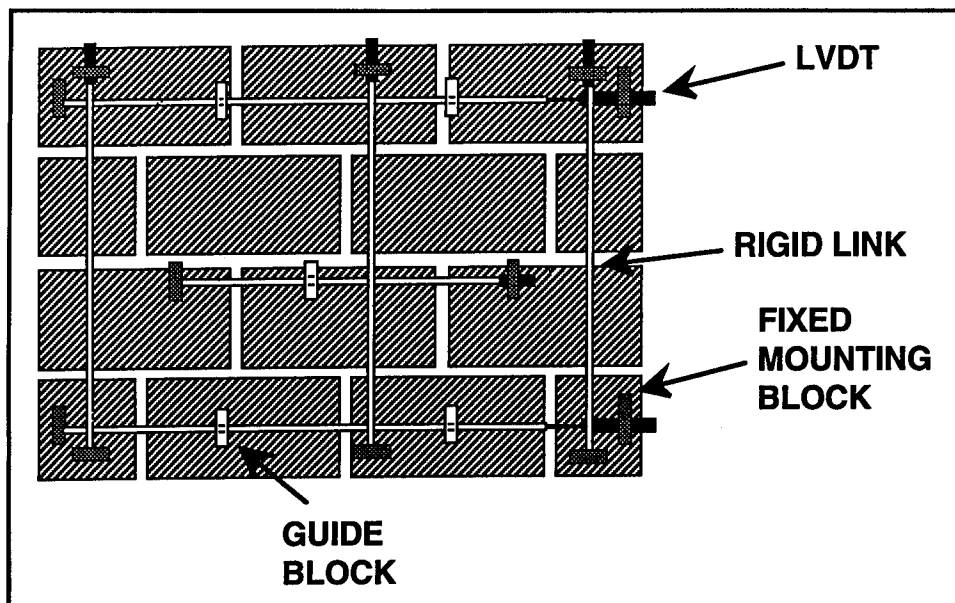

Figure 57. Typical instrumentation plan for masonry panel (identical each side)
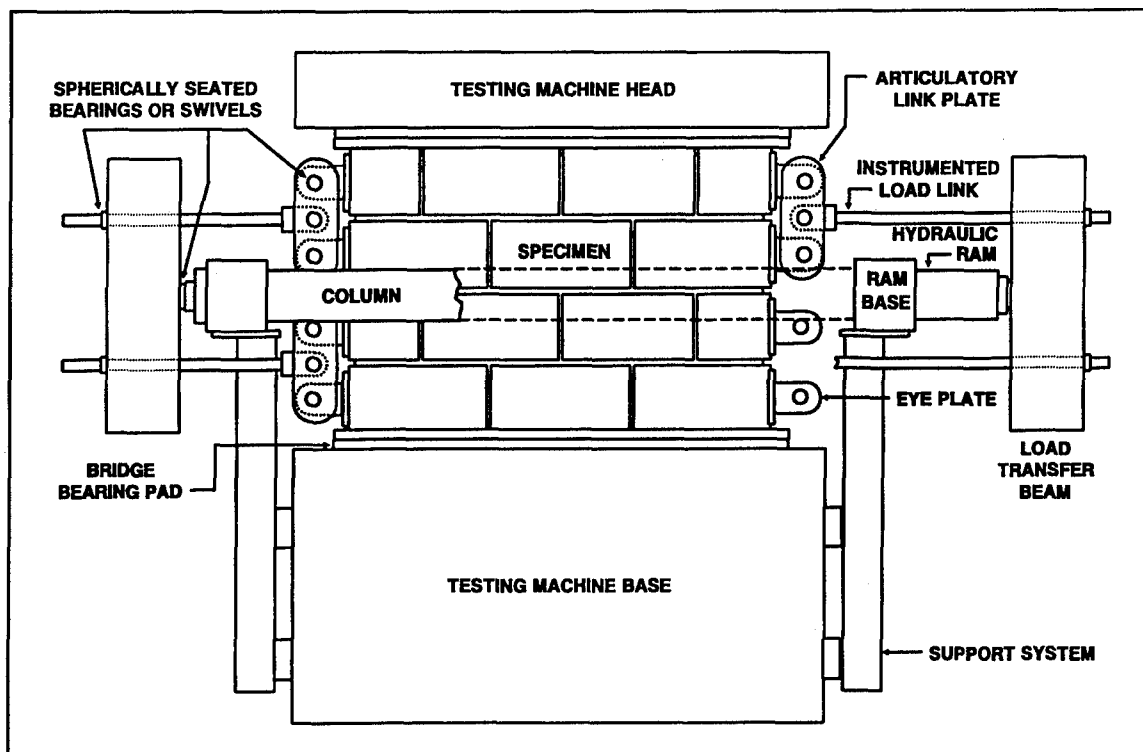
Figure 58. Biaxial load frame

hydraulic jack with an in-line pressure transducer. The force from the ram
was transferred through a load transfer beam to two rigid load links. The
load links were strain-gauged so that the loads in each link could be moni-
tored individually. Each load link terminated in a pair of articulating load
transfer plates. The loads were transferred from these plates to eye plates
which were bolted to the internal embedded load transfer plates described
below. At each of the contact points in the wiffletree system, spherically
seated bearings or swivels were used to minimize friction, thus allowing
the load to be equally distributed to the four application points on each
side of the panel. On the passive side, a similar wiffletree arrangement
was used to equally distribute the tensile reaction forces. The lateral
thrust in the wiffletree system was reacted by a series of beams and col-
umns so that all the lateral forces were contained in the test frame. Test
data indicate that the lateral wiffletree loading system accomplished the
objectives of equally distributing the loads to the ends of the specimens.
The maximum variation in the loads recorded from the four load links was
on the order of 10 percent of the applied load.

Testing procedures

In preparing for a test, both the upper and lower platens of the univer-
sal testing machine were cleaned and greased with petroleum-based
grease. A 1⅛-in.-thick high-strength neoprene bridge bearing pad with a
40-mil polyethylene cover was placed on the lower platen of the testing

machine. A ⅞-in.-thick steel plate was subsequently placed on top of the bearing pad. The bridge bearing pad was used to evenly distribute the vertical load from the large universal testing machine. The fabricated masonry panel, complete with the internal load transfer plates, was then placed on the steel plate and carefully centered in the testing machine and in the lateral loading frame. All connections from the lateral loading frame to the internal load transfer plate were completed at this time. Subsequently, the upper surface of the panel was capped with a gypsum cement capping material to achieve a planar bearing surface at the top of the panel. This cap was allowed to harden, and a steel plate and bridge bearing pad identical to those used on the bottom were centered on the top of the panel.

The test procedure for testing the masonry panels include a seating stage, a lateral loading stage, and a vertical loading stage. In some cases, the second and third stages were repeated to determine postfailure strength. The seating stage included loading the wall vertically in compression to 200 kips in 25-kip increments, then unloading to 50 kips in 25-kip increments. For Tests 6, 7, and 8, this seating stage followed the lateral loading stage to minimize lateral friction.

In the second stage, concrete masonry panels were tensioned laterally to a predetermined strain. Data were collected intermittently during this stage, at 25-kip increments during the elastic portion and at timed intervals after yielding. In the third stage, vertical compressive load was applied under deflection control until the ultimate strength was reached. Data recording scans were conducted at 25-kip load increments. After the ultimate strength was reached, the vertical load was removed and the lateral strain changed to a different level, and the vertical load was once again increased to the ultimate strength of the specimen.

Test matrix

Table 19 presents a summary of the eight tests conducted and a listing of the primary and secondary test parameters. In some cases, only the primary test was conducted because the specimen failed before it was possible to unload the vertical force. Test number one was a shakedown test. This test was used to check the seating of the specimen, the relative deflections in the instrumentation, the loading regime, and the data acquisition system. The results from this test were not used in the analysis because the specimen was not taken to failure and was tested only 18 days after grouting. Table 20 shows the fabrication schedule for all the specimens.

Table 19
Test Matrix

Test Number	Primary Test Parameter	Secondary Test Parameter
1	Shakedown test of experimental setup	None
4	Uniaxial Test ($\varepsilon_t = 0$)	$\varepsilon_t = 0.0024, 0.0042$
3	$\varepsilon_t = 0.0024$	Specimen failed before unloading
5	$\varepsilon_t = 0.0032$	Reload at $\varepsilon_t = 0.0032$
6	$\varepsilon_t = 0.0042$	Specimen failed before unloading
7	$\varepsilon_t = 0.0068$	Specimen failed before unloading
8	$\varepsilon_t = 0.0068$	Specimen failed before unloading
2	$\varepsilon_t = 0.0100$	Specimen failed before unloading

Table 20
Testing Program

Specimen Number	Fabrication Date	Grouting Date	Testing Date	Comments
1	6-23-92	6-29-92	7-16-92	Uniaxial
2	7-15-92	7-17-92	8-11-92	Biaxial
3	7-15-92	7-17-92	8-14-92	Biaxial
4	7-22-92	7-24-92	8-18-92	Uniaxial
5	7-22-92	7-24-92	8-21-92	Biaxial
6	7-29-92	8-1-92	8-26-92	Biaxial
7	7-29-92	8-1-92	10-7-92	Biaxial
8	7-29-92	8-1-92	10-13-92	Biaxial

Cast Prisms, cubes, and cylinders with specimens 4 and 5.

Materials and Quality Assurance

General

The materials used in this test program were representative of those used in the construction of reinforced concrete masonry unit structures. Appendix A contains the results of material property tests conducted on the concrete block, cement, lime, and reinforcing bars used in the biaxial tests.

Block

The concrete masonry block was a 6-in. concrete bond beam unit with a compressive strength of 3,180 psi on net area or 2,000 psi on gross area. The block was provided by Blocklite, Selma, CA, and was identical to the block used in the rest of this program.

Mortar

The mortar was an ASTM C 270 (ASTM 1990n) Type S mortar consisting of 1 lb Type I portland cement, 0.35 lb Type S lime, 3.71 lb sand (oven dry), and 0.80 lb water. The average compressive strength of the mortar was 2,300 psi determined from 2-in. cubical specimens tested following ASTM C 109-90 (1990d). The mixture proportions are shown in Table 21.

Table 21
Mortar Proportions

Material	Proportions Based on Volume	Specific Gravity	Weight, lb	Proportions Based on Weight
Cement	1.0 ft³	3.15	196.56	1.00 lb
Type S Lime	0.5 ft³	2.20	68.64	0.35 lb
Sand	4.5 ft³	2.60	730.08	3.71 lb
Water	2.5 ft³	1.00	157.25	0.80 lb

Grout

The grout consisted of 1 lb Type I portland cement, 2.5 lb sand (oven dry), 1.6 lb, 3/8-in. nominal maximum sized aggregate (oven dry), 0.01 lb of a commercial chemical admixture (Sika Grout Aid), and 0.57 lb water. The chemical admixture was used to compensate for shrinkage and enhance mobility of the grout. The grout mixture, conforming to ASTM C 476-83 (ASTM 1990q), was placed using internal vibration to obtain good consolidation. The grout proportions and properties are listed in Tables 22 and 23.

**Table 22
Grout Proportions**

Material	Proportions Based on Volume	Specific Gravity	Weight/yd^3	Proportions Based on Weight
Cement	3.12 ft^3	3.15	613	94 lb
3/8-in. Aggregate*	6.24 ft^3	2.55	992	152 lb
Sand**	9.37 ft^3	2.60	1,520	233 lb
Grout Aid	0.05 ft^3	NA†	6.15	0.94 lb
Air	2.70 ft^3	0.00	0.00	0.00 lb
Water	5.51 ft^3	1.00	343	52.6 lb

* (1.0% absorption)
** (0.3% absorption)
† This parameter not measured.

**Table 23
Grout Quality Assurance Testing**

Batch Date	6-26-92	7-17-92	7-24-92	7-30-92
Slump, in.	10.5	9.5	9.5	9.75
Air, percent	10.0	10.0	10.2	10.5
Unit Wt. #/ft^3	131	141	135	128

ASTM C 1019-89a (ASTM 1990t) grout prisms were cast from the grout batch used to grout Specimens 4 and 5. The compressive strength of the prisms was determined within 24 hours after the companion panels were tested. The compressive strength results are shown in Table 24.

**Table 24
Grout Prism Test Results (Specimens 4 and 5 only)**

Test Numbers	Age of Grout Prism	Compressive Strength
1	11 days	2,340 psi
2, 5	24 days	3,960 psi
3, 4	21 days	4,130 psi

Steel

The No. 4 reinforcing bars were grade 60 with a yield strength of 72,300 psi and ultimate strength of 117,000 psi following ASTM A 370-88a (ASTM 1990a). The modulus of elasticity of the bars was 29,300 ksi.

Masonry prisms

Three compressive strength prisms were fabricated and tested according to ASTM E 447-89 (ASTM 1990u). These specimens were constructed using the masonry prism jig described in Chapter 2. The specimens were three courses in height. The mean strength of these three prisms was 3,270 psi.

Results of Testing

Eight tests were performed to determine the compressive strength of reinforced masonry subjected to lateral strain in this testing program. The specimens and materials were described in the previous section. The test results are presented in this section and a discussion of the importance of the tests is presented in the succeeding section.

Typical test results

Upon the application of the lateral tensile forces, uniform tensile cracking occurred along each of the five lines of vertical mortar joints as shown in Figure 59. The cracking typically first occurred at the vertical lines of mortar joints near the ends of the panels and proceeded toward the central line of the panels as the level of tensile strain increased. Vertical compressive failures were characterized by spalling of the face shells, usually occurring first on one side of the panel, leading to an asymmetrical cross section. Once this asymmetrical condition developed, failure of the wall followed rather quickly.
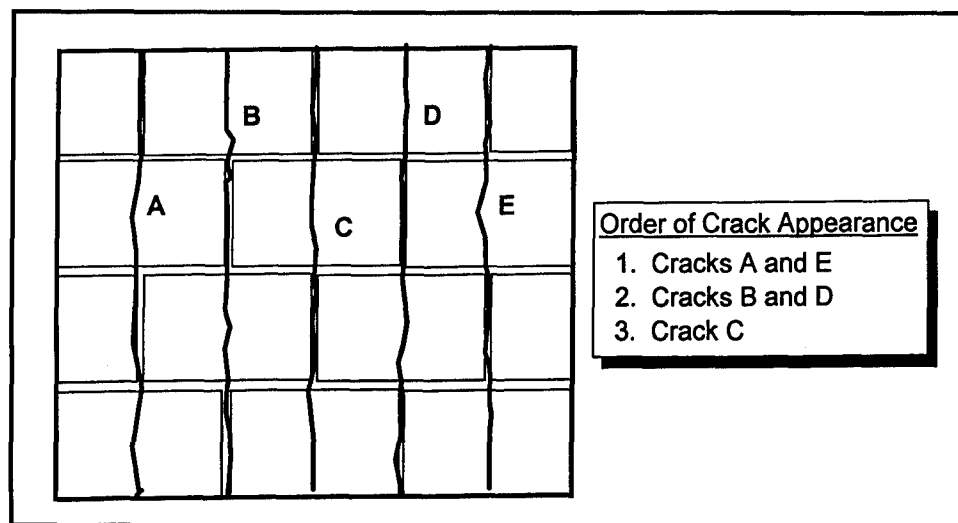

Figure 59. Typical tensile cracking pattern

Typical data from Test 4 are shown in Figures 60 through 63. In these figures, compressive stresses and strains are plotted as positive, and tensile stresses and strains are plotted as negative. From Table 20, Test 4 included a uniaxial loading followed by reloading at transverse tensile strain levels of 0.24 percent and 0.42 percent. In Figure 60, recorded loads from each of the four lateral rigid load links are plotted versus applied vertical load. The maximum variation in the loads recorded from the four load links is on the order of 10 percent of the applied load.
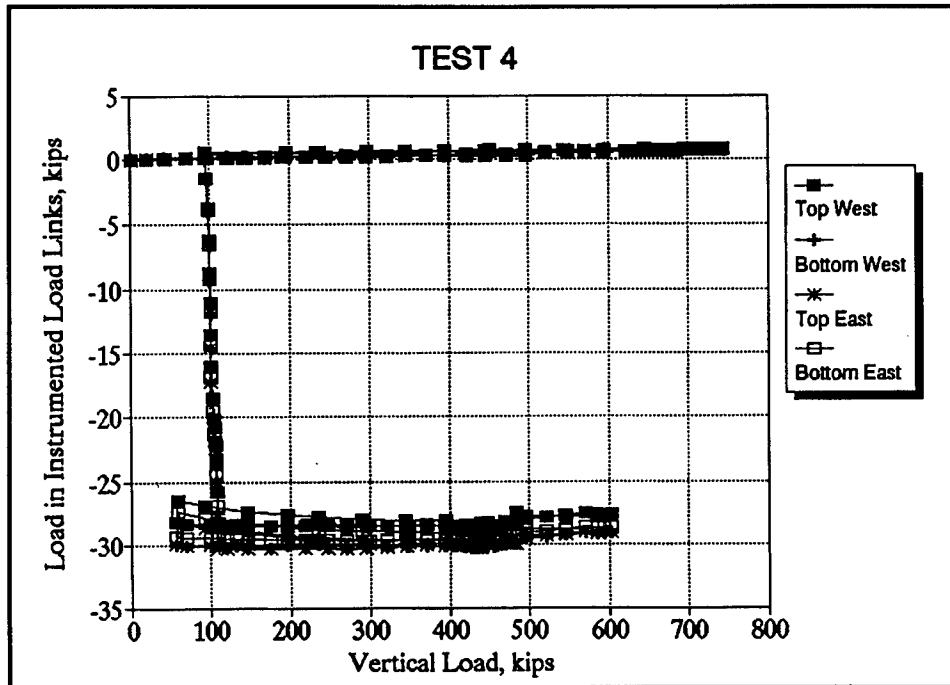

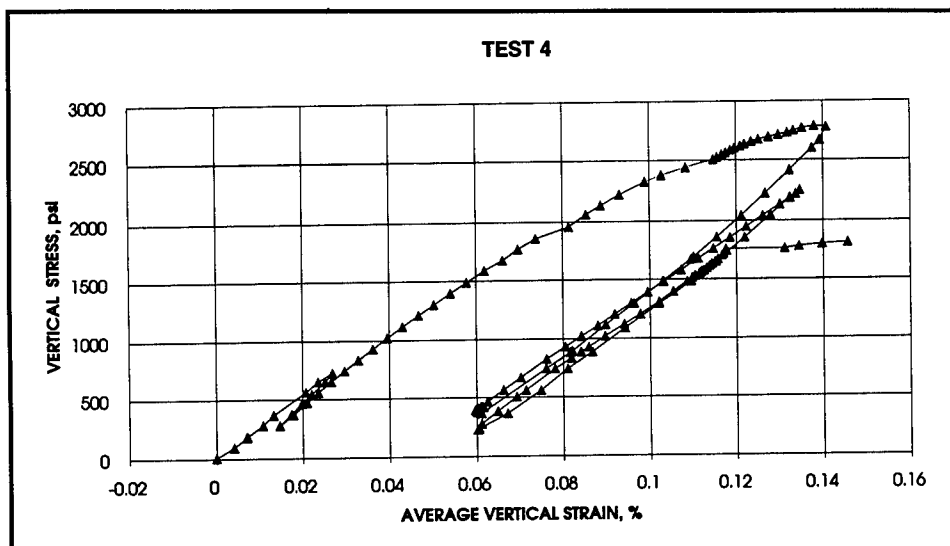Figure 60.   Comparison of data from instrumented load links, Test 4

Figure 61.   Vertical stress-strain data, Test 4

In Figure 61, vertical compressive stress is plotted against the average vertical compressive strain as recorded by the six vertical LVDT's (three per side). The vertical application of stress was continued until the vertical load-deformation curve indicated that peak resistance had been obtained. Vertical stress was calculated as the vertical load divided by the gross area of the top surface of the panel. The compressive modulus of elasticity for the initial loading was 2.5 million psi.

In Figure 62, transverse tensile stress is plotted against average transverse tensile strain for Test 4. The transverse stress was calculated as the total transverse load divided by the gross area of the end of the panel. For this test, the onset of tensile cracking occurred at a tensile stress of approximately 180 psi. For Tests 2 through 8, the range of tensile stress at
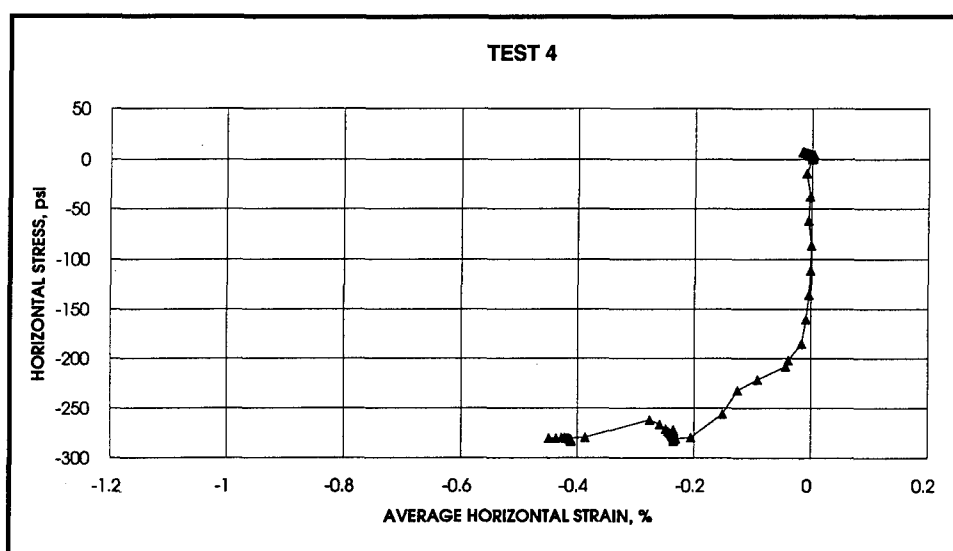
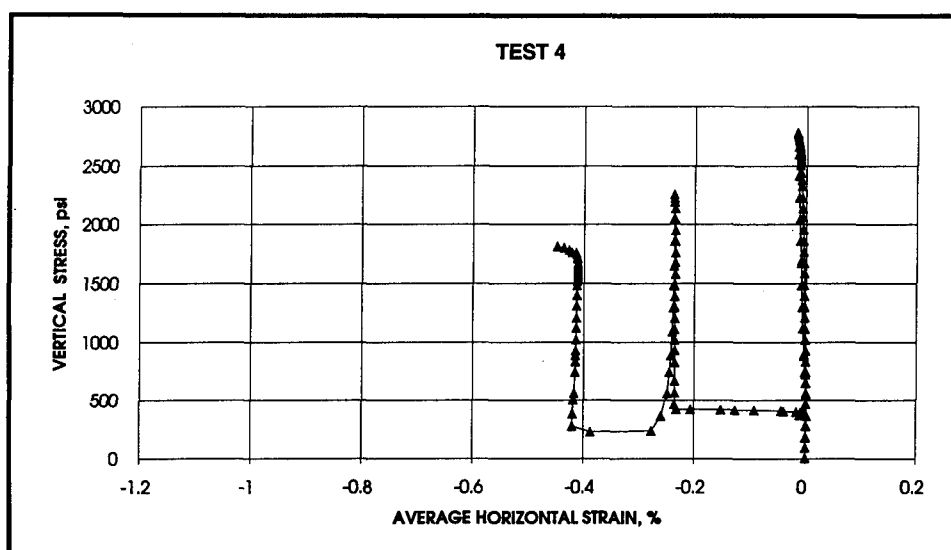Figure 62. Lateral stress-strain data, Test 4

Figure 63. Compressive stress-lateral strain data, Test 4

onset of tensile cracking was from approximately 120 psi to 180 psi, with the mean value of 155 psi.

In Figure 63, vertical compressive stress has been plotted against average transverse strain for Test 4. These data show the degradation of compressive strength for the three loading cycles as transverse tensile strain was progressively increased.

Test Results

Test 1 was performed as a trial test of the loading apparatus and data acquisition devices. This test provided valuable information on the load setup for the reinforced masonry specimens. The testing was performed in load control. The loading regime for this test was divided in three stages. In the first stage, vertical compressive load was applied to 200 kips in 25-kip increments. The load was subsequently incrementally decreased to 50-kips, and then increased to 400 kips in 25-kip increments. Next, the load was again decreased to 50 kips, and a third loading was applied to ultimate in 25-kip increments. The maximum uniaxial compressive stress was approximately 1,780 psi. Seventeen channels of data were collected. All 17 channels functioned throughout the test. These data are not presented herein, because the primary purpose of this test was to check out the loading and instrumentation systems.

In Test 2, a vertical compressive load of 200 kips was applied to the specimen in 25-kip increments in displacement control. The load was then incrementally decreased to 50 kips, and a lateral tensile load was applied to the specimen to produce a lateral strain of 0.0100 in./in. The lateral strain was then held constant, while the vertical compressive load was increased to ultimate strength in 25-kip increments. The ultimate biaxial compressive strength was approximately 1,460 psi. The stress-strain curve for Test 2 is shown in Figure 64. All data channels functioned throughout the test with the exception of the south-east vertical LVDT.

In Test 3, the masonry panel was preloaded to a vertical compressive load of 200-kips in 25-kip increments, and then the load was decreased to 50 kips. A lateral tensile load was applied to the specimen to cause a lateral tensile strain of 0.0024 in./in. and held constant throughout the remainder of the test. The vertical compressive force was then increased to ultimate in 25-kip increments. The ultimate biaxial compressive strength was approximately 2,850 psi. The stress-strain curve for Test 3 is shown in Figure 65.

In Test 4, the vertical compressive load was increased to 200 kips in 25-kip increments, followed by a decrease to 50 kips, and then an increase to ultimate in 25-kip increments. During this loading, the imposed lateral tensile strain was zero. The ultimate uniaxial compressive load with zero-imposed lateral stain was approximately 2,850 psi. Because the specimen

was still in excellent condition, the load was incrementally decreased to 50 kips and a lateral tensile load applied to produce a tensile strain of 0.0012 in./in. before the compressive load was again increased to ultimate. The ultimate compressive strength with an imposed lateral tensile stain of 0.0012 in./in. was 2,310 psi. The specimen was still in good condition, so the load was once again incrementally decreased to 50 kips. In the final load stage, a lateral load was applied to the specimen to cause an imposed tensile strain of 0.0024 in./in. before the compressive load was again increased to ultimate. With the imposed lateral tensile strain of 0.0024 in./in., the compressive strength was 1,850 psi. The stress-strain curve for Test 4 is shown in Figure 66.
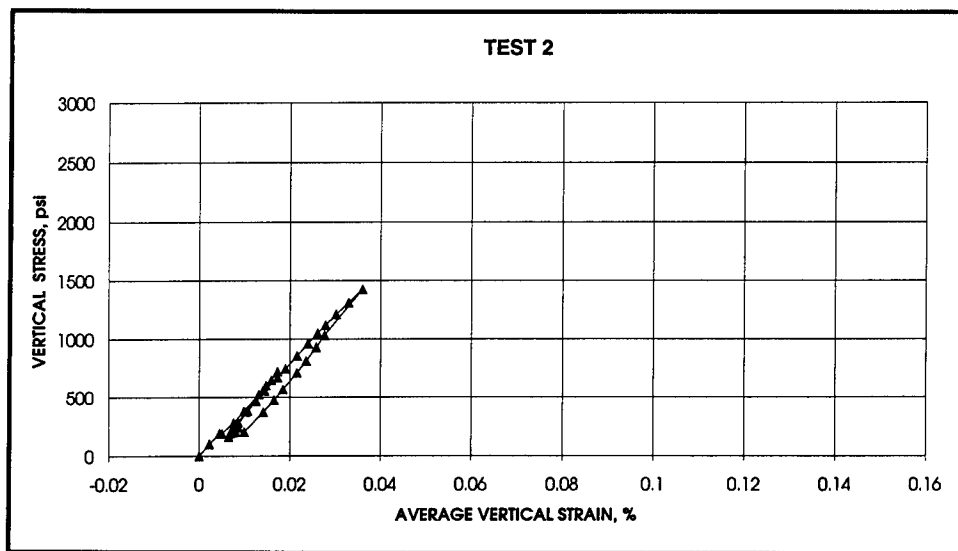

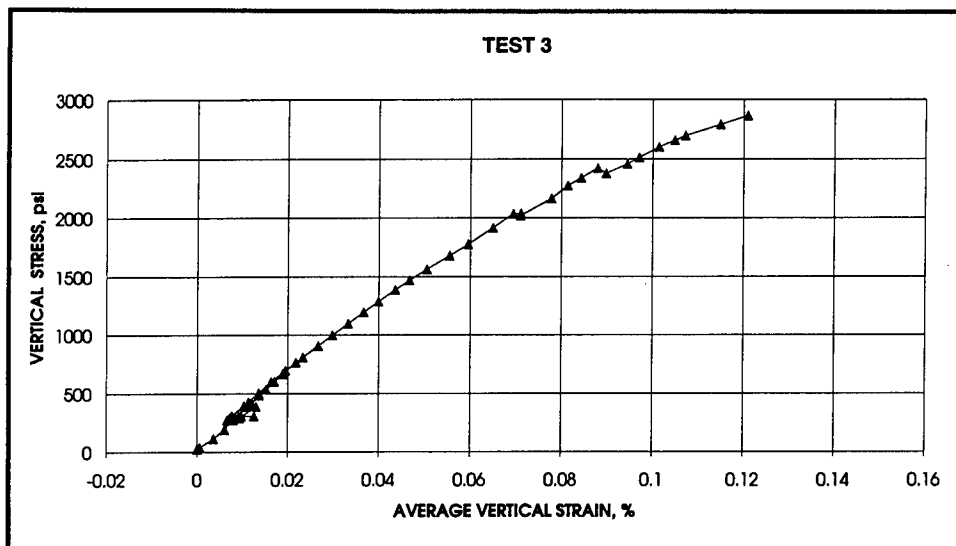Figure 64. Vertical stress-strain data, Test 2

Figure 65. Lateral stress-strain data, Test 3

The vertical compressive load was increased in 25-kip increments to 200 kips in Test 5 and then decreased to 50 kips with no imposed lateral strain. Subsequently, a lateral tensile load was applied to produce a lateral tensile strain of 0.0032 in./in. The load was incrementally increased to ultimate strength in 25-kip increments. The ultimate biaxial compressive strength at the imposed lateral tensile strain of 0.0032 in./in. was approximately 2,840 psi. The stress-strain curve for Test 5 is shown in Figure 67.

In Tests 6, 7, and 8, the lateral tensile strains were imposed prior to applying the vertical compressive loads. In Test 6, lateral load was applied to the specimen to produce a lateral tensile strain of 0.0042 in./in. A compressive load of 200 kips was then applied in 25-kip increments. Next, the load was incrementally decreased to 50 kips and then increased to ultimate in 25-kip increments. The ultimate biaxial compressive strength was approximately 2,620 psi. The stress-strain curve for Test 6 is shown in Figure 68.

In Test 7, a lateral tensile load was applied to the specimen to produce a lateral tensile strain of 0.0068 in./in. before a compressive load was applied. The loading regime for this test was again divided in two stages. In the first load stage, the vertical compressive force was applied to 200 kips in 25-kip increments. The load was incrementally decreased to 50 kips and then increased to ultimate in 25-kip increments. The ultimate
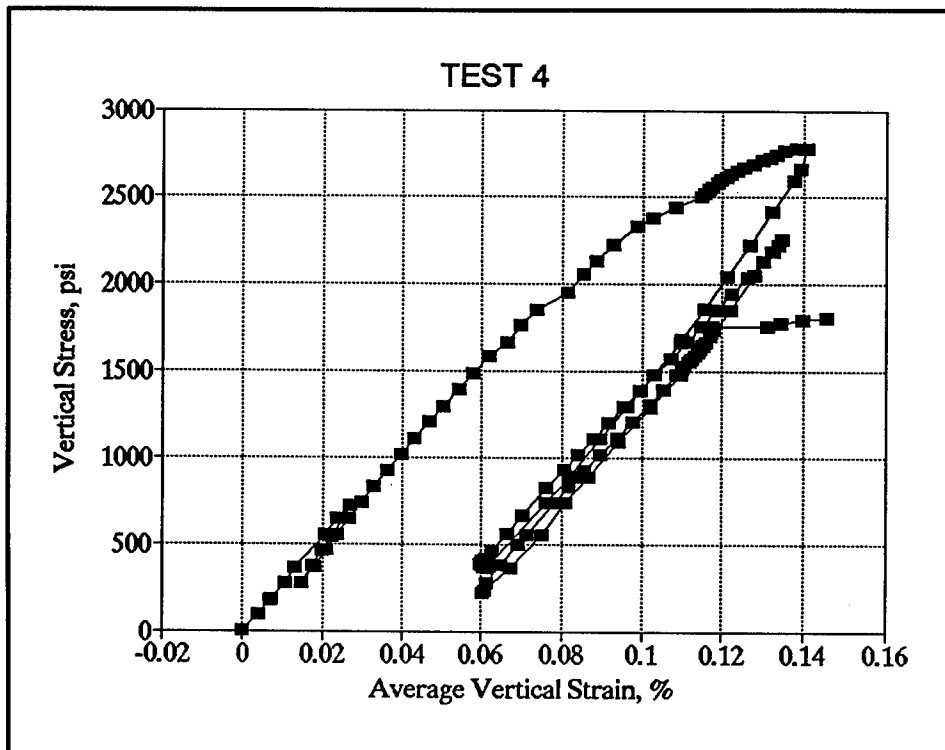
Figure 66.   Compressive stress-strain data, Test 4

biaxial compressive strength was approximately 1,990 psi. The stress-strain curve for Test 7 is shown in Figure 69.

For Test 8, a lateral tensile load was applied to the specimen to cause a 0.0088-in./in. tensile strain before a compressive load was applied. The loading regime for this test was divided in three stages. The first load stage consisted of a loading up to 200 kips in 25-kip increments. The load was then incrementally decreased to 50 kips and subsequently increased to ultimate strength in 25-kip increments. The ultimate biaxial compressive strength was approximately 1,960 psi at a lateral tensile strain of 0.0088 in./in. The load was then decreased in 50-kip increments to 10 kips. In the final load stage, the lateral load was controlled to impose a lateral tensile strain of 0.0068 in./in. before the compressive load was increased to
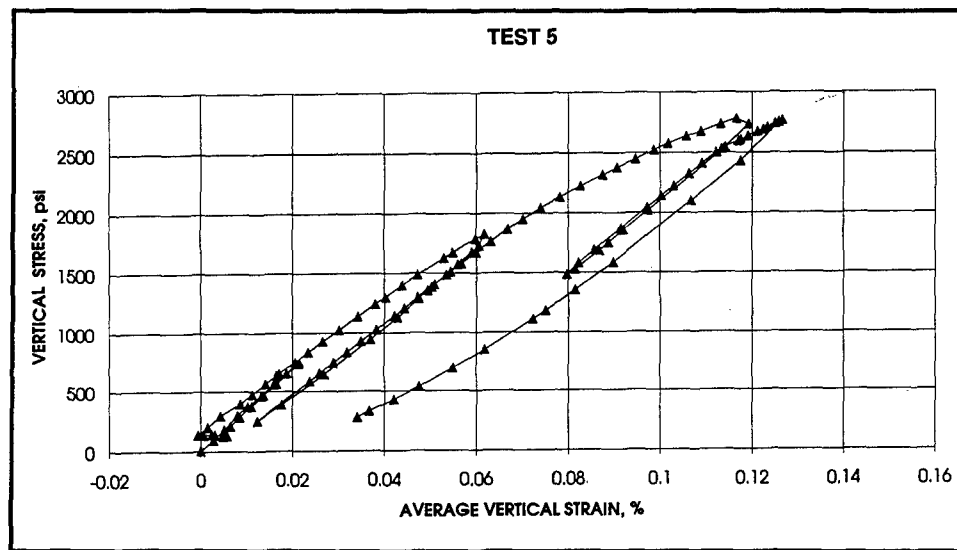
Figure 67. Lateral stress-strain data, Test 5
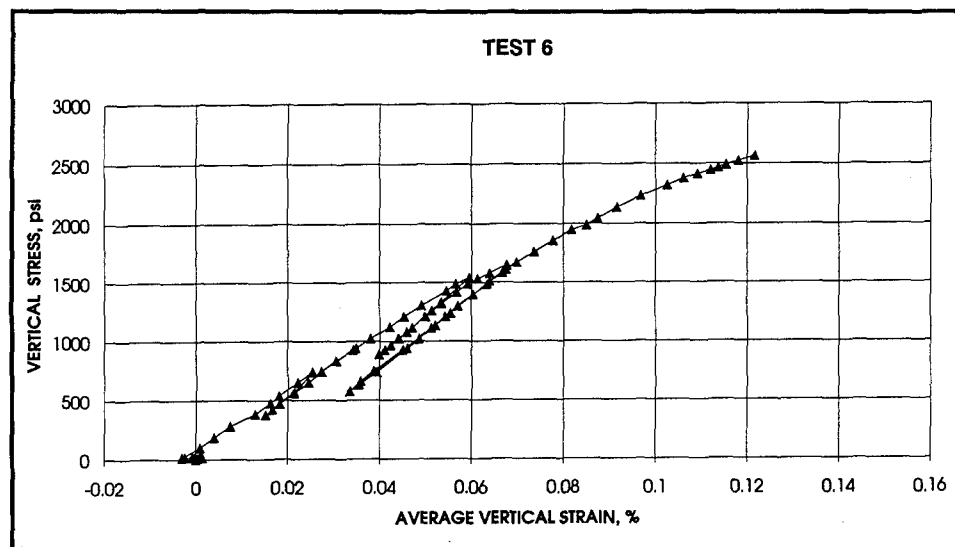
Figure 68. Vertical stress-strain data, Test 6

ultimate strength. The postfailure compressive strength was 2,650 psi.
The stress-strain curve for Test 8 is shown in Figure 70.

The modulus of elasticity and Poisson's ratio were computed from the
measured vertical and horizontal stresses and strains. In Tests 2, 3, 4, and
5, the initial load cycle was conducted with zero imposed lateral strain.
From this load cycle the modulus of elasticity and Poisson's ratio in com-
pression were calculated. These results are tabulated in Table 25. The
modulus was calculated as a secant value between approximately 5 and 40
percent of the applied 200-kip load. Poisson's ratio was calculated from
the average vertical and horizontal strains recorded at the same values of
load. After the lateral strain was imposed, the compressive elastic modu-
lus was determined as a chord modulus between approximately 5 and 40
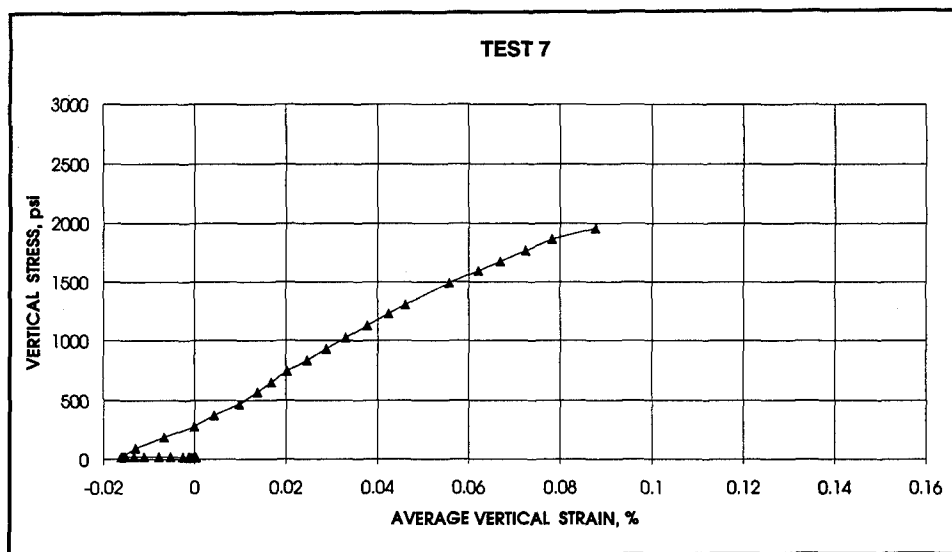
Figure 69. Lateral stress-strain data, Test 7
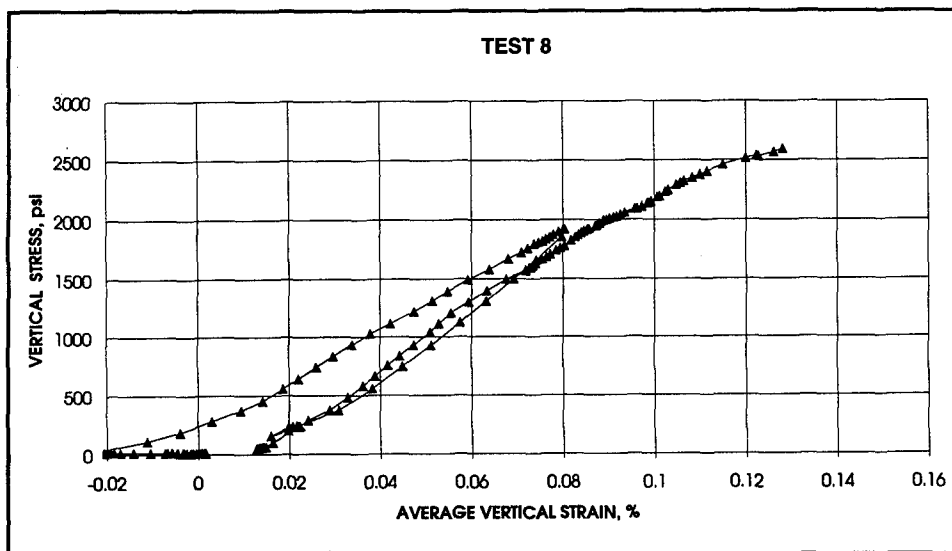
Figure 70. Lateral stress-strain data, Test 8

percent of ultimate load. In Tests 6, 7, and 8, the lateral tensile strains were imposed prior to applying the vertical compressive load. From this lateral tensile loading, the tensile modulus of elasticity was calculated for the portion of the tensile stress-strain curve before initial cracking. These data are also shown in Table 25. Subsequently, the compressive modulus of elasticity was calculated at the imposed lateral strain levels indicated.

Table 25
Calculated Modulus of Elasticity and Poisson's Ratio

| Test No. | Loading Phase | Lateral Strain in./in. | Compressive | | Tensile Modulus of Elasticity, million psi |
			Modulus of Elasticity, million psi	Poisson's Ratio	
2	1	0	4.55	0.174	--
	2	0.01	4.14	--	--
3	1	0	3.43	0.151	--
	2	0.0024	2.99	--	--
4	1	0	2.8	--	--
	2	0.0024	2.5	--	--
5	1	0	3.29	0.134	--
	2	0.0032	2.71	--	--
6	1	0.0042	--	--	3.49
	2	0.0042	2.67	--	--
7	1	0.0068	--	--	3.35
	2	0.0068	2.2	--	--
8	1	0.0088	2.28	--	4.06
	2	0.0068	2.28	--	--

Note: Blanks imply that parameter not calculated.

The compressive strain at failure, ε_c, was plotted versus the strain ratio, $\varepsilon_t/\varepsilon_o$, Figure 71. An approximately linear inverse relation exists with the compressive strain at failure decreasing as the lateral strain magnitude and strain ratio, $\varepsilon_t/\varepsilon_o$, increases. Linear regression gives the following relation with an R^2 value of 0.82:

$$\varepsilon_c = 0.001486 - 0.0013\left(\frac{\varepsilon_t}{\varepsilon_o}\right) \qquad (19)$$

Analysis and Discussion of Test Results

Table 26 summarizes the results of the biaxial test conducted under this test program. The purpose of the test program was to determine the relationship between the compressive strength of the concrete masonry with a
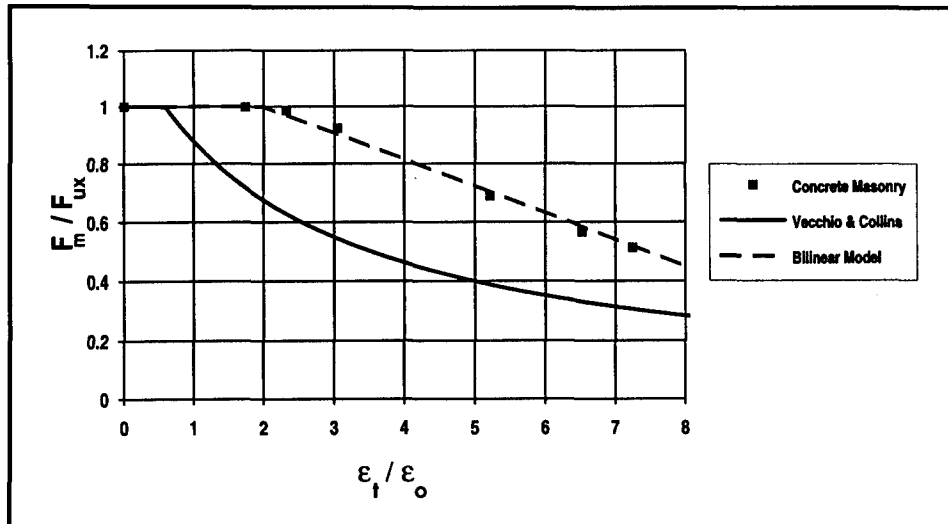
Figure 71. Relationship between compressive strength ratio and strain ratio

uniform lateral tension field. The data collected from Tests 2 through 8 showed a consistent behavioral pattern. Under small lateral tensile strains the reinforced masonry retains its full compressive strength. The compressive strength remains nearly constant to lateral tensile strains of 0.0032 in./in. When lateral tensile strains reached 0.0042 in./in., an 8-percent drop in compressive strength was noted. A 49-percent decrease in the compressive strength was measured when the lateral tensile strains were 0.0100 in./in. A regression analysis of the test results shows a linear relationship between lateral tensile strain and compressive strength for lateral tensile strains greater than 0.032 in./in., defined in the equation below.

$$F_m = -153,133\ \varepsilon_t + 3,340 \tag{20}$$

Figure 71 shows the failure data from Tests 2 through 8 summarized with dimensionless parameters. The vertical axis is the ratio of the compressive strength of the masonry panel (F_m) to the compressive strength of the masonry panel with no lateral tensile loads (F_{ux}). The value of F_{ux} was 2,850 psi from Test 4. The horizontal axis is the ratio of applied lateral tensile strain ε_t to the vertical compressive strain at uniaxial compressive failure (ε_o). The value of ε_o was 0.14 percent from Test 4. From Figure 71, it can be observed that the compressive strength remains nearly constant for strain ratios ($\varepsilon_t / \varepsilon_o$) of less than 2. For strain ratios greater than 2 and less than 8, the compressive strength ratio (F_m / F_{ux}) decreases linearly with increasing strain ratio. Based upon these results, the following model is proposed to describe the biaxial tension-compressive strength behavior of reinforced masonry:

$$\frac{F_m}{F_{ux}} = \begin{cases} 1 & for \ \frac{\varepsilon_t}{\varepsilon_o} \leq 2 \\ 1.18 - 0.092\left(\frac{\varepsilon_t}{\varepsilon_o}\right) & for \ \frac{\varepsilon_t}{\varepsilon_o} > 2 \end{cases}$$

(21)

The test results from Test 4 illustrate the progressive loss of strength as the same specimen was reloaded under increasing levels of lateral tensile strain. Under uniaxial load and zero imposed lateral tensile strain, the ultimate strength was 2,850 psi. When the specimen was reloaded with a lateral tensile strain of 0.0024 in./in., an ultimate strength of 2,310 psi was recorded, and when the lateral tensile strain was increased to 0.0042 in./in. on the third loading, the ultimate stress decreased to 1,850 psi.

Table 26
Biaxial Reinforced Masonry Panel Tests

Test No.	Lateral Tensile Strain, ε_t in./in.	Vertical Compressive Strain at Failure, ε_u, in./in.	Compressive Strength, F_m psi	$\varepsilon_t/\varepsilon_o$	Masonry Model	Vecchio and Collins Model
4	0	0.00141	2,850	0	1	1
3	0.0024	0.00126	2,850	1.714	1	0.723
5	0.0032	0.00095	2,840	2.286	0.970	0.634
6	0.0042	0.00122	2,620	3.00	0.904	0.549
7	0.0068	0.00088	1,990	4.857	0.733	0.408
8	0.0088	0.00129	1,960	6.286	0.602	0.340
2	0.0100	0.00037	1,460	7.143	0.523	0.310

Conclusions

Masonry panels subjected to biaxial tension and compression were tested to determine the relationship between the compressive strength of reinforced masonry and constant induced lateral strain. The results show that for large lateral tensile strains the compressive strength deterioration of a masonry panel is nearly linear with respect to the lateral tensile strain ratio. A bilinear model describing this relationship was proposed. The compressive strain at failure decreased linearly with increasing lateral tensile strain.

Tensile cracking stress for reinforced masonry was determined to be approximately 155 psi for these large-scale concrete masonry panels. It was confirmed that the compressive strength of masonry deteriorates with repeated loadings at or near the ultimate capacity.

Experimental stress-strain relationships for reinforced masonry in biaxial tension-compression loading were obtained. These data will provide useful information for verifying finite element models used to predict biaxial behavior of reinforced masonry.

Recommendations for Future Research

Future testing should consider the effect of other combinations of material properties such as block type and strength, grout strength, etc., on the biaxial relationship. Other load paths could be investigated to further define the biaxial relationship.

5 Summary and Conclusions

General

An experimental research program was conducted to determine critical material and design parameters of reinforced masonry which are necessary for the formulation of a new limit-states design standard for reinforced masonry. The new limit-states design standard for reinforced masonry, currently being drafted by the Masonry Standards Joint Committee (MSJC), will bring the design of reinforced masonry structures to the same level of practice as that used for reinforced concrete and steel structures. The results from this study provide critical behavioral knowledge necessary to prescribe requirements for lap-splice length, maximum and minimum amounts of reinforcing steel, and strength reduction factors for biaxial behavior.

The experimental study was conducted at the laboratories of WES. The design of the experiments was undertaken jointly by WES and by Atkinson-Noland & Associates. The overall objectives of the experimental program as well as the parameters to be studied and the range of these parameters were closely coordinated with other researchers involved with the U.S. Coordinated Program for Masonry Building Research through its TCCMAR committee. The interim results from this study have been presented to the TCCMAR committee for review and have served as the basis for formulating specific technical recommendations for design provisions to be included in the Limit-States Design Standard being formulated by the Masonry Standards Joint Committee (in preparation).

This research conducted in this study was divided into three subprograms: lap-splice behavior, tension-stiffening behavior, and biaxial compression-tension behavior. Although each subprogram was conducted independently, common materials, specimen preparation methods, and testing techniques were employed in each. The masonry units used in this study as well as the mix designs for mortar and grout were common with other experimental studies conducted under the U.S. Coordinated Program permitting direct transfer of knowledge gained from this program to, for example, results from tests on the five-story masonry structure tested at the University of California-San Diego.

126

Lap-Splice Behavior

Current design standard provisions for lap-splice design in reinforced masonry are based on working stress methods and are derived in large part from reinforced concrete behavior. An earlier experimental study conducted under the U.S. Coordinated Program tested a limited range of bar and unit sizes and from this data proposed a design equation for lap splices in masonry (Soric and Tulin 1987). The purpose of this study was to expand the range of test parameters to permit evaluation of the general applicability of design equation.

The experimental program on lap-splice behavior focused on specimen parameters which affect the strength and ductility of the lap splice in grouted concrete and clay unit masonry. A total of 62 lap-splice specimens were tested in this program. A performance criteria that a lapped connection in masonry should be able to sustain a tensile load equal to 125 percent of the yield load of the reinforcement was adopted and used to establish critical lap lengths and maximum bar sizes.

The experimental results from this study are, in general, in good agreement with the design equation proposed by Soric for masonry lapped splice behavior. The empirical coefficient determined by Soric from his limited range of test parameters was shown, in fact, to be a variable function of the reinforcement bar size. The observed tensile behavior and cracking behavior was used to define limits on the maximum reinforcement ratio and maximum bar size as a function of unit size so that longitudinal cracking leading to a potential brittle failure mode can be prevented. This information permits the establishment of important prescriptive limits for the design of masonry structures.

Tension-Stiffening Behavior

The knowledge of the tensile load-deformation behavior of reinforced masonry is essential in several aspects for safe and economical design. Reinforced masonry buildings are designed to respond to lateral loads in a bending mode and not in a shear mode. Knowledge of the bending deformations is critical in assuring that sufficient ductility exists and that limiting interstory drift angles are not exceeded. Strain localization effects occurring at tensile cracks impose significantly greater local strains on the reinforcing bar than indicated by the average calculated tensile strain value. Assurance that these local strains do not exceed critical levels is important. Finite element analysis of masonry buildings require a quantitative expression for the tension stiffening behavior of the reinforced masonry to achieve reliable predictions of structural deformations. Previous to data from this study, tension stiffening data from reinforced concrete were employed in the absence of any experimental data for reinforced masonry.

The experimental program tested 35 tension stiffening specimens with variables including bar sizes from No. 3 to 11, unit widths from 4 to 12 in., and considering both concrete and clay unit masonry. Localized and average strain data were obtained for the full range of tensile behavior from initial elastic to maximum strains up to 5 percent. Location and type of cracking behavior were observed as a function of bar size and steel ratio.

Experimental results have permitted the quantitative expression of tension-stiffening behavior in both the pre- and postyield range of tensile loading. Significant levels of tension stiffening and loss of ductility were observed for the case of small-diameter bars grouted in large masonry units (small reinforcement ratios). The averaged tensile stress-strain curve for specimens with low reinforcement ratios did not exhibit the yield plateau expected from reinforcing steel but rather transitioned from elastic to strain hardening behavior. Most significantly, however, was that all specimens were strained to levels far in excess of those permitted by design codes without suffering tensile bar failure. The quantitative results have been employed to determine limiting design standard parameters for maximum flexural reinforcement.

Biaxial Behavior

Masonry walls loaded in-plane by seismic loads are subject to cyclic reversed lateral loads. These loadings create a system of cracks in the wall. Tensile cracks normal to compressive in-plane loads have been shown in reinforced concrete to reduce compressive failure strength. In the absence of data on similar behavior for reinforced masonry, finite element analyses of masonry structures have used material behavior models from concrete research.

As part of this CPAR research program, a series of tests were conducted to determine the biaxial compressive-tensile behavior of reinforced concrete masonry panels. The tests were conducted in a unique load frame which permits independent control of lateral tensile and vertical compressive loads. Eight test panels, 32-in. (80-cm) high by 48-in (120-cm) wide, were loaded to compressive failure under various levels of imposed lateral strain. Biaxial stress and strain data were recorded over the full loading range.

From the test results, a model describing the influence of lateral tensile strain on the compressive stress and strain at compressive failure was obtained. No reduction in the compressive strength was observed until the lateral tensile strain exceeded a value equal to twice the strain at the masonry compressive failure. After this point, the experimental data produced a well-defined linear reduction in compressive strength with increasing lateral tensile strain. This behavior is significantly different from that determined for reinforced concrete.

General Conclusions

The results from this study on the behavior of reinforced masonry have provided important behavior data which will assist the drafting of a limit-states design standard for masonry. Results will permit authors of the limit-states standard to incorporate limits, parameters, and requirements in the standard which accurately reflect masonry behavior. This should produce savings in materials, since in the absence of applicable experimental data, the authors of design standards typically adopt very conservative parameters. The end result of this research program will assist in the development of a reinforced masonry design standard which improves the competitiveness of masonry as a building material.

References

American Concrete Institute. (1988a). "Building code requirements for masonry structures," ACI 530-88, American Concrete Institute, American Society for Civil Engineers, and The Masonry Society, Detroit, MI.

_____. (1988b). "Specifications for masonry structures," ACI 530.1-88, American Concrete Institute, American Society for Civil Engineers, and The Masonry Society, Detroit, MI.

American Concrete Institute Commitee 224. (1986). "Cracking of concrete members in direct tension," *ACI Journal.*

American Concrete Institute Committee 318. (1989). "ACI 318-89, building code requirements for reinforced concrete," The American Concrete Institute, Detroit, MI.

American Society of Testing and Materials. (1990). *1990 annual book of ASTM standards.* Philadelphia, PA.

   a. Designation A 370-88a, "Standard methods and definitions for mechanical testing of steel products."

   b. Designation A 615-87a, "Standard specification for deformed and plain billet-steel bars for concrete reinforcement."

   c. Designation C 67-89a, "Standard test methods of sampling and testing brick and structural clay tile."

   d. Designation C 109-90, "Standard test method for compressive strength of hydraulic cement mortars (using 2-in. or 50-mm cube specimens)."

   e. Designation C 136-84a, "Standard method for sieve analysis of fine and coarse aggregates."

   f. Designation C 138-81, "Standard test method for unit weight, yield, and air content (gravimetric) of concrete."

g. Designation C 143-90a, "Standard test method for slump of hydraulic cement concrete."

h. Designation C 140-75, "Standard methods of sampling and testing concrete masonry units."

i. Designation C 144-89, "Standard specification for aggregate for masonry mortar."

j. Designation C 150-89, "Standard specification for portland cement."

k. Designation C 190, "Standard test method for tensile strength of hydraulic cement mortars."

l. Designation C 207-76, "Standard specification for hydrated lime for masonry purposes."

m. Designation C 231-89a, "Standard test method for air content of freshly mixed concrete by the pressure method."

n. Designation C 270-89, "Standard specification for mortar for unit masonry."

o. Designation C 305-82, "Standard practice for mechanical mixing of hydraulic cement pastes and mortars of plastic consistency."

p. Designation C 404-87, "Standard specification for aggregates for masonry grout."

q. Designation C 476-83, "Standard specification for grout for masonry."

r. Designation C 496-90, "Standard test method for splitting tensile strength of cylindrical concrete specimens."

s. Designation C 780-90, "Standard method for preconstruction and construction evaluation of mortars for plain and reinforced unit masonry."

t. Designation C 1019-89a, "Standard method of sampling and testing grout."

u. Designation E 447-84, "Standard test methods for compressive strength of masonry prisms."

Atkinson-Noland & Associates. (1985). *Preparation of stack-bond masonry prisms*. Boulder, CO.

_____. (1988). *Preparation and testing of masonry mortar in the laboratory*. Boulder, CO.

Barzegar-Jamshidi, F., and Schnobrich, W. C. (1986). "Nonlinear finite element analysis of reinforced concrete under short term loading," Structural Research Series No. 530, University of Illinois at Urbana-Champaign.

Baynit, R. A. (1990). "Bond and development length in reinforced concrete block masonry," Master of Engineering Thesis, Carleton University, Ottawa, Can.

Bortolotti, L. (1991). "First cracking load of concrete subjected to direct tension," *ACI Materials Journal*, 70-73.

Cervenka, Vladimir. (1985). "Constitutive model for cracked reinforced concrete," *ACI Journal 82*, 877-882.

Cheema, T. S. (1981). "Anchorage behavior and prism strength of grouted concrete masonry," Ph.D. Dissertation, University of Texas at Austin.

Cheema, T. S., and Klingner, R. E. (1985). "Tensile anchorage behavior of deformed reinforcement in grouted concrete masonry," *American Concrete Institute Journal*, Title No. 82-34.

Dhanasekar, M., Page, A. W., and Kleeman, P. W. (1985). "The failure of brick masonry under biaxial stresses." *Proceedings Institution of Civil Engineers*, 79 Part 2.

Dialer, C. (1990). "Bruch-und Verformungsverhalten von schubbeanspruchten Mauerwerksscheiben, zweiachsige Versuche an verkleinertem Modellmauerwerk," Dr.-Ing. Dissertation, Technical University Munchen.

Ewing R. D., El-Mustapha, A. M., and Kariotis, J. C. (1987). "Fem/i, a finite element computer program for the nonlinear static analysis of reinforced masonry building components," (Revised June 1989), draft report, EKEH, Rancho Palos Verdes, CA.

Ferguson, Phil M. (1979). *Reinforced concrete fundamentals*. 4th ed., Wiley, New York, NY.

Ferguson, P. M., et al. (1966). "Bond stress - the state of the art," ACI Committee 408, *Journal of the American Concrete Institute*, Title No. 63-53.

Gerstle, W., and Ingraffea, A. R. (1991). "Does bond-slip exist?," *Concrete International*, 44-48.

Gilbert, R. I., and Warner, R. F. (1978). "Tension stiffening in reinforced concrete slabs." *Proceedings ASCE 105*, ST12, 1885-1900.

Gopalaratnam, V. S., and Shah, S. P. (1985). "Softening response of plain concrete in direct tension," *ACI Journal*, 310-323.

Goto, Y. (1971). "Cracks formed in concrete around deformed tension bars," *ACI Journal 68*, 244-251.

Gupta, A. K., and Maestrini, S. R. (1990). "Tension-stiffness model for reinforced concrete bars," *ASCE Journal of Structural Engineering 116(3)*, 769-790.

Hegemier, G. A., Murakami, H., and Hageman, L. J. (1985). "On tension stiffening in reinforced concrete," *Mechanics of Materials 4*, 161-179.

Hegemier, G. A., Murakami, H., and Kendall, D. M. (1990). "On the prediction of response, damage, and failure in rcm panels under monotonic and cyclic loadings." *Proceedings Sixth Meeting of the Joint Technical Coordinating Committee on Masonry Research*. Port Ludlow, WA.

Hegemier, G. A., Nunn, R. O., and Arya, S. K. (1978). "Behavior of concrete masonry under biaxial stresses." *Proceedings North American Masonry Conference*. Boulder, CO.

Houston, R. T., and Tadros, M. K. (1990). "Deflection of reinforced concrete masonry members," *ACI Structural Journal*, 453-463.

International Conference of Building Officials. (1988). "Masonry," *Uniform building code*. Whittier, CA.

International Conference of Building Officials. (1992). *Uniform building code*. Whittier, CA.

Khattab, M. M., and Drysdale, R. G. (1992). "Tests of concrete block masonry under biaxial tension-compression," Sixth Canadian Masonry Symposium.

_____. (1993). "The effect of reinforcement on the shear response of grouted concrete masonry." *Proceedings Sixth North American Masonry Conf.* Philadelphia, PA, 1121-1132.

Kubota, T., and Kamogawa, N. (1985). "On the lap joint of flexural reinforcement in concrete masonry." *Proceedings of the First Joint Technical Coordinating Committee on Masonry Research*. U.S.-Japan Coordinated Program for Masonry Building Research, Tokyo.

Lutz, L. A., and Gergely, P. (1967). "Mechanics of bond and slip of deformed bars in concrete," *ACI Journal 64*, 711-721.

Masonry Standards Joint Committee. (1992). *Building code requirements for masonry structures*. ACI 530-92/ASCE 5-92/TMS 402/92, American Concrete Institute, American Society of Civil Engineers, The Masonry Society.

_____. (1993). *Draft, masonry limit states design standard,* The Masonry Society, American Concrete Institute, American Society of Civil Engineers.

Massicotte, B., Elwi, A. E., and MacGregor, J. G. (1990). "Tension-stiffening model for planar reinforced concrete members," *ASCE Journal of Structural Engineering* 116(11), 3039-3058.

Matsumura, A. (1990). "Test on lap splices of relatively large size bars in masonry." *Proceedings of the Sixth Meeting of the U.S.-Japan Joint Technical Coordinating Committee on Masonry Research.* Port Ludlow, WA.

Naraine, Krishna, and Sinha, Sachchidanand. (1992). "Stress-strain curves for brick masonry in biaxial compression," *ASCE Journal of Structural Engineering* 118(6).

Noland, J. L. (1990). "1990 Status Report: U.S. coordinated program for masonry building research." *Proceedings, Fifth North American Masonry Conference,* 1, 57-68.

Nunn, Robert O. (1980). "Planar mechanics of fully grouted concrete masonry," Report UCSD/AMES/TR-80/001, Department of Applied Mechanics and Engineering Sciences, University of California, San Diego.

Paulay, T., and Priestlay, M. J. N. (1993). "Stability of ductile structural walls," *ACI Structural Journal,* 385-392.

Perry, E. S., and Jundi, N. (1969). "Pullout bond stress distribution under static and dynamic repeated loadings," *American Concrete Institute Journal,* Title No. 66-28.

Prakhya, G. K. V., and Morley, C. T. (1990). "Tension-stiffening and moment-curvature relations of reinforced concrete elements," *ACI Structural Journal* 87(5), 597-605.

Scrivener, J. C. (1986). "Bond of reinforcement in grouted hollow-unit masonry: a state-of-the-art," TCCMAR Report No. 6.2-1, U.S.-Japan Coordinated Program for Masonry Building Research.

Seible, F. , LaRovere, H. L., and Kingsley, G. R. (1990). "Nonlinear analysis of reinforced masonry shear wall structures - monotonic loading," *The Masonry Society Journal* (9)1, 60-69.

Soric, Z., and Tulin, L. G. (1987). "Bond & splices in reinforced masonry," TCCMAR Report No. 6.2-2, U.S.-Japan Coordinated Program for Masonry Building Research.

_____. (1988). "Length of lap for spliced reinforcement in masonry structures." *Proceedings of the 8th International Brick/Block Masonry Conference.* Dublin, Ire.

Stevens, N. J., Vzumeri, S. M., Collins, M. P., and Will, G. T. (1991). "Constitutive models for reinforced concrete finite element analysis," *ACI Structural Journal,* 49-59.

Suter, G. T., Fenton, G. A. (1985). "Splice length tests of reinforced concrete masonry walls." *Proceedings of the Third North American Masonry Conference.* University of Texas at Arlington.

The Masonry Society. (1991). *Draft masonry limit states design standard,* Boulder, CO.

The Masonry Society Codes and Standards Committee. (1990). "Commentary to chapter 24, masonry of the uniform building code 1988 edition," The Masonry Society, Boulder, CO.

Thompson, M. A., Jirsa, J. O., Breen, J. E., and Meinheit, D. F. (1979). "Behavior of multiple lap splices in wide sections," *American Concrete Institute Journal,* Title No. 76-12.

Thürlimann, B., and Ganz, H. R. (1985). "Plastic strength of masonry shear walls." *Proceedings 7th International Brick Masonry Conference,* Melbourne, 837-846.

Thürlimann, B., Lurati, F., and Graf, H. (1990). "Versuche zur Festlegung der Festigkeitswerke von Zementsteinmaurwerk," Institut fur Baustatik & Konstrucktion ETH, Zurich.

Vecchio, F. J. (1989). "Nonlinear finite element analysis of reinforced concrete membranes," *ACI Structural Journal,* 26-35.

Vecchio, F., and Collins, M. P. (1982). "The response of reinforced concrete to in-plane shear and normal stresses," Dept. of Civil Engineering, University of Toronto.

Vecchio, F. J., and Collins, M. P. (1986). "The modified compression-field theory for reinforced concrete elements subjected to shear," *ACI Journal* 83, 219-231.

Watanabe, M. (1985). "Bond and anchorage of reinforcement in masonry." *Proceedings of the First Joint Technical Coordinating Committee on Masonry Research.* U.S.-Japan Coordinated Program for Masonry Building Research, Tokyo.

Williams, S. (1986). "Tests on large reinforced concrete elements subjected to direct tension," Technical Report 562, Cement and Concrete Association, Wexham Springs, England.

Appendix A
Material and Index Properties

The results of material and index property tests on all materials used in this project including concrete masonry units, clay masonry units, steel reinforcing bars, aggregates, grout, mortar, and cementitious materials are given in this appendix. From the outset of this research, it was intended that all materials and procedures used in the test program match, to whatever extent possible, the materials and procedures used by other participating Technical Coordinating Committee For Masonry Research (TCCMAR) researchers.

Concrete and Clay Masonry Units

The concrete masonry and clay brick units used in this study were supplied to the U.S. Army Engineer Waterways Experiment Station (WES) by industry and are typical of units used elsewhere by TCCMAR. The index properties characterize the units based upon determinations of net areas (American Society of Testing and Materials (ASTM) C 67 (1990c)),[1] compressive strengths (ASTM C 140 (1990h) and ASTM C 67), 24-hour absorptions (ASTM C 140 and ASTM C 67), initial rate of absorption, (ASTM C 67), and associated parameters.

Concrete masonry units

All concrete masonry units used for this project were donated by the Blocklite Company, Selma, CA. For the concrete masonry units, six different size units were included. The nominal sizes of these units were 8 × 12 × 16 in., 8 × 10 × 16 in., 8 × 8 × 16 in., 8 × 6 × 16 in., 8 × 4 × 16 in., and 4 × 8 × 16 in. One 8- × 6- × 16-in. bond beam and one half-block 8 × 6 × 8 in. were included. The physical properties of these units were determined in accordance with ASTM standards listed above and given in Table A1. Typical dimensions of these units are shown in Figures A1 through A4.

---

[1] References cited in this appendix are listed following main text.

Table A1
Dimensions and Properties of Concrete Masonry Units Per ASTM C 140 (1990h)

Description	Nominal Unit Size, in.							Half Block
	Full Blocks							
	12	10	8	6	6*	4*	4†	6
Width, in.	11.64	9.62	7.62	5.62	5.63	7.63	3.63	5.63
Height, in.	7.63	7.62	7.62	7.54	7.62	3.59	7.65	7.60
Length, in.	15.56	15.59	15.59	15.56	15.58	15.61	15.55	7.66
Min. face shell thick., in. Top / Bottom	1.74 / 1.49	1.51 / 1.41	1.46 / 1.28	1.21 / 1.02	1.37 / 1.35	1.36 / 1.27	1.40 / 1.40	1.38 / 1.25
Min. web thick., in. Top / Bottom	2.08 / 1.31	1.63 / 1.30	1.80 / 1.03	1.36 / 1.03	1.66 / 1.59	1.18 / 1.04	1.43 / 1.10	
Min. end web thick., in. Top / Bottom	1.69 / 1.55	1.52 / 1.37	1.46 / 1.28	1.26 / 1.07	1.42 / 1.34	1.37 / 1.28	1.43 / 1.24	1.37†† / 0.71††
Gross areas, in.^{2}	181.12	149.98	118.80	87.45	87.72	119.10	56.45	43.13
Net area, in.^{2}	50.56	51.52	53.10	52.25	54.97	50.04	73.10	53.49
Density, pcf	101.12	98.87	97.95	98.49	98.78	100.05	96.34	99.70
Absorption, pcf / %	11.59 / 11.46	12.62 / 12.77	12.24 / 12.60	13.76 / 14.12	12.23 / 12.38	10.80 / 10.80	13.22 / 13.74	11.59 / 11.65
Moisture content, %	36.20	18.13	42.09	48.56	37.24	38.64	31.83	40.91
Axial compressive strength, psi Net area / Gross area	6,280 / 1,760	3,850 / 1,320	3,800 / 1,960	3,090 / 1,850	3,180 / 2,000	4,500 / 1,890	1,900 / 2,470	1,668 / 2,070

* Bond Beam
** See Figure A1.
† See Figure A2.
†† See Figure A4.

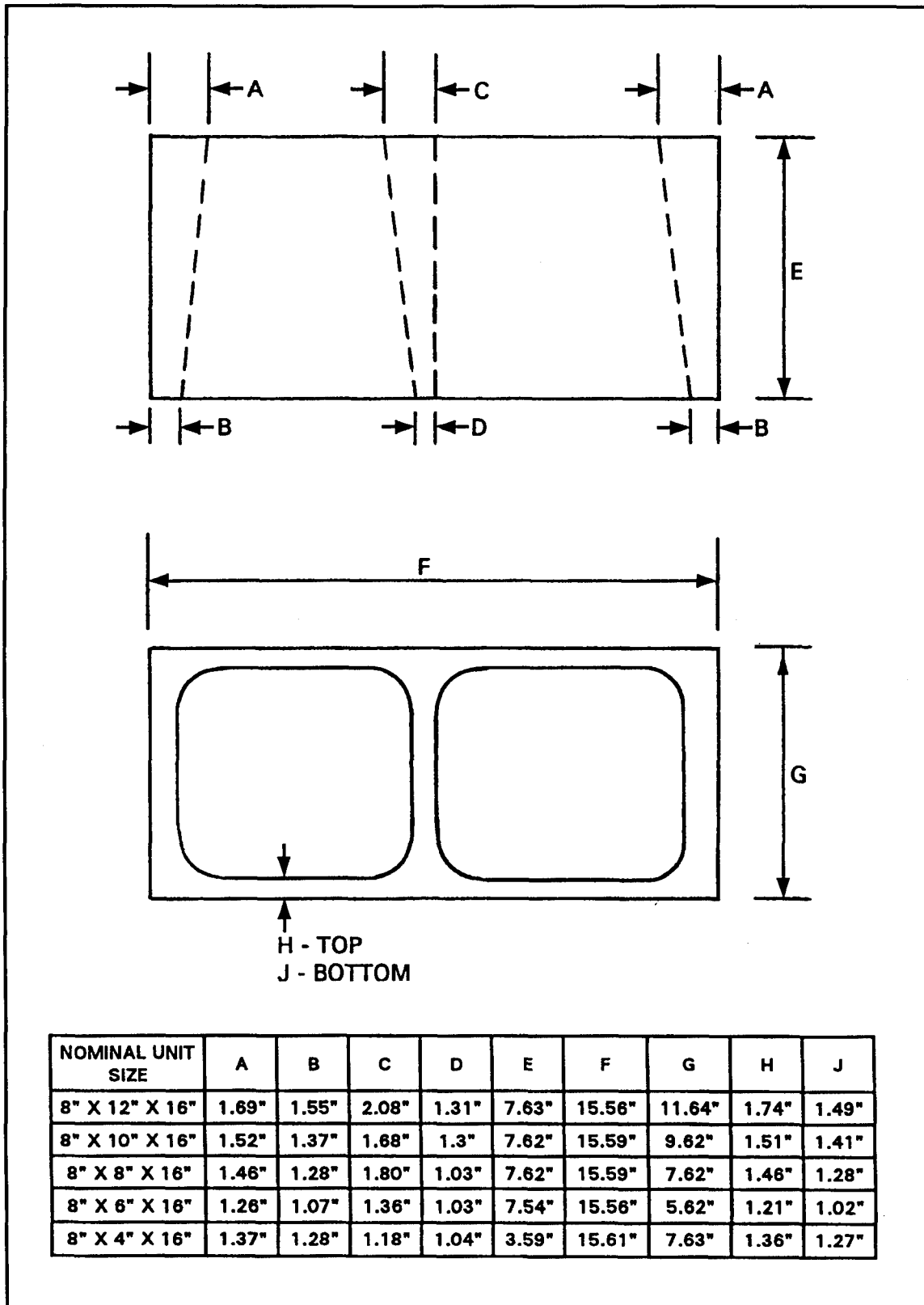| NOMINAL UNIT SIZE	A	B	C	D	E	F	G	H	J
8" X 12" X 16"	1.69"	1.55"	2.08"	1.31"	7.63"	15.56"	11.64"	1.74"	1.49"
8" X 10" X 16"	1.52"	1.37"	1.68"	1.3"	7.62"	15.59"	9.62"	1.51"	1.41"
8" X 8" X 16"	1.46"	1.28"	1.80"	1.03"	7.62"	15.59"	7.62"	1.46"	1.28"
8" X 6" X 16"	1.26"	1.07"	1.36"	1.03"	7.54"	15.56"	5.62"	1.21"	1.02"
8" X 4" X 16"	1.37"	1.28"	1.18"	1.04"	3.59"	15.61"	7.63"	1.36"	1.27"

Figure A1. Typical elevation and cross section of the 12-, 10-, 8-, 6-, and 4-in. concrete masonry units
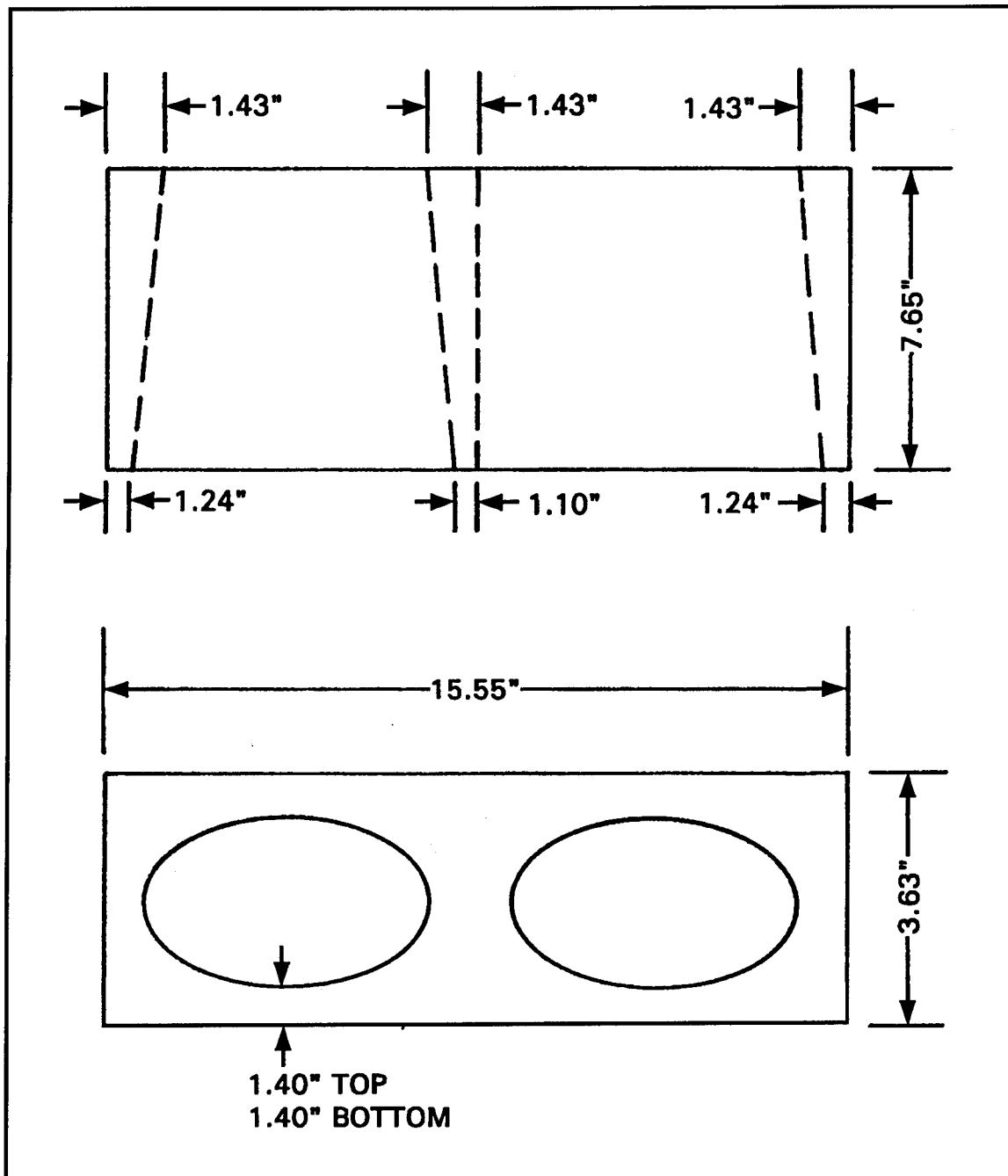
Figure A2. Typical elevation and cross section of 4-in. concrete masonry unit
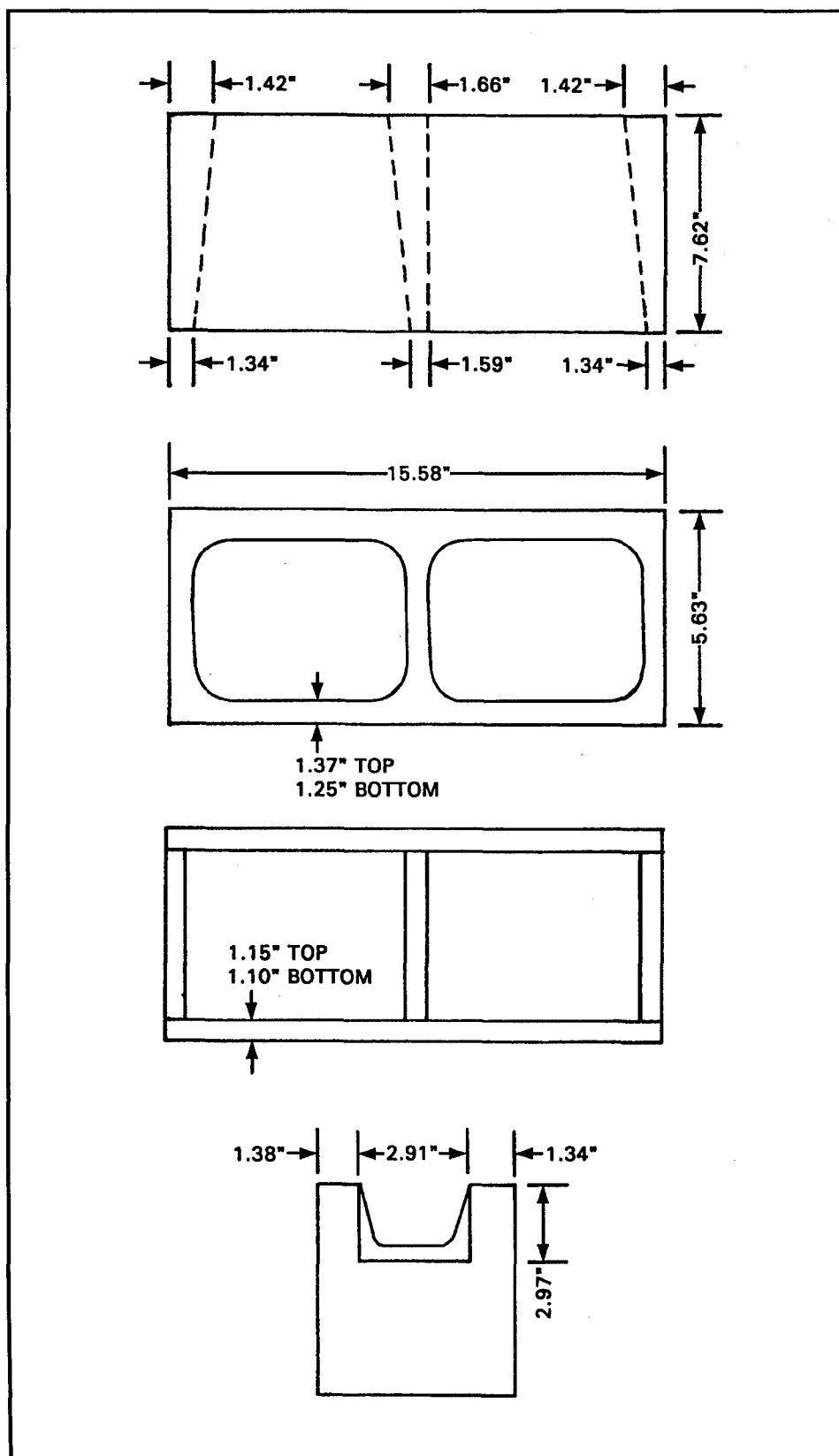
Figure A3. Typical elevation and cross section of 6-in. bond beam concrete masonry unit
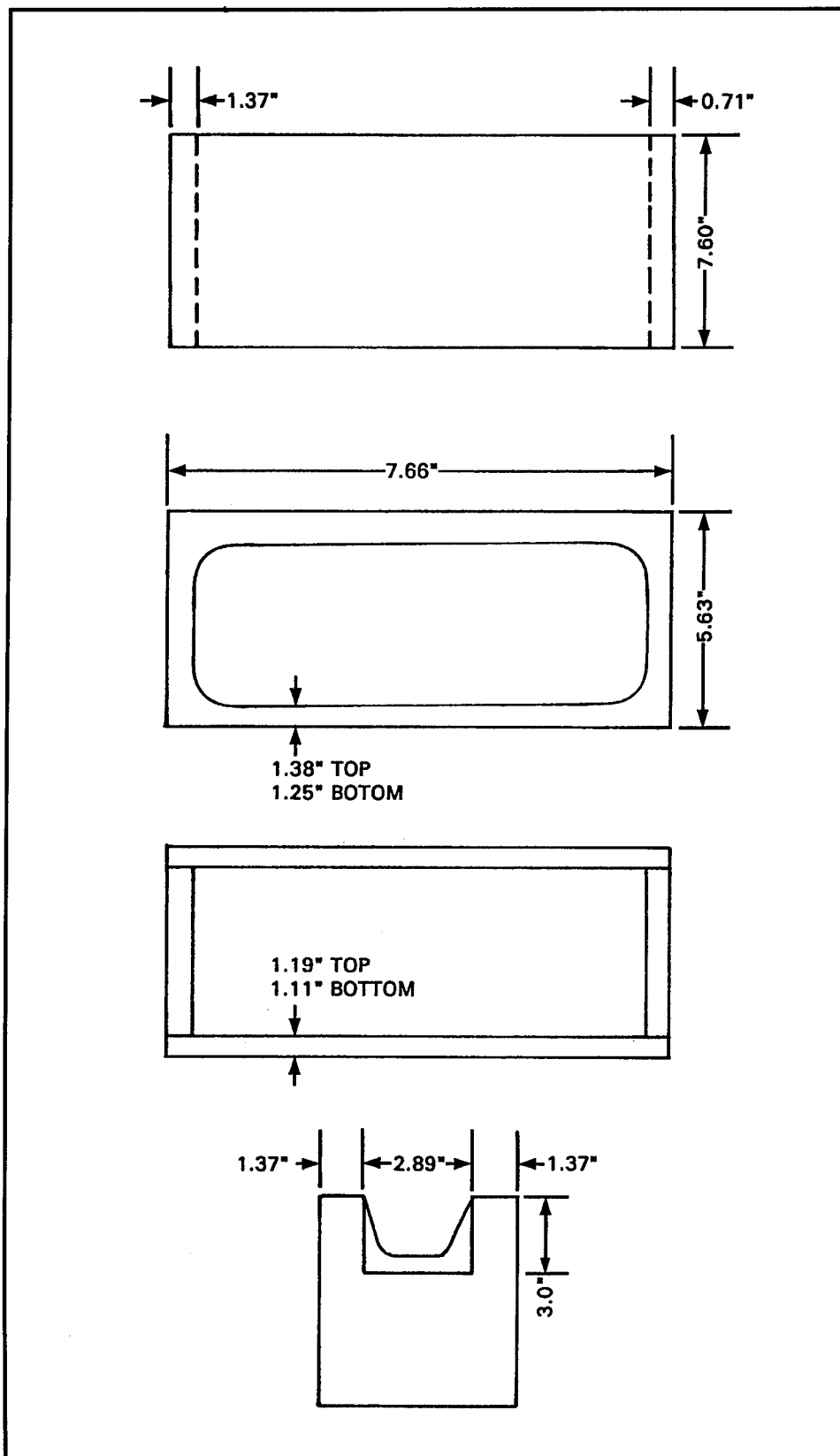
Figure A4. Typical elevation and cross section of 6-in. half-block concrete masonry unit

Clay masonry units

All clay masonry units used for this project were donated by the Interstate Brick Company, West Jordon, UT. For the hollow clay masonry units, three different sizes units were included. The nominal sizes are 4 × 8 × 16 in., 4 × 6 × 16 in., and 4 × 4 × 16 in., respectively. Additionally, one 4 × 6 × 16 in. bond beam clay brick was included. The physical properties were determined in accordance with ASTM standards and are given in Table A2. The typical dimensions of these units are shown in Figures A5 and A6.

Table A2
Dimensions and Properties of Clay Masonry Units Per ASTM C 67 (1990c)

Description	Nominal Unit Size, in.			
	8	6	6*	4
Width, in.	7.56	5.51	5.50	3.43
Height, in.	3.55	3.57	3.52	3.59
Length, in.	15.65	15.50	15.55	15.58
Gross area, in.^{2}	118.32	85.40	85.52	53.10
Net area, in.^{2}	64.00	55.52	55.52	35.40
Absorption, %	7.39	6.87	6.23	6.52
Initial rate of absorption, g/30 in.^{2}	22.8	15.2	14.41	
Axial compressive strength, psi (net area)	10,890	14,200	11,380	15,640
Axial compressive strength, psi (gross area)	5,890	9,230	7,390	10,070
*Refers to bond beam.				

Cementitious Materials

The cement used in this study was required to be an ASTM C 150 (1990j) Type I cement. All cement used in grout and mortar batches were supplied by the same supplier. Likewise, all lime used in the mortar batches were supplied by one manufacturer. The lime was required to be an ASTM C 207 (1990l) hydrated, Type S lime. The results of chemical analyses and physical tests on the cement and lime are given in Figures A7 and A8, respectively.

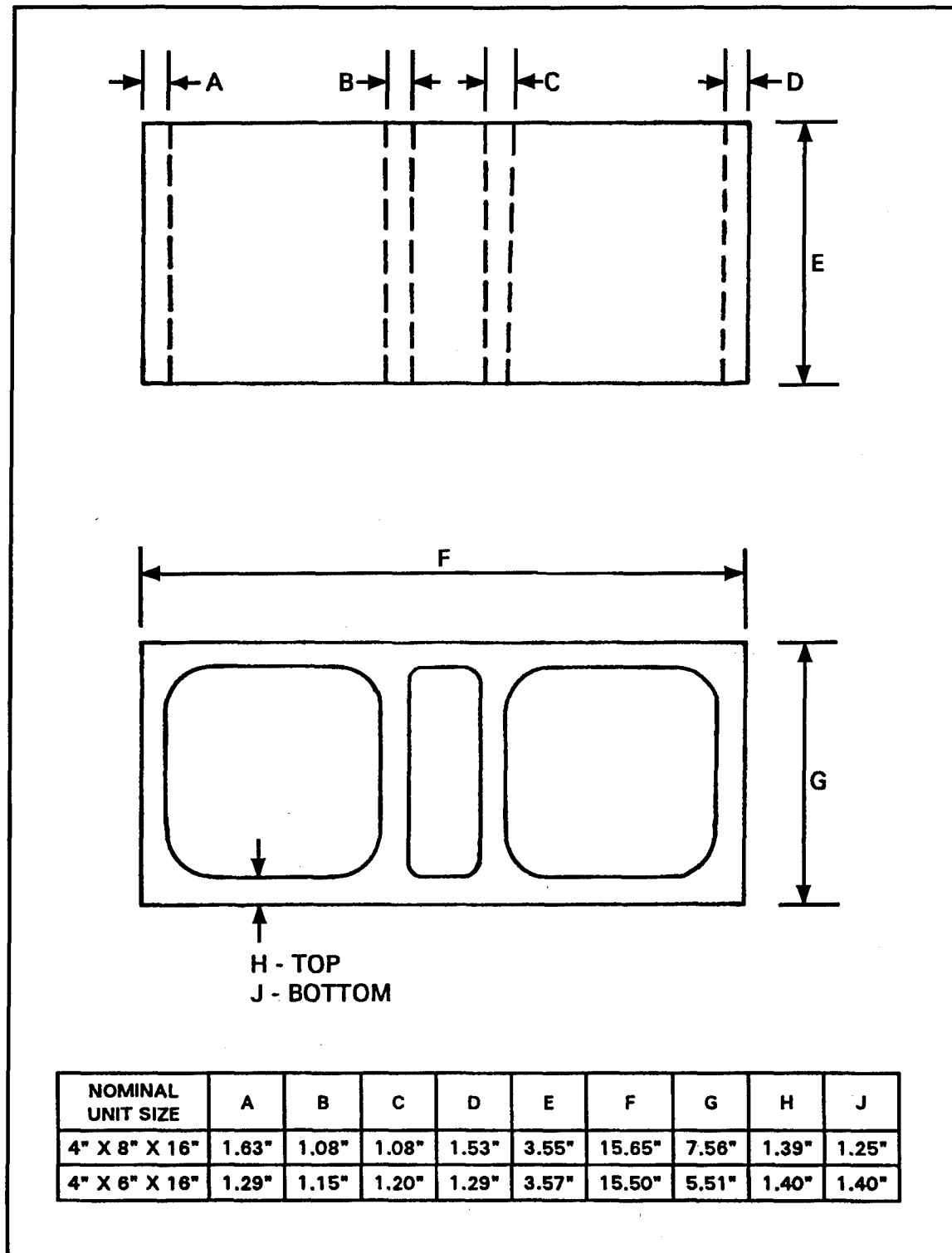| NOMINAL UNIT SIZE	A	B	C	D	E	F	G	H	J
4" X 8" X 16"	1.63"	1.08"	1.08"	1.53"	3.55"	15.65"	7.56"	1.39"	1.25"
4" X 6" X 16"	1.29"	1.15"	1.20"	1.29"	3.57"	15.50"	5.51"	1.40"	1.40"

Figure A5. Typical elevation and cross section of 8- and 6-in. clay masonry units
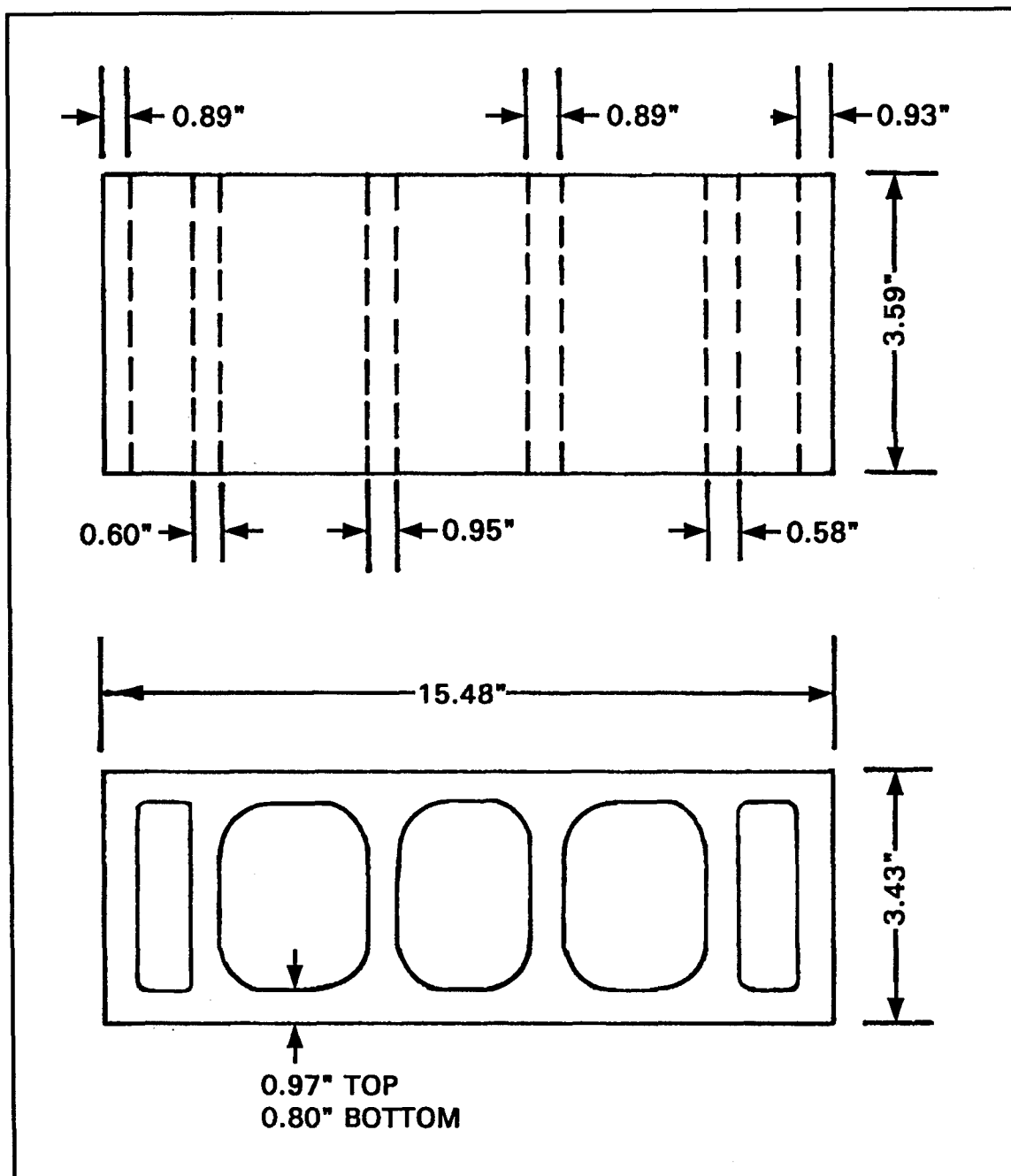
Figure A6. Typical elevation and cross section of 4-in. clay masonry units

```
Company:  Lone Star Industries          Test Report No.:  WES-52-91
Location:  Cape Girardeau, Missouri     Program:  Single Sample
Specification:  ASTM C 150, Type I      CTD No.:
Contract No.:                           Job No.:
Project:  CPAR-Masonry                  Date Sampled: 22 March 1991


_____Partial test result

4/5/91   Tests complete, material ____does, ____does not meet specification


                                     Result    Retest    Spec Limits
                                                          "Type I"
        Chemical Analysis


SiO₂, %. . . . . . . . . . . . . . . . .    21.6                 -
Al₂O₃, % . . . . . . . . . . . . . . . .     4.4                 -
Fe₂O₃, % . . . . . . . . . . . . . . . .     2.8                 -
CaO, % . . . . . . . . . . . . . . . . .    63.0                 -
MgO, % . . . . . . . . . . . . . . . . .     3.3           6.0 max
SO₃, % . . . . . . . . . . . . . . . . .     2.6        3.0,3.5 maxᵃ
Loss on ignition, %. . . . . . . . . . .     0.8           3.0 max
Insoluble residue, % . . . . . . . . . .     0.10         0.75 max
Na₂O, %. . . . . . . . . . . . . . . . .     0.03                -
K₂O, % . . . . . . . . . . . . . . . . .     0.79                -
Alkalies-total as Na₂O,% . . . . . . . .     0.55         0.60 max
TiO₂, %. . . . . . . . . . . . . . . . .     0.13                -
P₂O₅, %. . . . . . . . . . . . . . . . .     0.07                -
C₃A, % . . . . . . . . . . . . . . . . .     7             15 maxᵇ
C₃S, % . . . . . . . . . . . . . . . . .    50                   -
C₂S, % . . . . . . . . . . . . . . . . .    24                   -
C₄AF, %. . . . . . . . . . . . . . . . .     8                   -


        Physical Tests


Heat of hydration, 7-day, cal/g. . . . .     -                   -
Surface area, m²/kg (air permeability) .   360           280 min
Autoclave expansion, % . . . . . . . . .     0.03         0.80 max
Initial set, min. (Gillmore) . . . . . .   170            60 min
Final set, min. (Gillmore) . . . . . . .   300           600 max
Air content, % . . . . . . . . . . . . .     9            12 max
Compressive strength, 3-day, psi . . . .  3060          1800 min
Compressive strength, 7-day, psi . . . .  3880          2800 min
False set (final penetration), % . . . .                 50 min


REMARKS:
ᵃSee ASTM C 150
ᵇCorps of Engineers specification.
```

Figure A7. Results of physical and chemical tests on cement

```
Company:  Blue Circle                    Test Report No.:  WES-41-91
Location: Birmingham, Alabama            Program:  Single Sample
Specification:  ASTM C 207               CTD No.: CPAR-2, LIME-1
Contract No.:                            Job No.: SOOKO7
Project: CPAR-Masonry                    Date Sampled:  7 March 1991


_____Partial test result

3/14/91   Tests complete, material __X_does, ____does not meet specification


                                     RESULT   RETEST   SPEC LIMITS

    Chemical Analysis

Carbon dioxide . . . . . . . . . . . . . .    0.00              7 max.
CaO. . . . . . . . . . . . . . . . . . . .   93.45              -
MgO. . . . . . . . . . . . . . . . . . . .    3.90              -
Total CaO & MgO oxides . . . . . . . . . .   97.35              95 min.



    Physical Tests

Fineness (#30 sieve), % retained . . . . .    0.25              0.5 max.
Fineness (#200 sieve), % retained. . . . .    9.26              -
Water retention, % . . . . . . . . . . . .   86.0               75 min.
```

Figure A8. Results of physical and chemical tests on lime

Steel Reinforcing Bars

Reinforcing steel used in this study included No. 3, 4, 6, 8, and 11 Grade 60 bars, conforming the specifications of ASTM A 615, Specification for Deformed and Plain Billet-Steel Bars for Concrete Reinforcement (1990b). All bars of a given bar diameter used for the project were supplied by the vendor from the same lot of steel, thus uniformity of material properties within the same bar diameter was assumed. Deformations on all bars sizes were in a diagonal pattern, at an angle of 70 deg to the longitudinal axial of the bar, with three longitudinal ribs.

Tensile tests were conducted on coupons (three from each diameter bar) obtained from randomly selected bars within each bar diameter. Tests were conducted in accordance with ASTM A 370, Standard Methods and Definitions for Mechanical Testing of Steel Products (1990a). The results of these tensile tests are tabulated in Table A3. Typical stress-strain curves from one test on a coupon from each diameter bar are shown in Figures A9 through A14.

Table A3
Results of Tensile Tests on Reinforcing Bar Coupons

Bar No.	Specimen	Yield Strength, psi	Ultimate Strength, psi	Rupture Strength, psi	Modulus of Elasticity, million psi
3	1	69,900	113,800	94,200	28.7
	2	68,800	109,200	87,000	28.0
	3	69,000	108,900	86,700	27.7
	Average	69,200	110,600	89,300	28.1
4	6	70,600	116,100	97,600	28.9
	2	73,800	118,600	99,900	29.4
	3	72,600	116,300	95,600	29.7
	Average	72,300	117,000	97,770	29.3
6	1	65,000	104,100	86,900	29.6
	2	65,900	103,500	86,800	29.3
	3	68,200	102,700	84,500	29.1
	Average	66,400	103,500	86,100	29.3
8	1	65,400	114,200	99,200	29.5
	2	71,800	118,500	106,100	29.6
	3	68,900	114,500	98,500	29.2
	Average	68,700	115,700	101,300	29.4
11	1	66,700	105,100	93,100	28.5
	2	70,600	105,500	91,700	29.5
	3	66,800	105,800	92,400	29.6
	Average	68,000	105,500	92,400	29.2

BAR NO. 3
Specimen No. 1

Figure A9. Typical tensile stress-strain curve, No. 3 reinforcing bar

BAR NO. 4
Specimen No. 2

Figure A10.   Typical tensile stress-strain curve, No. 4 reinforcing bar

BAR NO. 6
Specimen No. 1
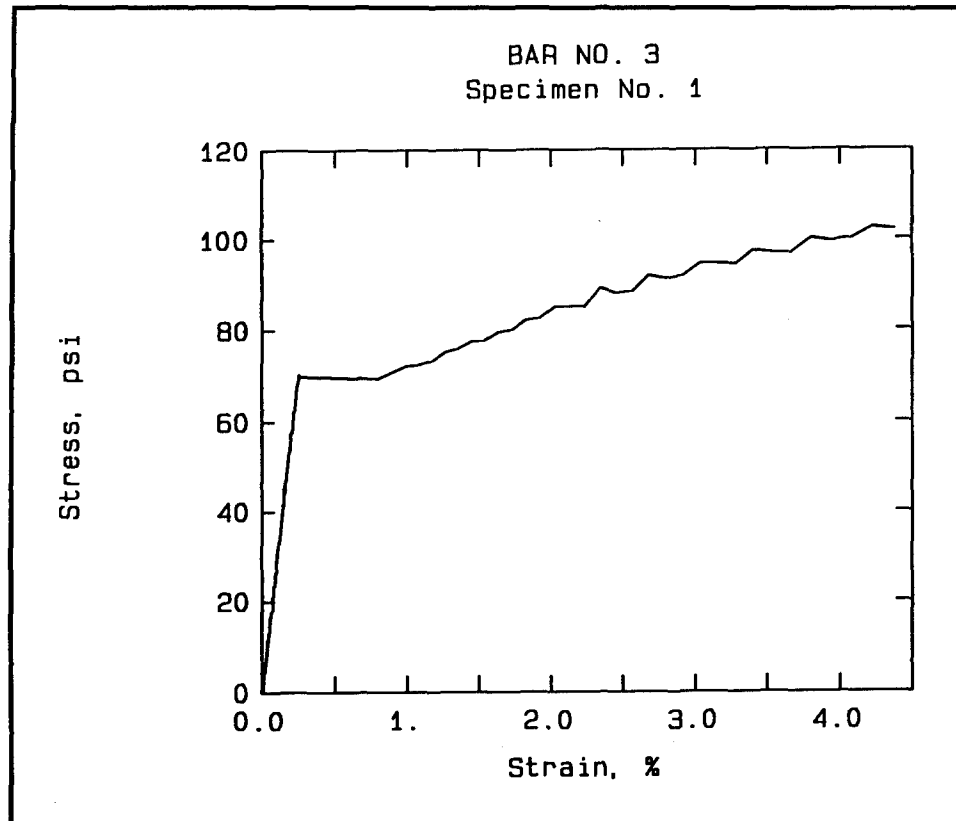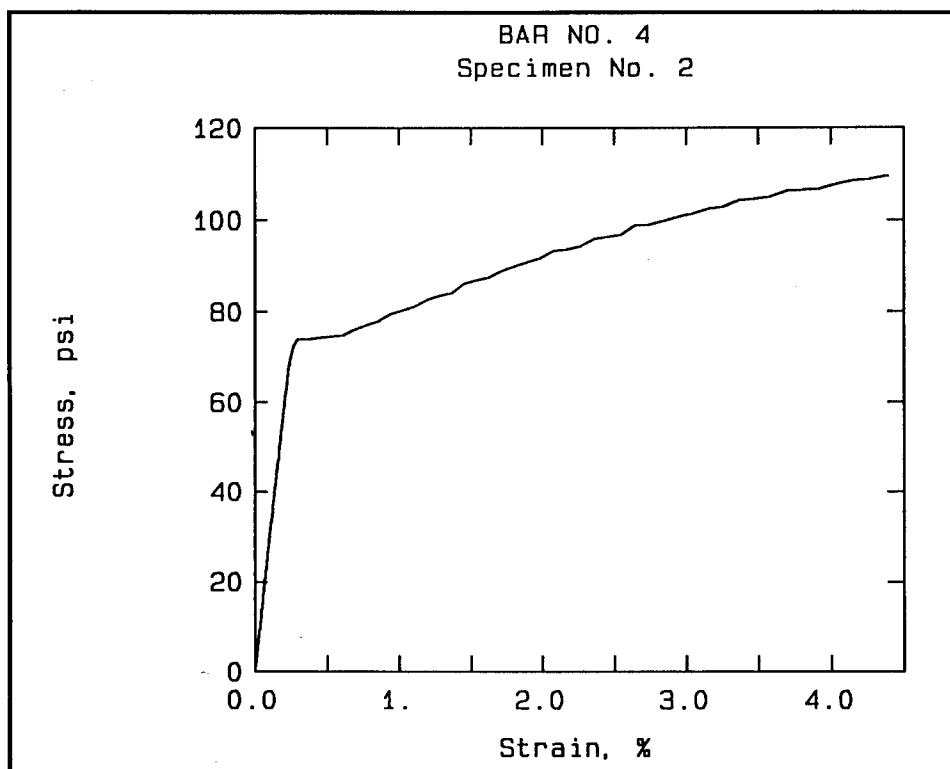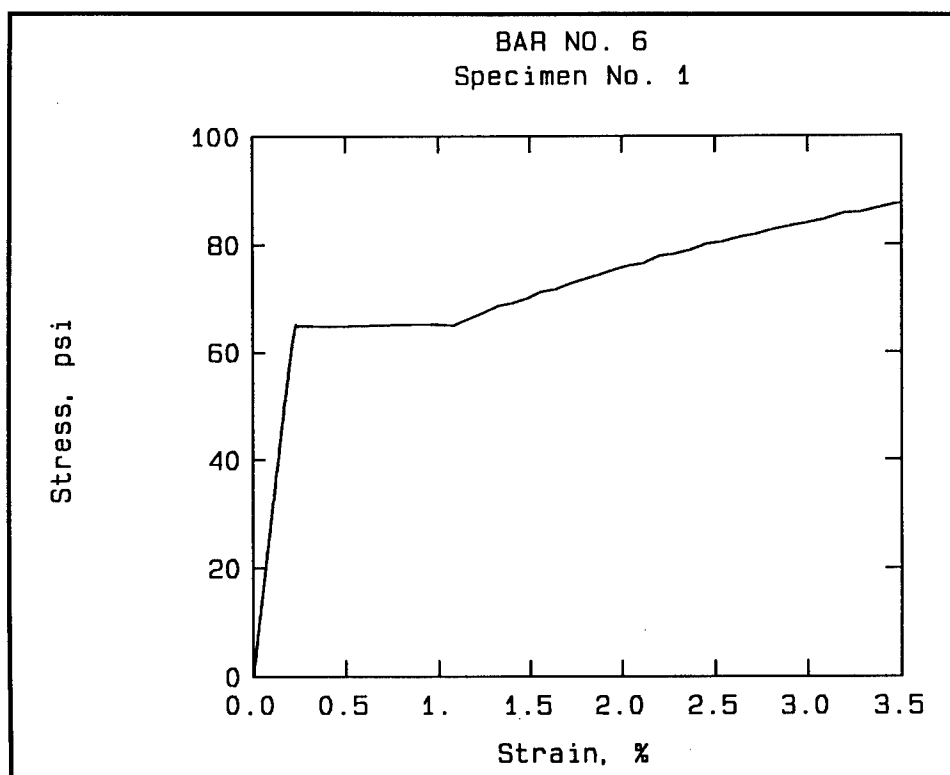
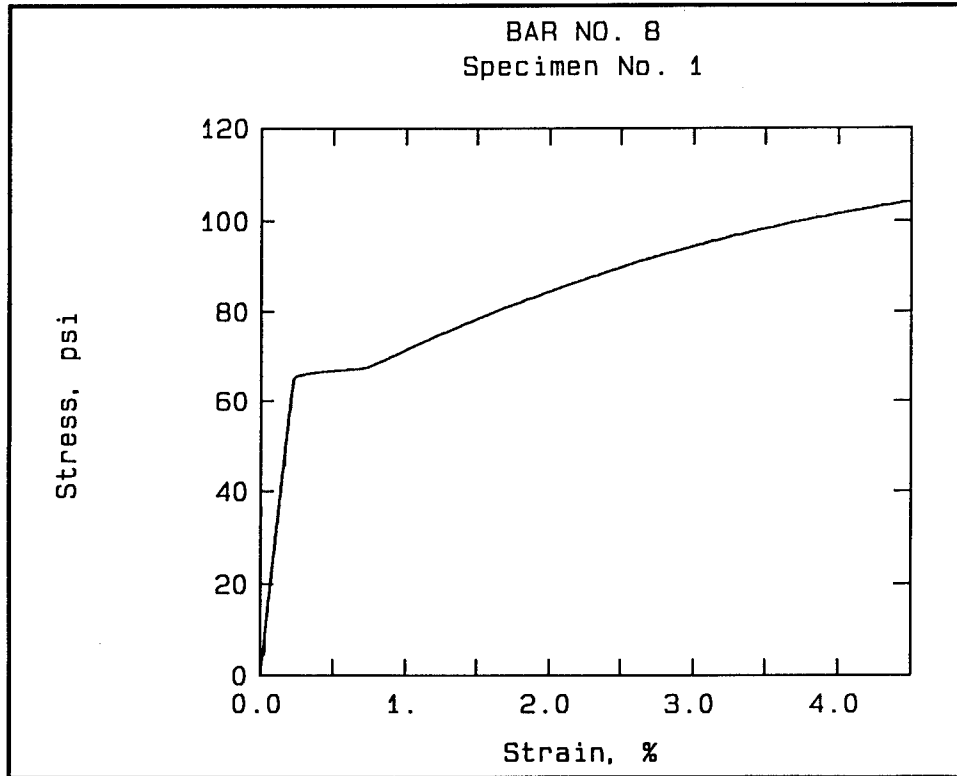Figure A11.   Typical stress-strain curve, No. 6 reinforcing bar

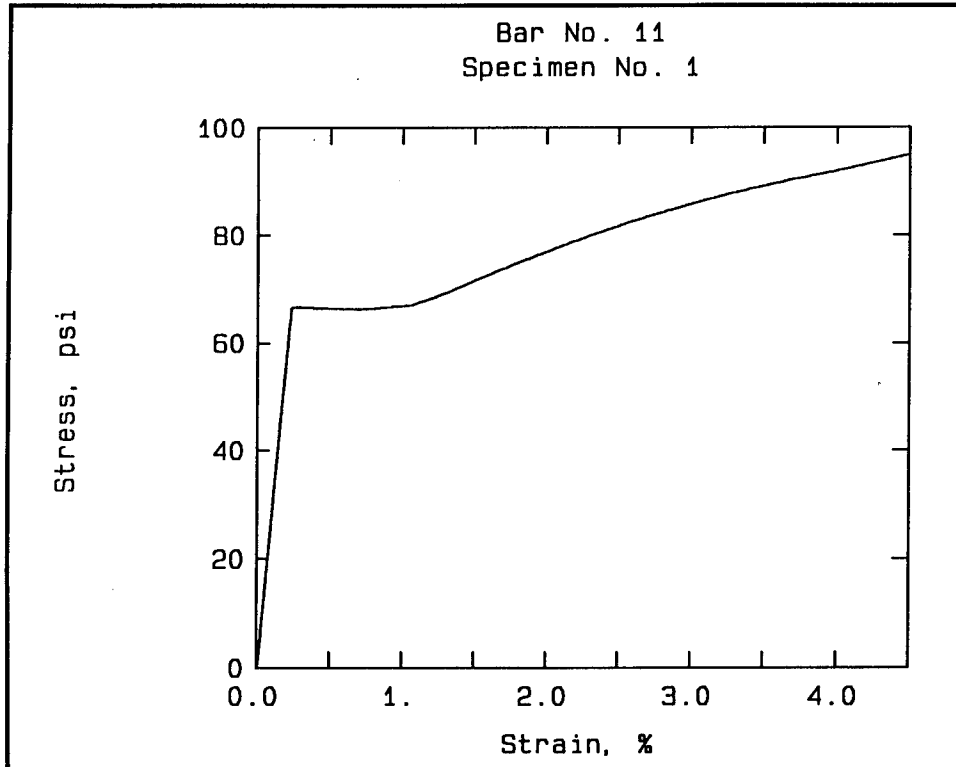Figure A12. Typical tensile stress-strain curve, No. 8 reinforcing bar

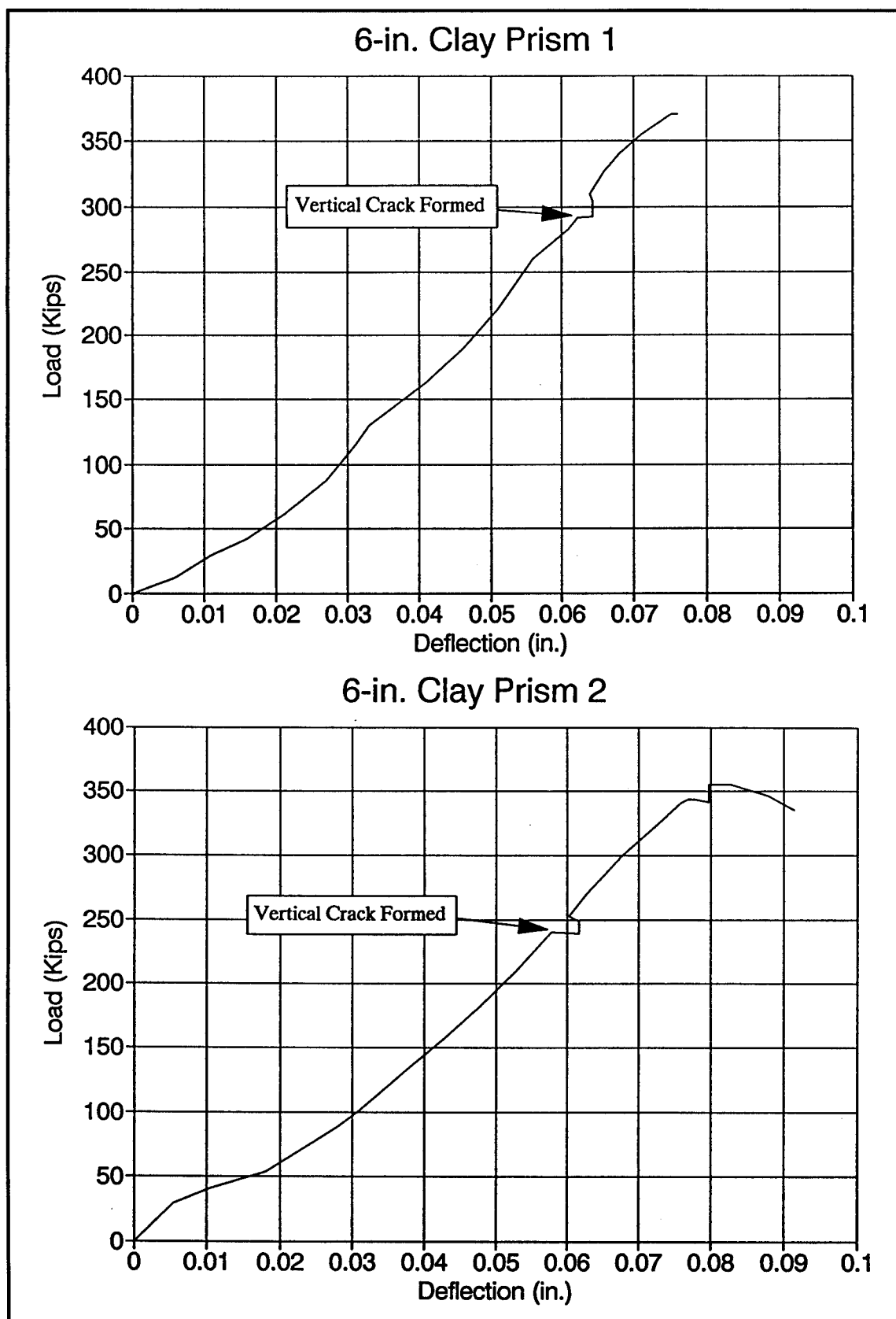Figure A13. Typical tensile stress-strain curve, No. 11 reinforcing bar

6-in. Clay Prism 1

6-in. Clay Prism 2

Figure A14.   Results of compressive strength tests on 6-in. clay masonry prisms

Aggregates

The coarse and fine aggregates used in this research project as a constituent of the grout batches were required to meet the specifications of ASTM C 404, Standard Specification for Aggregates for Masonry Grout (1990p), with the exception that manufactured aggregate were not allowed. A locally available, 3/8-in. nominal maximum size, silicious river gravel was used as the coarse aggregate. Also, a locally available silicious masonry sand was used for the fine aggregate. The results of ASTM C 136 (1990e) sieve analysis of the coarse and fine aggregates are shown in Table A4.

Table A4
Aggregate Gradings for Masonry Grout and Mortar

| | Cumulative Percent Passing | | | |
| | Coarse Aggregate | | Fine Aggregate | |
Sieve Size	Sample	ASTM C 404 (1990p) Requirements	Sample	ASTM C 404 and C 144 (1990p & I) Requirements
12.5 mm (1/2 in.)	100	100		
9.5 mm (3/8 in.)	85	85 to 100		
4.75 mm (#4)	12	10 to 30		100
2.36 mm (#8)	3	0 to 10	100	95 to 100
1.18 mm (#16)	3	0 to 5	99	70 to 100
600 μm (#30)	2		74	40 to 75
300 μm (#50)	1		38	10 to 35
150 μm (#100)			2	2 to 15

The aggregate used for preparation of mortar batches was required to meet the specifications of ASTM C 144, Aggregates for Masonry Mortar (1990i). For the preparation of mortar, the same masonry sand that was used in the fine aggregate in the grout mixture was used.

Note that the masonry sand was out of specification slightly on the No. 50 sieve. Because this was the only local source of masonry sand available and because the gradings were very close to specification, the sand was used for the project with the slight discrepancy noted.

Mortar

All masonry mortar used for this study was proportioned to meet the requirements of ASTM C 270, Standard Specification for Mortar for Unit Masonry (1990n), Type S mortar. In general, three cubical samples, each

2- by 2- by 2-in., and three (or six) cylindrical samples, each 2- by 4-in., were obtained from each batch of mortar prepared in the laboratory. All mortar cubes and cylinders were cast, stored, and tested as per the methods contained in the Atkinson-Noland and Associates report, "Preparation and Testing of Masonry Mortar in the Laboratory" (Atkinson-Noland and Associates 1988). The results of compression and splitting tensile tests conducted on each batch of grout are tabulated in Table A5.

Table A5 Results of Index Tests on Mortar			
Mixture	Compressive Strength, psi		Splitting Tensile Strength, psi
	Cube	Cylinder	
M114-1	1,990		
M114-2	2,490	2,150	
M115-1	2,060	1,980	
M119-1	2,420	2,240	
M121-1	2,070	2,030	
M122-1	3,240	2,710	
M122-2	1,900		
M123-1	1,910	1,660	
M212-1	2,750	1,950	
M213-1	2,430	1,860	250
M255-1	1,830	1,860	250
M259-1	4,390	3,770	
M260-1	4,580	3,030	
M260-2	3,580	2,370	
M261-1	3,040	2,690	
M289-1	4,530	3,960	
M290-1	5,800	4,390	
M290-2	5,010	4,650	
M293-1	4,370	4,030	
M293-2	2,430	2,250	
M130-1	3,800	3,020	
M132-1	5,050	4,760	
M132-2	4,780	4,260	

Grout

The proportions of the masonry grout used in this study met the requirements of ASTM C 476, Standard Specifications for Grout for Masonry (1990q). Selected tests were run on the freshly mixed grout including

slump per ASTM C 143, Standard Test Method for Slump of Portland Cement Concrete (1990g), unit weight per ASTM C 138, Standard Test Method for Unit Weight, Yield, and Air Content (Gravimetric) of Concrete (1990f), and air content per ASTM C 231, Standard Test Method for Air Content of Freshly Mixed Concrete by the Pressure Method (1990m). Compressive strength tests were performed on three prisms, each 3- by 3- by 6-in., from each batch. These specimens were prepared, cured, and tested in the laboratory as per ASTM C 1019, Standard Method of Sampling and Testing Grout (1990t). When appropriate, specimens were cast using either concrete masonry units or clay masonry units to mold the specimens. The results of these tests are given in Table A6. For Batch G129-2, 2- by 4-in. cylindrical specimens were cored from 3- by 3- by 6-in. prisms prepared and cured in accordance with ASTM C 1019. These specimens were then tested in splitting tension in accordance with the methods of ASTM C 496, Standard Test Method for Splitting Tensile Strength of Cylindrical Concrete Test Specimens (1990r). The results of these tests are tabulated in Table A6.

Table A6
Results of Fresh and Hardened Properties Tests on Grout

Mixture	Slump, in.	Unit Weight, pcf	Air Content, perecent	ASTM C 1019 (1990t) Compressive Strength, psi		Splitting Tensile Tensile Strength, psi	
				Clay Unit	Concrete Unit	Clay Unit	Concrete Unit
G93-1	10-1/4	129.8	8.5	2,950	3,030		
G129-2	9-1/4	128.2	10.0	3,700	2,130	500	430
G164-1	9-1/4	129.2	9.8	3,450	3,340		
G207-1	9-1/2	127.6	11.2	2,700	3,000		
G217-1	10	128.8	13.0	3,440	3,460		
G295-1	10	129.2	9.5	3,040	3,140		
G268-1	10	128.8	13.8	4,770	4,400		
G294-1	10	128.0	10.5		3,220		
G294-2	10	128.0	10.3		3,380		
G133-1					4,850		

Prism Tests

Uniaxial compression tests on stack-bond masonry prisms were conducted to provide typical strength and stiffness values per ASTM E 447 (1990u). Two specimens each were fabricated and tested using 6-in. clay masonry units and 8-in. concrete masonry units. Load-deflection curves for the prism tests are shown in Figure A15. The mean compressive strength (net area) for the concrete masonry prisms was 3,120 psi; for the clay masonry prisms, 4,160 psi.
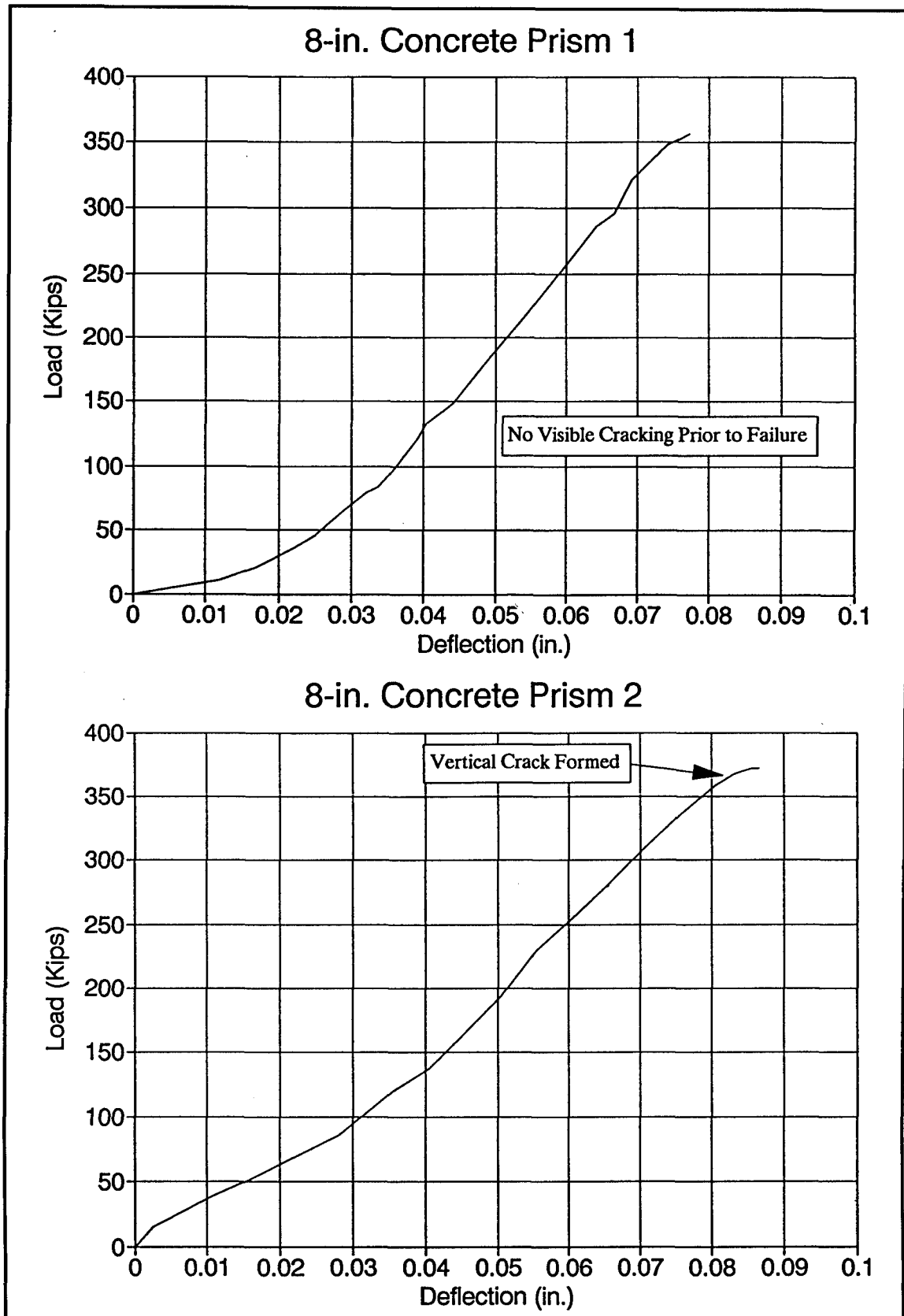
8-in. Concrete Prism 1

No Visible Cracking Prior to Failure

(Plot: Load (Kips) vs. Deflection (in.); Load axis 0 to 400, Deflection axis 0 to 0.1)

8-in. Concrete Prism 2

Vertical Crack Formed

(Plot: Load (Kips) vs. Deflection (in.); Load axis 0 to 400, Deflection axis 0 to 0.1)

Figure A15.   Results of compressive strength tests on 8-in. concrete masonry prisms

REPORT DOCUMENTATION PAGE

Public reporting burden for this collection of information is estimated to average 1 hour per response, including the time for reviewing instructions, searching existing data sources, gathering and maintaining the data needed, and completing and reviewing the collection of information. Send comments regarding this burden estimate or any other aspect of this collection of information, including suggestions for reducing this burden, to Washington Headquarters Services, Directorate for Information Operations and Reports, 1215 Jefferson Davis Highway, Suite 1204, Arlington, VA 22202-4302, and to the Office of Management and Budget, Paperwork Reduction Project (0704-0188), Washington, DC 20503.

1. AGENCY USE ONLY *(Leave blank)*	2. REPORT DATE October 1994	3. REPORT TYPE AND DATES COVERED Final report

4. TITLE AND SUBTITLE
Masonry Research for Limit-States Design

5. FUNDING NUMBERS

6. AUTHOR(S)
Michael I. Hammons, Richard H. Atkinson, Michael P. Schuller,
Paul J. Tikalsky

7. PERFORMING ORGANIZATION NAME(S) AND ADDRESS(ES)
U.S. Army Engineer Waterways Experiment Station, 3909 Halls Ferry Road,
Vicksburg, MS 39180-6199; Atkinson-Noland & Associates, 2619 Spruce St.,
Boulder, CO 80302; Santa Clara University, Santa Clara, CA 75053

8. PERFORMING ORGANIZATION REPORT NUMBER
Technical Report CPAR-SL-94-1

9. SPONSORING/MONITORING AGENCY NAME(S) AND ADDRESS(ES)
U.S. Army Corps of Engineers
Washington, DC 20314-1000

10. SPONSORING/MONITORING AGENCY REPORT NUMBER

11. SUPPLEMENTARY NOTES
Available from National Technical Information Service, 5285 Port Royal Road, Springfield, VA 22161.

12a. DISTRIBUTION/AVAILABILITY STATEMENT
Approved for public release; distribution is unlimited.

12b. DISTRIBUTION CODE

13. ABSTRACT *(Maximum 200 words)*

An experimental research program was conducted to determine certain critical material and design parameters of reinforced masonry necessary for the formulation of a new limit-states design standard. The research was divided into three subprograms: lap-splice, tension-stiffening, and biaxial compression-tension behavior. Tests were conducted to investigate lap splices in reinforced masonry, focusing on parameters which affect the strength and ductility of lap splices in both concrete and clay masonry construction. A performance criteria of 125 percent of the yield load of the reinforcement was adopted and used to establish critical lap lengths and maximum bar sizes. Tension-stiffening tests were conducted to develop data on the tensile behavior of reinforced masonry, especially in the postcracked state. The results of these experiments permitted the quantitative expression of tension-stiffening behavior in both the pre- and postyield range. Tests were conducted to determine the biaxial compressive-tensile behavior of reinforced concrete masonry panels. The tests were conducted in a unique load frame which permitted independent control of lateral tensile and vertical compressive loads. A model describing the influence of lateral tensile strain on the compressive stress and strain at compressive failure was obtained.

14. SUBJECT TERMS

Biaxial failure	Limit-states design	Strength
Design criteria	Masonry construction	Tension stiffening
Ductility	Reinforced masonry	
Lap splice	Reinforced masonry design	

15. NUMBER OF PAGES
165

16. PRICE CODE

17. SECURITY CLASSIFICATION OF REPORT UNCLASSIFIED	18. SECURITY CLASSIFICATION OF THIS PAGE UNCLASSIFIED	19. SECURITY CLASSIFICATION OF ABSTRACT	20. LIMITATION OF ABSTRACT